TRPM2 Channel-Mediated Signalling Mechanisms for Neuronal Cell Death

Xin Li

Submitted in accordance with the requirements for the degree of

Doctor of Philosophy

The University of Leeds

Faculty of Biological Sciences

August, 2017

The candidate confirms that the work submitted is her own and that appropriate credit has been given where reference has been made to the work of others.

Acknowledgements

I would like to express my sincere thanks to all the people who had generously offered assistant to me during my PhD.

Special thanks and appreciation go to my primary supervisor Dr. Lin-Hua Jiang for offering me an opportunity to engage in science and giving me tremendous academic support throughout my PhD. I appreciate his time, patience, constant trust and encouragement to my work. I am also grateful to my second supervisor, Prof. Asipu Sivaprasadarao, and my assessor, Dr. Jonathan Lippiat for the valuable advice to my research project.

I would like to thank the Faculty of Biological Sciences and the China Scholarship Council for providing a scholarship to me. I am hugely appreciative to Dr. Yang Wei (Zhejiang University, China) for his contribution to this project, to Ms. Fatema Mousawi, Dr. Emily Caseley for their kind help while working together, to Mr. Timothy Munsey, Ms. Hong-Lin Rong, Dr. Joan Sim (University of Manchester), Dr. Sally Boxall, Dr. Brian Jackson and all the staff in the Centre for Biomedical Service for their technical support. Similar gratitude goes to all the research groups in Gastang 6.45.

Last but not least, special thanks to my family and my friends for all the unconditional support and sacrifices they have made.

Abstract

Transient receptor potential melastatin-related 2 (TRPM2) channel is gated by ADP-ribose (ADPR) and potently activated by reactive oxygen species (ROS) through stimulating ADPR-generating mechanisms. Recent studies provide evidence to show a crucial role for TRPM2 in neuronal death and cognitive impairment associated with ischemic stroke and Alzheimer's disease. However, the underlying mechanisms are poorly understood. Studies described in this thesis adopted genetic and pharmacological interventions, in conjunction with immunofluorescent and live cell imaging, to investigate TRPM2-dependent cell death induced by H_2O_2 and the 42-residue of amyloid β ($A\beta_{42}$) in cultured hippocampal neurons. H_2O_2 and $A\beta_{42}$ induced significant neuronal death, which was reduced or prevented by TRPM2 knock-out (TRPM2-KO), TRPM2 channel inhibitors, or Zn^{2+} chelator TPEN. H_2O_2 and $A\beta_{42}$ induced intracellular Zn^{2+} increase, lysosomal dysfunction and Zn^{2+} release, mitochondrial Zn^{2+} accumulation, dysfunction and ROS generation. Bafilomycin A1-induced lysosomal dysfunction also resulted in mitochondrial Zn^{2+} accumulation and ROS generation. These events were abolished by TRPM2-KO or suppressed by inhibiting poly(ADP-ribose) polymerase-1 (PARP-1) or TRPM2 channel. Immunofluorescent imaging suggests mitochondrial localization of TRPM2. ADPR enhanced Zn^{2+} accumulation in isolated mitochondria from wild-type (WT) but not TRPM2-KO neurons. Finally, the inhibition of protein kinase C (PKC) and NADPH oxidases (NOX), particularly NOX1/4, suppressed H_2O_2/$A\beta_{42}$-induced neuronal death and $A\beta_{42}$-induced intracellular Zn^{2+} increase, lysosomal and mitochondrial dysfunction, and mitochondrial ROS generation. The inhibition of the proline-rich tyrosine kinase 2 (Pyk2) and the downstream MEK/ERK kinases protected against $A\beta_{42}$-induced neuronal death. Taken together, these results provide evidence to support a vicious positive feedback signalling loop that drives hippocampal neuronal death in response to ROS and $A\beta_{42}$, in which the TRPM2 channel in mitochondria integrates multiple

mechanisms comprising PKC/NOX-mediated ROS generation, lysosomal dysfunction and Zn^{2+} release, mitochondrial Zn^{2+} accumulation, mitochondrial dysfunction and ROS generation. In addition, the Pyk2-MEK-ERK signalling pathway is critically involved in $A\beta_{42}$-induced TRPM2-dependent neuronal death. These findings provide novel insights into the mechanisms underlying neuronal death and cognitive impairment related to ischemic stroke and AD.

Table of Contents

List of Tables

List of Figures

List of Abbreviations

α-KGDHG	α-Ketoglutarate dehydrogenase
Aβ	Amyloid β
ACA	N-(p-amylcinnamoyl)anthranilic acid
Ac-DVED-CMK	N-acetyl-L-α-aspartyl-L-α-glutamyl-N-[(1S)-1-(carboxymethyl)-3-chloro-2-oxopropyl]-L-valinamide
AD	Alzheimer's disease
ADP	Adenosine diphosphate
ADPR	ADP-ribose
AIF	Apoptosis-inducing factor
AMP	Adenosine monophosphate
AMPAR	α-Amino-3-hydroxy-5-methyl-4-isoxazolepropionic acid receptor
2-APB	2-Aminoethoxydiphenyl borate
APP	Amyloid precursor protein
AR	Aspect ratio
Arg	Arginine
AraC	Cytosine β-D-arabinofuranoside
Asp	Aspartic acid
ATP	Adenosine triphosphate
BBB	Blood-brain barrier
BCCAO	Bilateral common carotid artery occlusion
BD	Bipolar disorder
BLCLs	B-lymphoblast cell lines
BSA	Bovine serum albumin
$[Ca^{2+}]_i$	Intracellular Ca^{2+} concentration
cADPR	Cyclic ADP-ribose
CaM	Calmodulin

cAMP	Cyclic AMP
CAT	Catalase
CBF	Cerebral blood flow
CGD	Chronic granulomatous disease
CGP37157	7-Chloro-5-(2-chlorophenyl)-1,5-dihydro-4,1-benzothiazepin-2(3H)-one
cIAP	Cellular inhibitor of apoptosis 1/2
Clioquinol	5-Chloro-8-hydroxy-7-iodoquinoline
CNS	Central nervous system
CXCL2/8	Chemokine interleukin-2/8
Cyt-c	Cytochrome-c
DA	Dopamine
DCFH-DA	2’,7’-Dichlorofluorescin diacetate
DI	Degeneration index
DIV	Days *in vitro*
DMEM/F12	Dulbecco's modified Eagle medium/nutrient mixture F-12
DMSO	Dimethyl sulfoxide
DNA	Deoxyribonucleic acid
D-PBS	Dulbecco’s PBS
DPI	Diphenylene iodonium
DPQ	3,4-Dihydro-5-[4-(1-piperidinyl)butoxy]-1(2H)-isoquinolinone
DUOX	Dual oxidase
EAE	Experimental autoimmune encephalomyelitis
EC_{50}	Half maximal effective concentration
EGFR	Epidermal growth factor receptor
EGTA	Ethylene glycol-bis(β-aminoethyl ether)-N,N,N',N'-tetraacetic acid
EPAC	Exchange protein activated by cAMP

ER	Endoplasmic reticulum
ERK	Extracellular-signal regulated kinase
ETC	Electron transport chain
Ex-4	Exendin-4
FAD	Flavin adenine dinucleotide
$FADH_2$	Reduced form of FAD
FF	Form factor
FFA	Fluofenamic acid
FITC	Fluorescein isothiocyanate
FMN	Flavin mononucleotide
FTS	Farnesylthiosalicylic acid
GABA	Gamma-aminobutyric acid
GLP-1	Glucagon-like peptide 1
Glu	Glutamic acid
Gly	Glycine
GÖ6976	5,6,7,13-Tetrahydro-13-methyl-5-oxo-12H-indolo [2,3-a]pyrrolo [3,4-c]carbazole-12-propanenitrile
GPx	Glutathione peroxide
GSH	Glutathione
GSK-3	Glycogen synthase kinase-3
GTP	Guanosine triphosphate
HEK293	Human embryonic kidney 293 cell
HEPES	4-(2-Hydroxyethyl)-1-piperazineethanesulfonic acid
His	Histidine
HNE	4-Hydroxy-2-nonenal
H_2O_2	Hydrogen peroxide
IC_{50}	Half maximal inhibitory concentration
IF	Immunofluorescent

IFN-γ	Interferon-γ
IgG	Immunoglobulin G
IL-1β	Interleukin-1β
IM-54	2-(1H-Indol-3-yl)-3-pentylamino-maleimide
I-V	Current-voltage
JNK	c-Jun N-terminal kinase
KO	Knock-out
Leu	Leucine
LMP	Lysosomal membrane permeabilization
LPS	Lipopolysaccharides
MAO	Monoamine oxidase
MAP-2	Microtubule-associated protein-2
MAPK	Mitogen-activated protein kinase
MCAO	Middle cerebral artery occlusion
MCU	Mitochondrial Ca^{2+} uniporter
MEK	MAPK/ERK kinase
Met	Methionine
MLKL	Mixed lineage kinase domain like protein
mPTP	Mitochondrial permeability transition pore
MPTP	1-Methyl-4-phenyl-1,2,3,6-tetrahydropyridine
MPP^+	1-Methyl-4-phenylpyridinum
MT	Metallothionein
NAADP	Nicotinic acid adenine dinucleotide phosphate
NAD	Nicotinamide adenine dinucleotide
NADPH	Nicotinamide adenine dinucleotide phosphate (reduced form)
NADP	Reduced form of NAD
NCX	Na^+/Ca^{2+} exchanger
NF-κB	Nuclear factor kappa-light-chain-enhancer of activated B cells

NMDA	N-methyl-D-aspartate
NMDAR	NMDA receptor
NOX	NADPH oxidase
NS	No significance
NUDT9-H	Homology to NUDT9
$O_2^{\cdot -}$	Superoxide
OGD/R	Oxygen glucose deprivation followed with re-oxygenation
PARP	Poly(ADP-ribose) polymerase
PARG	Poly(ADP-ribose) glycohydrolase
PBS	Phosphate buffered saline
PBS-T	PBS with Tween-20
PD	Parkinson's disease
PF431396	N-methyl-N-[2-[[[2-[(2,3-dihydro-2-oxo-1H-indol-5-yl)amino]-5-(trifluoromethyl)-4-pyrimidinyl]amino]methyl]phenyl] methanesulfonamide
pH	Potential of hydrogen
PI	Propidium iodide
PJ34	N-(6-Oxo-5,6-dihydrophenanthridin-2-yl)-(N,N-dimethylamino) acetamide hydrochlorid
PKA/C	Protein kinase A/C
PMCA	Plasma membrane Ca^{2+}-ATPase
PS	Presenilin
PSD-95	Postsynaptic density-95
Pyk2	Proline-rich tyrosine kinase 2
$Q^{\cdot -}$	Semiquinone
Q	Ubiquinone
QH_2	Ubiquinol
RET	Reverse electron transport

RIPK1/3	Receptor-interacting protein kinase-1/3
RNA	Ribonucleic acid
ROS	Reactive oxygen species
SBS	Standard bath solution
SDS	Sodium dodecylsulphate
S.E.M	Standard error of the mean
Ser	Serine
SERCA	S/ER Ca^{2+}-ATPase
shRNA	Short hairpin RNA
siRNA	Small interfering RNA
SMAC	Second mitochondria-derived activator of caspases
SNc	Substantia nigra pars compacta
SNr	Substantia nigra pars reticulata
SOD	Superoxide dismutase
SR	Sarcoplasmic reticulum
Thr	Threonine
TM	Transmembrane
TNF-α	Tumour necrosis factor-α
TNFR1	TNF receptor 1
TPEN	N,N,N',N'-tetrakis(2-pyridylmethyl)ethane-1,2-diamine
TRADD	TNFR-associated death domain
TRITC	Tetramethylrhodamine isothiocyanate
TRP	Transient receptor potential
TRPA	TRP Ankyrin
TRPC	TRP canonical
TRPP	TRP polycystin
TRPM2	TRP melastatin-related 2 channel
TRPM2-L	Full-length TRPM2

TRPM2-S	Short form TRPM2
TRPM2-SSF	Striatum short form of TRPM2
TRPML	TRP mucolipin
TRPV	TRP vanilloid
U0126	1,4-Diamino-2,3-dicyano-1,4-bis[2-aminophenylthio] butadiene
VGCC	Voltage-gated Ca^{2+} channel
WT	Wild-type
ZIP	Zrt-/Irt-like protein family
$[Zn^{2+}]_i$	Intracellular Zn^{2+} concentration
ZnT	Zn^{2+} transporter

Chapter 1

General Introduction

1.1 ROS generation

The molecular oxygen has two unpaired electrons in its outer electron shell, which makes it highly reactive and susceptible to radical formation (Turrens, 2003). Free radicals and molecules which are derived from molecular oxygen are defined as reactive oxygen species (ROS), such as superoxide ($O_2^{\bullet -}$), hydroxyl radical, hydrogen peroxide (H_2O_2), hypochlorous acid and lipid peroxide (Nimse and Pal, 2015).

ROS generation was originally described in the respiratory burst of phagocytic cells such as macrophages and neutrophils (Forman and Torres, 2002). Later studies have shown ROS production in a variety of non-phagocytes such as vascular cells, myocytes and neurons (Griendling et al., 2000; Tammariello et al., 2000). ROS such as $O_2^{\bullet -}$ and H_2O_2 can be produced as a by-product within the respiratory pathways of mitochondria and peroxisomes, or during the oxidation processes of some enzyme systems, like xanthine oxidoreductase and cytochrome P-450 uncoupling in microsomal monooxygenase system (Murphy, 2009; Schrader and Fahimi, 2006; Harrison, 2004; Zangar et al., 2004). Among the above-mentioned sources, oxidative phosphorylation during mitochondrial electron transport and the activation of nicotinamide adenine dinucleotide phosphate (NADPH) oxidases (NOX) are two major mechanisms or processes for ROS generation.

1.1.1 ROS generation in mitochondria

The generation of ROS in mitochondria mainly takes place at the electron transport chain (ETC) in mitochondria inner membrane (**Fig. 1.1**). During the process of oxidative phosphorylation, electrons donated by nicotinamide adenine dinucleotide (NADH) at complex I and flavin adenine dinucleotide ($FADH_2$) at complex II pass through the ETC and ultimately reduce O_2 to water at complex IV. Electrons leaked

from the ETC reducing molecular oxygen to $O_2^{\cdot -}$, the primary ROS generated in mitochondria (Orrenius et al., 2007).

In mitochondrial ETC, there are several redox centre-containing complexes that serve as sites for ROS generation by providing electrons to molecular oxygen. Complex I (NADH-ubiquinone oxidoreductase) and III (ubiquinol-cytochrome c oxidoreductase) are considered as two major sources of mitochondrial ROS (**Fig. 1.1**) (Fato et al., 2009; Chen et al., 2003; Murphy, 2009). At complex I, flavin mononucleotide (FMN) accepts electrons from NADH and passes them through a chain of seven FeS centres to reduce ubiquinone (Q) (Hirst et al., 2003). $O_2^{\cdot -}$ is formed by transferring electrons from the fully reduced FMN to O_2 (Kussmaul and Hirst, 2006; Hirst et al., 2008). Its generation has been shown in isolated mitochondrial complex I (Hirst et al., 2008; Murphy, 2009). However, the conventional forward electron transport only exhibits minimal ROS generation, large amounts of $O_2^{\cdot -}$ are produced during reverse electron transport (RET). RET occurs when no adenosine triphosphate (ATP) is made by mitochondria, which results in a high proton-motive force and a reduced ubiquinone pool. Electrons flowing back to complex I through RET drive extensive $O_2^{\cdot -}$ generation (Kushnareva et al., 2002). Apart from complex I, complex III has also been identified as a principal site for ROS generation in mitochondria (Chen et al., 2003). The function of complex III is to funnel electrons to cytochrome-c (Cyt-c) and pump protons across the inner mitochondrial membrane through the Q-cycle (Murphy, 2009; Osyczka et al., 2005). There are two ubiquinone-reaction centres in the Q-cycle, ubiquinol-oxidation centre (Q_o site) and ubiquinone-reduction centre (Q_i site), which are located on the opposite sites of the mitochondrial inner membrane. The Q-cycle starts with the oxidation of ubiquinol (QH_2) to ubiquinone at the Q_o site, with two electrons being transferred via two alternate routes. One of the electrons is transferred through FeS cluster to Cyt-c; simultaneously, two protons are released to the mitochondrial intermembrane space. The other electron is transferred to ubiquinone bound to the

Q_i site, leading to the formation of semiquinone ($Q^{\cdot-}$) (Zorov et al., 2014). To complete the Q-cycle, the second QH_2 is oxidized at the Q_o site, releasing two more protons to the intermembrane space while $Q^{\cdot-}$ is reduced to QH_2. The $Q^{\cdot-}$ thereby serves as an electron donor, leading to high levels of $O_2^{\cdot-}$ production when the Q_i site is inhibited, for example, by antimycin A (Chen et al., 2003; Cape et al., 2007).

Several other sites that are ubiquitously present in mammalian mitochondria are likely to have the capability for ROS generation, although their contribution to the total mitochondrial ROS production is significantly lower than that of mitochondrial respiratory chain. For example, monoamine oxidases (MAO) A and B in the outer mitochondrial membrane catalyse the oxidation of neurotransmitters such as dopamine and produce H_2O_2. Therefore, MAOs are responsible for oxidative stress-related neurodegenerative diseases, including ischemia, Alzheimer's disease (AD) and Parkinson's disease (PD) (see further discussion below) (Youdim et al., 2006). The α-ketoglutarate dehydrogenase (α-KGDHG) complex, which is associated with the matrix side of the inner membrane, generates significant ROS when complex I is blocked by rotenone (Starkov et al., 2004).

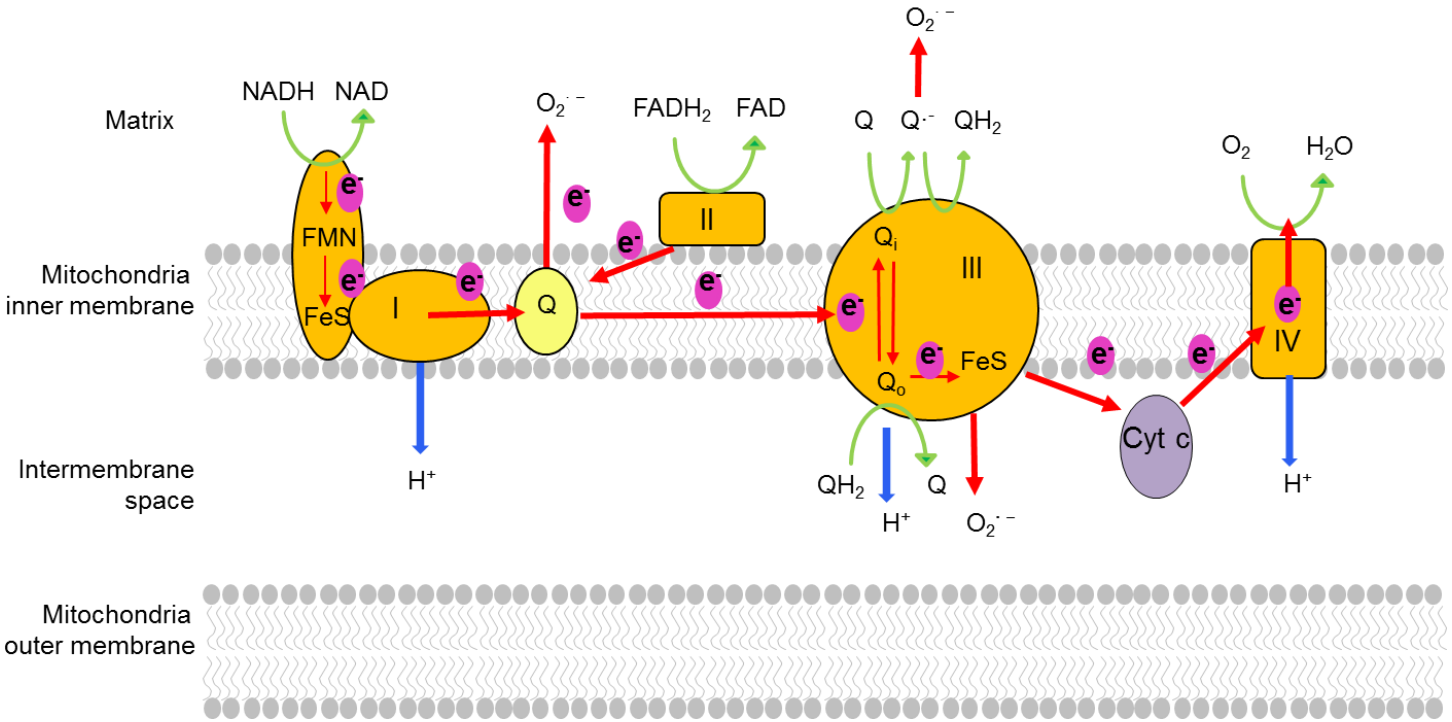

Figure 1.1 Main sites of mitochondrial ROS generation

Electrons provided by NADH and $FADH_2$ are passed through the electron transport chain and ultimately reduce molecular oxygen to water at complex IV. Superoxide can be produced as a by-product of oxidative phosphorylation at several sites in the electron transport chain such as complex I and complex III. (NADH: Nicotinamide adenine dinucleotide (reduced form); NAD: Nicotinamide adenine dinucleotide; FMN: Flavin mononucleotide; FeS: Iron-sulpher cluster; $FADH_2$: Flavin adenine dinucleotide (reduced form); FAD: Flavin adenine dinucleotide; Q: Ubiquinone; QH_2: Ubiquinol; $Q\cdot^-$: Semiquinol; Cyt-c: Cytochrome-c; $O_2\cdot^-$: Superoxide; e^-: Electron; H^+: Proton.)

1.1.2 ROS generation by NADPH oxidases

1.1.2.1 NOX activation

The NOX family is composed of catalytic subunit gp91^{phox}, regulatory subunits p22^{phox} p47^{phox}, p40^{phox}, p67^{phox} and a major binding partner small guanosine triphosphate (GTP)-binding protein, Rac (Lambeth, 2004) (**Fig. 1.2**). Genomic studies have identified 7 homologs of gp91^{phox} in animals, including NOX1-5, and dual oxidase (DUOX)-1 and 2 (Lambeth et al., 2000; Cheng et al., 2001). DUOXs and NOX5 enzymes have additional cytosolic EF-hands on their N-terminus which is crucial for Ca^{2+} binding (Bedard and Krause, 2007). Each member of the NOX family has particular tissue distributions, for example, previous studies have shown the expression of NOX1 and NOX4, especially NOX2 in the central nervous system (CNS) (Zhang et al., 2012; Vallet et al., 2005; Coyoy et al., 2008; Reinehr et al., 2007); however, little data reported the presence of NOX3 and NOX5 in the same regions.

Under resting conditions, most NOXs are inactive except for NOX4 which is constitutively active (Bedard and Krause, 2007). Activation of NOX is associated with the migration of cytosolic components to the plasma membrane (**Fig. 1.2**). For example, in the case of the well-characterized isoform NOX2, p22^{phox} is located in the plasma membrane with gp91^{phox} and functions as a docking site for the adaptor protein p47^{phox}. PKC-induced serine phosphorylation leads to the conformational change of p47^{phox} which thereby exposes its interacting domains to p22^{phox}. Subsequently, p47^{phox} binds to p22^{phox} and brings the entire cytosolic complex composed of p47^{phox}, p40^{phox}, p67^{phox} to the plasma membrane to form active oxidase (El-Benna et al., 2009). The activation of NOX also requires Rac, which binds to GTP upon activation and migrates to membrane along with the cytosolic complex (Bedard and Krause, 2007). Once the assembly is completed, the NOX complex becomes active and generates $O_2^{\bullet -}$ by transferring an electron from NADPH in cytosol to oxygen (Babior, 2004).

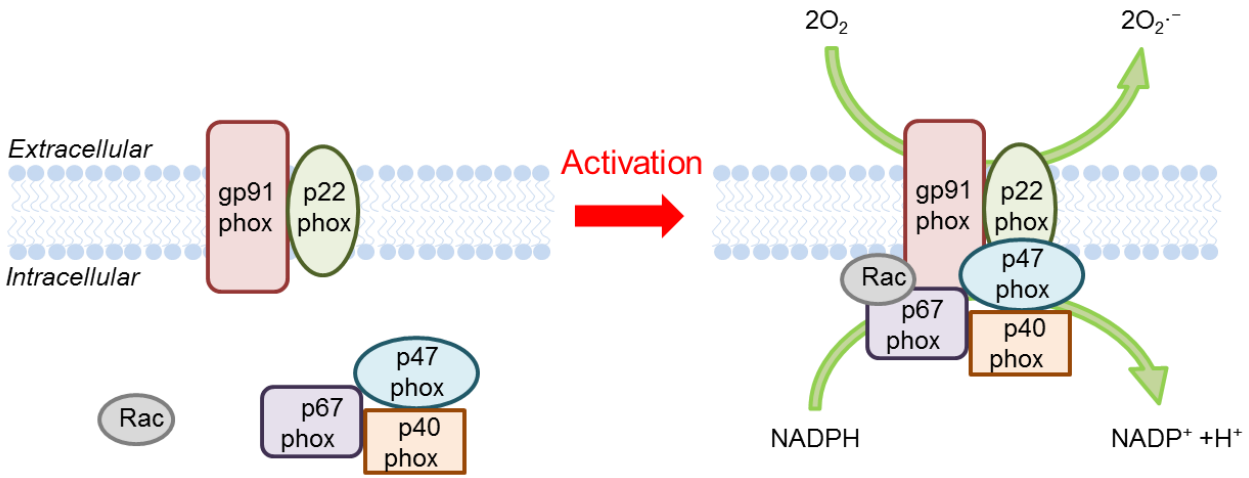

Figure 1.2 NADPH oxidase assembly and activation

Under resting conditions, the NADPH oxidases (NOX) are inactive (*left*). Activators of NOX trigger the migration of cytosolic components to the plasma membrane (*right*). Once the assembly is completed, the NOX complex becomes active and generates superoxide by transferring an electron from NADPH in cytosol to oxygen.

1.1.2.2 Activators of NOX

The NOX-dependent ROS production is regulated by a diversity of factors. For example, as mentioned above, serine phosphorylation of $p47^{phox}$ is essential for the assembly of active NOX and PKC is involved in this process (El-Benna et al., 2009). PKC can also phosphorylate $gp91^{phox}$ or $p22^{phox}$ to promote the interaction with other regulatory subunits and ultimately increase ROS production (Raad et al., 2009; Lewis et al., 2010). Pro-inflammatory cytokines such as tumour necrosis factor (TNF)-α, stimulatory molecules like lipopolysaccharides (LPS), PKC activator phorbol-12-myristate-13-acetate and chemoattractant N-formylmethionyl leucyl phenylalanine are known as phosphorylation inducers of $p47^{phox}$, contributing to NOX activation (Mittal et al., 2014). In addition, Rac1 which is required for the activation of NOX2, is activated by TNF-α, and interleukin-1β (IL-1β) (Mittal et al., 2014). NOX5 and DUOXs are directly regulated by Ca^{2+} through the above-mentioned Ca^{2+}-binding EF-hand domain in the N-terminus (Banfi et al., 2001; Wong et al., 2004; Ameziane-El-Hassani et al., 2005). Notably, studies have shown that ROS such as H_2O_2 can induce the production of $O_2{\cdot}^-$ by activating NOX in different types of cells, such as vascular smooth muscle, fibroblast and endothelial cells (Li et al., 2001; Coyle et al., 2006). Last but not least, NOX enzymes can be stimulated by physical challenges, for example, intracellular acidosis facilitates H^+ efflux which enhances the rate of ROS generation by NOX in astrocytes (Abramov et al., 2005).

1.1.2.3 NOX inhibitors

Diphenylene iodonium (DPI) and apocynin, with the half maximal inhibitory concentration (IC_{50}) of 0.02-0.24 μM and 10 μM respectively, represent the most frequently used generic NOX inhibitors (Drummond et al., 2011; Jaquet et al., 2011; Petronio et al., 2013). DPI inactivates flavoprotein-containing systems including NOX enzymes by preventing electron flow through the enzyme complex (O'Donnell et al., 1993; O'Donnell et al., 1994). Apocynin is capable of suppressing the

expression as well as the translocation of $p47^{phox}$ and $p67^{phox}$ (Li et al., 2013; Johnson et al., 2002; Petronio et al., 2013). In addition, several NOX inhibitors have been identified with selectivity towards to particular NOX isoforms. For example, GKT137831 is potent in inhibiting NOX1 and NOX4 with the IC_{50} of 0.14 and 0.11 μM, respectively (Aoyama et al., 2012).

1.1.3 Antioxidants

To defend against oxidative damage, cells are equipped with antioxidant capacity which serves to neutralize the effects of ROS. Based on the activity, antioxidants are categorised to enzymatic and non-enzymatic (Pisoschi and Pop, 2015).

Enzymatic antioxidants, such as superoxide dismutase (SOD), catalase (CAT) and glutathione peroxidase (GPx), work by breaking down and removing free radicals (Nimse and Pal, 2015). SOD located in cytosol (SOD1) and mitochondria (SOD2) catalyse the dismutation of $O_2^{\bullet -}$ to O_2 and H_2O_2 in the presence of metal ions such as Cu^{2+}, Zn^{2+} or Mn^{2+} (Fukai and Ushio-Fukai, 2011). CAT and GPx convert H_2O_2 to water that lowers the risk of hydroxyl radical formation from H_2O_2 via the Fenton reaction (Bechtel and Bauer, 2009; Tanaka et al., 2002; Baud et al., 2004).

Low-molecule-weight non-enzymatic antioxidants, such as vitamins (vitamin C and E) and glutathione (GSH), function as direct scavengers of ROS (Valko et al., 2007). Vitamin E is the principal defence against oxidant injury in the cell membrane. It donates electrons to peroxyl radical produced during lipid peroxidation to terminate the lipid peroxidation chain reaction (Nimse and Pal, 2015). Similarly, vitamin C scavenges $O_2^{\bullet -}$ and hydroxyl radical, preventing the lipid peroxidation chain reaction. Moreover, vitamin C reacts with oxidised vitamin E and reduces it, contributing to the regeneration of active vitamin E in the cell membrane together with GSH (Traber and Stevens, 2011). As a major antioxidant in cytosol, nucleus and mitochondria, GSH donates its electrons to H_2O_2 to reduce it into H_2O and O_2.

In addition to scavenge ROS by itself, GSH serves as a cofactor of several detoxifying enzymes against H_2O_2 or lipid peroxide, such as GPx (Masella et al., 2005).

1.1.4 Physiological role of ROS

A large amount of ROS are produced by phagocytes during NOX-mediated respiratory burst, in which ROS serve as critical components in the immune system against pathogens (Paiva and Bozza, 2014). The critical role of ROS in host immunity has been identified through the discovery of chronic granulomatous disease (CGD) that is characterized by low respiratory burst due to the deficiency in NOX2 (Panday et al., 2015). ROS can directly eliminate pathogens by causing oxidative damage such as lipid peroxidation, deoxyribonucleic acid (DNA) strand breakage, and oxidation of bases and amino acid residues (further discussed below) in microbes (Olagnier et al., 2014; Bhattacharyya et al., 2014). Neutrophils from CGD patients are thereby deficient in killing pathogens during phagocytosis (Panday et al., 2015). In addition to the intracellular killing, ROS leads to the formation of neutrophil extracellular traps that kill bacteria and degrade microbial toxins (Brinkmann et al., 2004).

Except for the respiratory burst by phagocytes, ROS, particularly at low levels, play a physiological role in the induction and maintenance of several signal transduction pathways involved in cell proliferation and differentiation. One broad class of signal transduction regulated by ROS is the mitogen-activated protein kinases (MAPK) that are comprised of extracellular signal regulated kinase (ERK), c-Jun N-terminal kinase (JNK) and p38 kinase. ERK has a well-established role in regulating cell proliferation (Zhang and Liu, 2002); JNK and p38 kinases are more strongly linked to stress responses ultimately leading to apoptosis and necrosis (Kim and Choi, 2010). ROS have been suggested to regulate the ERK pathway by activating the

epidermal growth factor receptor (EGFR) in the absence of growth factor ligand. The EGFR, once activated, undergoes auto-phosphorylation that initiates the Ras/Raf/ERK signalling cascade (Son et al., 2013; McCubrey et al., 2007). On the other hand, direct inhibition of MAPK phosphatases by ROS has been shown to regulate JNK and p38 activity (Ray et al., 2012). Moreover, the MAPK can be elicited as a consequence of ROS-induced PKC activation, contributing to cancer proliferation (Dempsey et al., 2000).

1.2 Oxidative stress

1.2.1 Oxidation of biomolecules

As discussed above, under physiological conditions, ROS generation is counterbalanced by antioxidant defense systems. However, when large amounts of ROS are produced, the antioxidant mechanisms become overwhelmed and oxidative stress may occur. Oxidative stress is typically detrimental to molecules such as lipids, proteins and DNA (Butterfield and Lauderback, 2002; Cooke et al., 2003).

Oxidants can attack polyunsaturated fatty acid, which initiates the lipid peroxidation and impairs cell membrane under the condition of oxidative stress (Butterfield and Lauderback, 2002). ROS react with DNA, resulting in DNA base modifications and DNA strand breaks. Such DNA damage responses are associated with cancer, neurodegenerative diseases, inflammation and many other diseases (Cooke et al., 2003). Oxidative stress can also trigger structural modification of proteins by oxidation of amino acid residues such as cysteine, methionine and tyrosine residues (Stadtman and Levine, 2000). Notably, oxidation of some amino acid residues like lysine, arginine and proline residues in proteins can lead to the formation of carbonyl derivatives. The production of carbonyls has been regarded as a marker for oxidative stress. Elevated protein carbonyls are detected in the

brains of rats and human undergoing aging or neurodegenerative diseases (Butterfield and Lauderback, 2002; Nicolle et al., 2001).

1.2.2 Oxidative stress and Ca^{2+} homeostasis

1.2.2.1 Regulation of extracellular Ca^{2+} entry

Substantial studies have demonstrated interactions between ROS and alterations in the intracellular Ca^{2+} concentrations ($[Ca^{2+}]_i$). ROS can regulate the Ca^{2+} homeostasis by either stimulating or suppressing the activity of Ca^{2+} transporting mechanisms such as ion channels on the cell membrane. The activity of voltage-gated Ca^{2+} channels (VGCC) has been shown to be modified by ROS, depending on the type of channels and expressing systems. For example, ROS suppress the L-type VGCC in guinea pig ventricular myocytes and the rabbit smooth muscle L-type VGCC heterologously expressed in Chinese hamster ovarian cells, but activate the L- and T-type VGCC channels in vascular smooth muscle cells (Gorlach et al., 2015). Ca^{2+} entry mediated by members of the transient receptor potential (TRP) superfamily has been associated with oxidative stress (Takahashi and Mori, 2011). ROS-induced activation of the non-selective Ca^{2+} permeable TRPM2 channel, the subject of this study, will be discussed in detail below. Oxidative stress has also been shown to activate store-operated Ca^{2+} channel-mediated Ca^{2+} entry by modifying the Ca^{2+} sensor stromal interaction molecule 1 in the endoplasmic reticulum (ER) (Grupe et al., 2010).

The plasma membrane Ca^{2+}-ATPase (PMCA) and Na^+/Ca^{2+} exchanger (NCX), two major Ca^{2+} extrusion pathways in the plasma membrane, are also sensitive to ROS regulation. In neurodegenerative diseases such as AD and PD, the oxidation of cysteine residues in the PMCA has been shown to trigger the uncoupling of ATP-binding and hydrolysis, reducing the PMCA activity and PMCA-mediated Ca^{2+} efflux (Zaidi, 2010). Of note, oxidative stress promotes the reverse mode of NCX, which

can function as a predominant route for Ca^{2+} entry under ischemia and hypoxia conditions (Eigel et al., 2004).

1.2.2.2 Intracellular Ca^{2+} release

Several intracellular mechanisms that play an important role in Ca^{2+} homeostasis are also targets for ROS. For example, as major Ca^{2+} release channels from the ER or sarcoplasmic reticulum (SR), the activity of ryanodine receptors (RyR) and inositol 1, 4, 5-trisphosphate receptors (IP_3R) are modulated by oxidants. Oxidation of RyR thiols augments Ca^{2+} leak from the SR; oxidants modify cysteine residues of IP_3R and increase its sensitivity to IP_3, promoting Ca^{2+} release from the ER or SR (Gorlach et al., 2015). The S/ER Ca^{2+} ATPase (SERCA) that involves in refilling Ca^{2+} in the ER or SR is also regulated by ROS-induced modification of cysteine residues (Sharov et al., 2006). Intriguingly, modification of the SERCA at different cysteine residues can result in either activation or inhibition of the pump activity (Gorlach et al., 2015).

Investigations using diverse tissues reveal that mitochondria serve as a large physiological buffer for Ca^{2+} (Williams et al., 2013). Ca^{2+} has been shown to flow into mitochondria through the mitochondrial Ca^{2+} uniporter (MCU) and mitochondrial NCX in a reversed mode (Chaudhuri et al., 2013; Santo-Domingo and Demaurex, 2010), and, as a result, Ca^{2+} stimulates the tricarboxylic acid cycle and oxidative phosphorylation by activating tricarboxylic acid cycle dehydrogenases, ATP synthase and adenine nucleotide translocase. As a consequence, enhanced metabolism consumes more O_2 to produce ATP and more electrons are thereby leaked from the ETC, resulting in an increase of mitochondrial ROS generation (Yan et al., 2006). Studies using isolated mitochondria suggest that alterations in mitochondrial membrane structure, such as opening of the mitochondrial permeability transition pore (mPTP) triggered by high concentrations of mitochondrial Ca^{2+}, are also intimately connected with mitochondrial ROS production (Sousa et al., 2003; Zorov et al., 2014).

1.2.3 Oxidative stress and Zn^{2+} homeostasis

Zn^{2+} is one of the most prevalent trace elements in the human body, mainly distributed in blood, kidney, liver, bone and brain (Sensi et al., 2009). Brain has the highest concentration of Zn^{2+} among all organs, especially in presynaptic vesicles at glutamatergic nerve terminals. Zn^{2+} is an essential cofactor for the structure and function of many proteins in cytosol and in many organelles, including the nucleus, lysosomes and mitochondria (Sensi et al., 2011). In the CNS, Zn^{2+} can be released upon neuronal activity and regulates the activity of ionotropic receptors for glutamate, such as N-methyl-D-aspartate receptor (NMDAR) and α-amino-3-hydroxy-5-methyl-4-isoxazolepropionic acid receptor (AMPAR), and receptors for gamma-aminobutyric acid (GABA) and glycine (Smart et al., 2004). Thus, Zn^{2+} deficiency can result in deleterious consequences on nervous system functions such as impairing the brain development and capabilities of learning and memory (Hagmeyer et al., 2014).

1.2.3.1 Maintenance of Zn^{2+} homeostasis

The cellular Zn^{2+} homeostasis or intracellular Zn^{2+} concentrations ($[Zn^{2+}]_i$) is tightly regulated by diverse cell membrane and intracellular mechanisms, as illustrated in **Fig. 1.3**. Numerous mechanisms on the cell membrane contribute in mediating Zn^{2+} influx and efflux from cytosol, including Zn^{2+} transporters (Kambe et al., 2015), Na^{+}/Zn^{2+} exchanger (Lovell, 2009) and various Ca^{2+}-permeable ion channels including the VGCC and AMPAR (Ohana et al., 2004). In addition, there are several intracellular Zn^{2+}-modulating mechanisms, located within intracellular organelles such as mitochondria (Sensi et al., 2003) and lysosomes (Kukic et al., 2014), as well as cytosolic Zn^{2+}-buffering proteins such as metallothioneins (MT) (Spahl et al., 2003).

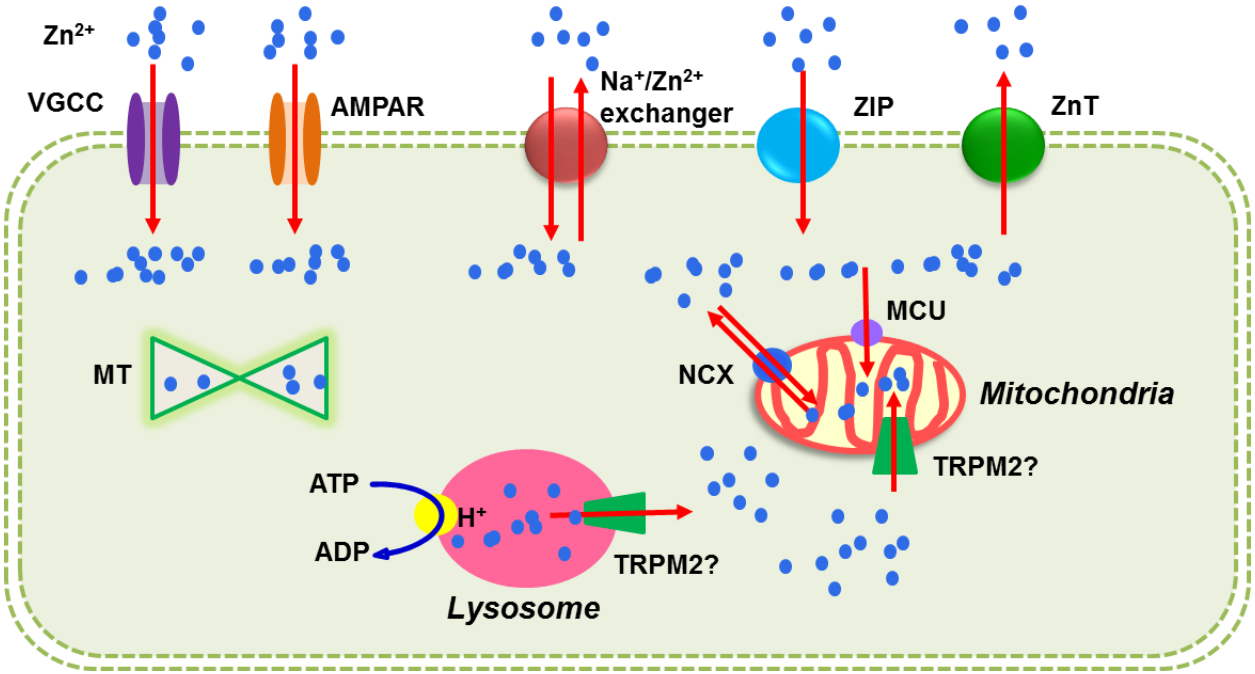

Figure 1.3 Key molecular mechanisms regulating the intracellular Zn^{2+} homeostasis

On the cell membrane, labile Zn^{2+} can be transported by voltage-gated Ca^{2+} channel (VGCC), AMPA receptor (AMPAR), Na^{+}/Zn^{2+} exchanger, Zrt-/Irt-like protein (ZIP) and Zn^{2+} transporters (ZnT). Within cytosol, Zn^{2+} is buffered by metallothioneins (MT), or stored in lysosomes, and mitochondria through the mitochondrial Ca^{2+} uniporter (MCU) and mitochondrial Na^{+}/Ca^{2+} exchanger (NCX). The role of intracellular TRPM2 in modulating Zn^{2+} transportation in lysosomes and mitochondria will be investigated in this thesis.

Zn^{2+} transporters

Zn^{2+}-transporting proteins can be divided into two distinct families, the Zn^{2+} transporter family (ZnT) and the Zrt-/Irt-like protein family (ZIP) (Kambe et al., 2015). ZnT mediates both Zn^{2+} efflux from cytosol (**Fig. 1.3**) and influx into the lumen of intracellular compartments such as secretory vesicles and Golgi apparatus (Huang and Tepaamorndech, 2013). There are at least 10 members in the ZnT (ZnT1-10) family, and among them, ZnT3 is more neuron-specific, expressed on Zn^{2+}-containing synaptic glutamatergic vesicles in the hippocampus and cerebral cortex (Palmiter et al., 1996) and in the cerebellar GABAergic and dopaminergic neurons in the spinal cord (Danscher et al., 2001). Moreover, ZnT3 has been shown to play an important role in transporting and concentrating Zn^{2+} into synaptic vesicles (Cole et al., 1999). ZnT3 knock-out (KO) mice showed a lack of synaptic vesicular Zn^{2+} uptake, and higher sensitivity to kainate-induced epileptic seizures (Cole et al., 2000) and age-dependent deficits in learning and spatial memory (Adlard et al., 2010; Sindreu et al., 2011). Other ZnT family members, although not brain-specific, have also been shown to mediate Zn^{2+} translocation in neurons and glia. For example, the reduction in the expression of ZnT1 protein in cortical neurons induces a significant decrease of Zn^{2+} efflux, suggesting the requirement of ZnT1 for neuronal Zn^{2+} release (Qin et al., 2009).

ZIP mediates Zn^{2+} transportation from the extracellular space or from intracellular vesicles to the cytoplasm (Kambe et al., 2015). There are 14 members in the ZIP family, ZIP1-14, mainly present in the plasma membrane. Notably, the membrane distribution of ZIP proteins, except ZIP5, is regulated by intracellular Zn^{2+}. For example, Zn^{2+} deficiency increased the membrane expression level of ZIP1 and ZIP3 and their Zn^{2+} uptake activity (Wang et al., 2004). Mice lacking one or multiple ZIP proteins are sensitive to the dietary Zn^{2+} deficiency during pregnancy (Kambe et al., 2015).

Na^+/Zn^{2+} exchanger

It was previously suggested that the NCX is involved in Zn^{2+} transport through plasma membrane. However, inhibitors of the NCX failed to entrap Na^+-dependent Zn^{2+} extrusion (Ohana et al., 2004). Moreover, Zn^{2+} influx was unchanged in human embryonic kidney (HEK)-293 cells heterologously expressing the NCX (Ohana et al., 2004). The findings suggest the existence of a Na^+/Zn^{2+} exchanger that is distinct from the NCX (**Fig. 1.3**), for Zn^{2+} extrusion in mammalian cells (Ohana et al., 2004; Qin et al., 2008). On the other hand, under conditions such as ischemic stroke, the increase of intracellular Na^+ concentrations induces depolarization of plasma membrane that lead to the reverse operation of the Na^+/Zn^{2+} exchanger and thereby the uptake of Zn^{2+} into cells (Qin et al., 2008).

Ca^{2+}-permeable ion channels

In neuronal cells, several Ca^{2+}-permeable channels are involved in Zn^{2+} influx into neurons, particularly Zn^{2+} translocation from presynaptic terminal to postsynaptic neurons. Studies in cultured cortical neurons have shown a significant role for NMDAR (Marin et al., 2000), AMPAR lacking GluA2 subunit (Yin et al., 2002) and VGCC (Kerchner et al., 2000) in mediating Zn^{2+} entry. The translocation of excessive Zn^{2+} through these mechanisms leads to excitotoxicity to post-synaptic neurons (Morris and Levenson, 2012).

Intracellular Zn^{2+} stores

Within cytosol, Zn^{2+} can accumulate and be released from intracellular compartments. For example, the MCU helps mitochondrial Zn^{2+} uptake when cytosolic Zn^{2+} buffering is impaired due to acidosis and oxidative stress in ischemia (Sensi et al., 2003; Clausen et al., 2013; Medvedeva and Weiss, 2014). Moreover, Zn^{2+} can be transported from cytosol into lysosomes either by ZnT (Falcon-Perez and Dell'Angelica, 2007) or through endocytosis or autophagy (Lee and Koh, 2010; Kukic et al., 2014). Lysosome was shown to be a pivotal Zn^{2+} sink in hippocampal

neurons under physiological conditions (Hwang et al., 2008). Upon exposure to oxidative stress, lysosomes lose their membrane integrity and release Zn^{2+} to cytosol (Hwang et al., 2008). In addition, as mentioned above, Zn^{2+} can accumulate in synaptic vesicles in the CNS via ZnT3 and is co-released with glutamate to modulate neuronal excitability (Cole et al., 1999).

Zn^{2+} binding proteins

MT, a group of metal-binding proteins (Ruttkay-Nedecky et al., 2013), represent another important Zn^{2+} buffering mechanism within cytosol (Kang, 2006). Among four subunits of MT proteins, MTI and MTII are expressed in all tissues, MTIII has particularly high expression in neurons but also in heart, kidney and reproductive organs, and MTIV is exclusively expressed in epithelia (Ruttkay-Nedecky et al., 2013).

As the primary isoform in neurons, MTIII is a cycteine rich protein and is readily oxidized (Maret and Vallee, 1998); hence, the association of Zn^{2+} with MTIII is extremely susceptible to oxidative stress, which leads to the liberation of bound Zn^{2+} (McCord and Aizenman, 2014). Intriguingly, MTIII has been shown to translocate to mitochondria and release Zn^{2+} within the mitochondrial intramembranous space (Ye et al., 2001), providing further evidence to support the important role of mitochondria in Zn^{2+} homeostasis.

1.2.3.2 Zn^{2+} homeostasis in oxidative stress-induced neuronal death

The increase in the $[Zn^{2+}]_i$ can induce numerous adverse effects on cell functions. A great number of studies have demonstrated the significance of Zn^{2+} in neurons undergoing oxidative stress. For example, chelatable Zn^{2+} accumulation has been shown in the hippocampus (Medvedeva et al., 2009) as well as in the cerebral cortex, thalamus, striatum and amygdala subjected to transient global ischemia insults (Koh et al., 1996), implicating disruption in the Zn^{2+} homeostasis as a critical mechanism underlying neuronal injury.

An increase in the $[Zn^{2+}]_i$ has been linked to oxidative stress in neurons, contributing to neurodegeneration (McCord and Aizenman, 2014). Zn^{2+} accumulation in mitochondria can trigger ROS production by either inhibiting complex III activity or interfering with complex I and α-KGDHG (Link and von Jagow, 1995; Sharpley and Hirst, 2006; Brown et al., 2000). Moreover, some studies suggest that Zn^{2+} at the concentration of 100-200 nM effectively impedes the cellular energy production by mitochondria and dissipates mitochondrial membrane potential. Such suppression of mitochondrial activities may contribute to the elevation of mitochondrial ROS generation, which eventually lead to Zn^{2+}-induced neuronal death (Dineley et al., 2005; Sensi et al., 2003). In addition, Zn^{2+} has been shown to stimulate PKC-dependent NOX activation (Kim and Koh, 2002; Noh and Koh, 2000; Noh et al., 1999). Exposure of cortical neurons to Zn^{2+} induced an increase in membrane PKC activity (Noh et al., 1999). The expression of $p47^{phox}$ and $p67^{phox}$ in plasma membrane is also subsequently elevated, resulting in NOX-mediated oxidative stress in cortical neurons (Noh and Koh, 2000). However, a recent study shows that inhibition of NOX activation substantially attenuates Ca^{2+}-induced ROS production in cortical neurons, but had no detectable effect on Zn^{2+}-triggered ROS generation. This finding challenges the contribution of NOX activation to Zn^{2+}-caused oxidative stress (Clausen et al., 2013).

Apart from inducing oxidative stress, Zn^{2+} can mediate neuronal death by triggering several cell death signalling pathways. For example, Zn^{2+} entry into mitochondria results in opening of the mPTP, followed by release of apoptotic mediators such as Cyt-c and apoptosis-inducing factor (AIF) which lead to apoptosis (as discussed below) (Jiang et al., 2001). Zn^{2+} may also elicit autophagy that contributes to neuronal death. Lysosomal Zn^{2+} accumulation during oxidative stress was shown to cause lysosomal membrane permeabilization (LMP), which led to the release of Zn^{2+} and acidic hydrolases such as cathepsin D, accompanied with the increased level of 4-hydroxy-2-nonenal (HNE) (Hwang et al., 2008). Recent studies have

speculated that autophagy and H_2O_2-induced LMP are mechanically linked in neuronal death (Lee et al., 2009). Removal of the intracellular Zn^{2+} substantially reduced autophagy; autophagy inhibitors not only attenuated LMP but also protected cells from H_2O_2-induced death (Lee et al., 2009). The results suggest Zn^{2+} is crucial in oxidative stress induced autophagy. Transient ischemia can induce excessive Zn^{2+} influx, which has been shown to decrease the nicotinamide adenine dinucleotide (NAD) level and inhibit glyceraldehyde-3-phosphate dehydrogenase. The resulting energy failure can contribute to neuronal death (Sheline et al., 2000). Moreover, a toxic level of Zn^{2+}-induced oxidative stress causes excessive DNA damage, which stimulates the activation of poly(ADP-ribose) polymerase (PARP) and poly(ADP-ribose) glycohydrolase (PARG) cycle (Kim and Koh, 2002). Prolonged PARP activation triggers the depletion of NAD and ATP, further contributing to energy failure-stimulated neuronal death (Alano et al., 2010).

Taken together, while Zn^{2+} plays an essential role in normal cellular function, excessive accumulation of labile Zn^{2+} results in deleterious consequences, such as neuronal death, that has been strongly implicated in oxidative stress-related neurodegeneration.

1.3 TRPM2 channel

The transient receptor potential (TRP) ion channels are a large family of mammalian homologues to proteins encoded by the *trp* gene. It was firstly identified in the study of photo-transduction mechanism in *drosophila melanogaster* (Montell, 2005). Based on amino acid sequence and structural similarity, the mammalian TRP superfamily is divided into six subfamilies: TRPC (canonical), TRPV (vanilloid), TRPM (melastatin), TRPP (polycystin), TRPML (mucolipin) and TRPA (ankyrin) (Montell, 2005).

The TRPM subfamily contains eight members, TRPM1-8. Their expression and major functions are briefly summarized in **Table 1.1**. TRPM1 was originally identified as a tumour suppressor gene in a melanoma cell line (Duncan et al., 1998). It has been proposed that TRPM1 is a constitutively active, non-selective cation channel (Fleig and Penner, 2004; Gees et al., 2010). TRPM1 expression was shown to be correlated with melanocytic tumour progression, melanoma tumour thickness, and the potential for melanoma metastasis (Duncan et al., 1998; Deeds et al., 2000). In addition, TRPM1 is expressed in retinal cells, and patients with *trpm1* mutation suffer congenital stationary night blindness, indicating that TRPM1 plays a role in retinal function (Audo et al., 2009; Koike et al., 2010). TRPM3 is also constitutively activated, permeable to cations like Na^+ and Ca^{2+} and Mg^{2+}, and thus has a role in ion homeostasis, particularly in determining the basal intracellular Ca^{2+} level. The channel activity is enhanced by extracellular hypotonic conditions (Grimm et al., 2003), suggesting volume-dependent regulation of TRPM3 channel. Studies have shown the critical role of TRPM3 channel in the renal Ca^{2+} homeostasis (Grimm et al., 2003), neurogenic inflammation and insulin release (Held et al., 2015). TRPM4 and TRPM5 are two closely-related channels that are essentially impermeable to Ca^{2+} (Gees et al., 2010). TRPM4 channel is voltage-dependent (Launay et al., 2002) and its opening is inhibited by nucleotide such as ATP, adenosine diphosphate (ADP) and adenosine monophosphate (AMP) (Nilius et al., 2003). In non-excitable cells that lack of VGCC, Ca^{2+}-activated TRPM4 channel mediates membrane depolarization that reduces the driving force for Ca^{2+} influx through the store-operated Ca^{2+} channel (Launay et al., 2002), while in excitable cells TRPM4 channel supports Ca^{2+} influx in a voltage-dependent mechanism (Nilius et al., 2003). TRPM4 has been shown to have a critical role in mediating insulin release from pancreatic β-cells (Cheng et al., 2007) and myogenic vasoconstriction of cerebral arteries (Earley et al., 2004). Similar to TRPM4, TRPM5 channel is voltage-dependent. The channel is crucial in taste transduction

and insulin release in pancreatic β-cells (Perez et al., 2002; Gilon and Henquin, 2001). TRPM6 shows substantial sequence homology with TRPM7. TRPM6 is activated by a reduction in free Mg^{2+} or Mg·ATP and is important in the Mg^{2+} homeostasis in kidney and intestine (Voets et al., 2004). Patients with non-functional TRPM6 mutants suffer from intestinal malabsorption and reduced renal reabsorption of Mg^{2+} (Walder et al., 2002; Fleig and Penner, 2004). TRPM7 is a constitutively active channel (Nadler et al., 2001) and responsible for the uptake of trace metal ions including Mg^{2+}, Zn^{2+} and Mn^{2+} (Monteilh-Zoller et al., 2003). Suppression of TRPM7 channel eliminates ischemia-induced Ca^{2+} uptake, ROS production and cell death in neurons (Aarts et al., 2003; Sun et al., 2009), providing evidence to the involvement of TRPM7 channel in brain ischemic injury. TRPM8 is activated by cold temperature (≤ 25°C) or by cooling agents such as methanol or icilin (Peier et al., 2002). Therefore, TRPM8 channel in peripheral nervous system plays an essential role in the thermosensation to cold stimuli (Bautista et al., 2007).

This study mainly focuses on TRPM2 channel. The following section is devoted to discussing molecular properties and physiological functions of TRPM2 channel as well as its role in mediating ROS-induced neuronal death and neurodegenerative diseases.

Table 1.1 The expression and major functions of the TRPM channels

Channel	Expression	Function
TRPM1	Brain and heart	Melanoma tumour progression; vision
TRPM2	Brain, peripheral blood, spleen, bone marrow, heart, leukocytes, liver, lung, kidney, prostate, testis, skeletal muscle and eye	Release of insulin from pancreatic β-cells; production of cytokines from immune cells; increased endothelial permeability
TRPM3	Kidney, liver, ovary, brain, spinal cord, pituitary, vascular smooth muscle, and testis as well as insulinoma cells and β-cells of the pancreas	Renal Ca^{2+} homeostasis; neurogenic inflammation; insulin release
TRPM4	Most adult tissues, with highest levels in heart, prostate and colon	Neuronal bursting activity; insulin release; cardiac rhythmicity
TRPM5	Intestine, pancreas, prostate, kidney, and pituitary	Taste transduction; insulin release
TRPM6	Gastrointestinal tract, kidney, colon epithelial cells, duodenum, jejunum, ileum and single distal renal tubule cells	Intestinal and renal absorption of Mg^{2+}
TRPM7	Ubiquitously expressed	Brain ischemia injury
TRPM8	Dorsal root ganglia and trigeminal ganglion, prostate	Thermosensation to cold stimuli in peripheral nervous system

1.3.1 Expression

TRPM2, originally known as TRPC7 or long TRPC2 (LTRPC2), forms a non-selective cation channel permeable to Ca^{2+}, Na^{+} and K^{+} with a linear current–voltage (I-V) relationship (Perraud et al., 2001; Sano et al., 2001; Hara et al., 2002). The TRPM2 messenger ribonucleic acid (mRNA) expression has been detected from various tissues such as pancreas, peripheral blood (Sano et al., 2001), spleen, bone marrow, heart, liver, lung, kidney, prostate, testis, skeletal muscle and eye (Perraud et al., 2001). Notably, TRPM2 is highly expressed in the brain (Perraud et al., 2001; Hara et al., 2002; Sumoza-Toledo et al., 2011), where it is widely distributed in the cerebral cortex, thalamus, midbrain and hippocampus (Hara et al., 2002; Kraft et al., 2004; Fonfria et al., 2006; Olah et al., 2009).

TRPM2 has been shown to be present in particular cell types within tissues mentioned above. This includes pancreatic β-cell (Togashi et al., 2006), pulmonary artery endothelial cells (Hecquet et al., 2008), cardiomyocytes (Yang et al., 2006) and several immune cells such as neutrophils, leucocytes and macrophages (Hiroi et al., 2013; Massullo et al., 2006; Zou et al., 2013). In the brain, TRPM2 expression has been demonstrated in microglia and neurons, but not in astrocytes (Kraft et al., 2004; Fonfria et al., 2006; Olah et al., 2009).

Several immortal cells have been shown to express TRPM2 channel, including human microglia C13 cell (Fonfria et al., 2006), T lymphocyte Jurkat cell (Gasser et al., 2006), rat CRI-G1 insulinoma cell (Inamura et al., 2003), rat pancreatic β-cell RIN-5F (Ishii et al., 2014), human monocytic THP-1 cell (Zou et al., 2013) and human monocytic U937 cell (Perraud et al., 2001).

Notably, immunostaining showed significant overlapping of the TRPM2 proteins and lysosome-associated membrane protein-1 in pancreatic β-cell and dendritic cell (Lange et al., 2009; Sumoza-Toledo et al., 2011). These findings suggest that in addition in plasma membrane, TRPM2 channel exists in the lysosomal membrane

and mediates lysosomal Ca^{2+} release (discussed further below). However, of note, a recent study has reported that the lysosomal Ca^{2+} release is similar between the wild-type (WT) and the TRPM2-KO pancreatic β-cells, arguing against the role of TRPM2 in mediating lysosomal Ca^{2+} release (Kashio and Tominaga, 2015).

1.3.2 Molecular and structural properties

TRPM2 channel, like all other TRP channels, is a tetramer with each subunit comprising an intracellular N-terminus, a region of six transmembrane (TM) segments with a pore-forming loop between the fifth and sixth TM segments, and an intracellular C-terminus (**Fig. 1.4**) (Perraud et al., 2001; Sano et al., 2001; Fleig and Penner, 2004). Among this, the N-terminus contains four TRPM homologous domains of unknown function (Perraud et al., 2001), and a calmodulin (CaM) binding IQ-like motif that mediates the modulation or activation of TRPM2 channel by intracellular Ca^{2+} (Du et al., 2009a; Tong et al., 2006). The C-terminus contains a short hydrophobic sequence that present in many TRP channels named TRP box (Montell, 2001), a coiled-coil domain, and a unique domain that exhibits homology to NUDT9 (NUDT9-H) and enables the gating of TRPM2 channel by ADPR (Fleig and Penner, 2004; Sano et al., 2001; Perraud et al., 2001; Kuhn and Luckhoff, 2004). NUDT9 is an adenosine diphosphate ribose (ADPR) pyrophosphatase which catalyses the hydrolysis of ADPR into AMP and ribose 5-phosphate, and the NUDT9-H domain when expressed on its own was shown to exhibit significant albeit reduced ADPR hydrolase ability, leading to the hypothesis that TRPM2 protein acts as a channel-enzyme (Perraud et al., 2001). However, this notion has been refuted by a recent study demonstrating that TRPM2 channel does not possess any ADPR hydrolase activity (Iordanov et al., 2016).

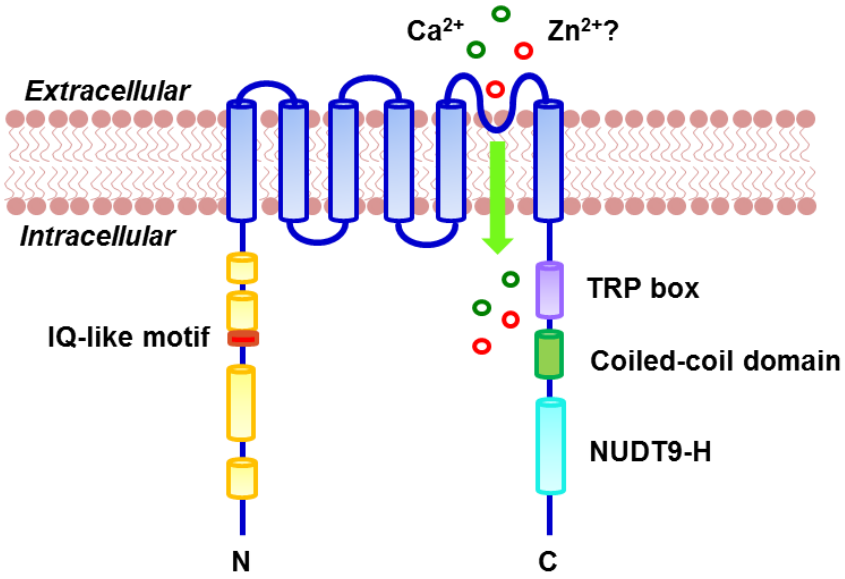

Figure 1.4 Major structural features of the TRPM2 channel protein

Each subunit of the tetrameric TRPM2 channel consists of an intracellular N-terminus, six transmembrane (TM) segments with a pore-forming loop between the fifth and sixth TM segments and an intracellular C-terminus. The N-terminus contains four TRPM homologous domains (denoted by yellow cylinders) and a calmodulin binding IQ-like motif. The C-terminus contains a TRP box, a coiled-coil domain and a NUDT9-H domain. TRPM2 channel is a Ca^{2+}-permeable cationic channel but its permeability to Zn^{2+} is not definitively established.

1.3.3 Alternative splicing isoforms

In addition to the full-length TRPM2 (TRPM2-L), several alternative splicing isoforms have been identified, including TRPM2-ΔN, TRPM2-ΔC, TRPM2-ΔNΔC, short form TRPM2 (TRPM2-S) and the striatum short form of TRPM2 (TRPM2-SSF) (Wehage et al., 2002; Zhang et al., 2003; Uemura et al., 2005; Orfanelli et al., 2008).

TRPM2-ΔN, TRPM2-ΔC and TRPM2-ΔNΔC, which were found in HL-60 cell and neutrophil granulocytes, contain deletions of amino acid residues in the N-terminus, C-terminus, or both (Wehage et al., 2002). ADPR-induced currents were not observed in cells expressing these alternative splicing isoforms, suggesting both C-terminus and N-terminus are required to ADPR-dependent TRPM2 channel activation (Wehage et al., 2002). Although insensitive to ADPR, the TRPM2-ΔC variant was robustly activated by H_2O_2 (Wehage et al., 2002). However, this was not verified in subsequent studies, which found neither H_2O_2 nor ADPR could induce detectable TRPM2 currents or Ca^{2+} influx in HEK293 cells expressing the TRPM2-ΔC variant (Perraud et al., 2005; Kuhn and Luckhoff, 2004). TRPM2-ΔN, TRPM2-ΔC and TRPM2-ΔNΔC were all activated by intracellular Ca^{2+} (Du et al., 2009a). The mechanisms by which ADPR, H_2O_2 and Ca^{2+} induce the activation of TRPM2 channel and its variant isoforms will be further discussed below.

TRPM2-S was identified in human bone marrow and other hematopoietic cells including human burst forming unit-erythroid-derived erythroblasts and TF-1 erythroleukemia cells, as well as in normal adrenal gland and neuroblastoma cells (Zhang et al., 2003; Chen et al., 2014). TRPM2-S only contains the N-terminus and the first two transmembrane domains and therefore does not form functional channel on its own (Zhang et al., 2003). In human pulmonary artery endothelial cells expressing both isoforms, deletion of the TRPM2-L suppress the expression of TRPM2-S (Hecquet et al., 2014). Intriguingly, overexpression of the TRPM2-S significantly inhibited ADPR-elicited TRPM2 channel currents and H_2O_2-induced Ca^{2+} influx through TRPM2-L (Chen et al., 2014; Zhang et al., 2003). Moreover,

TRPM2-S attenuated H_2O_2 or TNF-α induced cell death in hematopoietic cells and rat striatal cells (Hecquet et al., 2008; Zhang et al., 2006; Fonfria et al., 2005). Hence, the short isoform was proposed to act as a dominant negative mutant to antagonise the function of TRPM2-L, or/and participate in the heterotetrameric formation of TRPM2-L (Zhang et al., 2006; Zhang et al., 2003). A recent study shows that Ser-39 residue in TRPM2-S is crucial for its interaction with TRPM2-L (Hecquet et al., 2014). H_2O_2- or TNF-α-activated PKCα induces phosphorylation of TRPM2-S at Ser-39, resulting in dissociation of TRPM2-S and TRPM2-L (Hecquet et al., 2014).

TRPM2-SSF has a short N-terminus without the first 214 amino acid residues found in TRPM2-L. This isoform was only detected in the striatum of human brain, but not mouse brain (Uemura et al., 2005). TRPM2-SSF can still form a functional channel with permeability to Ca^{2+}. However, H_2O_2-induced Ca^{2+} influx was slightly, albeit significantly lower in TRPM2-SSF (Uemura et al., 2005).

1.3.4 TRPM2 channel activation

1.3.4.1 ADPR

As mentioned above, the C-terminal NUDT9-H domain confers specific activation of TRPM2 channel by ADPR (Perraud et al., 2005; Du et al., 2009a; Yu et al., 2017; Kuhn and Luckhoff, 2004). Depending on the cell type examined, ADPR induces TRPM2 channel activation with the half maximal effective concentration (EC_{50}) of 1-90 μM (Perraud et al., 2001; Kuhn and Luckhoff, 2004; Perraud et al., 2005; Sano et al., 2001; Inamura et al., 2003; Beck et al., 2006; Yamamoto et al., 2008). A recent study has disclosed several residues in the NUDT9-H domain to be critical in coordinating ADPR binding, including His-1346, Thr-1347, Thr-1349, Leu-1379, Gly-1389, Ser-1391, Glu-1409, Asp-1431, Arg-1433, Leu-1484, and His-1488 (Yu et al., 2017).

1.3.4.2 NAD and structurally related compounds

A number of studies have reported that NAD, cyclic-ADPR (cADPR) or nicotinic acid adenine dinucleotide phosphate (NAADP) could directly activate TRPM2 by binding to the NUDT9-H domain (Sano et al., 2001; Kolisek et al., 2005; Beck et al., 2006; Togashi et al., 2006). They were also shown as co-activators that potentiate the efficacy of ADPR-induced channel activation (Beck et al., 2006; Kolisek et al., 2005; Sano et al., 2001). However, recent studies have revealed that purified NAD, cADPR and NAADP do not evoke TRPM2 channel opening, suggesting the contamination of ADPR in commercial preparation results in TRPM2 gating (Toth et al., 2015; Toth and Csanady, 2010).

In contrast, ADP-ribose-2'-phosohate has recently been shown to be a novel true TRPM2 agonist. Of note, even at saturating concentrations, ADP-ribose-2'-phosohate only induces smaller TRPM2 currents compared to ADPR (Toth et al., 2015), indicating it is a partial agonist. In addition, 2'-O-acetyl-ADP-ribose was shown to induce TRPM2 channel currents in HEK293 cell expressing TRPM2 channel, which was thought to bind to the NUDT9-H domain as ADPR (Grubisha et al., 2006).

1.3.4.3 ROS

TRPM2 channel is potently activated by ROS such as H_2O_2. Both exogenous oxidants tert-butyl hydroperoxide, dithionite and endogenous ROS generation have been shown to contribute to the TRPM2 channel activation (Hara et al., 2002; Kolisek et al., 2005; Hecquet et al., 2008; Fonfria et al., 2005).

TNF-α is able to trigger a non-specific cation current, an increase in the $[Ca^{2+}]_i$ and cell death. Those effects were found to be significantly reduced by suppressing TRPM2 expression, implicating the role of TNF-α in eliciting TRPM2 channel activation (Hara et al., 2002; Roberge et al., 2014; Tong et al., 2006). Moreover, TNF-α evoked current was abolished by non-specific antioxidant N-acetyl-cysteine,

indicating the TRPM2 channel activation by TNF-α depends on ROS production (Roberge et al., 2014).

$A\beta_{42}$ induces a TRPM2-dependent increase in the $[Ca^{2+}]_i$ and cell death in neurons and brain endothelial cells (Fonfria et al., 2005; Ostapchenko et al., 2015; Park et al., 2014). Such $A\beta_{42}$ cytotoxicity was attenuated by inhibiting the PARP activity that is known to be required for ROS-induced TRPM2 channel activation as discussed below, suggesting that $A\beta_{42}$ can activate TRPM2 channel (Fonfria et al., 2005; Park et al., 2014). Moreover, $A\beta_{42}$ triggers substantial increase in intracellular ROS level. Therefore, it is likely that $A\beta_{42}$ exposure-induced oxidative stress eventually leads to the TRPM2 channel activation (Fonfria et al., 2005; Park et al., 2004).

The main mechanisms by which ROS induce TRPM2 channel activation are through generating free ADPR in mitochondria or nucleus. Free ADPR is a product of NAD hydrolysis or a breakdown product of cADPR. Within mitochondria, oxidative stress induces the opening of mPTP. An increase in mitochondria membrane permeability facilitates the conversion of mitochondrial NAD to ADPR by NAD-glycohydrolase located in the outer mitochondrial membrane. ADPR is subsequently diffused to cytosol through the permeable mitochondria membrane (Dolle et al., 2013). Cells expressing a mitochondria-targeted isoform of NUDT9 ADPR pyrophosphatase suppressed H_2O_2-induced Ca^{2+} influx, implicating the role of mitochondria-derived ADPR for oxidative stress-induced TRPM2 channel activation (Perraud et al., 2005).

On the other hand, oxidative stress is known to trigger deleterious DNA damage in the nucleus, which stimulates poly(ADP-ribose) metabolism that participate in DNA repair (Wei and Yu, 2016). A large amount of ADPR are generated in poly(ADP-ribose) metabolism arising from the cooperation of PARP-1 and PARG. The binding of PARP-1 to DNA strand breaks leads to the hyper-activation of PARP-1. Activated PARP-1 uses NAD as a substrate to catalyse the covalent attachment of poly(ADP-

ribose) on its acceptor proteins or on PARP-1 itself, generating ADPR polymers. PARG terminates the transduction of DNA damage signals, degrading poly(ADP-ribose) into free ADPR monomers (Schreiber et al., 2006) (**Fig. 1.5**). PARP expression was shown to be increased by ROS and, moreover, PARP inhibitors potently attenuated ROS-evoked TRPM2 channel currents, increase in the $[Ca^{2+}]_i$ and cell death, supporting the critical involvement of PARP in ROS-induced TRPM2 activation (Hecquet et al., 2008; Roberge et al., 2014; Fonfria et al., 2005).

As discussed below, TRPM2 channel is sensitive to the activation by temperature. There is evidence to show that exposure to H_2O_2 lowered the temperature threshold for TRPM2 channel activation in macrophage through the oxidation of Met-214 residue in the cytosolic N-terminus (Kashio et al., 2012). Moreover, H_2O_2-induced reduction in temperature threshold was partly and insignificantly attenuated by PARP inhibitors (Kashio et al., 2012), perhaps arguing that PARP-dependent ADPR generation is involved in such ROS-induced effect on the sensitivity of TRPM2 channel to temperature.

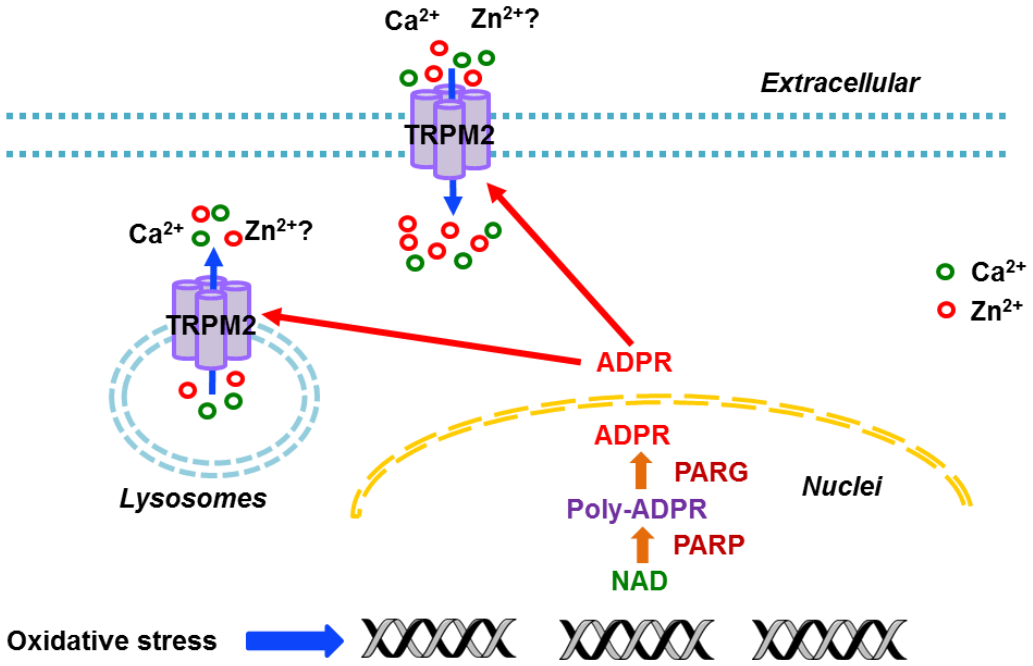

Figure 1.5 Oxidative stress-induced PARP-dependent TRPM2 channel activation

Oxidative stress induces DNA damage in nucleus that triggers the DNA repair process mediated by PARP and PARG using NAD and the generation of ADPR. ADPR is released to cytosol and activates the plasma membrane and lysosomal TRPM2 channels, resulting in the extracellular Ca^{2+}/Zn^{2+} influx or lysosomal Ca^{2+}/Zn^{2+} release. (PARP: Poly(ADP-ribose) polymerase; PARG: Poly(ADP-ribose) glycohydrolase; NAD: Nicotinamide adenine dinucleotide; ADPR: Adenosine diphosphate-ribose).

1.3.4.4 Ca^{2+}

TRPM2 channel opening requires intracellular Ca^{2+}, which could facilitate the channel activation by ADPR (Du et al., 2009a; Toth and Csanady, 2010; Starkus et al., 2007; McHugh et al., 2003). Moreover, the intracellular Ca^{2+} alone is shown to activate TRPM2 channel with an EC_{50} of 16.9 µM (Du et al., 2009a). Intriguingly, as mentioned above, not only TRPM2-L, the TRPM2 mutants with disrupted ADPR-binding sites and TRPM2-ΔC are activated by intracellular Ca^{2+}, suggesting this channel opening mechanism is ADPR-independent (Du et al., 2009a). Such intracellular Ca^{2+}-induced TRPM2 channel activation has been shown to be closely associated with the IQ-like CaM-binding motif located in the N-terminus of TRPM2 (Tong et al., 2006; Du et al., 2009a; Starkus et al., 2007). Co-expression of the mutant CaM in TRPM2-expressing cells significantly suppressed the amplitude of intracellular Ca^{2+}-induced current, implicating a crucial role for CaM in Ca^{2+}-induced TRPM2 channel activation (Du et al., 2009a). On the other hand, addition of CaM to internal solutions substantially potentiated ADPR-induced current amplitude which was suppressed by calmidazolium, a known CaM antagonist (Starkus et al., 2007). These findings provide evidence to the role of CaM in facilitating the effect of Ca^{2+} on TRPM2 channel activation. Given the mutation of the IQ-motif was sufficient to abolish CaM binding (Tong et al., 2006), the replacement of the IQ-like motif with its non-functional mutant also considerably attenuated the TRPM2 channel activation in response to intracellular Ca^{2+} (Du et al., 2009a), and H_2O_2-induced cell death (Tong et al., 2006), suggesting the IQ-like motif as a CaM binding site plays an important role in mediating intracellular Ca^{2+}-induced TRPM2 channel activation.

The extracellular Ca^{2+} is also critical for the full activation of TRPM2 channel. Similar to intracellular Ca^{2+}, extracellular Ca^{2+} strongly facilitates ADPR-induced TRPM2 channel activation, even with the depletion of intracellular Ca^{2+} (McHugh et al., 2003; Starkus et al., 2007; Hara et al., 2002). The rate of ADPR-induced TRPM2 channel activation is substantially influenced by extracellular Ca^{2+} in a

concentration-dependent manner (Starkus et al., 2007). Several residues in the pore-forming region, including His-958, Asp-964, and Glu-994, are shown to be responsible to the sensitivity of TRPM2 channel to extracellular Ca^{2+} (Du et al., 2009b).

1.3.4.5 Temperature

TRPM2 channel has been recently shown to be activated by warm temperature (Togashi et al., 2006; Kashio et al., 2012; Kashio and Tominaga, 2015). For example, human TRPM2-expressing HEK293 cells and RIN-5F cell both showed a significant increase in the $[Ca^{2+}]_i$ upon heating, with a threshold of about 40°C (Togashi et al., 2006). As discussed above, exposure to H_2O_2 lowers the temperature threshold for TRPM2 opening by mediating the oxidation of Met-214 residue (Kashio et al., 2012).

Recent studies have disclosed that the TRPM2 channel mediates the warm sensitivity of a particular population of neurons such as somatosensory and autonomic neurons, and preoptic area neurons (discuss further below) (Tan and McNaughton, 2016; Song et al., 2016). These findings provide further evidence to show heat-evoked TRPM2 channel activation.

1.3.5 TRPM2 inhibitors

1.3.5.1 Pharmacological inhibitors

ADPR is subjected to enzymatic hydrolysis by ADPR pyrophosphatase into AMP and ribose 5-phosphate (Iordanov et al., 2016). AMP exhibits a potent inhibition of ADPR-induced current with an IC_{50} of 70 μM. In contrast, it was ineffective in suppressing the currents induced by cADPR and H_2O_2 (Kolisek et al., 2005). AMP is thought to inhibit TRPM2 channel activation by competing with ADPR for the same binding site (Grubisha et al., 2006). However, a later study found that AMP failed to affect ADPR-induced TRPM2 currents in inside-out patch-clamp recording,

strongly arguing against a direct interaction of AMP with TRPM2 channel (Toth and Csanady, 2010).

2-Aminoethoxydiphenyl borate (2-APB) can inhibit ADPR- or H_2O_2-induced TRPM2 channel currents with an IC_{50} of ~1 μM (Togashi et al., 2008; Chen et al., 2012). The inhibition is rapid and reversible upon washout, and including 2-APB in recording pipette solution had no effect on ADPR-evoked currents. These results indicate that 2-APB inhibits TRPM2 channel activation via an extracellular mechanism (Togashi et al., 2008; Chen et al., 2012).

N-(p-amylcinnamoyl)anthranilic acid (ACA) shows a rapid and complete inhibition of ADPR-induced currents in whole cell patch-clamp recording and H_2O_2-induced Ca^{2+} responses with an IC_{50} of ~1.7 μM (Kraft et al., 2006). Similar to 2-APB, ACA reversibly blocks ADPR-evoked TRPM2 currents when applied extracellularly but not intracellularly. Intriguingly, the inhibition efficacy of ACA is significantly enhanced by lowering extracellular pH and the current inhibition is irreversible (Kraft et al., 2006).

The fenamate non-steroidal anti-inflammatory drug, fluofenamic acid (FFA), inhibits ADPR-induced TRPM2 channel, and the inhibition is irreversible and concentration-independent (Chen et al., 2012; Hill et al., 2004a). A structure-activity study shows that the trifluoromethyl group on the 2-phenylamono ring of fenamate skeleton is critical for blocking TRPM2 channel (Chen et al., 2012). The sites for FFA action are still ambiguous. An early study using whole-cell patch clamp recording demonstrated that FFA blocked ADPR-elicited currents when applied extracellularly but not intracellularly (Hill et al., 2004a). In contrast, a recent study using outside-out single channel recording shows that FFA has no effect on TRPM2 channel activity, suggesting the action is not extracellular (Chen et al., 2012). Extracellular pH influences the blocking rate of FFA; it is accelerated by acidification and slowed by alkalisation (Hill et al., 2004a).

Clotrimazole and econazole are structurally related imidazole antifungal agents. Both compounds suppress ADPR-evoked currents in a concentration-independent fashion (Hill et al., 2004b). It was shown that the inhibition was irreversible in cells expressing recombinant TRPM2 channels, but the antagonism of ADPR-induced currents in CRI-G1 cell by clotrimazole was reversible (Hill et al., 2004b). When applied from the inside of the cell, clotrimazole and econazole failed to inhibit ADPR-activated currents. Nevertheless, extracellular exposure resulted in rapid channel inhibition, suggesting the extracellular site for their actions. Moreover, the blocking rate of clotrimazole and econazole was observed to be pH-dependent, similar to FFA (Hill et al., 2004b).

As an analogue of cADPR, 8-Br-ADPR has complex effects on TRPM2 channel. Intracellular application of 8-Br-cADPR completely suppressed TRPM2 channel activation induced by cADPR or H_2O_2. However, 8-Br-cADPR did not attenuate but slightly accelerated the current induced by ADPR or NAD (Kolisek et al., 2005). This dual mode action of 8-Br-cADPR suggests that, on one hand, it interferes with cADPR-induced TRPM2 channel activation by competing with cADPR for the same binding site; on the other hand, it mimics cADPR in synergizing with ADPR and potentiates ADPR/NAD-elicited TRPM2 channel activation (Kolisek et al., 2005; Walseth and Lee, 1993).

As discussed above, oxidative stress-induced activation of PARP, particularly PARP-1 in the nucleus, leads to the generation of ADPR and subsequent activation of TRPM2 channel. Thus, several structurally distinct PARP inhibitors, including SB750139-B, 3-aminobenzamide, 3,4-dihydro-5-[4-(1-piperidinyl)butoxy]-1(2H)-isoquinolinone (DPQ) and N-(6-Oxo-5,6-dihydrophenanthridin-2-yl)-(N,N-dimethylamino)acetamide hydrochloride (PJ34) have been shown to inhibit H_2O_2-induced elevation in the $[Ca^{2+}]_i$ and cell death in a concentration-dependent manner, suggesting that PARP activation is important for ROS-induced TRPM2 channel activation (Fonfria et al., 2004; Hecquet et al., 2008).

Recent studies have found that tyrphostin AG-compounds, the well-known inhibitors for Janus kinase 2, have inhibitory effects on oxidative stress-induced TRPM2 channel activation (Shimizu et al., 2014; Toda et al., 2016; Yamamoto et al., 2017). AG490, AG555 and AG556 concentration-dependently reduce H_2O_2-induced increase in the $[Ca^{2+}]_i$ in HEK293 cells heterologously expressing TRPM2 channel and U937 cells which endogenously express TRPM2 channel (Toda et al., 2016; Yamamoto et al., 2017). The inhibition of AG490 on TRPM2 channel is rapid and reversible. Of note, AG490 inhibits H_2O_2-induced TRPM2 channel activation through scavenging hydroxyl radical rather than Janus kinase 2-dependent mechanism (Shimizu et al., 2014).

Curcumin has been shown to have powerful antioxidant effects. A recent study demonstrates that curcumin almost completely abolished H_2O_2-elicited TRPM2 channel currents in SH-SY5Y cells (Oz and Celik, 2017).

1.3.5.2 Acidic pH

Acidic extracellular pH significantly inhibits TRPM2 channel activation in a reversible and concentration-dependent manner with an IC_{50} of pH 5.3 (Du et al., 2009b; Yang et al., 2010). The H^+-binding sites are inconclusive due to the inconsistent results reported by different studies. The first study demonstrated that TRPM2 channel is impermeable to external protons. Acidic pH may cause the conformation change in TRPM2 channel by interacting with several pH-sensitive residues of the pore-forming region that interfere with extracellular Ca^{2+}-mediated channel gating, including His-958, Asp-964, and Glu-994 (Du et al., 2009b). However, a later study indicated that external protons permeate the open TRPM2 channel to gain access to an intracellular site that regulates the channel activity (Starkus et al., 2010). This study showed acidic pH-induced TRPM2 channel inactivation requires the channel opening (Starkus et al., 2010). Moreover, negative membrane potential that increased the driving force for proton influx accelerated

extracellular pH-induced inactivation, supporting the intracellular location of proton interaction sites (Starkus et al., 2010).

Acidic intracellular pH can also inhibit ADPR-evoked TRPM2 channel activation in a concentration-dependent manner, with an IC_{50} of pH 6.7 (Du et al., 2009b; Starkus et al., 2010). Further investigation revealed the Asp-933 residue at the C-terminus of the S4-S5 linker is responsible for intracellular pH-induced TRPM2 channel inhibition (Du et al., 2009b). Intracellular pH 6.0, which robustly blocked the WT TRPM2 channel, was ineffective at the TRPM2 channel with Asp-933 mutations (Du et al., 2009b), suggesting that Asp-933 is important in the inhibition of the TRPM2 channel by intracellular pH.

It is worth pointing out that none of the inhibitors discussed above is TRPM2 specific. For example, 2-APB is also an inhibitor of a wide spectrum of ion channels in the TRPC and TRPM subfamily. And so far, TRPM2-specific pharmacological inhibitors are not commercially available. Therefore, the genetic methods, such as genetic knock-out and knock-down of TRPM2 channel expression are frequently adopted to investigate the function of TRPM2 channel.

1.3.6 Physiological roles

1.3.6.1 Insulin release

Intracellular Ca^{2+} is the primary trigger of insulin secretion from pancreatic islet. Oral and intraperitoneal glucose tolerance experiments showed that the fasted TRPM2-KO mice had significantly higher blood glucose levels and lower plasma insulin levels compared to WT mice (Uchida et al., 2011). Glucose-induced increase in the $[Ca^{2+}]_i$ and insulin secretion were significantly reduced in pancreatic β-cells isolated from TRPM2-KO mice, providing evidence to support a crucial role of TRPM2 channel in glucose-induced insulin secretion (Uchida et al., 2011).

Moreover, the TRPM2 channel is also required for incretin hormones potentiated insulin secretion (Uchida et al., 2011; Yosida et al., 2014). The incretin hormones glucagon-like peptide (GLP)-1 and exendin (ex)-4, which is the agonist of GLP-1 receptor, were shown to activate TRPM2 channel and potentiate glucose-induced insulin secretion (Uchida et al., 2011). GLP-1 receptor activation leads to the generation of cyclic AMP (cAMP), initiating cAMP-dependent signalling pathways, via such as PKA and EPAC (exchange protein activated by cAMP) (Doyle et al., 2008). CAMP and the activator of EPAC were shown to increase TRPM2 channel currents and by contrast, activators and inhibitors of PKA had no effects. These results suggest that the cAMP/EPAC/TRPM2 pathway contributes in insulin secretion in pancreatic islets in response to glucose and incretin hormones (Yosida et al., 2014).

1.3.6.2 Immune responses

TRPM2 channel activation is important in the generation of pro-inflammatory cytokines in immune cells (Yamamoto et al., 2008; Wehrhahn et al., 2010; Melzer et al., 2012). H_2O_2 elicited a robust increase in the $[Ca^{2+}]_i$ and the generation of chemokine interleukin-8 (CXCL8) in the human monocytes. Removal of extracellular Ca^{2+} or knock-down of TRPM2-expression with small interfering RNA (siRNA) significantly reduced H_2O_2 induced CXCL8 production, suggesting the generation of CXCL8 was regulated by TRPM2-mediated Ca^{2+} influx (Yamamoto et al., 2008). As a potent monocyte activator, LPS also triggered an increase in the $[Ca^{2+}]_i$ and the generation of TNF-α, CXCL2, IL-1β, IL-6, IL-8 and IL-10 in the human monocytes. Using short hairpin RNA (shRNA) to downregulate the TRPM2 expression or removal of extracellular Ca^{2+} remarkably impaired this LPS-induced production of cytokines (Wehrhahn et al., 2010; Haraguchi et al., 2012). Moreover, genetic deletion and pharmacological inhibition of the TRPM2 channel dampened proliferation and pro-inflammatory cytokine secretion in $CD4^+$ and $CD8^+$ T cells following polyclonal stimulation by anti-CD3/CD28-coated beads (Melzer et al.,

2012). Taken together, the results suggest a central role of TRPM2 channel in stress-induced cytokines release.

H_2O_2-induced CXCL8 secretion in monocytes was suppressed by inhibitors of the ERK pathway or NF-κB (nuclear factor kappa-light-chain-enhancer of activated B cells). TRPM2-mediated Ca^{2+} influx was shown to be responsible for the activation of Ras and proline-rich tyrosine kinase 2 (Pyk2), the upstream signalling molecules of the ERK pathway. The resulting activation of the ERK pathway leads to nuclear translocation of NF-κB and CXCL8 expression (Yamamoto et al., 2008). The same mechanism underlies CXCL2 expression in the mouse monocytes induced by LPS and TNF-α (Yamamoto et al., 2008). The TRPM2-mediated increase in the $[Ca^{2+}]_i$ is also responsible for LPS/interferon (IFN)-γ-induced microglia activation. However, the mechanism appears to be independent of the ERK pathway but involves the p38 and JNK pathways (Miyake et al., 2014).

In striking contrast, a study found that LPS triggered the generation of more chemokines and pro-inflammatory cytokines, including TNF-α, CXCL2 and IL-6 in lungs of TRPM2-KO mice. Moreover, TRPM2-KO mice challenged with LPS showed enhanced lung infiltration of inflammatory cells, more lung edema and reduced survival compared with WT mice. Therefore, TRPM2 channels play a protective role in LPS-induced lung inflammatory (Di et al., 2011). These inflammatory responses in the lung were induced by ROS production. TRPM2 channel-mediated Na^+ influx resulted in the depolarization of plasma membrane potential, which thereby diminished ROS production mediated by the membrane potential-sensitive NOX and suppressed ROS-induced inflammatory responses (Di et al., 2011).

1.3.6.3 Temperature sensing

Recent studies have identified a subpopulation of heat-sensitive neurons, which were unable to be activated by the agonists for any known heat-sensitive TRP

channels (Tan and McNaughton, 2016). This novel heat-sensitivity channel in those neurons was shown to be permeable to Ca^{2+} and Na^{+}, and exhibit a linear I-V current with a reversal potential at zero and no time-dependent gating by membrane voltage. Moreover, the channel activation is potentiated by H_2O_2 and suppressed by 2-APB (Tan and McNaughton, 2016). TRPM2 is therefore the most probable candidate possessing all these properties. Indeed, genetic deletion of TRPM2 expression had striking impacts on the thermal preference in mice. TRPM2-KO mice showed little preference to the non-toxic warm temperature (38°C), whereas WT mice avoided such condition. Moreover, TRPM2-KO mice showed stronger aversion to non-toxic cool temperature (23°C) than the WT mice. These results support that the expression of TRPM2 in heat-sensitive neurons provides a non-toxic warm signal which thereby drives WT mice to seek cooler temperature (Tan and McNaughton, 2016).

TRPM2 expression has been shown in another study to confer the preoptic area neurons, the key brain structure controlling the thermal homeostasis in fever, with pronounced temperature sensitivity (Song et al., 2016). In a mouse fever model, injection with a high dose of prostaglandin E_2 resulted in increased fever response in TRPM2-KO mice compared to WT littermates, suggesting that the TRPM2 channel is required to maintain core body temperature. The excitatory population of preoptic area neurons plays a dominant role in thermoregulatory effect. Those neurons are proposed to detect the increase in body temperature that activates TRPM2 channel to initiate the thermoregulatory defence mechanism through the activation of corticotropin-releasing hormone positive neurons in the paraventricular nucleus of the hypothalamus (Song et al., 2016).

1.3.7 Pathophysiological roles

1.3.7.1 Diabetes

Altered insulin secretion from pancreatic-β cell is the primary mechanism for diabetes. Type 1 diabetes is an autoimmune disease characterised by the destruction of insulin-secreting pancreatic-β cells (Xie et al., 2014). Type 2 diabetes is a complex metabolic disorder. The pathophysiological abnormalities of type 2 diabetes including insulin resistance and defects in pancreatic-β cell functions (Muoio and Newgard, 2008). Therefore, the pancreatic-β cell death is central to the progression of both types of diabetes. A number of studies have shown that TRPM2 channel regulates pancreatic β-cell death (Ishii et al., 2006; Ishii et al., 2014; Manna et al., 2015; Hara et al., 2002). Treatment with TRPM2-specific antisense oligonucleotide reduced H_2O_2 or TNF-α induced increase in the $[Ca^{2+}]_i$ and cell death in RIN-5F cells (Hara et al., 2002). In addition, TRPM2-mediated Ca^{2+} release from lysosomes led to significant death of INS-1 cell in the absence of extracellular Ca^{2+} influx (Lange et al., 2009). A recent study has revealed that H_2O_2-induced cell death in INS-1 cell results from TRPM2-mediated increase in the $[Zn^{2+}]_i$ due to lysosomal Zn^{2+} release via TRPM2 channel (Manna et al., 2015). Suppression of the TRPM2 channel activation or the increase in the $[Zn^{2+}]_i$ attenuated H_2O_2-induced INS-1 cell death and streptozotocin-induced islet destruction (Manna et al., 2015), suggesting TRPM2-mediated rise in the $[Zn^{2+}]_i$ is responsible for pancreatic cell death and the onset of diabetes. Furthermore, TRPM2-KO mice were remarkably resistant to the hyperglycaemia induced by injection of multiple low doses of streptozotocin, providing evidence to show a critical role of the TRPM2 channel in diabetes (Manna et al., 2015).

1.3.7.2 Inflammatory diseases

The TRPM2 channel has been implicated in oxidative stress-related inflammatory diseases. In a mouse model of colitis induced by dextran sulfate sodium, TRPM2-KO reduced mucosal ulceration, serosa destruction and infiltration of neutrophil in

colon (Yamamoto et al., 2008). Another study showed that TRPM2-KO mice exhibited an ameliorated phenotype of the experimental autoimmune encephalomyelitis (EAE) (Melzer et al., 2012). In addition, the inflammatory infiltration and demyelination in spinal cord were significantly reduced in TRPM2-KO mice (Melzer et al., 2012). These findings provide a novel strategy for treating ulceration colitis and autoimmune CNS inflammation.

Emerging evidence suggest that neuroinflammation mediated by the interaction between immune cells and nociceptive neurons contributes to pathological pain (Haraguchi et al., 2012; So et al., 2015). TRPM2-KO mice showed significantly attenuated formalin or carrageenan-induced inflammatory pain, acetic acid-induced writhing behaviour, monosodium iodoacetate-induced osteoarthritis pain, chronic pain in the EAE model, paclitaxel-induced peripheral neuropathy, and streptozotocin-induced painful diabetic neuropathy (Haraguchi et al., 2012; So et al., 2015). The results indicate that TRPM2 channel plays a crucial role in inflammatory and neuropathic pain. On the contrary, TRPM2-KO had no effect on capsaicin- or H_2O_2-evoked chemical nociceptive pain or mechanical allodynia in postoperative incisional pain (So et al., 2015; Haraguchi et al., 2012).

1.3.7.3 Cardiovascular diseases

There is increasing evidence for the contribution of TRPM2 channel to the pathophysiology of oxidative stress-related cardiovascular diseases. ROS are important mediators of vascular barrier dysfunctions. It is known that oxidants increase the Ca^{2+} permeability of endothelial cell membrane resulting in an elevation in the $[Ca^{2+}]_i$ and inter-endothelial gap formation or barrier dysfunction (Vandenbroucke et al., 2008). Genetic or pharmacological inhibition of the TRPM2 channel diminished H_2O_2-induced Ca^{2+} entry and endothelial permeability (Hecquet et al., 2008). The results provide evidence to support a role of the TRPM2 channel in ROS-induced endothelial barrier dysfunction.

In addition, TRPM2 activation plays an essential role in oxidant-induced death of cardiomyocytes (Yang et al., 2006; Roberge et al., 2014). H_2O_2 was shown to induce caspase-3-depedent apoptosis of myocytes by triggering mitochondrial Ca^{2+} and Na^+ overload (Crow et al., 2004; Yang et al., 2006). Moreover, H_2O_2 treatment resulted in PARP-dependent ATP depletion and plasma membrane permeabilization, indicating necrotic death of myocytes. Inhibition of the TRPM2 channel by clotrimazole abolished H_2O_2-induced Cyt-c release, caspase-3 activation and nuclear condensation. In addition, inhibition of the PARP activity, which indirectly suppressed ROS-elicited TRPM2 channel activation, completely abolished H_2O_2-induced membrane permeabilization. Therefore, the results suggest that the TRPM2 channel activation contributes both apoptosis and necrosis in myocytes (Yang et al., 2006). The binding of TNF-α with its receptors is associated with necroptosis, resulting in the activation of caspase-8, mitochondrial ROS production and cell death (discuss further below) (Fauconnier et al., 2011). Inhibition of caspase-8 or ROS production significantly reduced TNF-α elicited TRPM2 currents in cardiomyocytes. Moreover, pharmacological inhibition of the TRPM2 channel activation reduced TNF-α induced cell death. The results provide evidence to show that TNF-α induces caspase-8 activation, ROS-production and TRPM2 channel activation that contribute to cardiomyocyte death (Roberge et al., 2014).

1.3.7.4 Bipolar disorder

Bipolar disorder (BD) is a psychiatric disease that causes mood swings between manic and depressed states. Genome-wide analyses led to the identification of the chromosomal region 21q22.3 as a susceptibility locus (Straub et al., 1994). This region contains the *trpm2* gene, and indeed, comparative analyses of the genomic DNA from BD patients suggest TRPM2 is a promising candidate contributing to the vulnerability to BD (Xu et al., 2006; McQuillin et al., 2006; Xu et al., 2009). A recent study using anxiety- and depression-related behavioural tests such as elevated plus

maze and light/dark transition tasks, has demonstrated that TRPM2-KO mice displayed increased anxiety and impaired social behaviour (Jang et al., 2015). Taken together, these studies provide important clues to suggest the involvement of TRPM2 channel in the pathophysiology of BD.

A number of independent studies have showed altered signalling transduction and impaired functions of second messengers, such as Ca^{2+} in mononuclear leukocytes and platelets from BD patients (Cipriani et al., 2016). The TRPM2 mRNA levels were significantly reduced in B-lymphoblast cell lines (BLCLs) from BD-I patients with elevated $[Ca^{2+}]_i$ compared with healthy subjects (Yoon et al., 2001), implying a role for TRPM2 channel in the disturbance of Ca^{2+} homeostasis. Chronic elevation of oxidative stress had no effect on TRPM2 expression in BLCLs of BD patients, but TRPM2 channel-mediated Ca^{2+} influx in these cells was significantly reduced by prolonged oxidative stress in BLCLs of BD patients, suggesting that oxidative stress alters TRPM2 channel function (Roedding et al., 2012; Roedding et al., 2013).

A recent study has identified a change from aspartic acid to glutamic acid at position 543 (Asp-543-Glu), which is located in the N-terminus of TRPM2 channel in BD patients, that causes the loss of TRPM2 channel function and phosphorylation of glycogen synthase kinase (GSK)-3 (Jang et al., 2015). The abnormal GSK-3 activity is closely related to BD. Li^+ as the first drug of choice for treating BD, inhibits GSK-3 activity either as a competitive inhibitor to Mg^{2+} that is necessary for the phosphorylation of target proteins, or by increasing the phosphorylation of the inhibitory serine residues in GSK-3 (Freland and Beaulieu, 2012). Li^+ treatment significantly reduced met-amphetamine-induced hyperactivity in WT mice. However, such anti-manic activity of Li^+ was not observed in TRPM2-KO mice. Intriguingly, a dramatic increase in the phosphorylation of inhibitory serine residues in GSK-3 was observed in the frontal cortices in TRPM2-KO mice, but not in WT mice. Overexpression of the loss-of-function mutant Asp-543-Glu significantly augmented the phosphorylation of GSK-3. These findings suggest that TRPM2 deficiency

results in the uncontrolled phosphorylation of GSK-3, which may contribute to the pathogenesis of BD (Jang et al., 2015).

1.4 TRPM2 channel in neurodegeneration

Oxidative stress is one of the common etiologies in various neurodegenerative diseases including AD and PD and ischemic stroke. The oxidative stress-related neurodegenerative diseases are normally characterized by progressive loss of neurons in specific brain regions (Uttara et al., 2009). Therefore, a brief introduction of major mechanisms for cell death is given before the discussion of evidence from recent studies that support a critical role for TRPM2 channel in oxidative stress-related neurodegenerative conditions.

1.4.1 Mechanisms in cell death

1.4.1.1 Apoptosis

There are a number of recognized pathways by which cells can die, including apoptosis, necrosis and necroptosis. Apoptosis represents a regulated form of cell death that occurs under normal physiological conditions. It manifests with morphological and biomedical changes including cell shrinkage, membrane blebbing, DNA fragmentation, formation of apoptotic bodies and externalization of phosphatidylserine (Elmore, 2007).

There are two main apoptosis pathways: the extrinsic and intrinsic pathway. The extrinsic pathway initiates apoptosis via interactions with transmembrane death receptors such as TNF receptor 1 (TNFR1) (Locksley et al., 2001). Activation of TNFR1 leads to the recruitment of adapter protein TNFR-associated death domain (TRADD), which associates with procaspase-8 to form a death-inducing signalling complex. The recruitment of procaspase-8 causes its dimerization and activation (Wang et al., 2008). Activated caspase-8 can directly initiate apoptosis by cleaving and thereby activating executioner caspases, including caspase-3, -6 and -7 or

activate the intrinsic apoptosis pathway described below (Slee et al., 2001). Caspase-3 can specifically activate endonuclease caspase activated deoxyribonuclease, which degrades chromosomal DNA and causes chromatin condensation. Moreover, caspase-3 can cleave gelsolin, an actin-binding protein, resulting in the disruption of cytoskeleton, cell division and subsequent signal transduction (Elmore, 2007).

The intrinsic signalling pathway is known as mitochondrial apoptosis pathway. It is activated by non-receptor-mediated stimuli, such as toxins, viral infections and free radicals (Elmore, 2007), which lead to opening of the mPTP, loss of mitochondrial membrane potential and release of pro-apoptotic proteins from the intermembrane space of mitochondria (Saelens et al., 2004), including Cyt-c and AIF (Garrido et al., 2006; Cande et al., 2002). Cyt-c binds and activates adaptor protein apoptotic protease activating factor-1 to form apoptosome, which recruits and activates procaspase-9 through its dimerization. Similar to caspase-8, activated caspase-9 cleaves and activates downstream executioner caspases, initiating apoptosis (Jiang and Wang, 2004). In contrast, AIF induces apoptosis in a caspase-independent manner by translocating to the nucleus and causing DNA fragmentation and condensation of peripheral nuclear chromatin (Joza et al., 2001). The intrinsic apoptosis pathway is regulated by Bcl-2 family proteins, which govern mitochondrial membrane permeability. There are two main groups of Bcl-2 family of proteins, namely the pro-apoptotic proteins that promote mitochondrial Cyt-c release and the anti-apoptotic proteins that inhibit such release (Shamas-Din et al., 2013). Caspase-8 is shown to cleave and activate the pro-apoptotic protein Bid, initiating mitochondria-dependent intrinsic apoptosis pathway (Huang et al., 2016).

1.4.1.2 Necrosis

In contrast to apoptosis, necrosis is often viewed as an accidental and unregulated event characterized by cytoplasmic swelling, irreversible plasma membrane damage, loss of ATP and random degradation of DNA (Festjens et al., 2006).

Necrotic cell death is usually caused by severe cellular stress, such as Ca^{2+} overload and oxidative stress, provoking damage to proteins, lipids and DNA (Zhivotovsky and Orrenius, 2011; Fiers et al., 1999; Festjens et al., 2006). The leakage of cytosolic contents and inflammatory cytokines accompanying necrotic cell death leads to the activation of pro-inflammatory signalling cascades (Rock and Kono, 2008).

Some forms of necrotic cell death, albeit being characterized by necrotic cell death morphologies, can be as well controlled and programmed as caspase-dependent apoptosis and is called necroptosis (Belizario et al., 2015). Necroptosis can be induced by either death receptors as apoptosis or pathogen recognition receptors in the innate immune response (Vandenabeele et al., 2010). Necroptosis depends on receptor-interacting protein kinase-3 (RIPK3) and its substrate mixed lineage kinase domain like (MLKL) protein (Galluzzi and Kroemer, 2008; Linkermann and Green, 2014).

Much of the knowledge of necroptosis comes from studies of TNF-α signalling (Vercammen et al., 1998). Except for extrinsic apoptosis pathway, the ligation of TNFR1 with TNF-α also initiates the association of TNFR1 intracellular domain with membrane-associated protein complex (complex I) assembling by TRADD, TNFR-associated factor 2, cIAP1/2 (cellular inhibitor of apoptosis 1/2) and RIPK1 (Zhou and Yuan, 2014). The formation of complex I leads to the activation of pro-survival NF-κB and MAPK pathways. Meanwhile, RIPK1 is polyubiquitinated by cIAPs. Nevertheless, in the presence of cIAP inhibitors, such as second mitochondria-derived activator of caspases (SMAC) or small-molecule SMAC mimetics, cIAPs are degraded, which promotes the deubiquitination of RIPK1 by deubiquitinases (Chen et al., 2016) and results in the dissociation of RIPK1 from plasma membrane to form complex II consisting of RIPK1, Fas-associated death domain and caspase-8 (Micheau and Tschopp, 2003). As a result, RIPK1 converts from pro-survival protein to pro-death proteins. The activation of caspase-8 leads to apoptotic cell

death and inhibits RIPK1 and RIPK3. However, if caspase-8 is inhibited, RIPK1 and RIPK3 bind to each other, to form a necrosome and switch to necroptosis (He et al., 2009). Activated RIPK3 binds to MLKL protein and promotes the phosphorylation of MLKL. The phosphorylated MLKL protein is further oligomerized and translocated from cytosol to plasma membrane, where it disrupts cell membrane and promotes necroptosis (Sun et al., 2012; Zhao et al., 2012; Chen et al., 2016).

1.4.2 Ischemic stroke

As one of the leading causes of mortality and morbidity, ischemic stroke is defined as the disruption of cerebral blood flow that leads to poor supply or deprivation of oxygen and glucose to the brain (Chen et al., 2011). Cerebral ischemia can be either transient, followed by reperfusion to restore blood flow, or permanent. Both ischemia and reperfusion trigger apoptotic and necrotic cell death and the formation of infraction via complex mechanisms (Lo et al., 2003; Hossmann, 2006). Therefore, brain damage can result from both ischemic insult and reperfusion process (Kalogeris et al., 2012). Certain populations of neurons such as the CA1 pyramidal neurons in hippocampus are highly susceptible to ischemia-reperfusion injury (Mattson et al., 2001).

1.4.2.1 The pathophysiology

The pathophysiology of ischemic stroke is complex, including the loss of ion homeostasis, excitotoxicity, oxidative stress and inflammatory responses (Mattson et al., 2001).

Excitatory amino acid-induced excitotoxicity and Ca^{2+} overload are major factors contributing to the early stages of neuronal death in ischemic brain. The reduction or termination of cerebral blood flow decreases glucose-dependent ATP generation and leads to the collapse of ATP-dependent Ca^{2+} extrusion mechanisms (as discussed in section **1.2.2.2**). The subsequent depolarization of cell membrane

induces the activation of VGCC and receptor-operated Ca^{2+} channels, and is coupled with enhanced release of glutamate into the extracellular space (Lai et al., 2014). Glutamate in return activates the AMPAR and NMDAR to cause substantial influx of ions, including Ca^{2+} and Zn^{2+} (Pochwat et al., 2015; Bano and Nicotera, 2007), leading to disruption in the Ca^{2+} and Zn^{2+} homeostasis that initiates a series of catastrophic events such as oxidative stress that leads to neuronal cell death.

Timely reperfusion is important clinically to restrict deleterious effects of acute ischemic stroke. However, the reintroduction of molecular oxygen during reperfusion leads to the generation of excessive ROS (Granger and Kvietys, 2015), leading to oxidative stress and neuronal degeneration after ischemic stroke (Murakami et al., 1998; Kawase et al., 1999). Indeed, the level of 8-hydroxy-2-deoxyguanosine, a biomarker of oxidative DNA damage, was shown to increase at the early stage of reperfusion and to be produced 24 hr after reperfusion (Chen et al., 2009).

It is noted that transient ischemia-induced CA1 pyramidal cell death in the hippocampus occurs with significant delay as it takes 2-3 days for those neurons to present the morphologies of cell death (Kirino, 2000). The phenomenon is therefore referred to as delayed neuronal death. Accumulative evidence supports that an increase in the $[Zn^{2+}]_i$ is a critical factor (Koh et al., 1996). A substantial increase in the $[Zn^{2+}]_i$ was shown to couple with the degeneration of CA1 pyramidal neurons after transient ischemia (Koh et al., 1996; Stork and Li, 2009). Exposure to exogenous Zn^{2+} with the presence of Zn^{2+} ionophore also conferred CA1 neurons with marked increase in neuronal death (Stork and Li, 2009; Koh et al., 1996). On the other hand, treatment with a Zn^{2+}-selective chelator significantly reduced the $[Zn^{2+}]_i$ and hippocampal neuronal death after ischemia or exposure to Zn^{2+} (Koh et al., 1996). These results strongly suggest the involvement of Zn^{2+} in delayed neuronal death.

Neuroinflammation is also crucial in the pathogenesis of ischemic stroke. A plenty of acute and prolonged inflammatory processes are observed during ischemic injury, including the rapid activation of microglia cells, production of pro-inflammatory mediators, and infiltration of inflammatory cells into the ischemic brain tissues (Jin et al., 2010). In the acute phrase of ischemic stroke, ROS and pro-inflammatory cytokines and chemokines are released rapidly from injured lesions (Amantea et al., 2009). These pro-inflammatory mediators induce the expression of adhesion molecules on cerebral endothelial cells and leucocytes, promoting adhesion and trans-endothelial migration of circulating leucocytes (Yilmaz and Granger, 2008). In the following hours and days after ischemic stroke, infiltrating leucocytes release cytokines and chemokines, especially excessive ROS, which amplify the brain-inflammatory responses by causing extensive activation of microglia cells and infiltration of leucocytes, eventually leading to the blood-brain barrier (BBB) disruption and neuronal death (Jin et al., 2010).

1.4.2.2 TRPM2 in ischemic stroke

Accumulative *in vivo* and *in vitro* evidence using either genetic depletion of TRPM2 expression or pharmacological inhibition of TRPM2 channel suggests a pivotal role for TRPM2 channel in neuronal death and brain damage during ischemic stroke and reperfusion. TRPM2-KO mice showed significantly less impairment in learning and spatial memory as compared to WT mice subjected to the bilateral common carotid artery occlusion (BCCAO) induced transient ischemia (Ye et al., 2014). Moreover, injection of clotrimazole significantly reduced the infarct volume in male mice subjected to the transient middle cerebral artery occlusion (MCAO) (Jia et al., 2011). WT male mice injected with lentivirus expressing TRPM2-specific shRNA and TRPM2-KO male mice also had significantly smaller infarct volumes compared with the matched control WT mice (Jia et al., 2011; Verma et al., 2012). In consistence with *in vivo* study, oxygen glucose deprivation followed with re-oxygenation (OGD/R), an *in vitro* ischemic stroke model-induced neuronal death

was significantly decreased by treatments with FFA, ACA, 2-APB and clotrimazole to inhibit TRPM2 channel (see section **1.3.5**), or with TRPM2-specific shRNA or TRPM2-KO neurons (Jia et al., 2011; Verma et al., 2012; Ye et al., 2014). Notably, there was no difference in the infarct volume between WT and TRPM2-KO mice subjected to permanent MCAO without reperfusion, indicating an exclusive role for TRPM2 in mediating reperfusion-induced brain damage (Alim et al., 2013).

Genetic depletion or pharmacological inhibition of the TRPM2 channel have no effect on the infarct volume or neuronal death in female mice subjected with MCAO-induced transient ischemia and reperfusion (Shimizu et al., 2013; Jia et al., 2011). TRPM2-dependent neuroprotection in male mice was suggested to depend on androgen receptor signalling and PARP activity (Shimizu et al., 2013). Clotrimazole had no effect on MCAO-induced infarct volume in male mice castrated to remove endogenous androgens before MCAO, but reduced the infarct volumes in those mice implanted with androgen (Shimizu et al., 2013). In addition, the PARP activity was strongly increased in peri-infarct region in male mice after ischemic insult. Clotrimazole failed to further decrease the total infarct volume in male PARP-KO mice (Shimizu et al., 2013). Taken together, these results suggest intact androgen signalling is required for ROS-induced TRPM2 channel activation. Nevertheless, a more recent study showed clotrimazole had no protective effect on MCAO-induced infarct volume in female mice lacking estrogen. Furthermore, implant of androgen in female mice did not cause an increase in ADPR levels and TRPM2-dependent neuroprotection (Quillinan et al., 2014). The findings argue against the role of androgen in TRPM2 channel activation, and suggest the existence of other signalling pathways in female mice involved in the suppression of the PARP activation.

A recent study shows that TRPM2 channel is involved in downregulating the pro-survival signalling in brain damage during reperfusion after MCAO (Alim et al., 2013). The ratio of two NMDAR subunits, GluN2A and GluN2B, was demonstrated

to govern the signalling pathways leading to cell survival and cell death: an increase in GluN2A/GluN2B facilitates survival, while the opposite promotes death (Martel et al., 2009; Hardingham and Bading, 2010). GluN2B expression was significantly decreased, whereas GluN2A expression was increased in hippocampal neurons in TRPM2-KO mice. The treatment with GluN2A selective inhibitors during OGD/R abolished the neuroprotective effects due to TRPM2-KO, without effects on WT neuron viability. However, treatment with GluN2B selective inhibitors preferentially suppressed OGD/R-induced WT neuronal death, but had no effect on TRPM2-KO neurons. These results suggest that TRPM2 deficiency leads to the alternation in the subunit composition of NMDAR subunits (Alim et al., 2013). It is known that the GluN2A-containing NMDAR promotes pro-survival mechanisms via activating the Akt and ERK signalling pathways. The activation of Akt is involved in the inhibition of GSK-3β, a protein kinase that facilitates the translocation of pro-apoptosis regulators. Indeed, phosphorylated forms of Akt and ERK, and the phosphorylated and the inactive form of GSK-3β were increased in TRPM2-KO mice as compared to WT mice. On the other hand, postsynaptic density-95 (PSD-95) was shown to interact with GluN2B and its activation is associated with neuronal death (Chung et al., 2004; Aarts et al., 2002). With the decrease of GluN2B-containing NMDAR, the PSD-95 expression was also reduced in TRPM2-KO mice, further supporting that the deficiency of TRPM2 suppresses the activation of GluN2B subunit-containing NMDAR and the pro-death pathway (Alim et al., 2013). Taken together, these results have led to the proposal that TRPM2 channel regulates NMDAR-dependent pro-survival and pro-death mechanisms.

As discussed above, an increase in the $[Zn^{2+}]_i$ is a critical factor in transient ischemia-induced delayed neuronal death in CA1 pyramidal neurons. Neuronal death and an increase in the $[Zn^{2+}]_i$ were observed in WT mice after MCAO-induced ischemia and reperfusion, or in WT hippocampal slices after OGD/R. However, both effects were completely abolished by TRPM2-KO. Given the discernible increase in

the $[Zn^{2+}]_i$ in WT mice after 48 hr, these results suggest that deletion of the TRPM2 expression suppresses delayed increase in the $[Zn^{2+}]_i$ during reperfusion. Further investigation using single cell imaging demonstrated OGD/R induced a similar increase in the $[Zn^{2+}]_i$ in WT and TRPM2-KO neurons that remained sustained in WT neurons but rapidly declined to the basal level in TRPM2-KO neurons during reperfusion. These results are consistent with the above-mentioned finding that TRPM2-KO preferentially reduces brain damage induced by transient ischemia with reperfusion, but not permanent ischemia (Alim et al., 2013). In particular, these results have disclosed an important and exclusive role for TRPM2 channel in reperfusion following transient ischemia. Such difference in the intracellular Zn^{2+} homeostasis during reperfusion between WT and TRPM2-KO neurons may attribute to the ROS production during reperfusion. Indeed, there was a strong increase in ROS generation in the CA1 region of WT mice that occurred considerably earlier than the increase in the $[Zn^{2+}]_i$. Such ROS production was significantly attenuated in TRPM2-KO mice (Ye et al., 2014). Taken together, TRPM2 is essential for the ROS production and ROS-induced increase in the $[Zn^{2+}]_i$ during reperfusion that triggers delayed hippocampal neuron death. However, mechanisms of how TRPM2 channel activation triggers ROS production during reperfusion are not fully understood. In Chapter 3 of this study, I will investigate mechanisms by which TRPM2 channel activation induces ROS generation and increase in the $[Zn^{2+}]_i$ in oxidative stress-induced hippocampal neuron death.

1.4.3 Alzheimer's disease

AD is an age-related disorder that is clinically characterized by a progressive decline in cognitive function. While a small proportion of AD cases are familial, early-onset and are associated with genetic mutations, most cases of AD are sporadic, late-onset events, occurring in individuals older than 65. There are two

main histopathological hallmarks of AD, including senile amyloid plaques with extracellular deposition of Aβ peptides and intracellular neurofibrillary tangles containing hyper-phosphorylated Tau protein (Murphy and LeVine, 2010). It is widely accepted that synapse loss and neuronal death lead to the progressive decline in cognitive function in AD (Murphy and LeVine, 2010).

1.4.3.1 Neurotoxic Aβ generation

An imbalance in the generation and clearance of Aβ peptides has long been considered as an early and initiating factor in AD pathogenesis. Aβ peptides are derived from the proteolytic processing of amyloid precursor protein (APP) via two membrane-bound enzymes, β-secretase and γ-secretase (O'Brien and Wong, 2011). The γ-secretase has been identified as a complex composed of presenilin (PS) 1 or 2, nicastein, anterior pharynx defective and presenilin enhancer 2 (LaFerla et al., 2007). Of note, the cleavage of APP by γ-secretase can occur at different positions, generating a variety of Aβ peptides (Benilova et al., 2012). $A\beta_{40}$ is the most abundant form that is produced in both health and AD brains. The slightly longer form, $A\beta_{42}$, is more hydrophobic and more prone to fibril formation than $A\beta_{40}$, and is the major species found in cerebral plaques (LaFerla et al., 2007; Murphy and LeVine, 2010).

The creation of transgenic mice with gross amyloid deposition provides a powerful tool to the exploration of AD pathophysiology and evaluation of potential treatments. For instance, the transgenic mice expressing human mutated APP or APP/PS genes exhibit age-dependent brain Aβ elevation and behavioural deficits, reproducing the pathological alterations in early-onset familial AD (Kokjohn and Roher, 2009).

1.4.3.2 Aβ neurotoxicity

It has long been proposed that oxidative stress plays a crucial role in AD pathogenesis by triggering lipid peroxidation and the oxidation of protein and DNA

(Pratico and Sung, 2004; Williams et al., 2006). *In vitro* studies show that Aβ is acutely toxic to cultured neuronal cells by increasing intracellular ROS levels (Fonfria et al., 2005; Wang et al., 2010; Park et al., 2005). In addition, the reduction of antioxidants with aging contributes to the oxidative stress in brain afflicted by AD. Supplementation of antioxidants such as vitamin E and C decreases the incidence of AD and provides neuroprotective effects on cognitive functions among the susceptible population (Boothby and Doering, 2005).

A number of studies have demonstrated Aβ peptides contribute to oxidative stress by triggering mitochondrial dysfunction and NOX activation. In the presence of Ca^{2+}, $A\beta_{35}$ promotes the opening of mPTP (Moreira et al., 2001), which initiates further mitochondria dysfunctions, such as decreased ATP production, mitochondrial morphological changes and ROS production (Casley et al., 2002; Du and Yan, 2010). $A\beta_{42}$ peptide was shown to prevent the entry of mortalin/mtHsp70 and Tom20 into mitochondria, which is associated with the loss of mitochondria membrane potential, leading to an increase in mitochondrial ROS production and morphology changes (Sirk et al., 2007). Aβ-induced mitochondrial dysfunction is associated with neuronal death via mitochondrial-dependent apoptosis (Deshpande et al., 2006). The activation of caspases-3, -6, -7, -8 and -9, had been reported in brains of both AD mice and post-mortem AD patients (Rissman et al., 2004; Rohn and Head, 2009). The transgenic caspase-2 or caspase-3 null mice were resistant to $A\beta_{42}$- or $A\beta_{40}$-induced neuronal loss (Troy et al., 2000; Takuma et al., 2004), which provides evidence to support the involvement of mitochondria-dependent oxidative stress and apoptosis in Aβ neurotoxicity.

The APP transgenic mice lacking the NOX2 expression showed improved spatial memory performance, implicating that the NOX activation is critical to Aβ-induced neurotoxicity. $A\beta_{35,}$ $A\beta_{40}$ and $A\beta_{42}$ were shown to activate NOX activation and the formation of $O_2{\cdot}^-$ in microglia, monocytes and neutrophils (Bianca et al., 1999). Application of NOX inhibitors or genetic deletion of NOX significantly reduced

oxidative stress in the APP transgenic mice (Han et al., 2015; Park et al., 2008; Park et al., 2005). Moreover, microglial activation is known to elicit neuroinflammation via the production of pro-inflammatory cytokines, chemokines and nitric oxide (Doens and Fernandez, 2014). Apocynin substantially attenuated the activation of microglia and astrocytes in aged APP transgenic mice (Han et al., 2015). Collectively, NOX-mediated oxidative stress contributes to Aβ neurotoxicity, particularly via activating microglia-induced neuroinflammatory responses.

An increasing number of studies indicate cerebrovascular dysfunctions, such as a reduction in cerebral blood flow (CBF), are associated with the pathogenesis of AD (Tong et al., 2005; Zlokovic, 2011). CBF is a critical mechanism for the delivery of O_2 and glucose, and the removal of deleterious metabolism by-products in the brain. It is regulated by local neuronal activity and metabolism, known as neurovascular coupling. Increased ROS level was observed in cerebral arteries in aged APP transgenic mice, suggesting an association of APP overexpression with oxidative stress in cerebral vessels (Han et al., 2015). $A\beta_{40}$ significantly reduced both the basal CBF and vasoactive factors stimulated CBF in somatosensory cortex in mice (Park et al., 2005). However, it had no effect on the CBF responses in mice lacking NOX subunit $gp91^{phox}$. Genetic deletion of $gp91^{phox}$ or NOX2 ameliorated the cerebrovascular dysfunction in aged WT mice and in APP transgenic mice (Park et al., 2005; Park et al., 2008). These results strongly suggest NOX-mediated oxidative stress is a key factor in $A\beta_{40}$-induced cerebrovascular dysfunction.

1.4.3.3 TRPM2 in AD

Emerging evidence shows the involvement of TRPM2 channel in mediating Aβ neurotoxicity and AD. A recent *in vivo* study has demonstrated that genetic deletion of TRPM2 expression rescued spatial memory deficits in aged APP/PS1 AD mice (Ostapchenko et al., 2015), supporting the role of TRPM2 in Aβ-induced neurotoxicity.

Exposure to $A\beta_{42}$ significantly augmented ADPR-induced TRPM2 channel currents in hippocampal neurons (Ostapchenko et al., 2015). Transfecting striatal neuron cultures with TRPM2-S or siRNA targeting TRPM2 inhibited $A\beta_{42}$-induced rise in the $[Ca^{2+}]_i$ and neuronal death (Fonfria et al., 2005), suggesting that $A\beta_{42}$ elicits TRPM2 channel activation, leading to Ca^{2+} influx and neuronal death. The protein misfolding-mediated ER-stress has been defined as a novel trigger for AD pathology (Salminen et al., 2009). However, decreased expression of ER stress protein was observed in APP/PS1 mice lacking TRPM2 expression, suggesting deletion of TRPM2 expression attenuated ER stress (Ostapchenko et al., 2015). In addition, elimination of the TRPM2 expression inhibited the loss of synapse and reduced microglia activation in the APP/PS1 mice (Pozueta et al., 2013; Ostapchenko et al., 2015). Taken together, these results suggest that TRPM2 channel activation contributes to AD pathogenesis.

Aβ-induced cerebrovascular dysfunction in AD has also been shown to associate with TRPM2 channel activation (Zlokovic, 2011). The treatment with 2-APB or ACA or genetic deletion of TRPM2 expression strongly prevented $A\beta_{40}$-induced CBF reduction in WT and reversed cerebrovascular dysfunction in APP transgenic mice. As discussed above, Aβ triggers cerebrovascular dysfunction by activating NOX-dependent ROS production. TRPM2 activated by oxidative stress can increase Ca^{2+} influx into endothelial cells, enhancing the permeability of endothelial cell. Collectively, the results provide implication that Aβ-induced oxidative stress evokes the TRPM2 channel activation , resulting in alterations in ionic homeostasis and thereby the neurovascular and endothelial impairment (Park et al., 2014).

In the Chapter 4, I will investigate the molecular mechanisms responsible for $A\beta_{42}$-induced TRPM2 channel-mediated neuronal death.

1.4.4 PD

1.4.4.1 Pathogenesis

PD is another common neurodegenerative disorder due to neuronal loss in the substantia nigra pars compacta (SNc), which causes striatal dopamine (DA) deficiency. Pathological hallmarks of PD include the presence of Lewy bodies that is largely made up of aggregated α-synuclein in degenerating neurons (Poewe et al., 2017). Increasing evidence indicates that oxidative stress acts as the principal molecular mechanism underlying the pathogenesis of PD (Moore et al., 2005; Hwang, 2013). A number of sources and mechanisms contributing to the ROS generation in PD are recognized, including the metabolism of DA itself, mitochondrial dysfunctions and the neuroinflammation (Dias et al., 2013).

DA is an unstable molecule that undergoes auto-oxidation catalysed by enzymes such as MAOs to form DA quinones and ROS (Munoz et al., 2012). Under normal conditions, the level of DA is regulated by the oxidative metabolism of MAO-A. However, during PD or aging-induced neuronal degeneration, MAO-B located in glia cells plays a predominant role in DA metabolism, leading to the production of H_2O_2 (Dias et al., 2013). H_2O_2 is subsequently converted to hydroxyl radical in the presence of Fe^{2+}, contributing to oxidative stress. DA quinones can also contribute to oxidative stress. Aminochrome, which is formed by the cycling of DA quinones, is highly reactive and leads to the generation of $O_2^{\cdot -}$ (Dias et al., 2013). Aminochrome is ultimately polymerized to form neuromelanin, a pigment which exacerbates neurodegeneration by triggering neuroinflammation (Zecca et al., 2008). In addition, DA quinones are shown to modify low-molecule-weight sulfhydryls such as GSH, an important antioxidant as discussed above, and a number of proteins which are associated with the pathophysiology of PD such as α-synuclein, parkin, DJ-1 (Hwang, 2013).

Compelling evidence suggests the impairment in mitochondrial functions is an essential element contributing to the pathogenesis of PD. Deficiency in mitochondrial complex I is considered as a primary source of ROS in PD (Vila and Przedborski, 2003). Reduced mitochondrial complex I activity in SNc as well as other brain regions is well described in PD patients (Parker et al., 2008; Hwang, 2013). Complex I inhibitors, such as rotenone and 1-methyl-4-phenyl-1,2,3,6-tetrahydropyridine (MPTP), exert preferential cytotoxicity to dopaminergic neurons (Hwang, 2013). MPTP is metabolised by MAO in endothelial cells to generate 1-methyl-4-phenylpyridinum (MPP^+) after crossing the BBB and entering the brain. MPP^+ is taken up into dopaminergic neurons by DA transporter and concentrated within mitochondria where it acts to inhibit complex I (Bartels and Leenders, 2009). As discussed in section **1.1.1**, the inhibition of complex I disrupts electron flow through the mitochondrial ETC, resulting in a decrease in ATP production and an increase in ROS generation.

Mutations in genes encoding mitochondrial proteins like parkin, PINK and DJ-1 have been linked with the familial form of PD. These mutations are responsible for mitochondrial dysfunction and oxidative stress, providing additional evidence to support the role of mitochondrial dynamics in PD pathogenesis. Parkin is essential for the mitochondria integrity. Cells derived from patients or mice bearing mutations in parkin gene showed decreased mitochondrial complex I activity along with oxidative damage (Muftuoglu et al., 2004; Palacino et al., 2004). Overexpression of parkin in mice reduced MPTP-induced dopaminergic neuron loss (Bian et al., 2012). PINK1 mutation can induce deficits in the mitochondrial ETC, leading to the loss of mitochondrial membrane potential and increased ROS generation (Amo et al., 2014; Wood-Kaczmar et al., 2008). Oxidative stress stimulates the translocation of DJ-1 into mitochondria, where it binds to the subunits of mitochondrial complex I and regulates its activity (Hayashi et al., 2009; Zhang et al., 2005a). Cells with DJ-1

deficiency exhibit aberrant mitochondrial respiratory and morphology, reduced membrane potential and elevated ROS production (Irrcher et al., 2010).

A number of studies provided evidence to indicate that sustained inflammatory responses, which are mainly mediated by microglial cells, play a vital role in the pathophysiology of PD (Wang et al., 2015). Microglia activated upon brain injuries are an important source of ROS, contributing to oxidative stress in the brain. Moreover, microglia activation in PD brain upregulate the production of pro-inflammatory cytokines, including TNF-α, IL-1β, IL-6 and IFN-γ, which promote the degeneration of dopaminergic neurons (Qian et al., 2010). As mentioned above, neuromelanin that produced from DA oxidation activates microglia and triggers neuroinflammation. α-Synuclein and matrix metallopeoteinase-3 released from damaged dopaminergic neurons also enhance microglia activation, further amplifying neuroinflammatory responses and neurodegeneration (Wilms et al., 2003; Zhang et al., 2005b; Kim et al., 2005; Wang et al., 2015).

1.4.4.2 TRPM2 in PD

A recent study has demonstrated that TRPM2 channel mediates MPP^+-induced dopaminergic neuronal death (Sun et al., 2016). MPP^+ significantly increased the expression of TRPM2 protein in SNc in mice and in SH-SY5Y cell line, a widely-used cell model for PD research. Moreover, the TRPM2 expression was elevated in SNc regions of PD patients when compared with age-matched subjects (Sun et al., 2016). Treatment with FFA and ACA effectively abolished MPP^+-induced Ca^{2+} influx and inward currents, suggesting that TRPM2 channel expression is upregulated and mediates enhanced Ca^{2+} influx in response to MPP^+. Treatment with FFA or TRPM2 knockdown attenuated MPP^+-induced Cyt-c release and activation of caspase-dependent apoptosis. On the contrary, overexpression of TRPM2 exacerbated MPP^+-induced cell death. The results provide evidence to show a critical role of TRPM2 channel in apoptotic cell death related to PD (Sun et al., 2016).

In addition, the increase in burst firing of substantia nigra pars reticulata (SNr) neurons is known to contribute to the pathophysiology of PD (Rivlin-Etzion et al., 2008). TRPM2 channel activation was shown to be required for NMDA-induced burst firing (Lee et al., 2013). In SNr GABAnergic neurons, intracellular application of ADPR resulted in a significant increase in the firing rate, which was completely abolished by FFA or selective anti-TRPM2 antibody (Lee et al., 2013). These results indicate that TRPM2 channel activation affects the burst firing in SNr GABAnergic neurons in PD.

1.5 Aim of the current study

Recent *in vitro* and *in vivo* studies using transgenic TRPM2-KO mice in conjunction with models of transient ischemia and AD support an important role for TRPM2 channel in mediating neuronal death and cognitive dysfunction associated with reperfusion or excessive Aβ generation. However, the molecular mechanisms underlying TRPM2-mediated neuronal death still remain contentious. As such, the investigations discussed in this thesis aimed to illustrate molecular mechanisms for TRPM2-mediated death in primary cultured hippocampal neurons.

The objectives of this study are:

1. To demonstrate the expression of TRPM2 channel in hippocampal neurons and its participation in neuronal cell death induced by ROS and $A\beta_{42}$.
2. To explore the role of TRPM2 channel in mediating the increase in the $[Zn^{2+}]_i$ in hippocampal neurons in response to ROS and $A\beta_{42}$.
3. To investigate the mechanisms responsible for the increase in the $[Zn^{2+}]_i$ and neuronal death induced by ROS and $A\beta_{42}$.
4. To examine the subcellular location of TRPM2 channel and its interaction with the PKC/NOX and MEK/ERK signalling mechanisms.

Chapter 2

Materials and Methods

2.1 Materials

2.1.1 Chemicals

All major chemicals used in this study are listed in **Table 2.1.**

Table 2.1 Chemicals used in the study

Chemical	Manufacture	stock
$A\beta_{42}$	China Peptides	0.5 mM in H_2O, -20°C
ACA	Calbiochem	20 mM in DMSO, -20°C
Ac-DVED-CMK	Cayman Chemical	10 mM in DMS0, -20°C
2-APB	Sigma	100 mM in H2O, -20°C
Apocynin	Cayman Chemical	10 mM in DMSO, -20°C
AraC	Sigma	100 mM in H_2O, -20°C
Bafilomycin A1	Cayman Chemical	100 mM in DMSO, -20°C
CGP37157	Calbiochem	10 mM in DMSO, -20°C
Clioquinol	Santa Cruz	10 mM in DMSO, room temperature
DPI	Cayman Chemical	10 mM in DMSO, -20°C
DPQ	Calbiochem	10 mM in DMSO, -20°C
EGTA	Sigma	0.5 M in H_2O, 4°C
FTS	Cayman Chemical	15 mM in DMSO, -20°C
GKT137831	Cayman Chemical	10 mM in DMSO, -20°C
GÖ6976	Calbiochem	10 mM in DMSO, -20°C
H_2O_2	Sigma	10 M in H_2O, 4°C
IM54	Sigma	5 mM in DMSO, -20°C
Ionomycin	Cayman Chemical	5 mM in DMSO, -20°C
Necrostatin-1	Alfa Aesar	75 mM in DMSO, -20°C

PF431396	Tocris	50 mM in DMSO, -20°C
PJ34	Calbiochem	10 mM in DMSO, -20°C
Pluronic Acid	Life Technologies	10% (w/v) in H_2O, room temperature
Poly-L-lysine	Sigma	10 mg/ml in H_2O, -20°C
Ru360	Calbiochem	10 mM in DMSO, -20°C
TNF-α	Cell signalling Technology	100 µg/ml stock in PBS containing 1% BSA, -20°C
TPEN	StressMarq Bioscience	10 mM in DMSO, -20°C
U0126	Cayman Chemical	10 mM in DMSO, -20°C
$ZnSO_4$	Sigma	0.15 M, room temperature

Abbreviations: Ac-DVED-CMK (N-acetyl-L-α-aspartyl-L-α-glutamyl-N-[(1S)-1-(carboxymethyl)-3-chloro-2-oxopropyl]-L-valinamide); araC (Cytosine β-D-arabinofuranoside); CGP37157 (7-Chloro-5-(2-chlorophenyl)-1,5-dihydro-4,1-benzothiazepin-2(3H)-one); clioquinol (5-Chloro-8-hydroxy-7-iodoquinoline); DPQ (3,4-Dihydro-5[4-(1-piperindinyl)butoxy]-1(2H)-isoquinoline); EGTA (Ethylene glycol-bis(β-aminoethyl ether)-N,N,N',N'-tetraacetic acid); FTS (Farnesylthiosalicylic acid); GÖ6976 (5,6,7,13-Tetrahydro-13-methyl-5-oxo-12H-indolo [2,3-a]pyrrolo [3,4-c]carbazole-12-propanenitrile); IM54 (2-(1H-Indol-3-yl)-3-pentylamino-maleimide); PF431396(N-Methyl-N-[2-[[[2-[(2,3-dihydro-2-oxo-1H-indol-5-yl)amino]-5-(trifluoromethyl)-4-pyrimidinyl]amino]methyl]phenyl] methanesulfonamide); TPEN (N,N,N',N'-tetrakis(2-pyridylmethyl)ethane-1,2-diamine); U0126 (1,4-Diamino-2,3-dicyano-1,4-bis[2-aminophenylthio] butadiene).

2.1.2 Animals

The wild-type C57BL/6 mice were purchased from the Central Biomedical Services, University of Leeds. The transgenic TRPM2-KO C57BL/6 mice expressing the *trpm2* gene without exons 17 and 18 encoding amino acid residuals from Leu-843 to Met-931 were generated in a previous study (Zou et al., 2013). All experiments and experimental protocols, including all those involving mice, were approved by the University of Leeds Ethical Review Committee and performed in accordance with the University of Leeds guidelines and procedure and conforming to the UK Home Office rules and regulations.

2.1.3 Antibodies

Antibodies used for immunofluorescent staining are listed in **Table 2.2**.

Table 2.2 Antibodies used in this study

Primary antibodies	**Host**	**Working concentration**	**Manufacture**
Anti-Cyt-c	Mouse	1:100	BD
Anti- MAP-2	Rabbit	1:1000	Millipore
Anti-Tau	Rabbit	1: 500	Dako
Anti-TRPM2	Rabbit	1:1000	Bethyl laboratories
Pan neuronal marker	Mouse	1: 100	Millipore
Secondary antibodies	**Target species**	**Working concentrations**	**Supplier**
FITC-conjugated IgG	Mouse or rabbit	1: 500	Sigma
TRITC-conjugated IgG	Mouse	1: 500	Sigma

Abbreviations: Cyt-c (Cytochrome-c); FITC (Fluorescein isothiocyanate); IF (Immunofluorescent staining); MAP-2 (Microtubule-associated protein 2); TRITC (Tetramethylrhodamine isothiocyanate).

2.1.4 Fluorescent indicators and fluorophores conjugated secondary antibodies

Fluorescent indicators and fluorophores conjugated to secondary antibodies are listed in **Table 2.3**.

Table 2.3 The spectral properties for fluorescent indicators and antibodies

Indicator	Excitation wavelength (nm)	Emission wavelength (nm)	Manufacture
DCFH-DA	504	529	Sigma
ER-Tracker Red	587	615	Life Technologies
FITC-conjugated secondary antibodies	493	528	Sigma
Fura-2/AM	340 and 380	510	Life Technologies
FluoZin-3/AM	494	516	Life Technologies
Fluo-4/AM	494	506	Life Technologies
Hoechst 33432	355	465	Cell Signalling Technologies
LysoTracker Red DND-99	577	590	Life Technologies
MitoTracker Red CMXRos	579	599	Life Technologies
MitoTracker Green FM	490	516	Life Technologies

MitoTracker Red CM-H_2Xros	579	599	Life Technologies
NucView488 Caspase-3 substrate	488	520	Biotium
PI	535	617	Sigma
RhodZin-3/AM	550	575	Life Technologies
TRITC-conjugated secondary antibodies	547	572	Sigma

Abbreviations: DCFH-DA (2',7'-Dichlorofluorescin diacetate); PI (Propidium iodide).

2.1.5 Solutions

The solutions used for immunofluorescent staining, live cell images or Ca^{2+} measurements were prepared in Milli-Q deionized water and pH values were adjusted to the indicated pH by 4 M NaOH or 37% HCl. Solutions for cell culture and mouse tissue dissection were commercially obtained in sterilized conditions or sterilized by autoclaving or filtering through 0.22-μm syringe filter. The compositions for solutions used in this study are listed in **Table 2.4**. All general chemicals were purchased from Sigma at the analytical reagent grade.

Table 2.4 Solutions used in the study

Solution	Compositions
Blocking solution/ antibody dilution buffer	10% goat serum in PBS-T
Borate acid buffer	100 mM boric acid; 75 mM NaCl; 25 mM sodium tetraborate; pH 8.5
Ca^{2+}-free SBS	130 mM NaCl; 5 mM KCl; 1.2 mM $MgCl_2$; 8 mM glucose; 10 mM HEPES; 0.4 mM EGTA, pH 7.4

PBS-T	0.4 % (v/v) Triton X-100 dissolved in PBS
Phosphate buffer saline (PBS)	One PBS tablet dissolved in 200 ml sterilized water
Standard bath solution (SBS)	130 mM NaCl; 5 mM KCl; 1.2 mM $MgCl_2$; 8 mM glucose; 10 mM HEPES; 1.5 mM $CaCl_2$, pH 7.4
Zamboni's fixative solution	15% (v/v) picric acid; 5.5% (v/v) 37% formaldehyde in PBS

2.1.6 Culturing media

The compositions for each medium are listed in **Table 2.5.** The medium were stored at 4°C and pre-warmed at room temperature prior to use. All medium and supplements were purchased from Life Technologies, if not indicated.

Table 2.5 Medium for primary hippocampal neuron culture

Type	Medium
Culturing medium	Neurobasal® Medium supplemented with 2% (v/v) B-27 supplement, 0.5 mM L-glutamine, 50 unit/ml penicillin and 50 µg/ml streptomycin
Dissection medium	DMEM/F12 + GlutaMax™ added with 50 unit/ml penicillin and 50 µg/ml streptomycin (Sigma)
Plating medium	DMEM/F12 + GlutaMax™ supplemented with 10% (v/v) horse serum, 50 unit/ml penicillin and 50 µg/ml streptomycin

2.2 Methods

2.2.1 Primary mouse hippocampal neuron culture

All the following primary neuron culture operations were carried in a laminar flow hood (Wolf Laboratories). Hippocampal neurons were maintained in appropriate medium in a 37°C incubator with humidified 5% CO_2 (Sanyo).

2.2.1.1 Preparing coverslips and culture containers

The 13-mm coverslips were commercially obtained from VWR. After being cleaned and boiled in sterilized water, coverslips were left in room temperature for cooling and boiled again. The sterilized water was changed to 100% ethanol when the liquid were completely cooled. Coverslips were kept in ethanol for at least one week, dried in the tissue culture hood and placed in 24-well plate for coating.

Poly-L-lysine was dissolve in sterilized water at stock concentration listed in **Table 2.1** and then diluted in 0.1 M borate acid buffer (see **Table 2.4**) to the working concentration of 0.1 mg/ml. Coverslips, 24-well plates and glass bottom petri-dishes used for primary cell culture were coated overnight before cells were seeded. After poly-L-lysine being aspirate entirely, coverslips, plates or petri-dishes were washed with sterilized water for 3 times and dried in the tissue culture hood. Plates or petri-dishes were wrapped with aluminium foil and kept in 4°C before use.

2.2.1.2 Hippocampal neuron isolation

All dissection tools was kept in 70% (v/v) ethanol and dried thoroughly before use. All procedures for the brain tissue dissection were performed on ice. Primary neurons were prepared from postnatal 1-2 day-old WT or TRPM2-KO mice using protocols described previously (Beaudoin et al., 2012). The mouse was euthanized by decapitation and the head was collected into a 3.5-cm petri-dish containing 1x ice-cold Hank's balanced salt solution (HBSS, Invitrogen). After the skin and skull were gently removed, the brain was exposed. The brain was pinched off from the base by forceps and transferred to 35-mm dish containing ice-cold HBSS. Under a

dissection microscope, the cerebellum, midbrain and thalamic tissues were carefully removed; only the intact hemisphere containing the cortex and hippocampus were kept. The meninges layers were completely removed and the C-shape hippocampus was separated from the cortex, and collected in a 35-mm dish containing dissecting medium.

The dissecting medium containing isolated hippocampi were gently removed and replaced with 2 ml 0.125% trypsin-EDTA. Tissues were incubated in trypsin-EDTA at 37°C for 15 min and dishes were gently shaken every 3 min. Then, trypsin-EDTA was thoroughly removed and the hippocampi were re-suspended using 2 ml plating medium (see **Table 2.5**). Tissues were gently triturated 50 times by using 1000 µl-pipette to dissociate cells and the suspension was left to stand for 2 min until all tissues were settled to the bottom. The supernatant was carefully transferred into a 70-µm cell strainer placed inserted in a 50-ml falcon centrifuge tube and the re-suspension step was repeated 3 times until no chunk tissues remained. Cell suspension was centrifuged at 100 x *g* for 5 min. The supernatant was discarded and the pellets containing single hippocampal neurons were suspended with plating medium. Cells were counted using a haemocytometer. Cells were seeded at the cell density of 100 cells per mm^2 for all assays.

2.2.1.3 Maintenance

The hippocampal neuron cultures were maintained in a tissue incubator for 2-6 hr. After neurons were settled, the plating medium was aspirated from each well or dish, and fresh Neurobasal medium supplemented with nutrients (see **Table 2.5**) were added. Two days after plating, araC was added into each well to a final concentration of 0.5 µM to inhibit the proliferation of non-neuronal cells. The araC-containing medium was then replaced with fresh maintenance medium after 48 hr. Hippocampal neurons cultured for 14-20 days *in vitro* (DIV14-20) were used in this study. To identify the purity of neuron culturing, anti-mouse MAP-2 antibody was used to label neurons.

2.2.2 Mitochondria isolation

The Mitochondria Isolation Kit for cultured cells was purchased from Thermo Scientific. Protease inhibitor cocktail (Roche) were added to Mitochondria Isolation Reagent A and C (Reagent A and C) freshly before use. A total number of 2 x 10^6 neurons were used for mitochondria isolation in each experiment. Cells were detached with 0.05% trypsin-EDTA and harvested in a 15-ml falcon tube by centrifugation at 850 x *g* for 2 min at room temperature. After the supernatant was carefully removed, 800 µl Reagent A were added to the cell pellet. Cells were suspended by vortex at 1000 rpm for 5 s and incubated on ice for exactly 2 min. Cell suspension were homogenized using a 1 ml-syringe with needle (25G) by sucking in and out the suspension for 80 strokes on ice. Then, 400 µl Reagent C were added into the cell suspension and gently mixed by inverting the centrifuge tube. After the mixture was centrifuged at 700 x *g* for 10 min at 4°C, the supernatant were transferred to a new falcon tube and centrifuged at 3000 x *g* for 15 min at 4°C and the pellet was washed with 250 µl Reagent C. The suspension was centrifuged at 12,000 x *g* for 5 min and the supernatant was discarded. The pellet containing isolated mitochondria were re-suspended in 800-1000 µl SBS or Ca^{2+}-free SBS and maintained on ice before being used for further experiments.

2.2.3 Live cell and isolated mitochondria confocal imaging

2.2.3.1 Fluorescent indicators

A number of fluorescent indicators or dyes for Ca^{2+} or Zn^{2+} and for intracellular organelles were used in this study. The excitation and emission wavelengths for each of these fluorescent indicators are listed in **Table 2.3**. Fluo-4 is a Ca^{2+} indicator that upon binding by Ca^{2+} exhibits an increase in the fluorescence excitation. FluoZin-3 is an indicator with a high affinity for labile Zn^{2+}. The indicator has been demonstrated to be suitable to detect Zn^{2+} at the concentration as low as

1 nM and thus is considered to be the most sensitive and specific Zn^{2+} indicator. RhodZin-3 is a Zn^{2+} indicator with a nanomolar affinity and preferentially localized into mitochondria and therefore, it is a valuable tool for monitoring mitochondrial Zn^{2+} concentration.

LysoTracker Red DND-99 is a membrane-permeable, red fluorescent dye. The probe consists of a fluorophore linked to a weak base that is only partially protonated at neutral pH, resulting in a selective accumulation of the dye in acidic compartments. Therefore, LysoTracker is used as a fluorescent probe for labelling and tracing acidic organelles such as lysosome in live cells. ER-Tracker Red is a membrane-permeable fluorescent indicator with high selectivity for the ER. It is conjugated with glibenclamide BODIOY TR that binds to the sulphonylurea receptor subunit of the ATP-sensitive K^+ channel prominently on the ER. MitoTracker Red CMXRos and MitoTracker Green FM are selective probes that passively diffuse across plasma membrane and concentrate in mitochondria. The accumulation of MitoTracker Red in mitochondria is dependent upon the mitochondrial membrane potential. MitoTracker Green appears to localize to mitochondria regardless of the mitochondrial membrane potential.

2.2.3.2 Single cell confocal imaging

Glass-bottom 35-mm petri-dishes (World Precision Instruments) used for single cell confocal imaging were pre-coated with poly-L-lysine before use as described above.

After the culture medium were removed, cells were gently rinsed with SBS (**Table 2.4)** and incubated in 500 µl of SBS containing 1 µM fluo-4, 0.5 µM FluoZin-3 or 1 µM RhodZin-3 with pluronic acid at the final concentration of 0.01% (w/v) for 1 hr. SBS containing Ca^{2+} or Zn^{2+} indicators were then removed and cells were gently rinsed with SBS to remove the remaining dyes. Cells were incubated in SBS for 30 min to de-esterify the AM esters or in SBS containing 1 µM LysoTracker, 25~100 nM MitoTracker or 1 µM ER-Tracker for 30 min to examine the subcellular

localization of Zn^{2+} in intracellular organelles. To measure $A\beta_{42}$-induced intracellular alterations, neurons were exposed to 1 μM $A\beta_{42}$ for 24 or 48 hr before replacing culture medium with SBS containing fluorescent indicators. To examine the effects of H_2O_2, after removal of the remaining dyes, cells were incubated in SBS or Ca^{2+}-free SBS containing 300 μM H_2O_2 for the durations indicated in result chapters. In experiments examining the effects of inhibitors, the inhibitors were added into the culture medium or SBS solution at indicated concentrations 30 min before and during exposure to $A\beta_{42}$ or H_2O_2. Cells were rinsed with SBS to remove H_2O_2 and maintained in 2 ml SBS during imaging. Images were captured immediately using an inverted LSM700 or LSM880 confocal microscope (Zeiss) housed in the Faculty of Biological Sciences (University of Leeds) with a 63x objective under environmental control of 37°C and humidified 5% CO_2. ImageJ software (National Institutes of Health, USA) was used to determine the fluorescent intensity.

For time-lapse confocal imaging, cells were labelled with the indicators as described above and incubated in 2 ml SBS. Similarly, inhibitors were added into the bathing solutions and incubated in a cell culture incubator for 30 min. Petri-dish was mounted on the scanning stage of confocal microscope and an area was randomly chosen for recording. H_2O_2 or bafilomycin A1 was added into the dish under indicated conditions, and images of the same area were captured every 5 min for a total duration of 30-40 min. ImageJ software was used to determine the fluorescence intensity.

2.2.3.3 Measurement of mitochondrial morphology

After exposure to indicated treatments, hippocampal neurons were labelled with MitoTracker and imaged as described above in section **2.2.3.2.** Confocal images were processed through a 7x7 convolve filter using ImageJ to obtain isolated and equalized fluorescent pixels. After converting to mask, the Particle Analyser was applied to acquire the circularity and length of major and minor axes of mitochondria particles. The morphology of mitochondria was characterized by

aspect ratio (AR: major axis/minor axis) and form factor (FF: the reciprocal of circularity value) (Koopman et al., 2005; De Vos et al., 2005). Both parameters have a minimal value of 1, with high values for AR indicating elongated tubular mitochondria and high values for FF indicating increased mitochondrial length and branching.

2.2.3.4 Confocal imaging of isolated mitochondria

Mitochondria were isolated as described above in section **2.2.2**, and were incubated in SBS or Ca^{2+}-free SBS containing 1 mM ADPR for 30 min. In some experiments, 1 μM TPEN was added 15 min before applying ADPR. $ZnSO_4$ was then added with a final concentration of 10 μM and incubated for 30 min. The mitochondria suspension was centrifuged at 12,000 x *g* for 5 min and the supernatant was discarded. The pellets were suspended and incubated in 200 μl SBS containing 1 μM RhodZin-3 with pluronic acid at final concentration of 0.01% (w/v) for 1 hr, and dyes were removed by centrifugation at 12,000 x *g* for 5 min. The pellets were re-suspended and incubated in SBS containing 50 nM MitoTracker Green for 30 min. Mitochondria in each tube were re-suspended with 50 μl SBS and dropped on a glass slide. Samples were covered by coverslips and sealed with nail polish. Images were captured immediately using an inverted LSM700 microscope and a 63x objective under environmental control of 37°C and humidified 5% CO_2. ImageJ software was used to determine the fluorescence intensity.

2.2.4 Immunofluorescence imaging

Immunofluorescent staining is a procedure to detect an antigen based on the specificity of an antibody and is widely used to determine the expression and distribution of target proteins. Solutions for immunofluorescent staining were prepared as described in **Table 2.4**. After gently rinsed with PBS, cells were fixed

with Zamboni's fixative solution for 1 hr at room temperature. Cells were washed with PBS for three times, 5 min for each time. The fixed cells were incubated with blocking goat serum solution for 1 hr and then with the primary antibody diluted in an antibody dilution buffer at concentrations listed in **Table 2.2** overnight at 4°C. On the next day, cells were washed three times with PBS and incubated with a FITC- or TRITC-conjugated secondary antibody for 1 hr at room temperature in dark. The secondary antibody was diluted in the antibody dilution buffer at concentrations detailed in **Table 2.2**. Cells were washed with PBS for 5 min and rinsed in water. Each coverslip was dried on tissue paper and mounted inversely on a glass slide with 6 µl DAPI-containing SlowFade Gold Antifade Mountant (Invitrogen) and kept in 4°C overnight. In some experiments, cells were treated with indicated activators before fixation as indicated in the result chapters. Images were captured using an inverted LSM 700 or LSM880 microscope. ImageJ software was used for image analysis.

2.2.5 Quantification of hippocampal neuron axonal degeneration

Following treatments with H_2O_2 or $A\beta_{42}$ at indicated concentrations and durations, hippocampal neurons were labelled with axon-specific anti-Tau antibody and imaged as described in section **2.2.4**. Levels of axonal degeneration were reported as a degeneration index (DI), which is defined as the ratio of the fragmented area over the total axonal area (Sasaki et al., 2009).

To process images for DI quantification, ImageJ was utilized to binarize the image and to remove all cell bodies, and total axonal area was determined as the black area against white background. To measure the area of fragments in a degenerating axon, the Particle Analyzer of ImageJ was applied to identify regions of fragmentation on the basis of size and circularity. The total area of detected

axonal fragments was then divided by the total axonal area to determine DI (Kraemer et al., 2014).

2.2.6 Measurement of cell death

2.2.6.1 Induction of cell death

Cells were treated with H_2O_2 or $A\beta_{42}$ at indicated concentrations and durations as detailed in result chapters. In some experiments, inhibitors at indicated concentrations were added 30 min prior to and during the whole experiment.

2.2.6.2 Measurement of dead cells

Propidium iodide (PI) is a red fluorescent dye which binds to DNA in the nucleus after entering cells without intact plasma membrane. Therefore, PI staining is commonly used for identifying dead cells, particularly those via necrotic cell death. Hoechst 33342 is a plasma membrane-permeable fluorescent dye binding DNA. Hoechst and PI are frequently used together for cell death analysis (Xu et al., 2012).

After indicated treatments, cells were incubated in culture medium containing 1 µM Hoechst 33342 and 5 µg/ml PI. The plates were wrapped with aluminium foil and incubated at 37°C in humidified 5% CO_2 incubator for 30 min. Medium containing dyes were replaced with pre-warmed D-PBS (Dulbecco's phosphate buffered saline; modified, without $CaCl_2$ and $MgCl_2$) before images were captured using an EVOS Cell Imaging Systems (Life Technologies). ImageJ was used for cell counting.

2.2.7 Measurement of whole cell ROS and mitochondrial ROS

2',7'-Dichlorofluorescin diacetate (DCFH-DA) was used to measure the whole cell ROS level (Ruiz et al., 2012). DCFH-DA is a plasma-permeable non-fluorescent probe that emits high fluorescent once hydrolysed intracellularly upon oxidative stress. MitoTracker Red CM-H_2Xros was used to determine mitochondrial ROS

production. This indicator is a reduced, non-fluorescent form of MitoTracker which becomes fluorescent upon oxidation.

Cells were exposed to H_2O_2 or $A\beta_{42}$ at concentrations and durations as detailed in result chapters. In some experiments, cells were treated with indicated inhibitors for 30 min before and during exposure to H_2O_2 or $A\beta_{42}$. After exposed to indicated treatments, cells were incubated in medium containing 3 μM DCFH-DA or 100 nM MitoTracker Red CM-H_2Xros for 30 min in a 37°C incubator with humidified 5% CO_2. Medium were replaced with fresh D-PBS to remove dyes before images were captured using an EVOS Cell Imaging System. The above procedures were performed in dark. ImageJ was used for analysis of fluorescence intensity.

2.2.8 Data presentation and analysis

Cell death was defined by PI positive cells as the percentage of Hoechst-stained cells in the same area. The increases in intracellular and mitochondrial Zn^{2+} levels, in response to indicated stimuli were defined by normalizing FluoZin-3 or RhodZin-3 fluorescence intensity in treated cells to the values in matched untreated cells. Inhibition of stimuli-induced Zn^{2+} increases by an inhibitor was defined as the relative fluorescence intensity in cells treated with the inhibitor to that in cells without treatment with the inhibitor. The changes of intracellular or mitochondrial Zn^{2+} concentrations during time-lapse recording were described by normalizing the fluorescence intensity at each time point to the value under basal conditions. The function of lysosomes or mitochondria was evaluated by the LysoTracker Red or MitoTracker Green fluorescent intensity at each condition related to the values in matched control cells. The co-localization of two fluorescent signals was quantified by Pearson's correlation coefficient as previously described (Dunn et al. 2011). The coefficient value varies between -1 to 1, with 1 being total positive correlation, 0 no correlation and -1 total negative correlation. Mitochondrial ROS production was

determined by normalizing the fluorescence intensity of MitoTracker Red-CMH_2Xros under indicated conditions to that in matched control cells.

Data were presented as mean ± standard error mean (S.E.M.), where appropriately. Numbers of cells used and numbers of independent experiments were indicated in figure legends. Statistical significance analyses were conducted using Student's *t*-test between two groups and ANOVA (analysis of variance) with post-hoc Tukey's test among multiple groups, with significance at the level of $P < 0.05$.

Chapter 3

Molecular mechanisms in H_2O_2-induced TRPM2-dependent hippocampal neuron death

3.1 Introduction

The hippocampus is crucial for learning and memory but represents one of the brain regions that are highly vulnerable to ischemia and reperfusion injury. Studies of ischemic stroke patients and rodent models of ischemia-reperfusion injury have revealed extraordinarily complicated mechanisms of brain damage due to ischemia and reperfusion (Deb et al., 2010; Doyle et al., 2008). It is well recognized that when oxygen becomes available during reperfusion following transient ischemia, it serves as a substrate for oxidation reactions, giving rise to the generation of excessive ROS and oxidative stress (Sanderson et al., 2013). In addition, increasing evidence supports an important role for oxidative stress-induced neuronal death in the pathogenesis of dementia-causing neurodegenerative conditions such as AD and PD (Zhu et al., 2007; Hwang, 2013). Thus, ROS-induced neuronal death represents a common mechanism contributing in neurodegeneration. ROS can cause oxidative damage to various biologically important molecules such as DNA (Uttara et al., 2009). PARPs, in particular PARP-1, are critical in the DNA damage repair process, during which ADPR is generated as a by-product (Dantzer et al., 2006). The TRPM2 channel, which is exclusively gated by ADPR (Perraud et al., 2001), has been increasingly recognized as an important oxidative stress sensor and as a key molecular mechanism responsible for ROS-induced cell death (Jiang et al., 2010; Miller, 2006). A good number of *in vivo* studies showed the activation of ROS-sensitive TRPM2 channel plays an important role in post-ischemic alterations in hippocampal neuronal death and cognitive dysfunction during reperfusion (Ye et al., 2014; Jia et al., 2011; Verma et al., 2012; Alim et al., 2013). In addition, a recent study disclosed an exclusive role for TRPM2 channel in reperfusion-induced increase in the $[Zn^{2+}]_i$ and a causative relationship of such intracellular Zn^{2+} elevation to post-ischemic neuronal death (Ye et al., 2014). However, mechanisms and signalling pathways of TRPM2-mediated

increase in the $[Zn^{2+}]_i$ leading to hippocampal neuronal death during reperfusion have not been fully recognised.

In this chapter, primary cultured mouse hippocampal neurons and H_2O_2, as an experimental paradigm of oxidative stress, were used to define molecular mechanisms and signalling pathways in TRPM2-mediated neuronal death during post-ischemia reperfusion. Results from genetic and pharmacological interventions showed that H_2O_2 induces lysosomal dysfunction, mitochondrial Zn^{2+} accumulation and ROS generation, axonal degeneration and the activation of PKC and NOX, and support mitochondrial TRPM2 channel as the nexus of such multiple molecular mechanisms and signalling pathways to form a vicious positive feedback loop and drive hippocampal neuronal death.

3.2 Results

3.2.1 Role of TRPM2 in H_2O_2-induced hippocampal neuron death

As reported in previous studies, hippocampal neurons are highly sensitive to ROS-induced injury (Wang and Michaelis, 2010). Exposure of hippocampal neurons to H_2O_2 at 30-300 μM for 2-24 hr induced concentration- and duration-dependent neuronal death as determined by PI staining assay (**Fig. 3.1**). Moreover, hippocampal neuron death induced by exposure to 300 μM H_2O_2 at 24 hr was significantly reduced by IM54 (**Fig. 3.2**), an inhibitor for necrosis, Ac-DVED-CMK (**Fig. 3.2**), an inhibitor for caspase-3-dependent apoptosis, and necrostatin-1 (**Fig. 3.2**), an inhibitor for necroptosis. The neuroprotective effects of these inhibitors suggested H_2O_2-induced hippocampal neuronal death occurs via multiple mechanisms including apoptosis, necrosis and necroptosis.

The immunofluorescent imaging showed strong TRPM2 immunoreactivity in hippocampal neurons (**Fig. 3.3a**), as previously reported (Ye et al., 2014). H_2O_2-induced neuronal death was significantly reduced by TRPM2-KO (**Fig. 3.3**) as well as by treatment with PJ34, a PARP inhibitor that as discussed in the Introduction chapter is known to suppress ROS-induced TRPM2 activation, prior and during exposure to H_2O_2 (**Fig. 3.3**). The above pharmacological and genetic intervention results provide strong evidence to confirm a significant role for the TRPM2 channel activation in H_2O_2-induced hippocampal neuron death. H_2O_2-induced hippocampal neuron death was significantly attenuated in the culturing medium added with 5 mM EGTA to remove extracellular Ca^{2+} as compared to that in normal culturing medium containing Ca^{2+} (**Fig. 3.3**), supporting a role for TRPM2 channel-mediated Ca^{2+} influx in inducing H_2O_2-induced neuronal death as previously reported in cortical neurons (Kaneko et al., 2006). Furthermore, H_2O_2-induced neuronal death was inhibited, to great extent, by treatment with 1 μM TPEN, a selective Zn^{2+} chelator (**Fig. 3.3**), consistent with the recent study showing that TRPM2-KO prevented reperfusion-induced increase in the $[Zn^{2+}]_i$ and post-ischemic neuronal death (Ye et

al., 2014). Therefore, increases in the $[Zn^{2+}]_i$ and $[Ca^{2+}]_i$ are critical in oxidative stress-induced hippocampal neuron death.

3.2.2 H_2O_2-induced TRPM2-dependent increase in the $[Zn^{2+}]_i$

Single cell confocal imaging using FluoZin3, a fluorescent indicator for free or labile Zn^{2+} (see section **2.2.3.1** in the Materials and Methods chapter), was performed to investigate the intracellular Zn^{2+} and its concentration changes in hippocampal neurons in response to H_2O_2, and the relationship to TRPM2 channel activation and TRPM2-mediated Ca^{2+} influx. In untreated neurons, there was a very low but discernible level of free Zn^{2+} that was predominantly present in puncta or vesicles (**Fig. 3.4**). Exposure to H_2O_2 gave rise to a massive increase in the $[Zn^{2+}]_i$ (**Fig. 3.4**), which was largely abolished by TRPM2-KO (**Fig. 3.4**), and also significantly reduced by treatment with PJ34 (**Fig. 3.4**), as well as treatment with the TRPM2 channel inhibitor 2-APB (**Fig. 3.4**). As anticipated, such H_2O_2-evoked Zn^{2+} response was prevented by treatment with TPEN (**Fig. 3.4**). Intriguingly, H_2O_2-induced increase in the $[Zn^{2+}]_i$ was completely lost in extracellular Ca^{2+}-free solution (**Fig. 3.4**). Taken together, these results support that TRPM2 channel activation and TRPM2-mediated Ca^{2+} influx stimulates H_2O_2-induced increase in the $[Zn^{2+}]_i$.

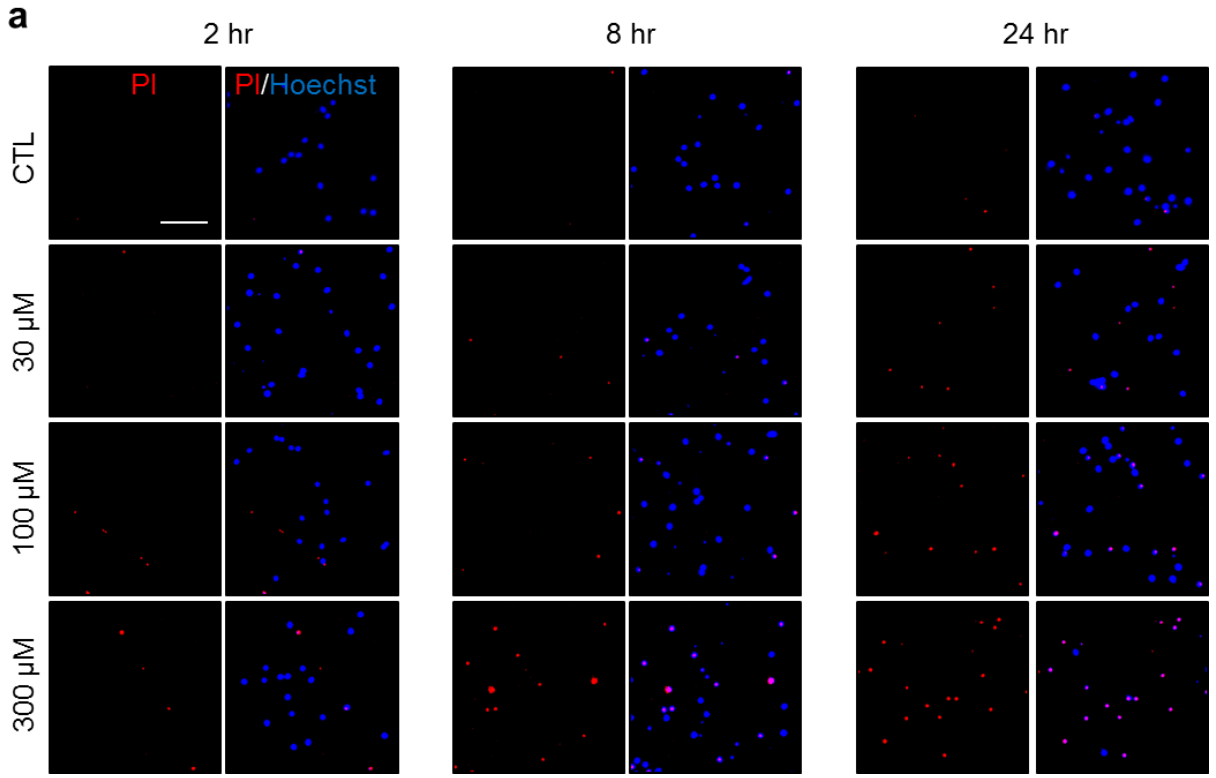
a
2 hr
8 hr
24 hr
PI
PI/Hoechst
CTL
30 μM
100 μM
300 μM

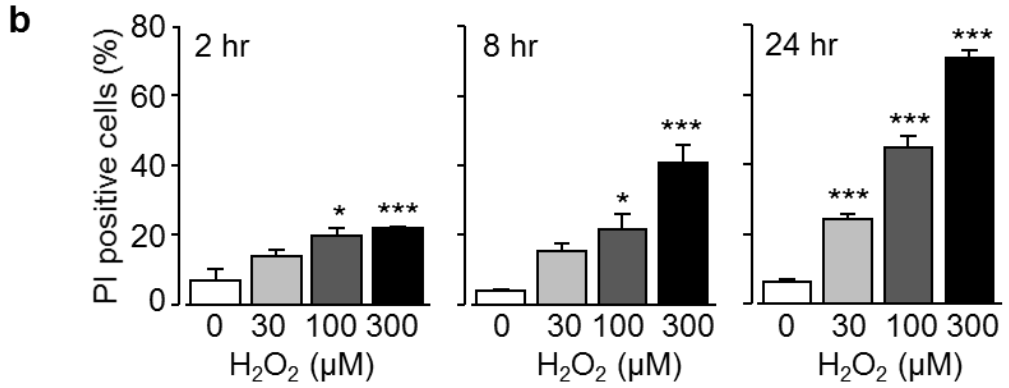

Figure 3.1 H_2O_2 induces death of primary cultured hippocampal neurons

(**a**) Representative PI staining images of cultured WT hippocampal neurons treated with indicated concentrations of H_2O_2 for 2 (*left panel*), 8 (*middle panel*) or 24 hr (*right panel*). Each panel consists of PI staining images showing dead cells (red color) and merged Hoechst (blue color)/PI staining image showing nuclei and dead cells. Scale bar is 100 μm. (**b**) The mean percentage of PI positive cells at indicated conditions from 3-8 independent experiments (350-500 cells for each independent experiment). *, $P < 0.05$ and ***, $P < 0.001$ indicate significant difference relative to untreated control.

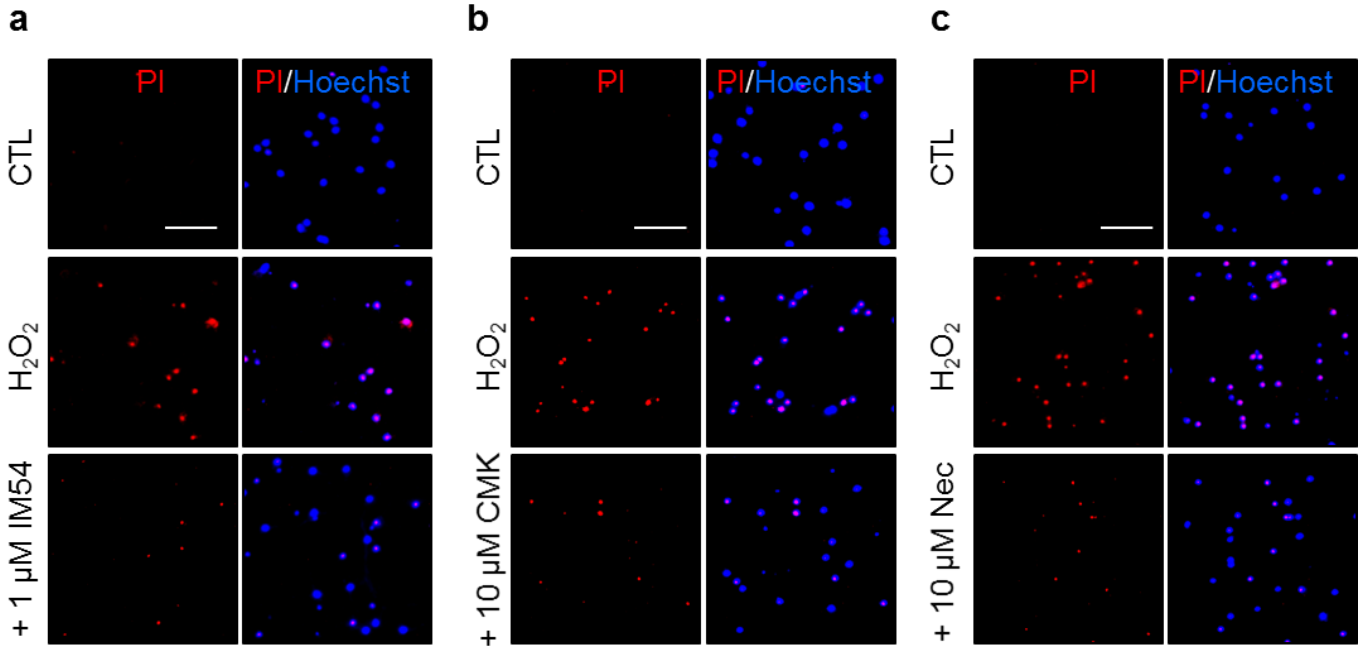
a
b
c
PI
PI/Hoechst
CTL
H2O2
+ 1 μM IM54
+ 10 μM CMK
+ 10 μM Nec

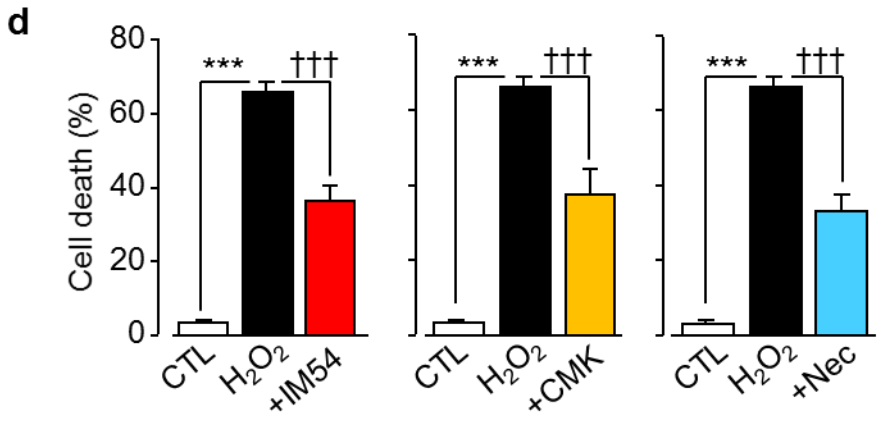

Figure 3.2 H_2O_2 induces hippocampal neuron death through multiple pathways

(**a-c**) Representative PI and PI/Hoechst staining images of WT cultured hippocampal neurons. The untreated control cells (CTL), or cells treated with 300 µM H_2O_2 alone for 24 hr, or pre-treated with 1 µM IM54 (**a**), 10 µM Ac-DVED-CMK (CMK) (**b**) or 10 µM necrostatin-1 (Nec) (**c**) 30 min before and during applying H_2O_2. Each panel consists of PI staining images showing cells, merged PI/Hoechst staining showing nuclei and dead cells. Scale bar is 100 µm. (**d**) Summary of the mean percentage of PI positive cells at indicated conditions from 3 independent experiments (350-500 cells for each independent experiment). ***, $P < 0.001$ indicates significant difference relative to control and †††, $P < 0.001$ represent significant difference in comparison with cells exposed to H_2O_2 alone.

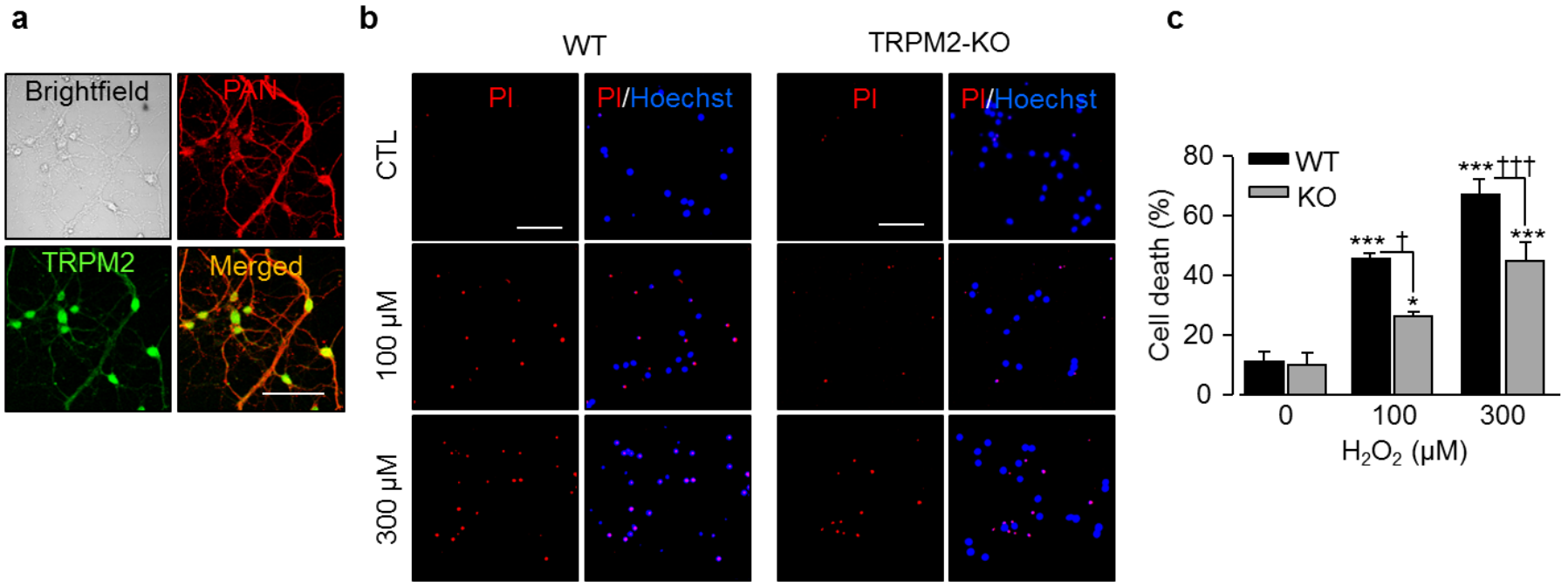
a
Brightfield
PAN
TRPM2
Merged
b
WT
TRPM2-KO
PI
PI/Hoechst
CTL
100 μM
300 μM
c
WT
KO
Cell death (%)
80
60
40
20
0
***
†
*
***
†††
***
0
100
300
H2O2 (μM)

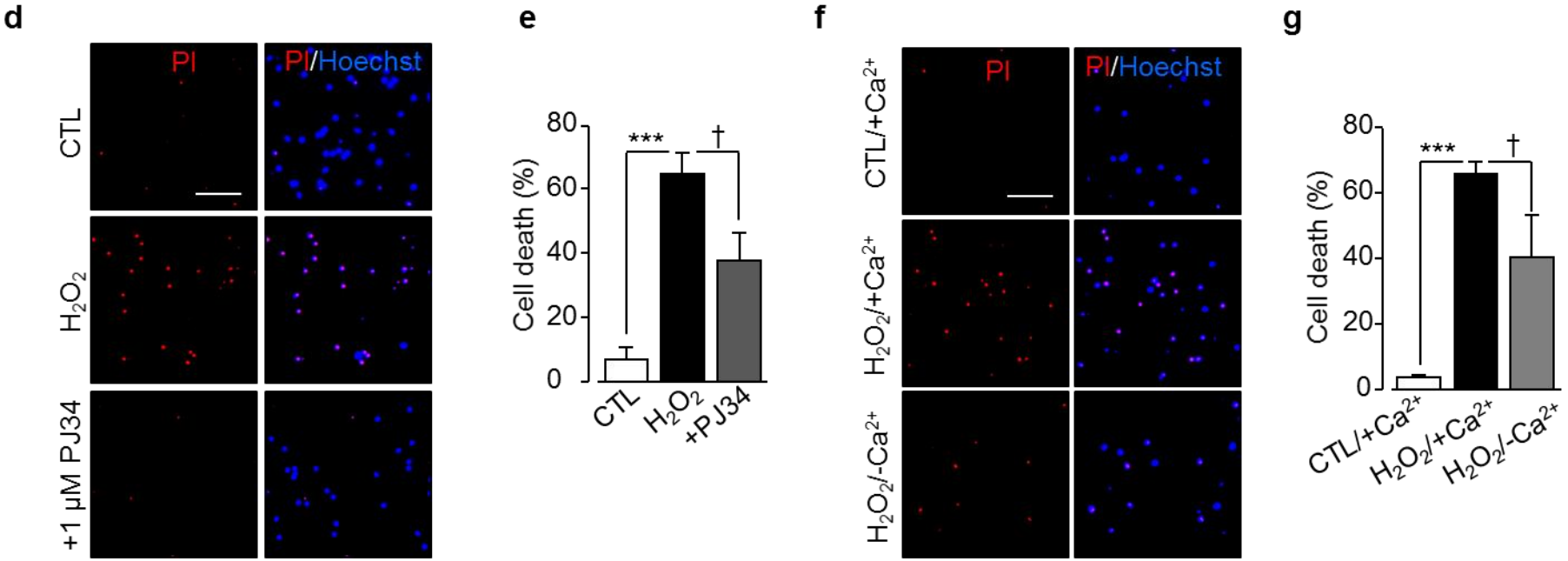
d
PI
PI/Hoechst
CTL
H2O2
+1 μM PJ34
e
Cell death (%)
80
60
40
20
0
***
†
CTL
H2O2
+PJ34
f
PI
PI/Hoechst
CTL/+Ca2+
H2O2/+Ca2+
H2O2/-Ca2+
g
Cell death (%)
80
60
40
20
0
***
†
CTL/+Ca2+
H2O2/+Ca2+
H2O2/-Ca2+

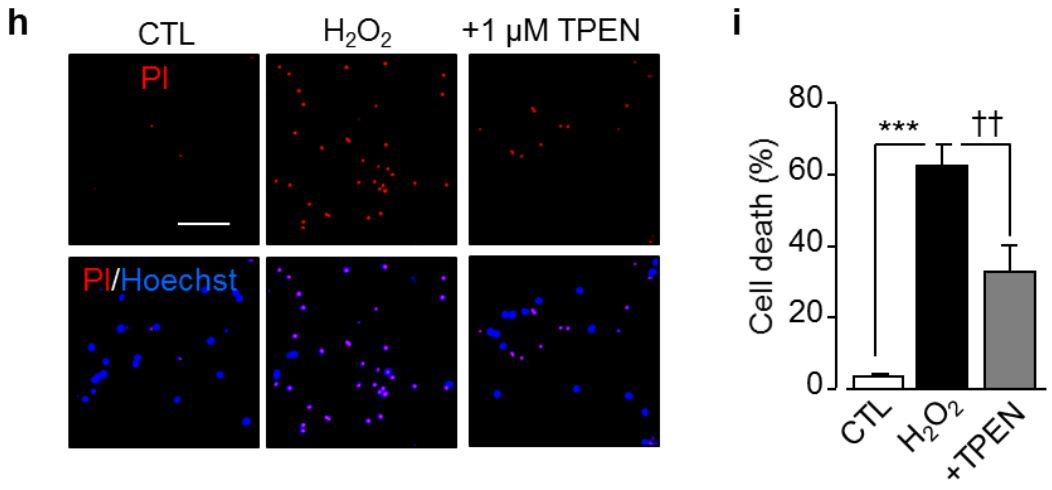

Figure 3.3 H_2O_2 induces TRPM2-dependent hippocampal neuron death

(**a**) Representative confocal images showing TRPM2 immunostaining (green) in cultured hippocampal neurons labelled with Pan neuronal marker antibody (red). Similar results were observed in 3 independent experiments with each experiment examining 45-70 neurons. Scale bar is 100 μm. (**b**) Representative images showing PI and PI/Hoechst staining in cultured hippocampal neurons from WT and TRPM2-KO neurons exposed to 100 or 300 μM for 24 hr in addition to untreated control conditions (CTL). Scale bar is 100 μm. (**c**) Summary of the percentage of PI positive neurons under indicated conditions, from 4-5 independent experiments with each experiment examining 350-550 neurons. Black and grey bars represent the percentage of cell death in WT and TRPM2-KO neurons, respectively. *, $P < 0.05$ and ***, $P < 0.001$ indicate significant difference from respective untreated neurons. †, $P < 0.05$ and †††, $P < 0.001$ represent significant difference between WT and TRPM2-KO neurons under the same treatment. (**d, f** and **h**) Representative images showing PI and PI/Hoechst staining in hippocampal neurons treated with 1 μM PJ34 (**d**), 5 mM EGTA (**f**) or 1 μM TPEN (**h**) prior to and during exposure to 300 μM H_2O_2 for 24 hr. Scale bar is 100 μm. (**e**, **g** and **i**) Summary of the mean percentage of PI positive neurons at each indicated condition, from 4-5 independent experiments with each experiment examining 350-550 neurons. ***, $P < 0.001$ indicates significant difference from untreated control. †, $P < 0.05$ and ††, $P < 0.01$, indicate difference with neurons exposed to H_2O_2 alone.

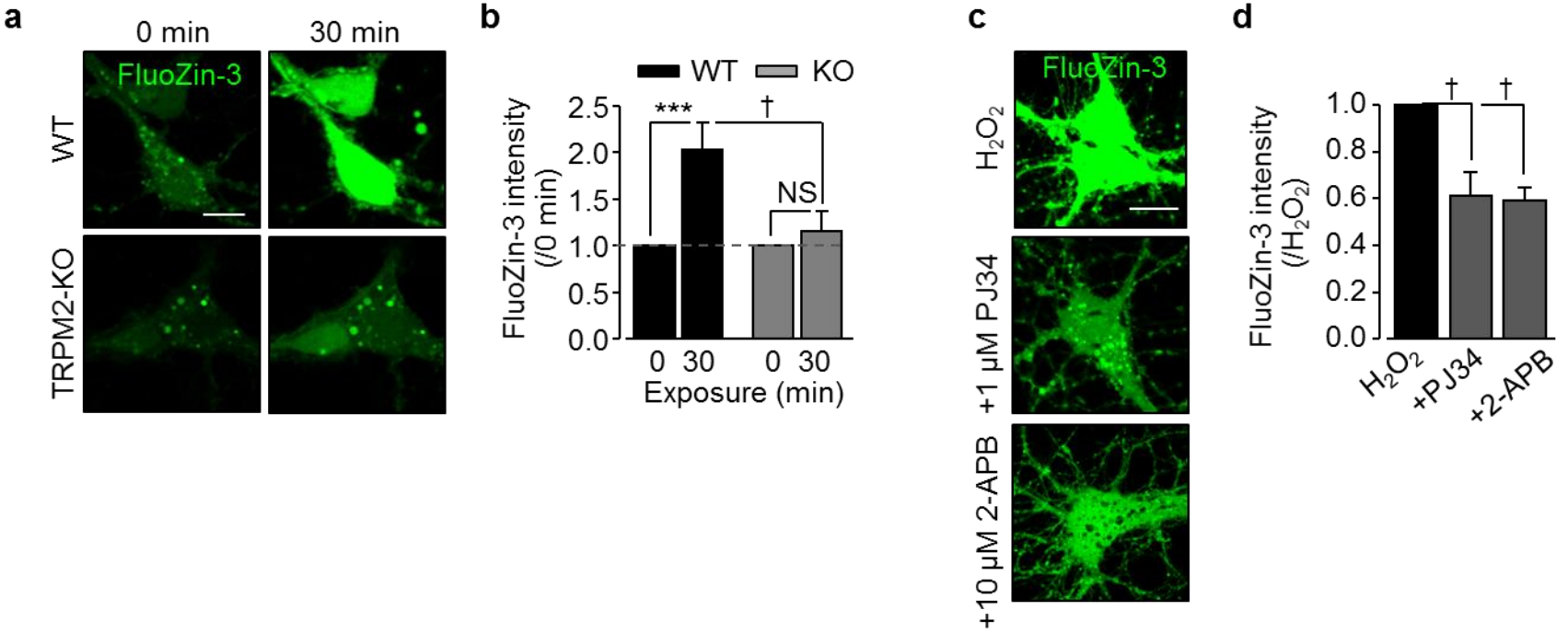
a
0 min
30 min
FluoZin-3
WT
TRPM2-KO
b
WT
KO
FluoZin-3 intensity (/0 min)
2.5
2.0
1.5
1.0
0.5
0.0
***
†
NS
0 30 0 30
Exposure (min)
c
FluoZin-3
H2O2
+1 μM PJ34
+10 μM 2-APB
d
FluoZin-3 intensity (/H2O2)
1.0
0.8
0.6
0.4
0.2
0.0
†
†
H2O2
+PJ34
+2-APB

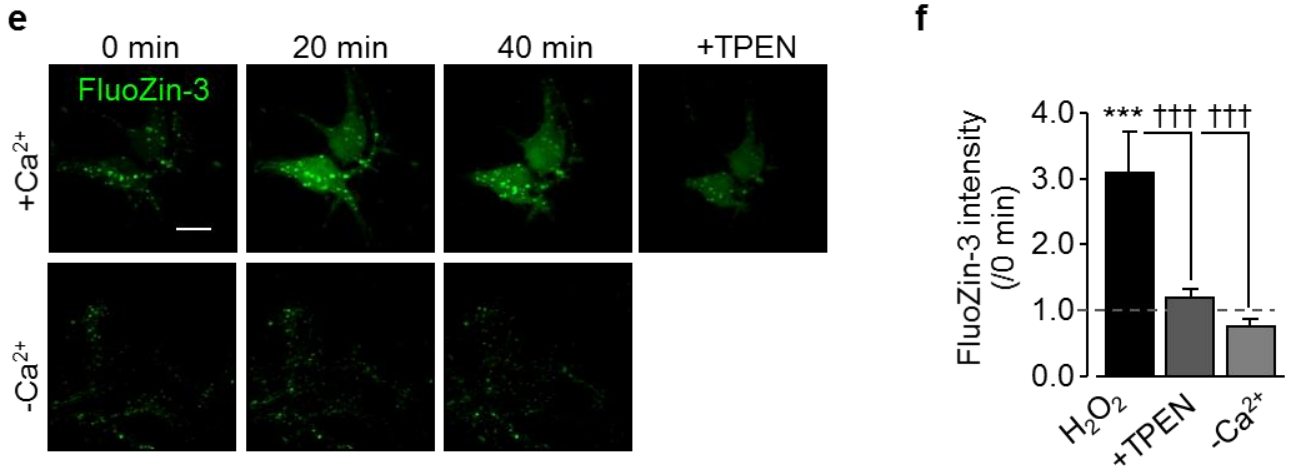

Figure 3.4 H_2O_2 induces TRPM2-dependent increase in the $[Zn^{2+}]_i$

(**a**) Representative confocal time-lapse images showing the FluoZin-3 (green) staining of WT and TRPM2-KO hippocampal neurons before and after exposed to 300 μM H_2O_2 for 30 min. Scale bar is 10 μm. (**b**) Mean of normalized fluorescent intensity of FluoZin-3 under indicated conditions, from 40 cells of 9-11 independent experiments. All values are relative to the basal condition for each type of neurons. ***, $P < 0.001$ indicates significant difference relative to the basal level, and †, $P < 0.05$ for the comparison between WT and TRPM2-KO neurons. NS stands for no significance. (**c**) Representative confocal images showing FluoZin-3 fluorescence in hippocampal neurons treated with 300 μM H_2O_2 for 30 min or pre-treated with 1 μM PJ34 or 10 μM 2-APB 30 min prior to and during exposure to H_2O_2. (**d**) Summary of the mean FluoZin-3 fluorescence intensity in neurons at indicated condition relative to cells exposed to 300 μM H_2O_2 alone. The means were acquired from 4-5 independent experiments and 20-25 cells for each independent experiment. †, $P < 0.05$ indicates significant difference relative to cells treated with H_2O_2 alone. (**e**) Representative images showing time-lapse recording of the $[Zn^{2+}]_i$ in cultured neurons exposure to H_2O_2 at indicated duration in Ca^{2+} containing or Ca^{2+}-free buffer, and TPEN was applied to Ca^{2+}-containing medium at the end of the recording. (**f**) Mean of normalized fluorescent intensity of FluoZin-3. All values were normalized to the basal condition in the presence of Ca^{2+}. ***, $P < 0.001$ indicates significant difference with untreated control; †††, $P < 0.001$ indicates significant difference with H_2O_2 treated cell in the presence of Ca^{2+} (**e-f** are contributed by Dr. Yang Wei).

3.2.3 H_2O_2-induced TRPM2-dependent lysosomal dysfunction and mitochondrial Zn^{2+} accumulation

Further single cell confocal imaging was conducted, using FluoZin-3 in combination with intracellular organelle specific fluorescent markers, to better understand H_2O_2-induced change in the intracellular Zn^{2+} homeostasis. Double labelling revealed that a majority of Zn^{2+} puncta or vesicles in untreated hippocampal neurons from both WT and TRPM2-KO mice exhibited considerable co-localization with LysoTracker (**Fig. 3.5**), suggesting primarily lysosomal location. Exposure to H_2O_2 induced substantial loss of LysoTracker fluorescence as well as an increase in the $[Zn^{2+}]_i$ (**Fig. 3.5**). Such H_2O_2-induced increase in the $[Zn^{2+}]_i$ and lysosomal dysfunction were not observed in TRPM2-KO neurons (**Fig. 3.5**), pointing out a critical role for TRPM2 channel. Moreover, the co-localization of lysosomes and Zn^{2+} were substantially decreased in WT hippocampal neurons but not in TRPM2-KO neurons after exposure to H_2O_2 (**Fig. 3.5**). In contrast with LysoTracker, there was little or poor co-localization of Zn^{2+} puncta and MitoTracker Red in untreated neurons (**Fig. 3.5**) and H_2O_2 strongly enhanced the co-localization of Zn^{2+} puncta with MitoTracker Red (**Fig. 3.5**). Such H_2O_2-induced increase in mitochondrial Zn^{2+} was also eliminated by TRPM2-KO (**Fig. 3.5**). Collectively, these results provide evidence to show that H_2O_2-induced TRPM2 channel activation gives rise to an increase in the $[Zn^{2+}]_i$, lysosomal dysfunction, and mitochondrial Zn^{2+} accumulation.

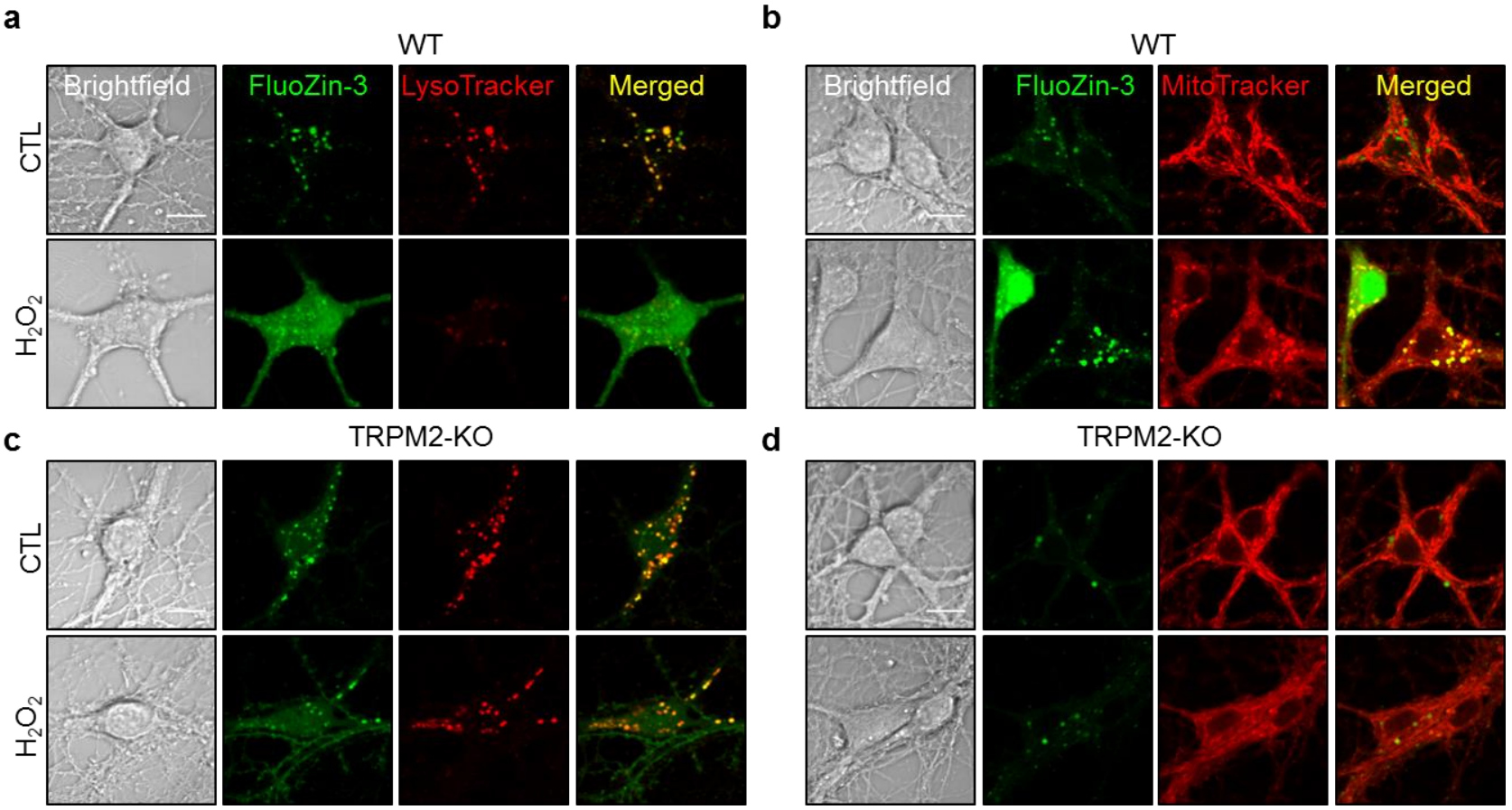
a
WT
Brightfield
FluoZin-3
LysoTracker
Merged
CTL
H2O2
b
WT
Brightfield
FluoZin-3
MitoTracker
Merged
c
TRPM2-KO
CTL
H2O2
d
TRPM2-KO

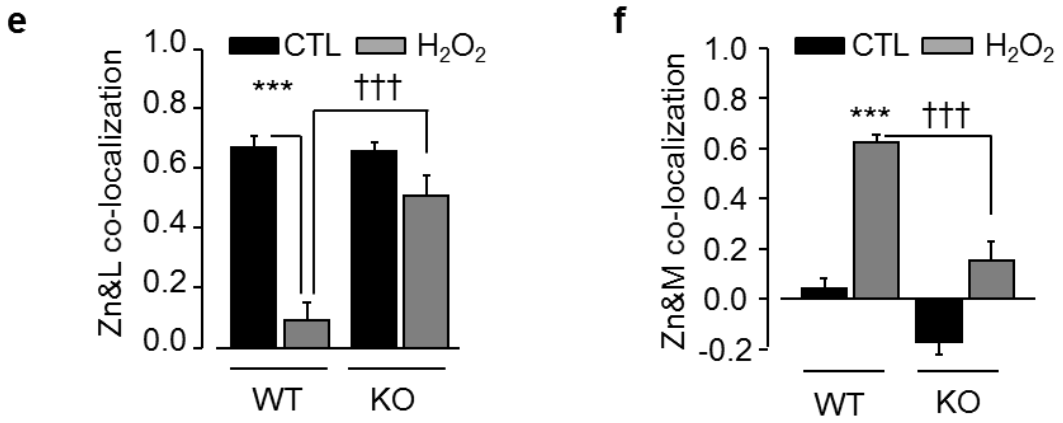

Figure 3.5 TRPM2 channel in H_2O_2-induced lysosomal dysfunction and Zn^{2+} release and mitochondrial Zn^{2+} accumulation

(**a, c**) Representative confocal images showing FluoZin-3 (green) and LysoTracker (red), and their co-localization in merged images in WT or TRPM2-KO hippocampal neurons untreated (CTL), or treated with 300 μM H_2O_2 for 30 min. Scale bar is 10 μm. (**b, d**) Representative confocal images showing FluoZin-3 and MitoTracker Red, and their co-localization in merged images in WT or TRPM2-KO hippocampal neurons untreated (CTL), or treated with 300 μM H_2O_2 for 30 min. Scale bar is 10 μm. (**e**-**f**) Quantification of the mean value of Pearson's correlation coefficient of the intracellular Zn^{2+} and lysosomes (**e**) or mitochondria (**f**) from 3 independent experiments (12-18 cells of each independent experiment). Black bars and grey bars indicate the values in WT or TRPM2-KO hippocampal neurons respectively. ***, $P < 0.001$ indicates significant difference relative to control, and †††, $P < 0.001$ for the comparison between WT and TRPM2-KO neurons.

3.2.4 H_2O_2-indued TRPM2-dependent mitochondrial morphological changes

It was noticeable from single cell confocal imaging using MitoTracker that exposure to H_2O_2 induced strong changes in mitochondrial morphology (**Fig. 3.5b**). Staining with MitoTracker Green, a fluorescent indicator with no or weak dependence of mitochondrial membrane potential (see section **2.2.3.1** in the Materials and Methods chapter) was performed to characterize H_2O_2-induced effects on mitochondrial morphology in hippocampal neurons. Exposure to H_2O_2 led to a significant reduction in MitoTracker Green fluorescence (**Fig. 3.6**). Mitochondria exhibited typical, tubular morphology in untreated neurons and became markedly fragmented in neurons after exposed to H_2O_2 (**Fig. 3.6**). This was further shown in quantitative analysis that both form factor and aspect ratio, two parameters widely used to describe mitochondrial morphology (see section **2.2.3.3** in the Materials and Methods chapter), were significantly reduced (**Fig. 3.6**). Immunofluorescence imaging was used to examine the release of Cyt-c, an indicative of cell death (discussed in section **1.4.1.1** in the Introduction chapter) in hippocampal neurons. Exposure to H_2O_2 at 100-300 μM for 2-24 hr induced considerable Cyt-c release in a concentration- and duration-dependent manner (**Fig. 3.6**). All H_2O_2-induced mitochondrial effects, that is, the reduction in MitoTracker Green fluorescence, change in the mitochondrial morphology and Cyt-c release, were virtually abolished by TRPM2-KO (**Fig. 3.6**), revealing a key role for TRPM2 channel.

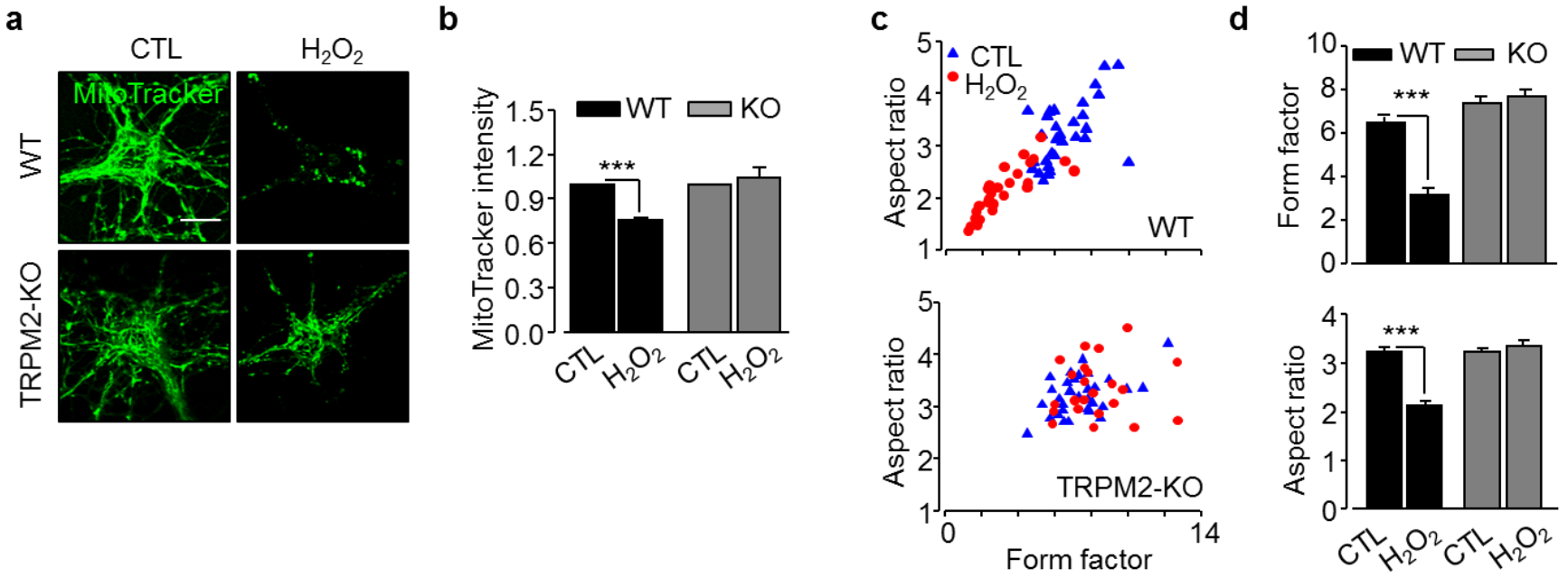
a
CTL
H2O2
MitoTracker
WT
TRPM2-KO
b
MitoTracker intensity
WT
KO
***
CTL
H2O2
c
Aspect ratio
CTL
H2O2
WT
TRPM2-KO
Form factor
d
Form factor
Aspect ratio
WT
KO
***

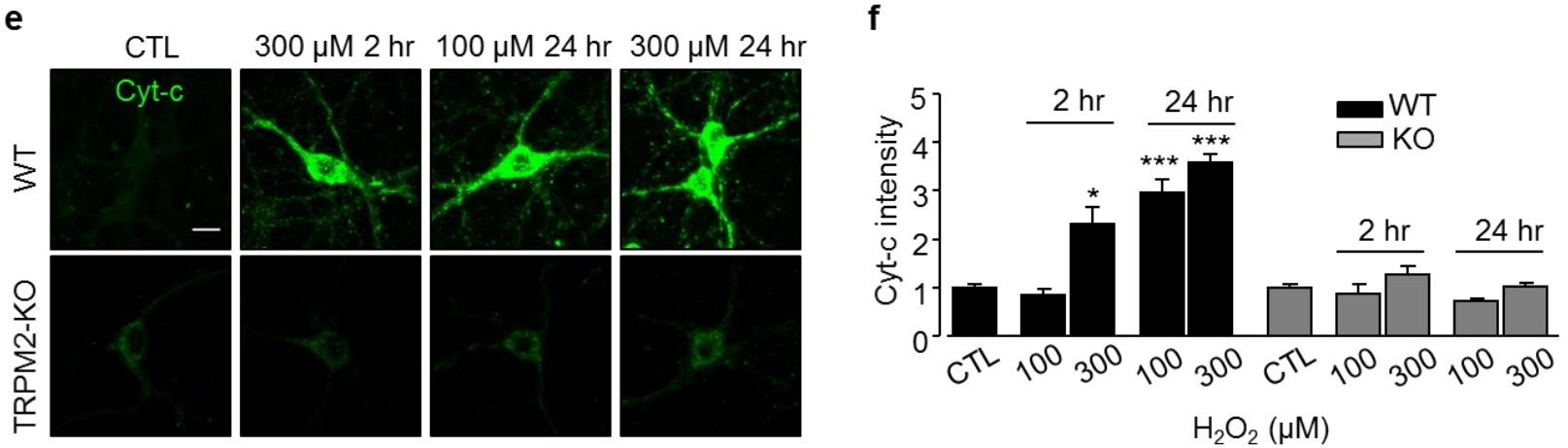

Figure 3.6 TRPM2 channel involves in H_2O_2-induced mitochondrial dysfunction

(**a**) Representative confocal images showing the MitoTracker Green fluorescence in WT or TRPM2-KO hippocampal neurons at basal condition (CTL) or treated with 300 μM H_2O_2 for 30 min. Scale bar is 10 μm. (**b**) Summary of normalized mean fluorescent intensity of MitoTracker in WT and TRPM2-KO neurons at indicated conditions from 3 independent experiments (10-12 cells in each independent experiment). All values were normalized to the basal level in each cell type. ***, $P < 0.001$, compared to the control in each cell type. (**c**) The computer-assisted morphology analyses of mitochondria at indicated conditions. The form factor and aspect ratio were quantified and plotted against each other. Blue triangles indicate the untreated control neurons (CTL); red circles represent neurons exposed to 300 μM H_2O_2 for 30 min. (**d**) Mean values of form factor (*top*) and aspect ratio (*bottom*) of neurons as shown from 3 independent experiments (10-12 cells for each independent experiment). Black bars and grey bars represent WT and TRPM2-KO hippocampal neurons respectively. ***, $P < 0.001$, compared to the control neurons in each type of cells. (**e**) The immunofluorescent staining images showing the expression of Cyt-c in WT (*top*) and TRPM2-KO (*bottom*) neurons at indicated conditions. Scale bar is 10 μm. (**f**) Normalized mean fluorescent intensity of anti-Cyt-c immunofluorescence from 3-4 independent experiments (15-25 cells for each independent experiment). The value at each indicated condition was relative to the untreated control neurons (CTL).*, $P < 0.05$ and ***, $P < 0.001$ indicate significant difference relative to untreated neurons.

3.2.5 H_2O_2-induced TRPM2-dependent ROS generation

Further experiments were carried out to examine whether mitochondrial Zn^{2+} accumulation stimulated mitochondrial ROS generation in hippocampal neurons, using MitoTracker-Red CM-H_2Xros (MitoROS), a fluorescent indicator for mitochondrial ROS generation. Exposure to 100-300 μM H_2O_2 resulted in a strong increase in MitoROS fluorescence in WT neurons, indicating enhanced mitochondrial ROS generation (**Fig. 3.7**). Such mitochondrial ROS generation was effectively inhibited by treatment with TPEN (**Fig. 3.7**), consistent with the notion that mitochondrial Zn^{2+} accumulation induces mitochondrial ROS generation (Clausen et al., 2013). Furthermore, H_2O_2-induced mitochondrial ROS generation was prevented by TRPM2-KO or treatment with PJ34 and 2-APB to inhibit TRPM2 channel activation or function (**Fig. 3.7**). Taken together, these results support mitochondrial ROS generation depends on H_2O_2-induced TRPM2 channel activation and mitochondrial Zn^{2+} accumulation.

3.2.6 Bafilomycin A1-induced TRPM2-dependent effects on mitochondria

According to the above results, it is a reasonable assumption that H_2O_2-induced lysosomal dysfunction gives rise to an increase in the mitochondrial Zn^{2+} accumulation and mitochondrial ROS generation. To address this, bafilomycin A1, the V-type H^+-ATPase inhibitor which interferes with the proton gradient responsible for Ca^{2+}/Zn^{2+} sequestration into lysosomes, was used (Collins et al., 2011). Exposure to 100 nM bafilomycin A1 induced a strong increase in the mitochondrial Zn^{2+} accumulation in WT hippocampal neurons (**Fig. 3.8**). In contrast, such an increase in the mitochondrial Zn^{2+} level was abolished by TRPM2-KO (**Fig. 3.8**), and also effectively prevented by treatment with PJ34 or 2-APB (**Fig. 3.8**). Moreover, bafilomycin A1 stimulated mitochondrial ROS generation in WT neurons, but not in TRPM2-KO neurons (**Fig. 3.8**). These results consistently support that

lysosomal dysfunction leads to the mitochondrial Zn^{2+} accumulation and mitochondrial ROS production.

3.2.7 The functional role of TRPM2 in mitochondrial Zn^{2+} uptake

An intriguing and important question arose from the experiments described above, regarding molecular mechanisms responsible for the Zn^{2+} entry into mitochondria. The findings that bafilomycin A1- and H_2O_2-indued mitochondrial Zn^{2+} accumulation exhibited strong TRPM2-dependence (**Fig. 3.4-3.8**) point to a role for the TRPM2 channel in mediating the mitochondrial Zn^{2+} accumulation. The immunofluorescence confocal imaging revealed significant co-localization of the TRPM2 immunoreactivity with MitoTracker Red in hippocampal neurons (**Fig. 3.9**). To demonstrate a functional role for TRPM2 channel in the mitochondrial Zn^{2+} accumulation, Zn^{2+} uptake into isolated mitochondria from WT and TRPM2-KO hippocampal neurons was examined. The addition of Zn^{2+} in Ca^{2+}-containing solutions used to suspend isolated mitochondria led to a significant increase in the mitochondrial Zn^{2+} level, which was further elevated by the addition of ADPR (**Fig. 3.9**). In contrast, there was no such Zn^{2+} increase in mitochondria isolated from TRPM2-KO neurons (**Fig. 3.9**). These results are in support of the mitochondrial expression of TRPM2 channel and its importance in mediating mitochondrial Zn^{2+} accumulation. Consistently with Ca^{2+} being critically required for ADPR-induced TRPM2 channel activation, ADPR-induced Zn^{2+} increase in isolated mitochondria was not observed in the Ca^{2+}-free solution (**Fig. 3.9**). Such findings provided additional support for the functional expression of TRPM2 in mitochondria, and furthermore, show a critical requirement for plasma membrane TRPM2 channel-mediated Ca^{2+} influx as described above for H_2O_2-induced neuronal death (**Fig. 3.3**) and increase in the $[Zn^{2+}]_i$ (**Fig. 3.4**).

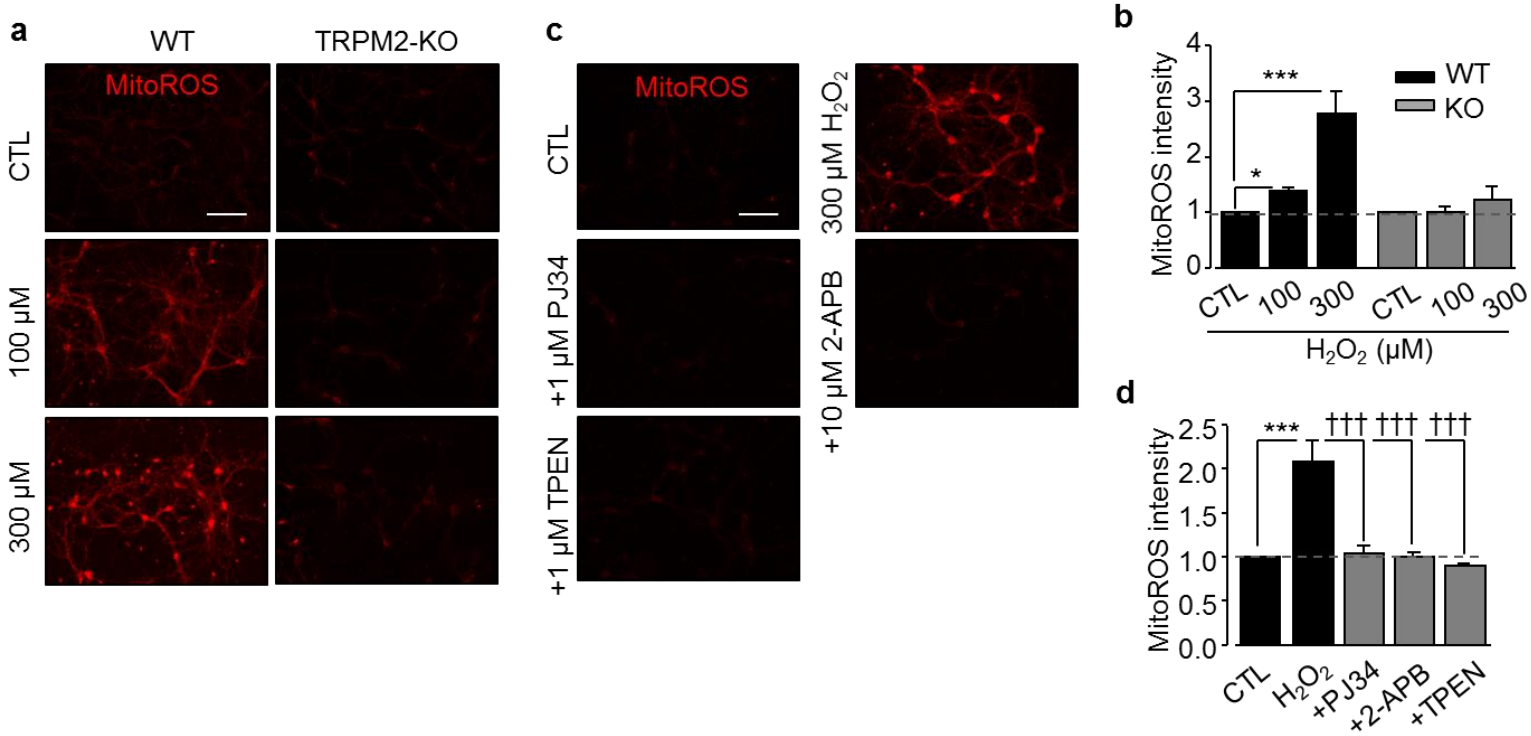

Figure 3.7 H_2O_2-induced mitochondrial ROS production in hippocampal neuron is TRPM2-dependent

(**a**, **c**) Fluorescence images of MitoTracker Red CM-H_2Xros (MitoROS) showing mitochondrial ROS production in WT or TRPM2-KO hippocampal neurons. Cells were treated by 100 µM or 300 µM H_2O_2 at indicated concentrations for 2 hr or pre-treated with 1 µM PJ34, 10 µM 2-APB or 1 µM TPEN 30 min before adding 300 µM H_2O_2. Scale bar is 100 µm. (**b**, **d**) Normalized mean of MitoROS fluorescence intensity from 3-5 independent experiments (35-70 cells for each independent experiment). *, $P < 0.05$ and ***, $P < 0.001$ indicate significant difference relative to untreated control cells (CTL); †††, $P < 0.001$ for comparison with cells exposed to 300 µM H_2O_2 for 30 min.

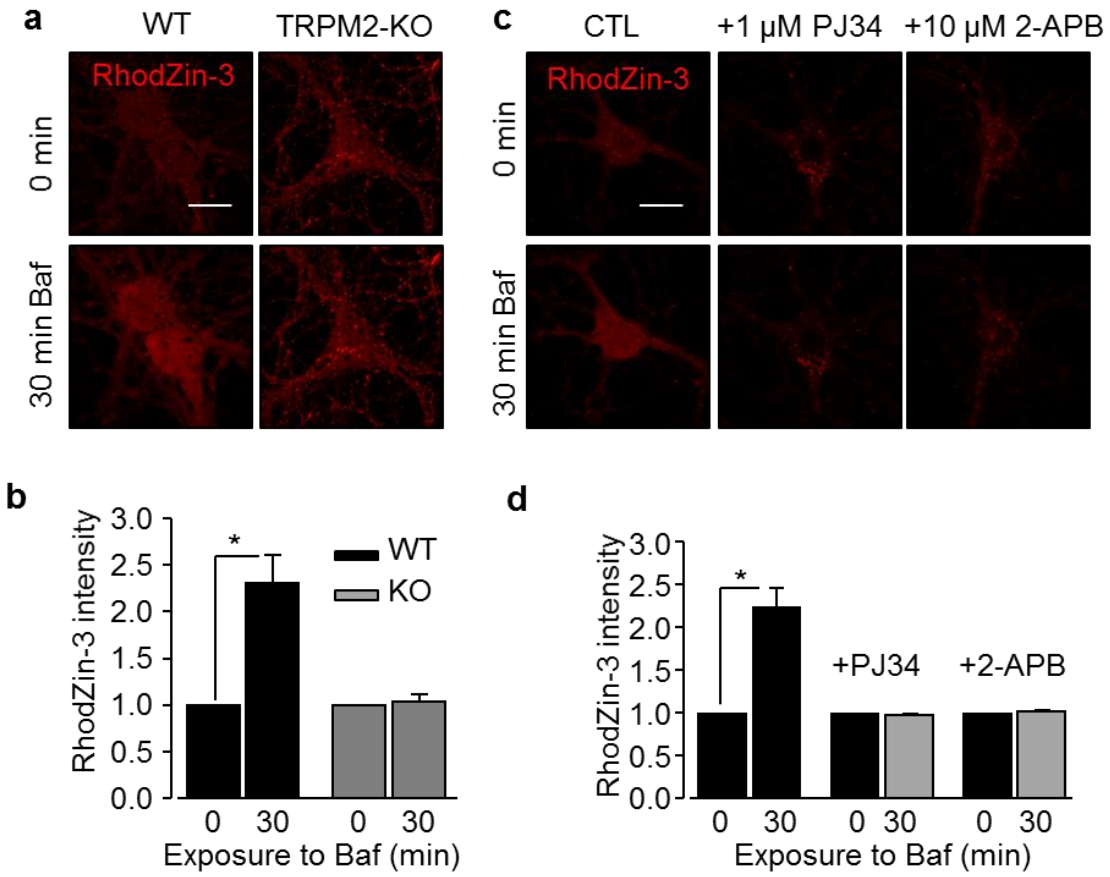
a
WT
TRPM2-KO
RhodZin-3
0 min
30 min Baf
c
CTL
+1 μM PJ34
+10 μM 2-APB
RhodZin-3
0 min
30 min Baf
b
RhodZin-3 intensity
3.0
2.5
2.0
1.5
1.0
0.5
0.0
*
WT
KO
0
30
0
30
Exposure to Baf (min)
d
RhodZin-3 intensity
3.0
2.5
2.0
1.5
1.0
0.5
0.0
*
+PJ34
+2-APB
0
30
0
30
0
30
Exposure to Baf (min)

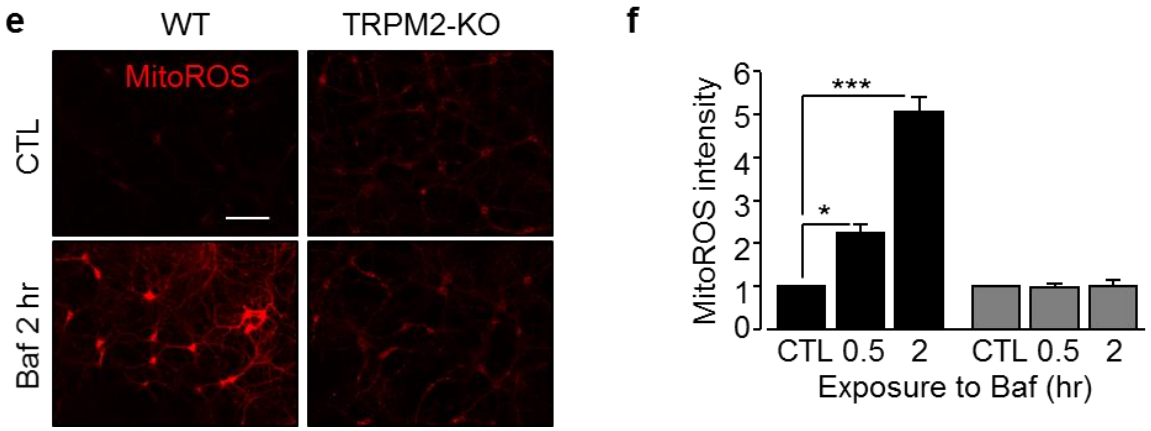

Figure 3.8 Bafilomycin A1 induces TRPM2-dependent mitochondrial Zn^{2+} accumulation and excessive mitochondrial ROS generation

(**a**, **c**) The time-lapse recording of RhodZin-3 fluorescence intensity during 30 min exposure to 100 nM bafilomycin A1 (Baf) in WT and TRPM2-KO hippocampal neurons (**a**), or WT neurons under control (CTL) and treatment with 1 μM PJ34 or 10 μM 2-APB (**c**). Scale bar is 10 μm. (**b**, **d**) Summary of the mean RhodZin-3 fluorescence intensity under indicated conditions, normalized to the basal level (0 min), from 3 independent experiments with each experiment examining 3 petri-dishes. *, $P < 0.05$ indicates difference from the basal level. (**e**) Representative images showing MitoROS fluorescence in WT and TRPM2-KO hippocampal neurons under untreated control (CTL) or after exposure to 100 nM bafilomycin A1 for 2 hr. Scale bar is 100 μm. (**f**) Summary of the mean MitoROS fluorescence intensity under indicated conditions, normalized to that in neurons under control conditions, from 3-5 independent experiments with each examining 40-70 neurons. *, $P < 0.05$ and ***, $P < 0.001$ indicate difference from neurons under control conditions.

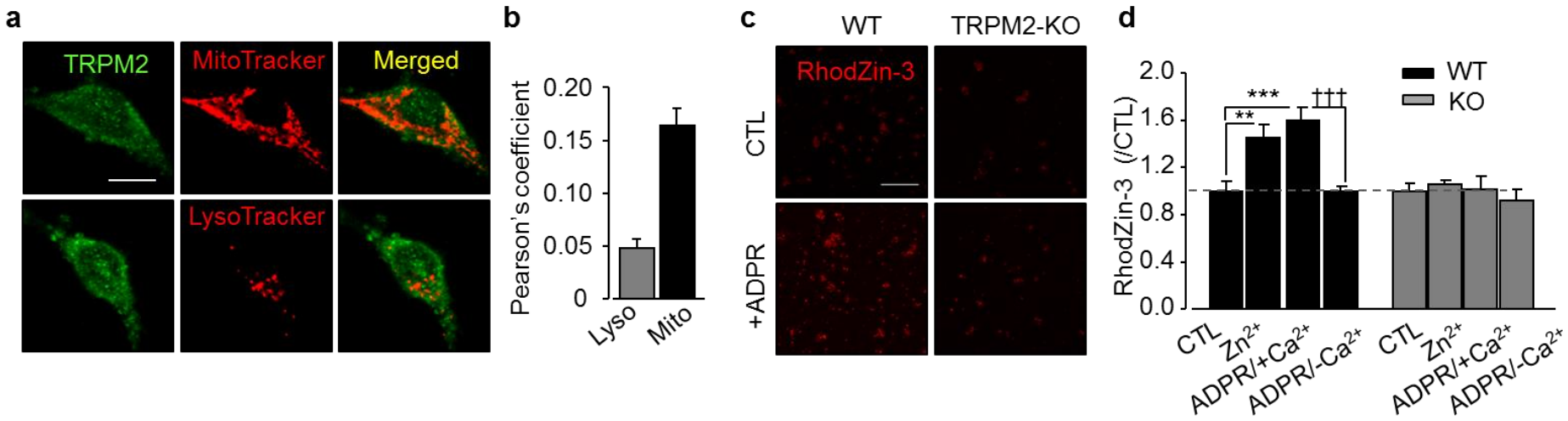

Figure 3.9 TRPM2 channel is required for the Zn^{2+} accumulation in isolated mitochondria

(**a**) Representative confocal images showing TRPM2 immunofluorescent staining (green) with LysoTracker or MitoTracker (red) in hippocampal neurons. Scale bar is 10 µm. (**b**) Summary of the mean Pearson's correlation coefficient, from 3 independent experiments each examining 10-15 neurons. (**c**) Representative images showing RhodZin-3 staining in isolated mitochondria from WT and TRPM2-KO hippocampal neurons under control (CTL) or the treatment with 5 mM ADPR and 30 µM Zn^{2+}. Scale bar is 20 µm. (**d**) Summary of the mean RhodZin-3 fluorescence intensity in isolated mitochondria under indicated conditions normalized to that under untreated control conditions (CTL), from 5 independent experiments each examining mitochondrial preparation from $2x10^6$ neurons. **, $P < 0.01$ and ***, $P < 0.001$ indicate difference from that under control. †††, $P < 0.001$ indicates difference from neurons exposed to Zn^{2+} and ADPR in solutions containing 1.5 mM or no Ca^{2+}.

3.2.8 TRPM2-dependent role of NCX and MCU in H_2O_2-induced mitochondrial ROS generation and neuronal death

As discussed in the Introduction chapter (see section **1.2.2**), the mitochondrial NCX and MCU have been shown to mediate in oxidative stress-induced alteration in the mitochondrial Ca^{2+} homeostasis (Rizzuto et al., 2012) and neuronal death (Cali et al., 2012). Evidence also exists that they are involved in regulating the mitochondrial Zn^{2+} homeostasis (Medvedeva and Weiss, 2014; Chaudhuri et al., 2013). It is interesting to examine whether these two molecular mechanisms participated in H_2O_2-induced mitochondrial Zn^{2+} homeostasis, particularly whether they functioned independently or in coupling with the mitochondrial TRPM2 channel. Treatment with the mitochondrial Na^+/Ca^{2+} exchanger inhibitor CGP37157, or the mitochondrial Ca^{2+} uniporter inhibitor Ru360, strongly reduced H_2O_2-induced hippocampal neuron death to the similar level by TRPM2-KO (**Fig. 3.10**), and did not further reduce H_2O_2-induced neuronal death in TRPM2-KO neurons (**Fig. 3.10**). H_2O_2-induced mitochondrial ROS generation was completely prevented by treatment with CGP37157 or Ru360 (**Fig. 3.10**). These results suggest the involvement of mitochondrial NCX and MCU in mediating H_2O_2-induced mitochondrial Zn^{2+} accumulation, ROS and hippocampal neuronal death. Furthermore, the results have implicated a role of functional interplay between TRPM2 channel and the NCX and MCU in mediating H_2O_2-induced mitochondrial Zn^{2+} accumulation and ROS generation.

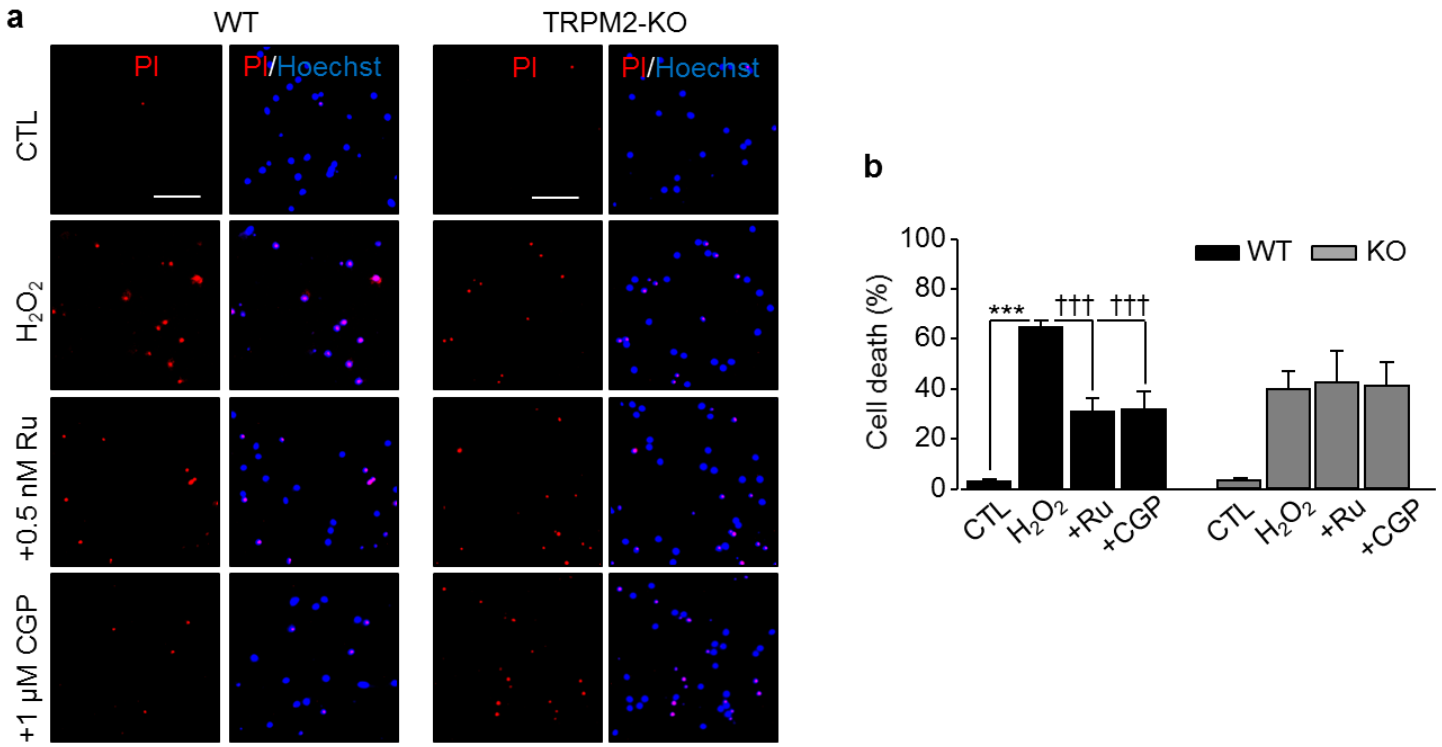
a
WT
TRPM2-KO
PI
PI/Hoechst
CTL
H2O2
+0.5 nM Ru
+1 μM CGP
b
Cell death (%)
100
80
60
40
20
0
WT
KO
***
†††
†††
CTL
H2O2
+Ru
+CGP

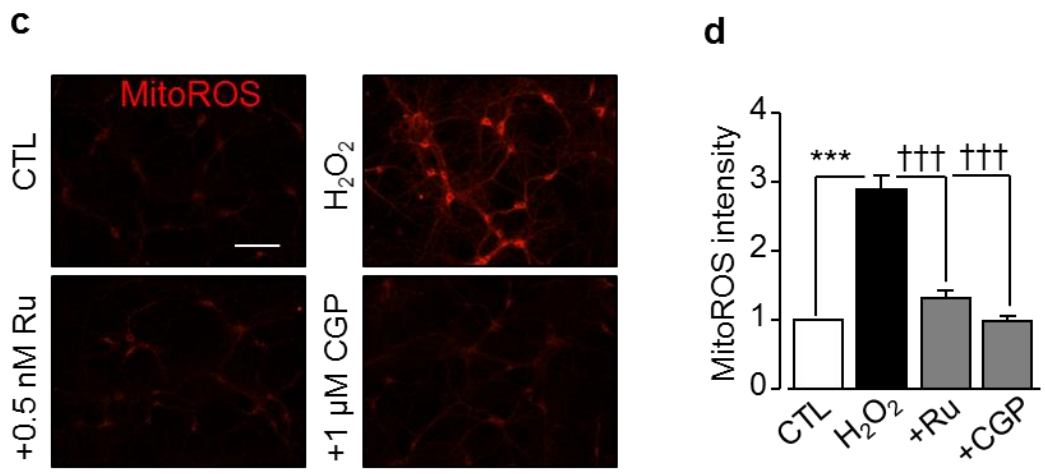

Figure 3.10 The interaction of TRPM2 channel with mitochondrial Zn^{2+} pathways

(**a**) Representative images showing PI and PI/Hoechst staining images in WT or TRPM2-KO hippocampal neurons treated with 300 μM H_2O_2 for 24 hr or treated with 0.5 nM Ru360 or 1 μM CGP37157 before and during exposure to H_2O_2. Scale bar is 100 μm. (**b**) The mean percentage of dead cells under indicated conditions in WT and TRPM2-KO neurons from 3 independent experiments (300-450 cells in each independent experiment). (**c**) Representative images showing MitoROS fluorescent images in hippocampal neurons exposed to 300 μM H_2O_2 for 2 hr or pre-treated with 0.5 nM Ru360 or 1 μM CGP37157 for 30 min. Scale bar is 100 μm. (**d**) Normalized MitoROS fluorescence intensity at indicated conditions from 3 independent experiments (55-80 cells of each independent experiment). All values were normalized to untreated control cells (CTL). ***, $P < 0.001$ indicates significant difference relative to control, and †††, $P < 0.001$ for comparison with cells exposed to H_2O_2 alone.

3.2.9 H_2O_2-induced TRPM2-dependent axonal degeneration

The axon is critical for neurons to receive, process, and transmit information. Previous studies show that mitochondrial dysfunction can lead to axonal degeneration, including the opening of mPTP (Barrientos et al., 2011). ROS, which activate mPTP, play an important role in axonal degeneration (Zorov et al., 2014; Court and Coleman, 2012). To investigate the role of TRPM2 channel in ROS-induced axonal degeneration, hippocampal neurons were examined using immunofluorescent confocal imaging in combination with using an antibody recognizing Tau, an axon-specific protein. The degeneration index (DI) was considerably increased in hippocampal neurons after exposure to 300 μM H_2O_2 for 2-24 hr (**Fig. 3.11**), indicating that axons were severely damaged. However, such detrimental effect was strongly attenuated in hippocampal neurons from TRPM2-KO mice (**Fig. 3.11**). The results suggest that the TRPM2 channel activation contributes to ROS-induced axonal degeneration.

3.2.10 The involvement of PKC and NOX in ROS generation and neuron death

It is long known that ROS can activate PKC that in turn activates NOX and that NOX-mediated ROS generation has been implicated in neuronal death in transient ischemia damage and neurodegenerative diseases (Bedard and Krause, 2007). H_2O_2-induced hippocampal neuron death was significantly inhibited by treatments with the PKC inhibitor GÖ6976, NOX generic inhibitor apocynin, and NOX1/4 inhibitor GKT137831 (**Fig. 3.12**). The results suggest a critical role of PKC and NOX in contributing in H_2O_2-induced ROS generation and neuronal death.

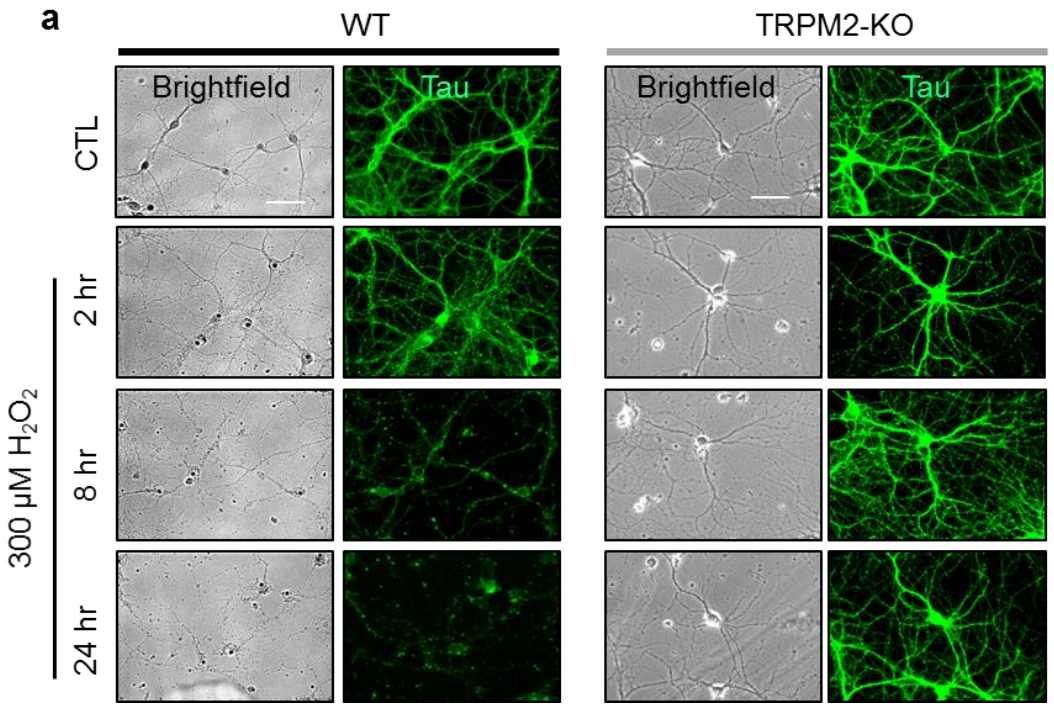
a
WT
TRPM2-KO
Brightfield
Tau
Brightfield
Tau
CTL
2 hr
8 hr
24 hr
300 μM H2O2

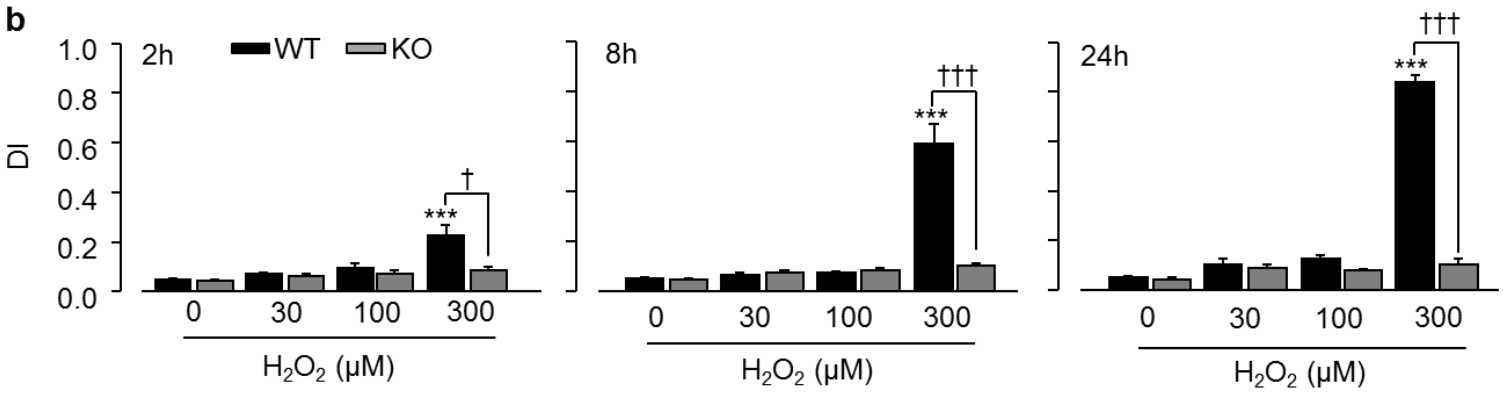

Figure 3.11 TRPM2 activation mediates axonal degeneration in hippocampal neurons induced by H_2O_2

(**a**) Representative immunofluorescent confocal images of hippocampal neurons labelled with an anti-Tau antibody (green) in hippocampal neurons from WT and TRPM2-KO neurons treated under indicated conditions. Scale bar is 100 μm. (**b**) Quantification of the axon degeneration index (DI) of WT and TRPM2-KO hippocampal neurons under indicated conditions. The results were from 3-5 (60-80 cells of each independent experiment). ***, $P < 0.001$ indicate significant difference relative to untreated control; †, $P < 0.05$ and †††, $P < 0.001$ for comparison between WT and TRPM2-KO neurons.

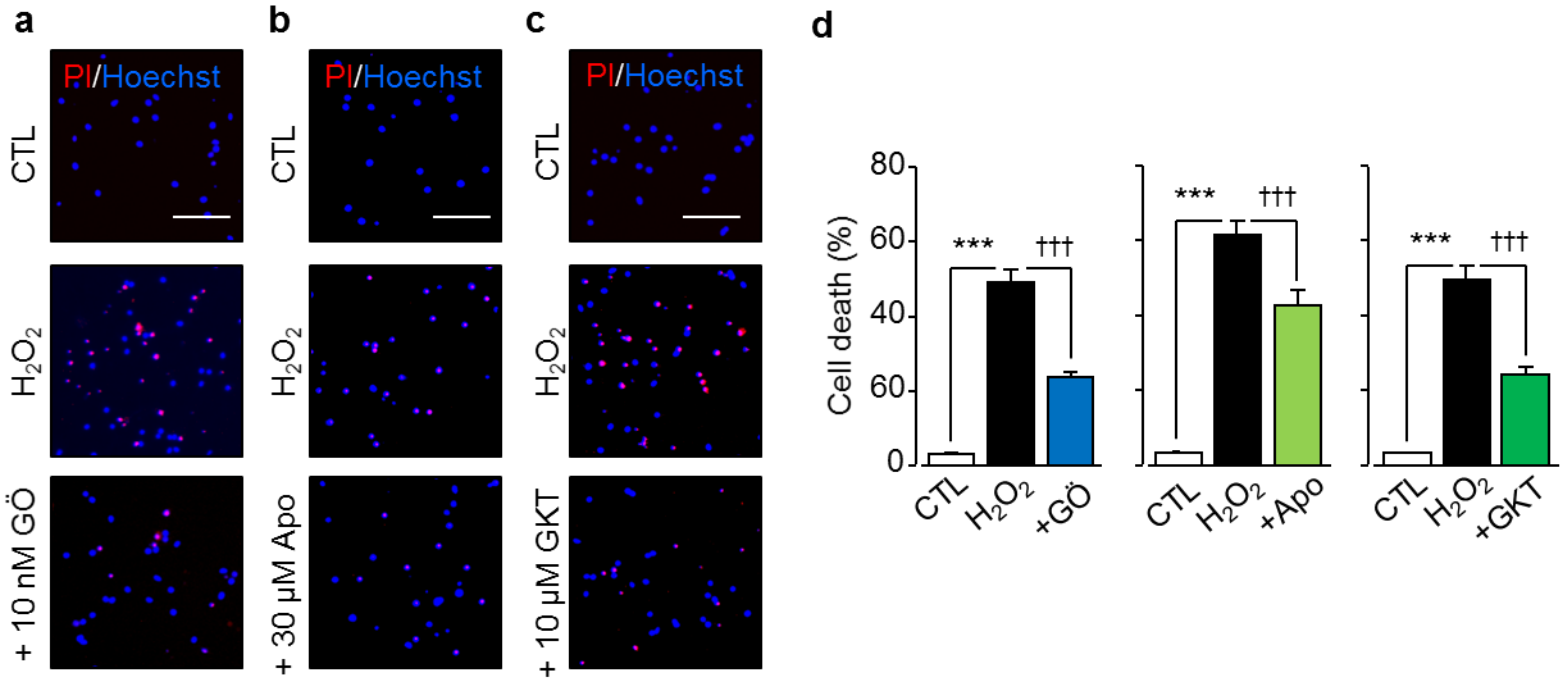

Figure 3.12 ROS-PKC-NOX signalling contributes to H_2O_2-induced hippocampal neuronal death

(**a-c**) Representative PI/Hoechst staining images of WT hippocampal neurons untreated (CTL), treated with 300 µM H_2O_2 or pre-treated with 10 nM GÖ6976 (**a**), 30 µM apocynin (**b**) or 10 µM GKT137831 (**c**). Scale bar is 100 µm. (**d**) Summary of the percentage of PI positive cells at indicated conditions from 3-5 independent experiments (400-600 cells for each independent experiment). ***, $P < 0.001$ indicates significant difference relative to untreated control (CTL), and †††, $P < 0.001$ for comparison with H_2O_2-treated cells.

3.3 Discussion

The study presented in this chapter provides evidence to identify multiple molecular mechanisms driving H_2O_2-induced hippocampal neuron death and show mitochondrial TRPM2 channel as a nexus to form a vicious positive feedback loop (**Fig. 3.13**).

It has well established that an increase in the $[Zn^{2+}]_i$, as a result from the extracellular Zn^{2+} influx or internal Zn^{2+} release through Zn^{2+}-specific transporters as well as diverse Ca^{2+} transporting mechanisms, can induce neuronal death (Chaudhuri et al., 2013; Medvedeva and Weiss, 2014). In this chapter, it was showed that H_2O_2-induced hippocampal neuronal death was strongly inhibited by TRPM2-KO (**Fig. 3.3**) or pharmacological inhibition of the TRPM2 channel activation (**Fig. 3.3**) and also by treatment with TPEN (**Fig. 3.3**), a Zn^{2+} chelator. Single cell imaging further demonstrated a prominent increase in the $[Zn^{2+}]_i$ in response to H_2O_2 (**Fig. 3.4**), which was completely prevented by TRPM2-KO (**Fig. 3.4**) or the pharmacological inhibition of TRPM2 channel activation or activity (**Fig. 3.4**), as well as by treatment with TPEN (**Fig. 3.4**). Taken together, the results provide consistent evidence to support a critical role for TRPM2-dependent increase in the $[Zn^{2+}]_i$ in oxidative stress-induced hippocampal neuronal death. As introduced above, reperfusion following transient ischemia gives rise to the generation of excessive ROS, leading to oxidative stress (Sanderson et al., 2013). A recent study shows that TRPM2 channel plays an important and exclusive role in determining reperfusion-induced increase in the $[Zn^{2+}]_i$ in hippocampal neurons and post-ischemia neuronal death *in vivo* and *in vitro* (Ye et al., 2014). Therefore, the results presented in this chapter consistently support a critical role for TRPM2-dependent Zn^{2+} signalling in H_2O_2 or oxidative stress-induced neuronal death.

The results in this chapter also provide further evidence to reveal multiple molecular mechanisms and signalling pathways in TRPM2-dependent alterations in the

intracellular Zn^{2+} homeostasis in hippocampal neurons. In consistence with a recent study (Ye et al., 2014), hippocampal neurons contained very low intracellular Zn^{2+} level present in puncta or vesicles, and a majority of Zn^{2+} puncta were co-localized with LysoTracker (**Fig. 3.5**), suggesting the lysosomal localization. Brief exposure to H_2O_2 induced substantial increase in the $[Zn^{2+}]_i$ (**Fig. 3.4**), similar to what was reported in previous studies (Hwang et al., 2008; Manna et al., 2015). Exposure to H_2O_2 resulted in a prominent reduction in LysoTracker fluorescence (**Fig. 3.5**), indicating lysosomal dysfunction. The lysosomal dysfunction was proposed in a previous study to be responsible for the lysosomal Zn^{2+} release to increase the $[Zn^{2+}]_i$ (Hwang et al., 2008). Lysosomal dysfunction can elicit either apoptosis or/and necrosis depending on the magnitude of rupture and as a consequence, the amount of proteolytic enzymes released into cytosol (Guicciardi et al., 2004). H_2O_2-induced reduction in LysoTracker fluorescence or lysosomal dysfunction was ablated by genetic deletion of the TRPM2 expression (**Fig. 3.5**), suggesting a strong dependence of the TRPM2 channel. TRPM2 channel was previously shown to function as a lysosomal Ca^{2+} release channel in pancreatic β-cells (Lange et al., 2009; Togashi et al., 2006). There was a low level of co-localization of the TRPM2 immunoreactivity with LysoTracker (**Fig. 3.9**) and, nonetheless, it is possible that TRPM2 channel mediates lysosomal Zn^{2+} release that contribute to H_2O_2-induced increase in the $[Zn^{2+}]_i$ in hippocampal neurons, as a recent study shows in pancreatic β-cells (Manna et al., 2015). There is evidence that oxidative stress induces Zn^{2+} release from the Zn^{2+}-binding MT proteins increase the $[Zn^{2+}]_i$ in neurons and results in ischemic brain damage (Shuttleworth and Weiss, 2011). The strong dependence of H_2O_2-induced increase in the $[Zn^{2+}]_i$ on TRPM2 channel appears to argue against such a possibility.

The second important finding of this chapter is to reveal a role for the TRPM2 channel in ROS-induced alteration in the mitochondrial Zn^{2+} homeostasis leading to hippocampal neuron death. As shown in this study, exposure to H_2O_2 induced

considerable mitochondrial Zn^{2+} accumulation (**Fig. 3.5**), mitochondrial loss (**Fig. 3.6**), change in the mitochondrial morphology (**Fig. 3.6**), Cyt-c release (**Fig. 3.6**) and mitochondrial ROS generation (**Fig. 3.7**). Exposure to bafilomycin A1 to induce lysosomal dysfunction gave rise to the similar mitochondrial Zn^{2+} increase and ROS production (**Fig. 3.8**). Furthermore, H_2O_2-induced mitochondrial ROS production was prevented by treatment with TPEN (**Fig. 3.7**). Taken together, these results suggest that H_2O_2-induced lysosomal dysfunction and increase in the $[Zn^{2+}]_i$ trigger mitochondrial Zn^{2+} accumulation, which in turn causes mitochondrial loss, changes in the mitochondrial morphology, Cyt-c release and mitochondrial ROS generation. H_2O_2-induced mitochondrial effects were prevented by the genetic or pharmacological inhibition of TRPM2 channel (**Fig. 3.5-3.7**). These results raised the intriguing question with regards to molecular mechanisms responsible for the mitochondrial Zn^{2+} accumulation. Immunofluorescence imaging supports the localization of TRPM2 to the mitochondria (**Fig. 3.9**). Moreover, ADPR, the TRPM2 channel specific agonist, significantly enhanced Zn^{2+} in the mitochondria isolated from the WT but not TRPM2-KO hippocampal neurons (**Fig. 3.9**). These results are consistent with the notion that the mitochondrial TRPM2 channel mediates mitochondrial Zn^{2+} accumulation, similarly to the role for TRPC3 channel in mediating the mitochondrial Ca^{2+} homeostasis proposed in a recent study (Feng et al., 2013).

In addition, ROS-induced mitochondria dysfunction had been shown to be associated with axonal degeneration, which leads to neuronal cell death and is an early feature of most neurodegenerative disorders (Court and Coleman, 2012; Barrientos et al., 2011). H_2O_2-induced considerable axonal degeneration in WT hippocampal neurons was largely abolished by TRPM2-KO (**Fig. 3.11**), suggesuing a critical role for the TRPM2 channel in mediating ROS-induced axonal degeneration. Further studies are required to understand the underlying mechanisms.

H_2O_2-induced mitochondrial ROS accumulation and cell death in the WT hippocampal neurons was also attenuated by pharmacological inhibition of the mitochondrial NCX and MCU (**Fig. 3.10**), implicating that two molecular mechanisms are critically involved in mediating the mitochondrial Zn^{2+} accumulation induced ROS generation and oxidative damage. However, intriguingly, the mitochondrial NCX and MCU exhibited a strong dependence on the TRPM2 channel as their inhibition was without effect in TRPM2-KO neurons (**Fig. 3.10**). Evidently, further investigations are required to gain better insights into the functional interplay of the mitochondrial NCX and MCU with the TRPM2 channel in mitochondria.

The activation of TRPM2 channel has been shown by recent studies to be important in mediating ROS-induced hippocampal neuron death (Jia et al., 2011; Verma et al., 2012; Ye et al., 2014), which has been further confirmed by the results in this chapter (**Fig. 3.3**). In consistence with previous reports, results described in this chapter showed plasma membrane expression of TRPM2 channel in hippocampal neurons (**Fig. 3.3**). In addition, H_2O_2-induced hippocampal neuron death in the absence of Ca^{2+} was significantly lower than in the presence of Ca^{2+} (**Fig. 3.3**), supporting a significant role for plasma membrane TRPM2-mediated Ca^{2+} influx in H_2O_2-induced hippocampal neuron death, as reported previously in H_2O_2-induced cortical neuron death (Kaneko et al., 2006). H_2O_2-induced increase in the $[Zn^{2+}]_i$ was completely prevented in Ca^{2+}-free solution (**Fig. 3.4**). Furthermore, ADPR-induced Zn^{2+} accumulation in isolated mitochondria was considerably reduced in the absence of Ca^{2+} (**Fig. 3.9**). Given that intracellular Ca^{2+} is critical required for facilitating ADPR-induced TRPM2 channel activation (Du et al., 2009a; Toth and Csanady, 2010), these results are consistent with the role of the plasma membrane TRPM2 channel in mediating Ca^{2+} influx that provides cytosolic Ca^{2+} for ADPR-induced mitochondrial TRPM2 channel activation.

It is well recognized that ROS activates PKC, which in turn stimulates NOX-mediated ROS generation (Bedard and Krause, 2007). There is increasing evidence to show a critical role for NOX-mediated ROS generation in neuronal death for ischemia-reperfusion damage and neurodegenerative diseases (Chen et al., 2009). Consistently, the present study showed that H_2O_2-induced neuronal death was strongly suppressed by GÖ6976, apocynin and GKT137831 (**Fig. 3.12**), suggesting the activation of PKC and NOX, particularly NOX1/4, as a vital molecular mechanism in oxidative stress-induced neuronal death. These results also implicate that oxidative stress can set in motion a positive feedback loop that drives neuronal death via the activation of PKC and NOX1/4-mediated ROS generation.

The results in this chapter suggest mitochondrial TRPM2 channel as a nexus integrating dynamic lysosome-to-mitochondria Zn^{2+} translocation, leading to the mitochondrial Zn^{2+} accumulation that in turn triggers mitochondrial ROS production. As mentioned in the Introduction chapter, Zn^{2+} can induce apoptotic cell death via disrupting mitochondrial function and ROS production, which is consistent with H_2O_2-induced Cyt-c release (**Fig. 3.6**) and the inhibition of H_2O_2-induced hippocampal neuron death by Ac-DVED-CMK (**Fig. 3.2**). H_2O_2-induced hippocampal neuron death was also sensitive to the inhibition by IM-54 (**Fig. 3.2**), and necrostatin-1 (**Fig. 3.2**), suggesting that necrosis and necroptosis mechanisms are also involved in H_2O_2-induced hippocampal neuron death.

As illustrated in **Figure 3.13**, the present study shows mitochondrial TRPM2 channel as a nexus for multiple molecular mechanisms and signalling pathways that form a positive feedback loop that drives ROS-induced neuronal death. Such novel mechanistic insights are useful for a better understanding of oxidative stress-induced neuronal death that is closely linked to post-ischemic stroke damage and oxidative stress-related neurodegeneration diseases, and therefore are helpful in the development of novel therapeutics treating these neurodegenerative conditions.

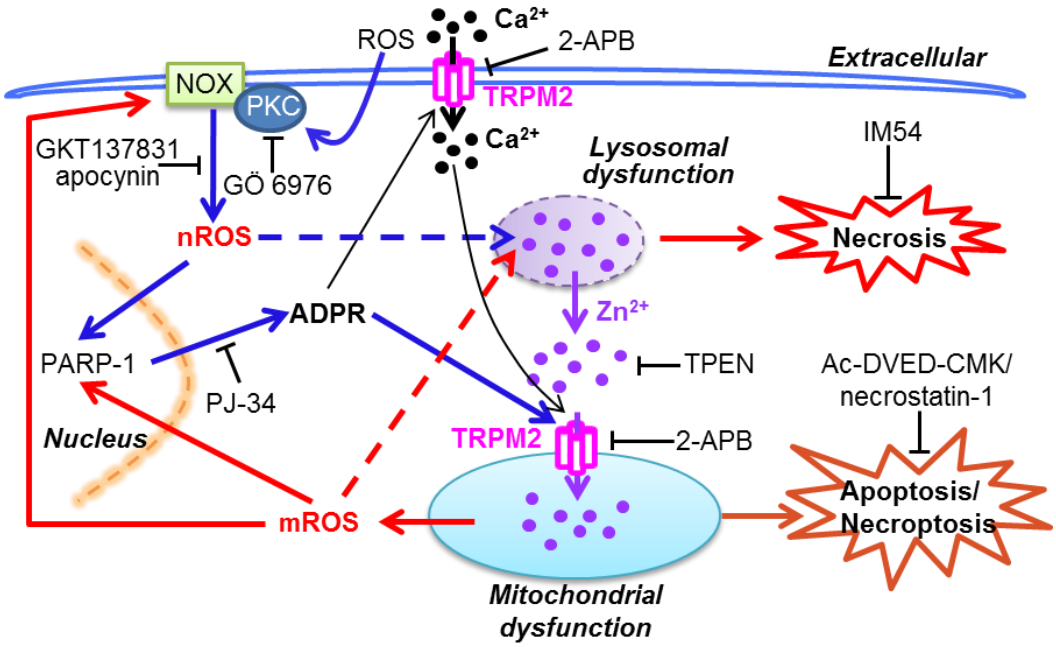

Figure 3.13 Proposed molecular mechanisms in ROS-induced TRPM2-mediated neuronal death

The initial exposure to ROS such as H_2O_2 stimulates NOX via PKC and NOX-mediated ROS production (nROS), a step inhibited by GÖ6976, apocynin and GKT137831, and nROS in turn stimulates PARP-1-mediated production of ADPR, a step sensitive to the inhibition by PJ34, and lysosomal dysfunction that leads to the lysosomal Zn^{2+} release and necrosis. ADPR activates cell surface TRPM2 channel to increase the $[Ca^{2+}]_i$ that facilitates ADPR-induced TRPM2 channel activation. The mitochondrial TRPM2 channel is required for the mitochondrial Zn^{2+} accumulation, triggering the production of mitochondrial ROS (mROS) and mitochondrial dysfunction that induces apoptosis and necroptosis. Mitochondrial ROS may in turn activate PKC and NOX to induce NOX-mediated ROS generation and/or PARP-1-mediated production of ADPR. These signalling pathways form a positive feedback mechanism that causes neuronal cell death. (ROS: Reactive oxygen species; NOX: NADPH oxidases; PKC: Protein kinase C; PARP-1: Poly(ADP-ribose) polymerase-1; ADPR: Adenosine diphosphate ribose).

Chapter 4

Signalling mechanisms in $A\beta_{42}$ peptide-induced TRPM2 channel activation and neurotoxicity

4.1 Introduction

AD is an age-related neurodegenerative disorder that is characterized by the formation of senile amyloid plaque with elevated deposits of the Aβ peptides. Aβ is known to induce neurotoxicity via multiple but yet fully understood molecular and cellular mechanisms, which lead to synaptic loss and neuronal network dysfunction in the hippocampus and other brain regions responsible for learning and memory (Mucke and Selkoe, 2012). Aβ-induced neurotoxicity thus plays a critical role in the AD pathogenesis (Haass and Selkoe, 2007; Scheltens et al., 2016). Aβ can stimulate the generation of ROS in hippocampal neurons (De Felice et al., 2007) and as a consequence, excessive ROS generation, lipid peroxides and the oxidative modification of proteins and lipids are widely observed in cell exposed to Aβ and in the brain tissues of APP/PS1 transgenic AD mice, consistent with a role for oxidative stress in Aβ-induced neurotoxicity (Querfurth and LaFerla, 2010; Swomley et al., 2014; Wang et al., 2014). In addition, Aβ-induced axonal degeneration also contributes to neuronal cell death (Alobuia et al., 2013; Christensen et al., 2014). Emerging evidence supports an important role for the ROS-sensitive TRPM2 channel in mediating the neurotoxicity of Aβ peptides (Ostapchenko et al., 2015; Park et al., 2014). It is well established that TRPM2 channel confers susceptibility to ROS stimuli, including $A\beta_{42}$ and TNF-α, induced cell death in diverse cell types (Jiang et al., 2010; Miller and Zhang, 2011). Consistently with an early *in vitro* study suggesting a role for TRPM2 channel in $A\beta_{42}$-induced neurotoxicity (Fonfria et al., 2005), a recent study has shown that TRPM2-KO in the APP/PS1 mice prevented Aβ-induced neurotoxicity in the hippocampus and age-related impairment in memory with an decreased level of cell-associated low molecular weight Aβ oligomers (Ostapchenko et al., 2015). These studies provide strong evidence to support TRPM2 channel as a previously unrecognized mechanism mediating neurotoxicity and cognitive impairment following the accumulation of excessive neurotoxic Aβ. As shown in Chapter 3,

H_2O_2 was shown to initiate a positive feedback loop involving an elevation in the $[Zn^{2+}]_i$ and substantial ROS generation from mitochondria as well as via NOX activation (Kim and Koh, 2002). Experiments described in the present chapter aimed to examine the underlying mechanisms in $A\beta_{42}$-induced neurotoxicity in cultured mouse hippocampal neurons. The results have revealed that TRPM2 channel activation coupling with the PKC/NOX and MEK (MAPK/ERK kinase)/ERK/PARP signalling pathways forms a positive feedback signalling mechanism for $A\beta_{42}$-induced cellular oxidative stress and neurotoxicity. These findings provide novel and mechanistic insights into the AD pathogenesis.

4.2 Results

4.2.1 $A\beta_{42}$ induces TRPM2-dependent hippocampal neurotoxicity

To investigate the role of TRPM2 channel in mediating Aβ neurotoxicity, PI staining assay was performed to determine hippocampal neuron death in response to the exposure to $A\beta_{42}$, one of the major neurotoxic Aβ peptides (LaFerla et al., 2007). Hippocampal neurons from the WT and TRPM2-KO mice were exposed to $A\beta_{42}$ at 1 μM for 24, 48 and 96 hr (**Fig. 4.1**). Exposure of the WT neurons to $A\beta_{42}$ resulted in substantial neurotoxicity (**Fig. 4.1**). Considerable, albeit slightly less, neurotoxicity was also observed in neurons exposed to $A\beta_{42}$ at lower concentrations, such as 22 and 66 nM (100 and 300 mg/ml) (**Fig. 4.1**). In striking contrast, $A\beta_{42}$ induced no significant neurotoxicity in TRPM2-KO neurons (**Fig. 4.1**). The treatment of 10 μM 2-APB or 1 μM ACA, prior to and during exposure to $A\beta_{42}$, strongly inhibited $A\beta_{42}$-induced neurotoxicity in WT neurons (**Fig. 4.2**). Moreover, the treatment of WT neurons with 1 μM PJ34 and 30 μM DPQ, also significantly reduced, albeit to less extent, $A\beta_{42}$-induced neurotoxicity (**Fig. 4.2**). These experiments using genetic and pharmacological approaches provide strong evidence to support a critical role for TRPM2 channel in mediating $A\beta_{42}$-induced neurotoxicity, highly consistent with the recent *in vivo* study (Ostapchenko et al., 2015). Moreover, Ac-DVED-CMK, IM-54 and necrostatin-1 all significantly inhibited $A\beta_{42}$-triggerred hippocampal neuron death (**Fig. 4.3**), which suggest that such TRPM2-dependent $A\beta_{42}$ neurotoxicity, similar to H_2O_2-mediated neuronal death described in the previous chapter, results from the activation of multiple cell death mechanisms including apoptosis, necrosis and necroptosis.

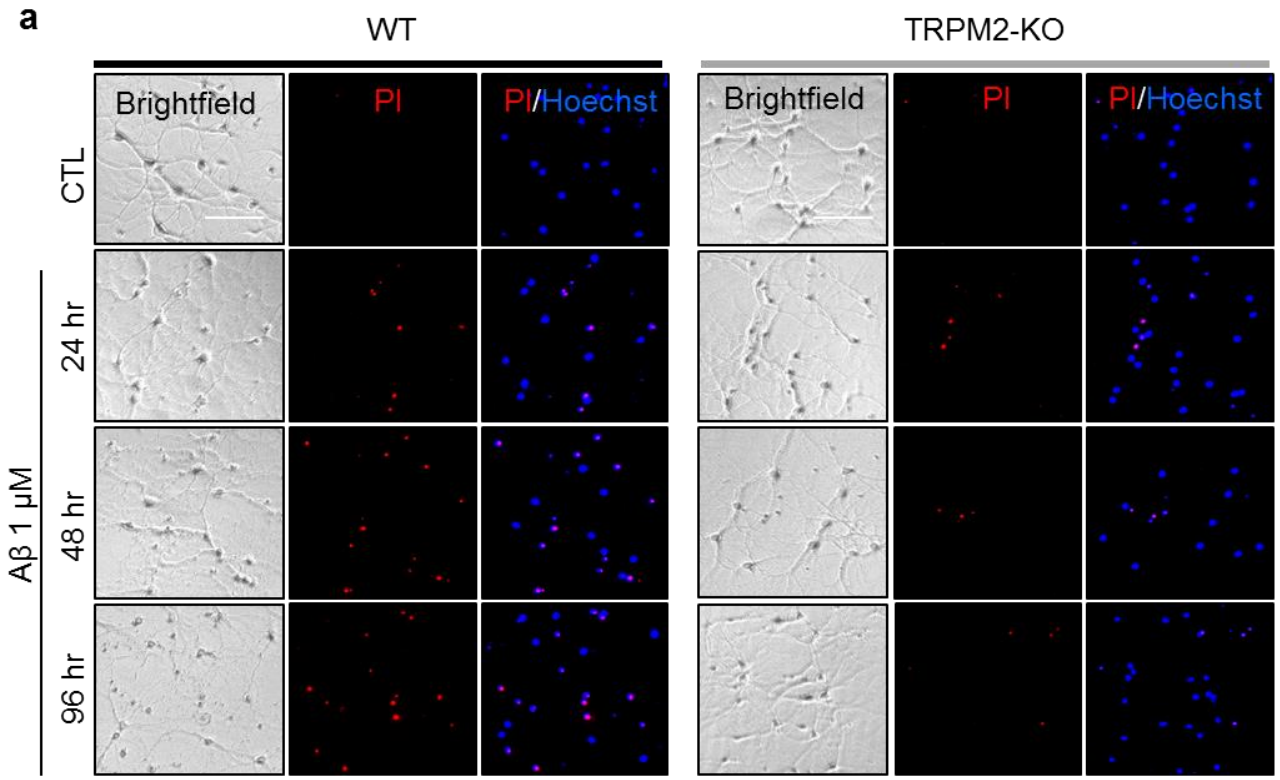
a
WT
TRPM2-KO
Brightfield
PI
PI/Hoechst
Brightfield
PI
PI/Hoechst
CTL
Aβ 1 μM
24 hr
48 hr
96 hr

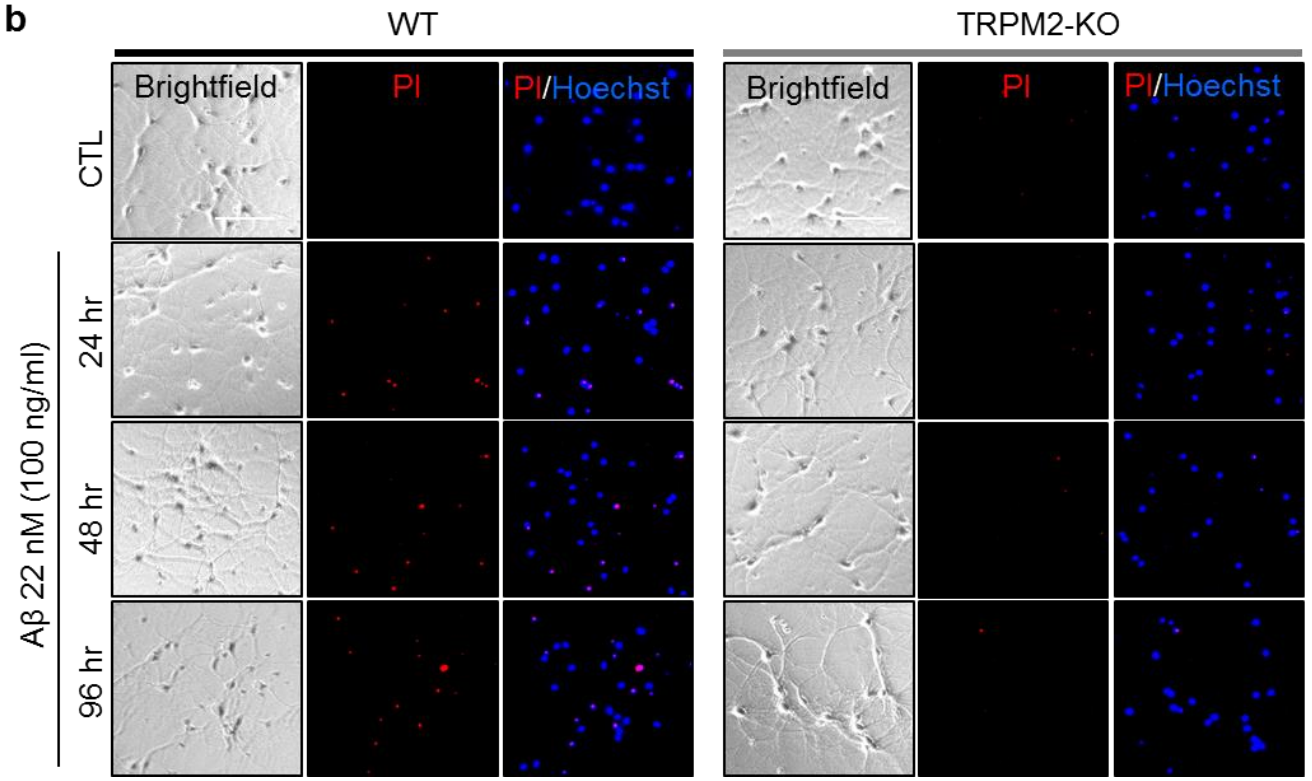
b
WT
TRPM2-KO
Brightfield
PI
PI/Hoechst
Brightfield
PI
PI/Hoechst
CTL
24 hr
48 hr
96 hr
Aβ 22 nM (100 ng/ml)

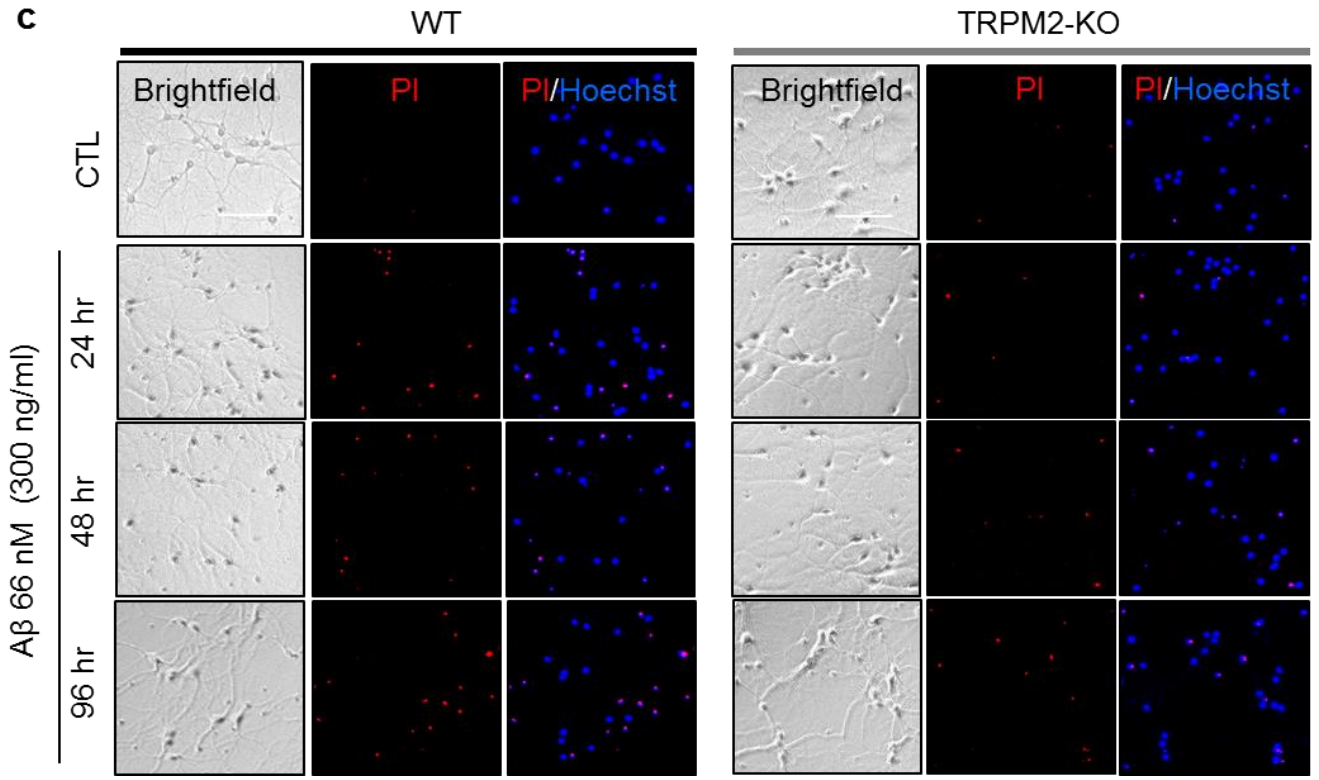
c
WT
TRPM2-KO
Brightfield
PI
PI/Hoechst
Brightfield
PI
PI/Hoechst
CTL
Aβ 66 nM (300 ng/ml)
24 hr
48 hr
96 hr

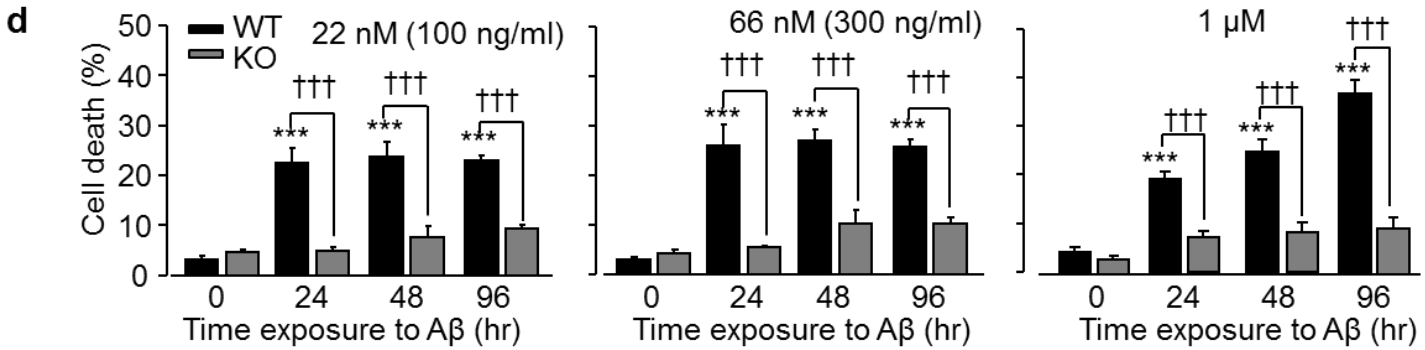

Figure 4.1 $A\beta_{42}$ induces cell death in WT and TRPM2-KO hippocampal neurons

(**a-c**) Representative images showing PI and PI/Hoechst staining in cultured hippocampal neurons from WT and TRPM2-KO mice exposed to 1 μM (**a**) as well as 22 nM (**b**) and 66 nM (**c**) $A\beta_{42}$ for 24, 48 or 96 hr in addition to under control (CTL) conditions. Each panel consists of brightfield image showing neurons. Scale bar is 100 μm. (**d**) Summary of the percentage of PI positive neurons under indicated conditions, from 3-5 independent experiments with each experiment examining 400-650 neurons. Black and grey bars represent the percentage of cell death in WT and TRPM2-KO neurons, respectively. ***, $P < 0.001$ indicates significant difference from respective untreated neurons. †††, $P < 0.001$ indicates significant difference between WT and TRPM2-KO neurons.

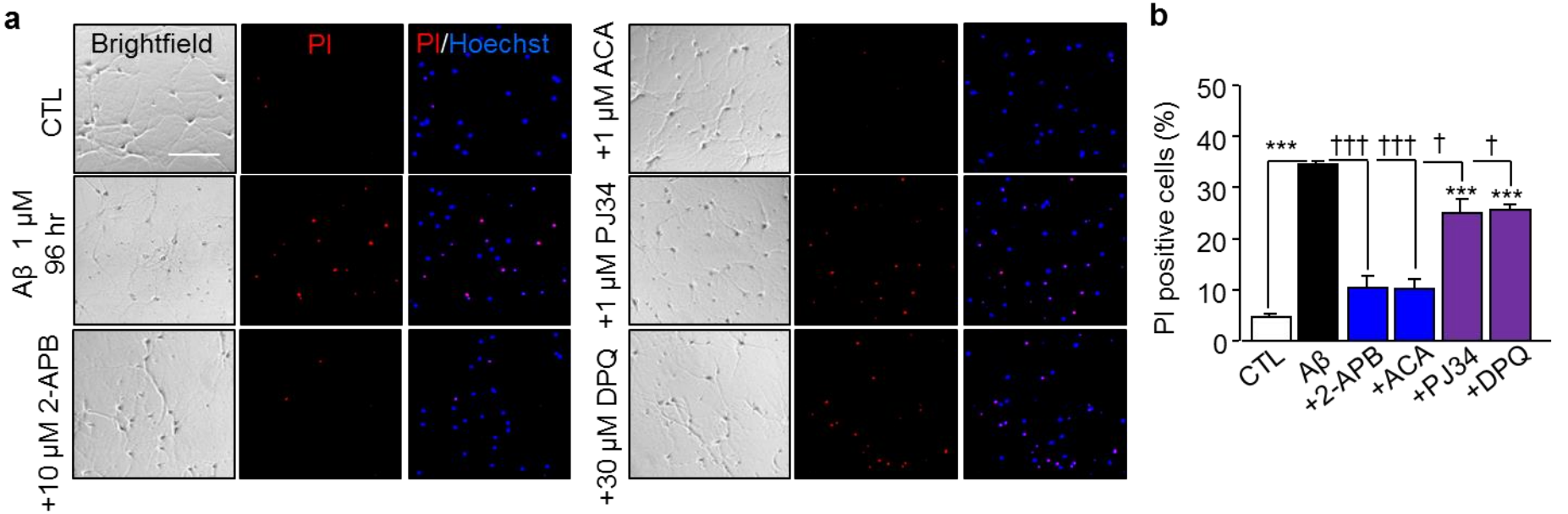

Figure 4.2 PARP/TRPM2 inhibitors protect hippocampal neurons from $A\beta_{42}$-induced death

(**a**) Representative images showing PI and PI/Hoechst staining in hippocampal neurons untreated (CTL), or treated with 10 μM 2-APB, 1 μM ACA, 1 μM PJ34 or 30 μM DPQ prior to and during exposure to 1 μM $A\beta_{42}$ for 96 hr. Scale bar is 100 μm. (**b**) Summary of the mean percentage of PI positive neurons, from 3-5 independent experiments with each experiment examining 400-600 neurons. ***, $P < 0.001$ indicates significant difference from untreated neurons. †, $P < 0.05$ and †††, $P < 0.001$ indicate difference from neurons exposed with $A\beta_{42}$ alone.

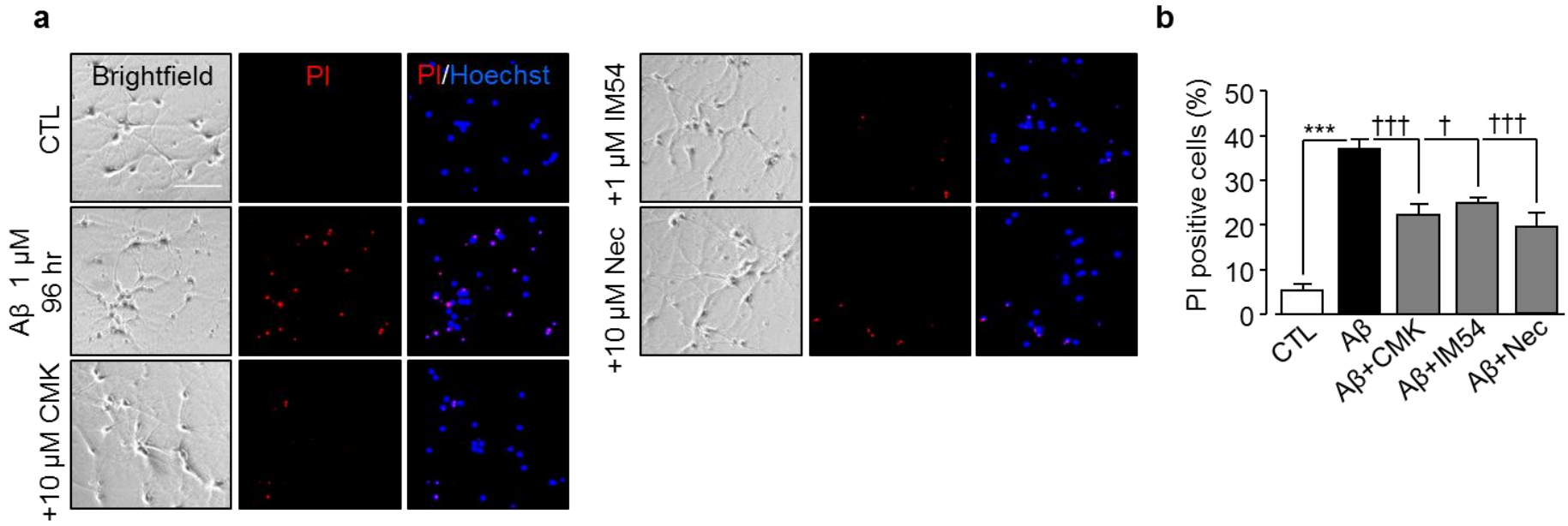

Figure 4.3 Mechanisms of $A\beta_{42}$-induced hippocampal neuron death

(**a**) Representative PI and PI/Hoechst staining images in hippocampal neurons treated with 10 μM Ac-DVED-CMK, 1 μM IM-54 or 10 μM necrostatin-1 prior to and during exposure to 1 μM $A\beta_{42}$ for 96 hr. Scale bar is 100 μm. (**b**) The mean percentage of PI positive neurons at indicated conditions from 3 independent experiments (350-500 cells for each independent experiment). ***, $P < 0.001$ indicates significant difference from untreated control neurons (CTL). †, $P < 0.05$ and †††, $P < 0.001$ indicate difference from neurons exposed with $A\beta_{42}$ alone.

4.2.2 $A\beta_{42}$ induces TRPM2-dependent increase in the $[Zn^{2+}]_i$ and lysosomal dysfunction

Intriguingly, $A\beta_{42}$-induced hippocampal neurotoxicity was almost completely prevented by treatment with 0.1 μM TPEN (**Fig. 4.4**), suggesting the importance of Zn^{2+} signalling in $A\beta_{42}$-elicited hippocampal neuron death. Indeed, as shown by single cell imaging together with using FluoZin3, the $[Zn^{2+}]_i$ was progressively increased in hippocampal neurons during prolonged exposure to $A\beta_{42}$ (**Fig. 4.4**). Moreover, single cell imaging with fluo-4 indicated no significant increase in the $[Ca^{2+}]_i$ in $A\beta_{42}$-exposed hippocampal neurons while there was massive Ca^{2+} responses upon subsequent exposure to ionomycin as a positive control (**Fig. 4.4**). Collectively, the above results suggests $A\beta_{42}$-induced hippocampal neurotoxicity results from an increase in the $[Zn^{2+}]_i$ (**Fig. 4.4**).

As shown in Chapter 3, the $[Zn^{2+}]_i$ was low in hippocampal neurons under control condition and highly concentrated in puncta that exhibited noticeable co-localization with LysoTracker. The exposure of WT neurons to $A\beta_{42}$ for 24 and 48 hr induced salient increase in the $[Zn^{2+}]_i$, which was accompanied with strong decline in LysoTracker intensity (**Fig. 4.5**). However, exposure to $A\beta_{42}$ induced no such discernible effects on the $[Zn^{2+}]_i$ and LysoTracker intensity in TRPM2-KO neurons (**Fig. 4.5**). $A\beta_{42}$-induced increase in the $[Zn^{2+}]_i$ and reduction in LysoTracker intensity in WT neurons were also strongly suppressed by treatments with PJ34 and 2-APB or with TPEN prior to and during exposure to $A\beta_{42}$ (**Fig. 4.5**). Taken together, the above results provide evidence to show the TRPM2 channel to be critical in $A\beta_{42}$-induced increase in the $[Zn^{2+}]_i$ and lysosomal dysfunction in hippocampal neurons.

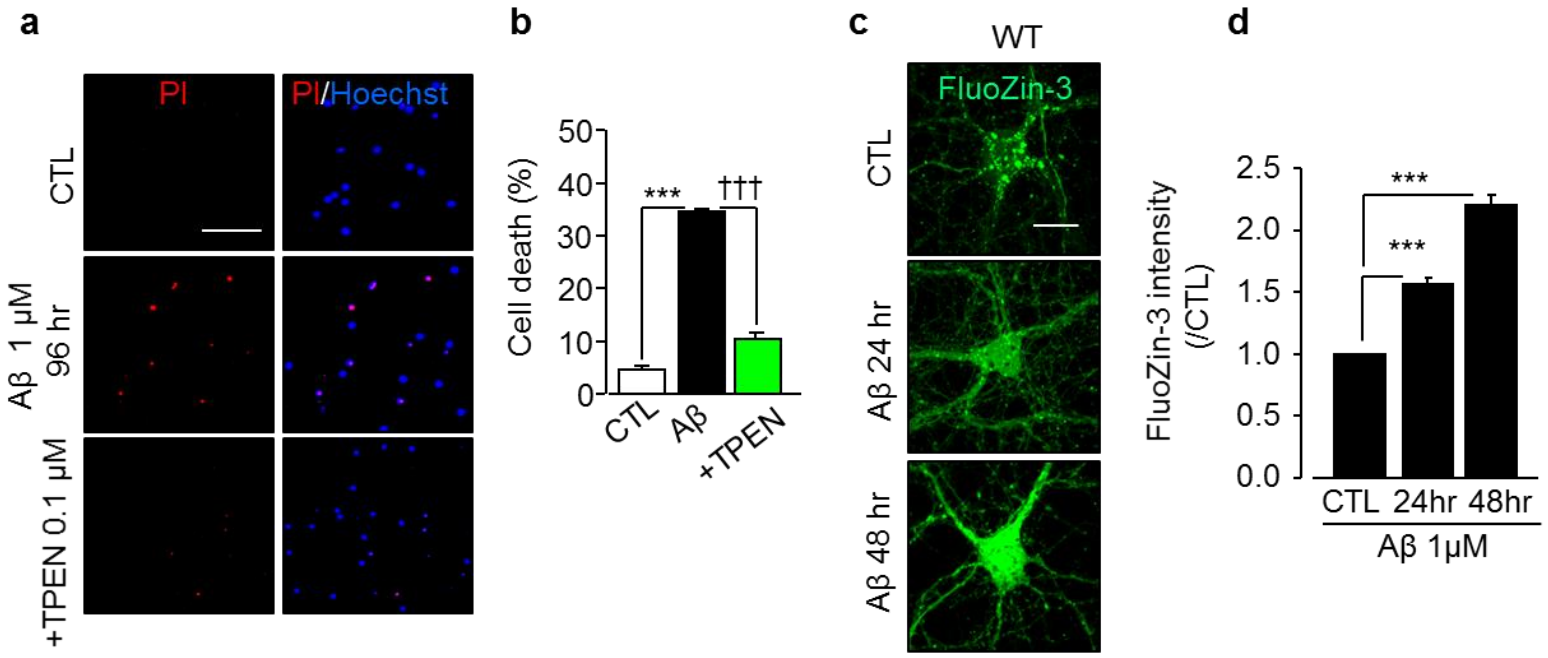
a
PI
PI/Hoechst
CTL
Aβ 1 μM
96 hr
+TPEN 0.1 μM
b
Cell death (%)
50
40
30
20
10
0
***
†††
CTL
Aβ
+TPEN
c
WT
FluoZin-3
CTL
Aβ 24 hr
Aβ 48 hr
d
FluoZin-3 intensity
(/CTL)
2.5
2.0
1.5
1.0
0.5
0.0
***
***
CTL 24hr 48hr
Aβ 1μM

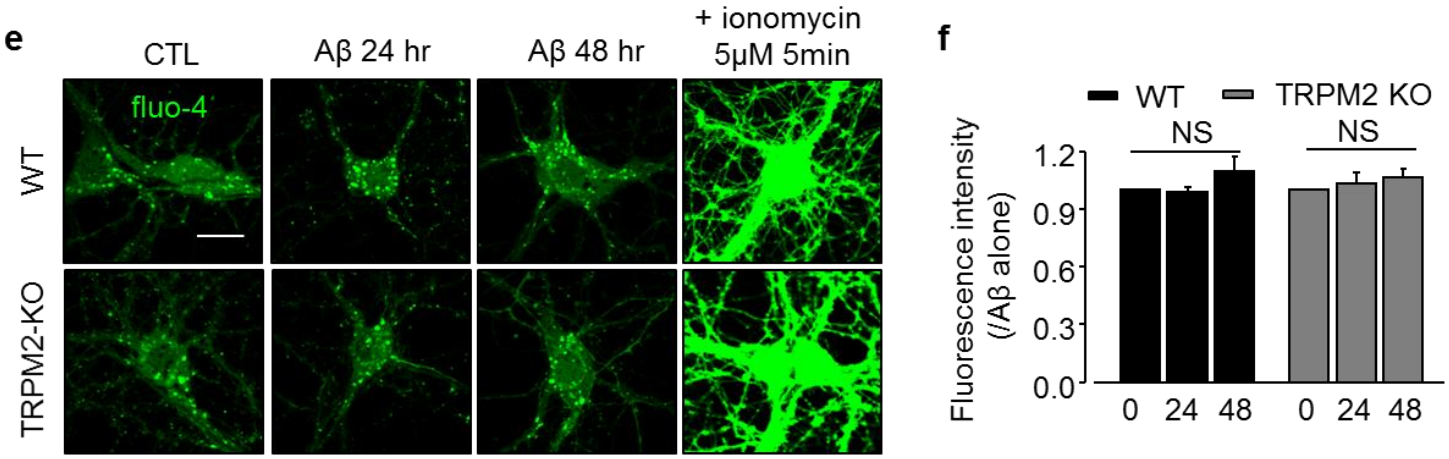

Figure 4.4 Effects of exposure to $A\beta_{42}$ on the $[Zn^{2+}]_i$ and $[Ca^{2+}]_i$ in WT and TRPM2-KO hippocampal neurons

(**a**) Representative images showing PI and PI/Hoechst staining in hippocampal neurons treated with 0.1 μM TPEN prior to and during exposure to 1 μM $A\beta_{42}$ for 96 hr. Scale bar is 100 μm. (**b**) The mean percentage of PI positive cells at indicated conditions, from 5 independent experiments with each experiment examining 400-600 neurons. ***, $P < 0.001$ indicates significant difference from untreated neurons (CTL). †††, $P < 0.001$ indicates difference compared to neurons exposed with $A\beta_{42}$ alone. (**c**) Representative confocal images showing the FluoZin-3 staining of WT hippocampal neurons untreated (CTL) or treated with 1 μM $A\beta_{42}$ for 24 or 48 hr. (**d**) Mean value of the fluorescence intensity of FluoZin-3 at indicated conditions from 5 independent experiments, 10-15 cells were examined in each independent experiment. All values were normalized to untreated cells. ***, $P < 0.001$ indicates significant difference with untreated neurons. (**e**) Representative confocal images showing the fluo-4 staining of WT and TRPM2-KO hippocampal neurons. Cells were untreated (CTL), treated with 1 μM $A\beta_{42}$ for 24 or 48 hr, or treated with 5 μM ionomycin for 5 min. Scale bar is 10 μm. (**f**) Summary of the normalized fluorescence intensity of fluo-4 at indicated conditions. All values were relative to the untreated cells. Black bars and grey bars represent the WT and TRPM2-KO neurons, respectively. NS stands for no significant difference.

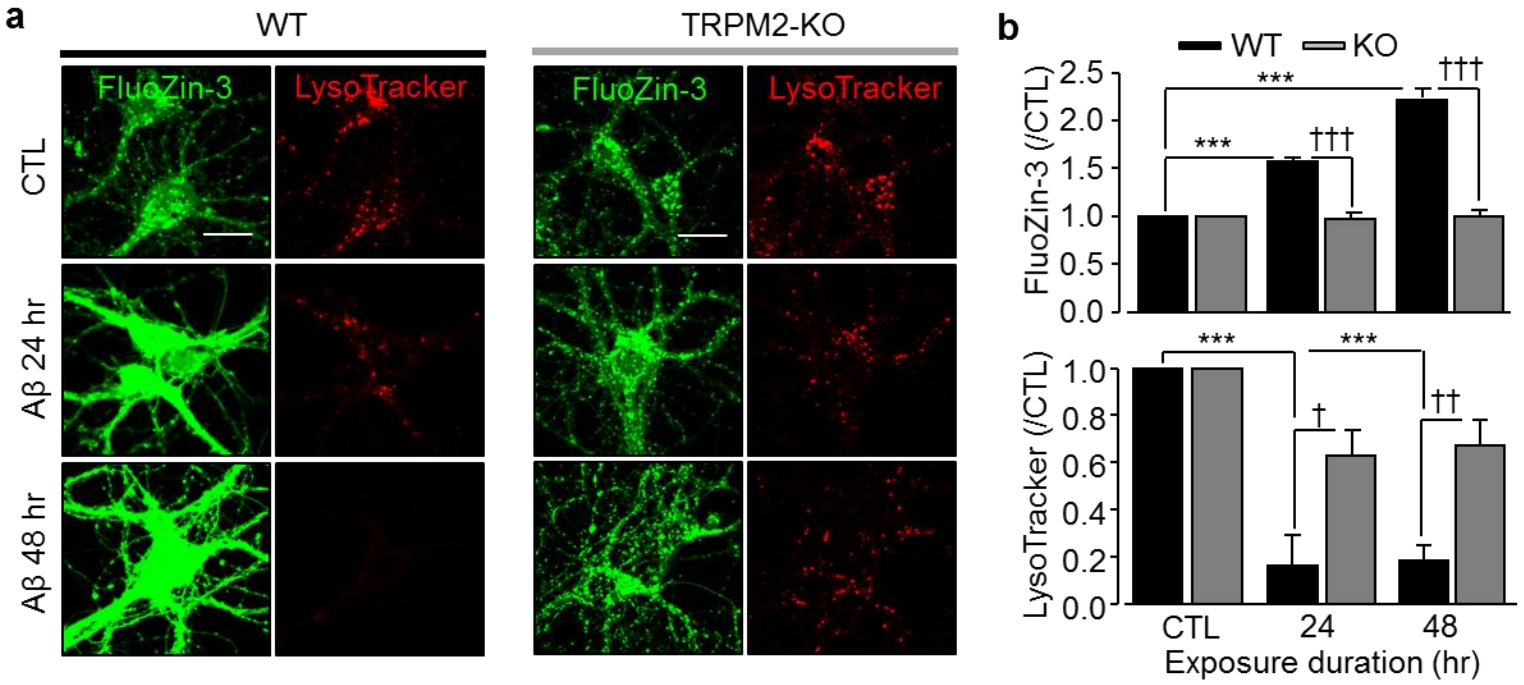
a
WT
TRPM2-KO
FluoZin-3
LysoTracker
FluoZin-3
LysoTracker
CTL
Aβ 24 hr
Aβ 48 hr
b
WT
KO
FluoZin-3 (/CTL)
2.5
2.0
1.5
1.0
0.5
0.0
***
***
†††
†††
LysoTracker (/CTL)
1.0
0.8
0.6
0.4
0.2
0.0
***
***
†
††
CTL
24
48
Exposure duration (hr)

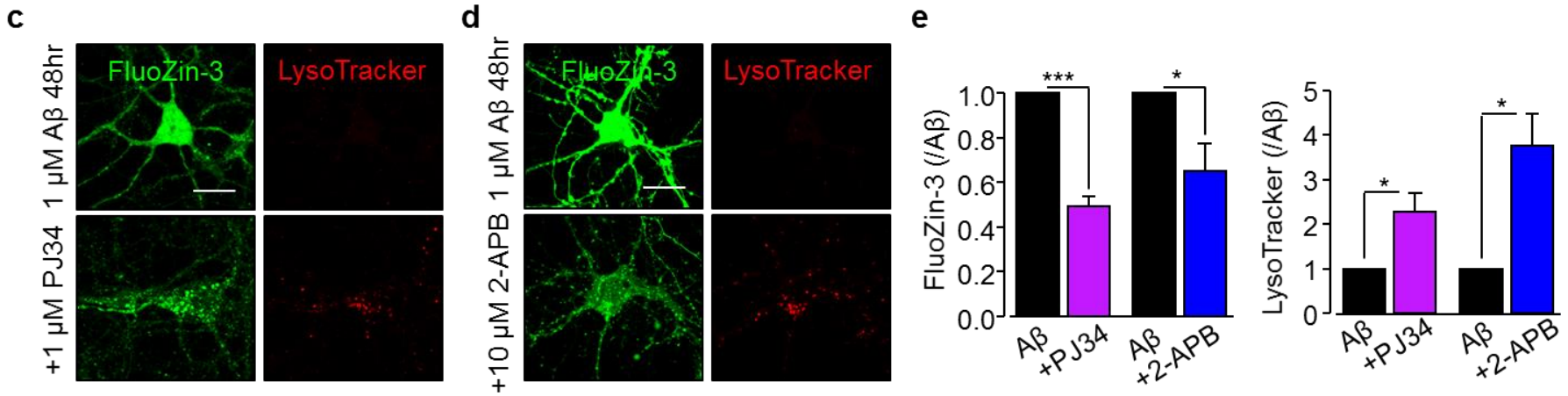
c
FluoZin-3
LysoTracker
1 μM Aβ 48hr
+1 μM PJ34
d
FluoZin-3
LysoTracker
1 μM Aβ 48hr
+10 μM 2-APB
e
FluoZin-3 (/Aβ)
1.0
0.8
0.6
0.4
0.2
0.0
***
*
Aβ
+PJ34
Aβ
+2-APB
LysoTracker (/Aβ)
5
4
3
2
1
0
*
*
Aβ
+PJ34
Aβ
+2-APB

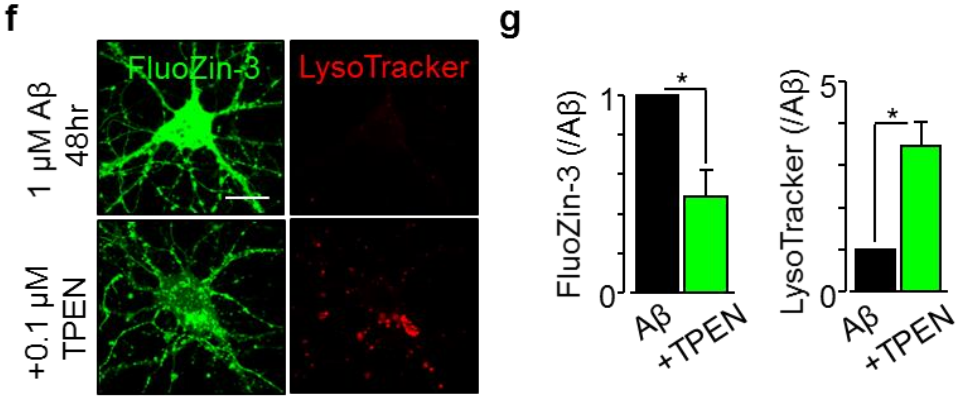

Figure 4.5 $A\beta_{42}$ induces TRPM2-dependent increase in the $[Zn^{2+}]_i$ and lysosomal dysfunction

(**a, c, d, f**) Representative confocal images showing the FluoZin-3 (green) and LysoTracker (red) staining of WT and TRPM2-KO hippocampal neurons under control (CTL) and the treatment with 1 μM $A\beta_{42}$ for 24 or 48 hr (**a**), or WT hippocampal neurons exposed to 1 μM $A\beta_{42}$ for 48 hr with or without treatments with 1 μM PJ34 (**c**), 10 μM 2-APB (**d**) or 0.1 μM TPEN (**f**). Scale bar is 10 μm. (**b, e, g**) Summary of the mean fluorescence intensity of FluoZin-3 (*top panel* in **b** and *left panels* in **e** and **g**) or LysoTracker (*bottom panel* in **b**, and *right panels* in **e** and **g**) under indicated conditions, from 3-4 independent experiments with each experiment examining 10-15 neurons. *, $P < 0.05$ and ***, $P < 0.001$ indicate significant difference from untreated neurons (**b**) or neurons treated with $A\beta_{42}$ alone (**e, g**). †, $P < 0.05$, ††, $P < 0.01$, and †††, $P < 0.001$ indicate significant difference between WT and TRPM2-KO neurons.

4.2.3 $A\beta_{42}$ induces TRPM2-dependent mitochondrial Zn^{2+} accumulation, alterations in morphology and ROS generation

As discussed in the Introduction chapter, Zn^{2+} has an intimate relationship with mitochondrial function and ROS generation. In particular, there is increasing evidence to show that mitochondrial dysfunctions and the loss of mitochondria occur in hippocampal neurons in the close vicinity or contact with Aβ-laden senile plaques (Reddy et al., 2010). Therefore, further experiments were carried out to examine whether $A\beta_{42}$ induces Zn^{2+} accumulation into mitochondria, using RhodZin-3, and the ensuring impacts on mitochondrial functions, using MitoTracker Green. Single cell imaging revealed a significant increase in the mitochondrial Zn^{2+} accumulation in WT neurons after exposure to $A\beta_{42}$ for 24-48 hr (**Fig. 4.6**). Meanwhile, there was profound decrease in MitoTracker Green fluorescence intensity, indicating the loss of mitochondria (**Fig. 4.6**). Furthermore, the remaining mitochondria became noticeably fragmented (**Fig. 4.6**). $A\beta_{42}$-induced Zn^{2+} accumulation and alterations in mitochondria were completely abolished in TRPM2-KO neurons (**Fig. 4.6**), and strongly inhibited in WT neurons treated with PJ34 or 2-APB, prior to and exposure to $A\beta_{42}$ (**Fig. 4.7**). Similarly, such $A\beta_{42}$-induced mitochondrial effects in WT neurons were suppressed by treatment with TPEN (**Fig. 4.7**).

It is interesting to know whether $A\beta_{42}$-induced mitochondrial Zn^{2+} accumulation promoted excessive ROS generation. ROS generation in WT neurons was increase by 1.5-fold and nearly 4-fold after exposure to $A\beta_{42}$ for 24 hr and 48 hr, respectively (**Fig. 4.8**). Such $A\beta_{42}$-induced increase in mitochondrial ROS generation was not observed in TRPM2-KO neurons (**Fig. 4.8**) and completely abolished in WT neurons by treatment with PJ34 or 2-APB (**Fig. 4.8**). Similarly, there was no significant increase in mitochondrial ROS generation in WT neurons treated with TPEN (**Fig. 4.8**). Collectively, these results show that TRPM2 channel plays an

important role in $A\beta_{42}$-induced mitochondrial Zn^{2+} accumulation, loss and dysfunction of mitochondria, and excessive mitochondrial ROS generation in hippocampal neurons.

4.2.4 The role of TRPM2 channel in $A\beta_{42}$-induced axonal degeneration

As shown in Chapter 3, exposure of H_2O_2 led to a substantial increase in axonal degeneration and such effect strongly depended on the TRPM2 channel. Previous studies indicate $A\beta_{42}$ can also induce axonal degeneration (Alobuia et al., 2013; Christensen et al., 2014). $A\beta_{42}$ induced excessive ROS generation (**Fig. 4.8**), thus whether the TRPM2 channal has a role in $A\beta_{42}$-induced axonal degeneration was examined. There was also significant axonal damage in WT hippocampal neurons after being exposed to 1 μM $A\beta_{42}$ for 48 and 96 hr (**Fig. 4.9**). However, the axons remained intact in TRPM2-KO hippocampal neurons (**Fig. 4.9**). These results taken together support a role of the TRPM2 channel in contributing to $A\beta_{42}$-induced axonal degeneration.

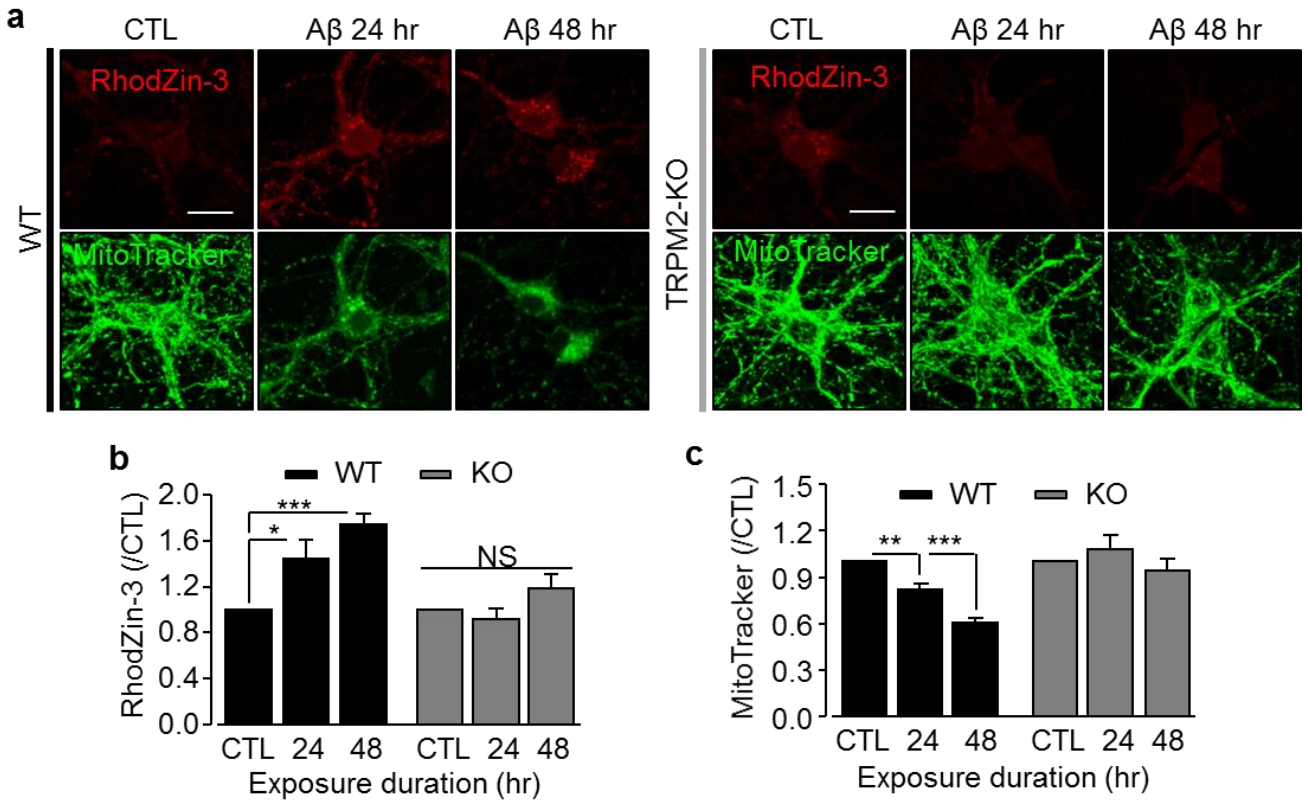
a
CTL
Aβ 24 hr
Aβ 48 hr
RhodZin-3
MitoTracker
WT
TRPM2-KO
b
WT
KO
RhodZin-3 (/CTL)
2.0
1.6
1.2
0.8
0.4
0.0
***
*
NS
CTL 24 48 CTL 24 48
Exposure duration (hr)
c
WT
KO
MitoTracker (/CTL)
1.5
1.2
0.9
0.6
0.3
0.0
**
***
CTL 24 48 CTL 24 48
Exposure duration (hr)

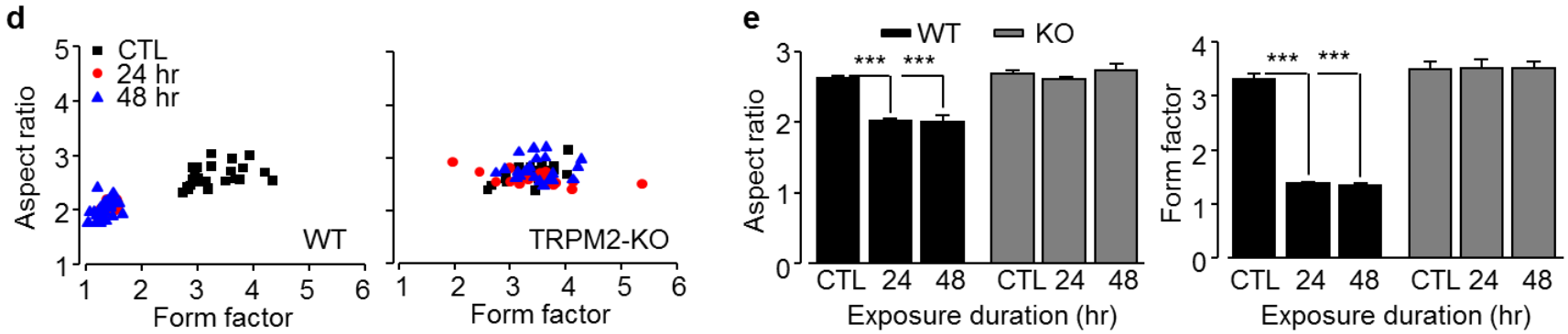

Figure 4.6 $A\beta_{42}$ induces mitochondrial Zn^{2+} accumulation, loss and fragmentation of mitochondria in WT and TRPM2-KO hippocampal neurons

(**a**) Representative confocal images showing the RhodZin-3 and MitoTracker Green staining of WT and TRPM2-KO hippocampal neurons under control (CTL) and treatment with 1 μM $A\beta_{42}$ for 24 or 48 hr. Scale bar is 10 μm. (**b, c**) Summary of the mean fluorescence intensity of RhodZin-3 (**b**) and MitoTracker (**c**) under indicated conditions, normalized to that in untreated neurons. The data were from 4 independent experiments with each examining 15-20 neurons. *, $P < 0.05$, **, $P < 0.01$, and ***, $P < 0.001$ indicate significant difference from untreated neurons in each type of neurons. NS, no significant difference. Black bars and grey bars indicate WT and TRPM2-KO hippocampal neurons, respectively. (**d**) Scatter plot of mitochondrial aspect ratio and form factor in cultured WT (*left*) or TRPM2-KO hippocampal neurons (*right*) under indicated conditions. Black squares, red circles and blue triangles represent untreated cells, cells exposed to $A\beta_{42}$ for 24 or 48 hrs, respectively. (**e**) Summary of the mean aspect ratio and form factor of mitochondria derived from computer-assisted analysis in WT (black bars) or TRPM2-KO (grey bars) hippocampal neurons under indicated conditions. The data were from 4 independent experiments with each examining 15-20 neurons. *, $P < 0.05$ and ***, $P < 0.001$ indicate significant difference from untreated neurons.

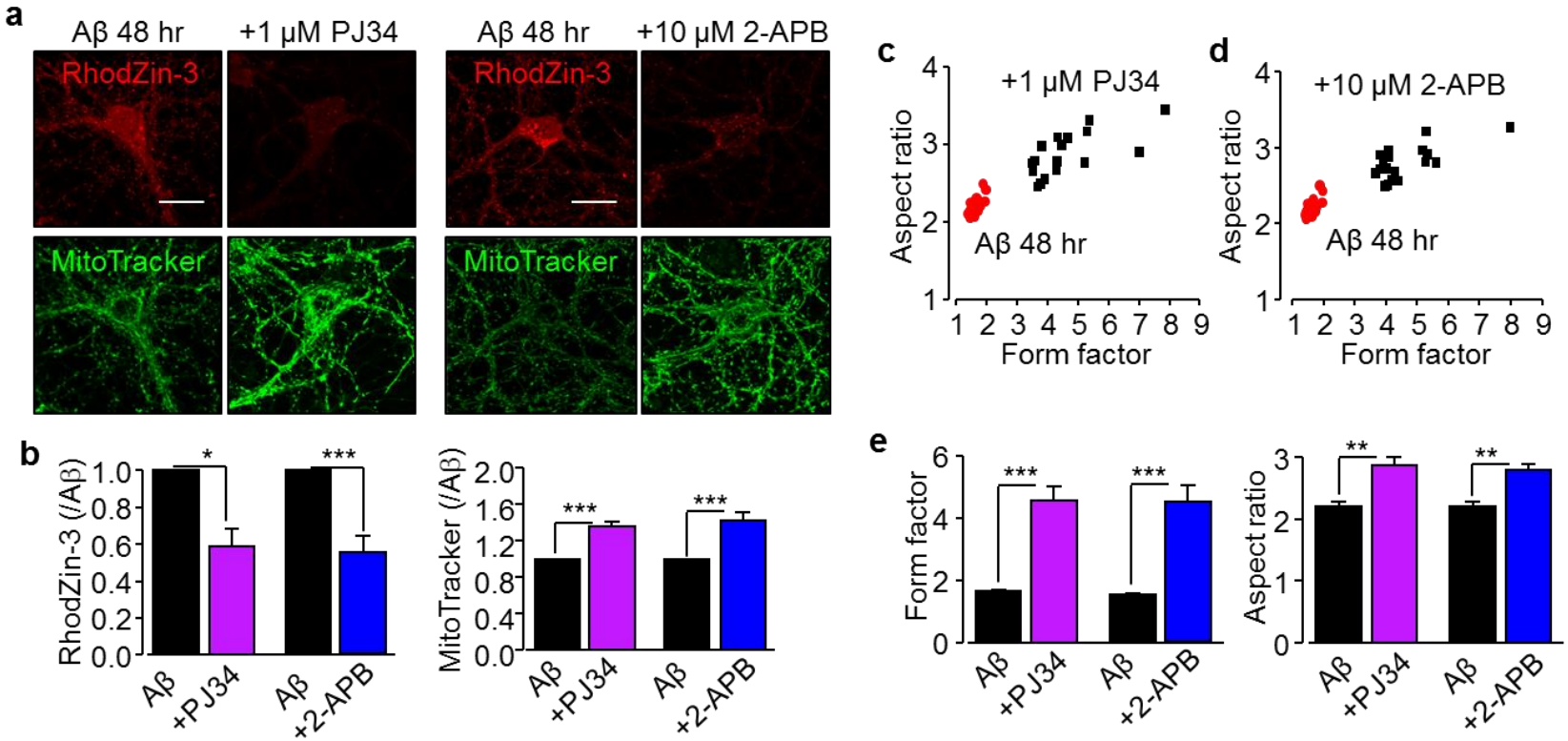
a
Aβ 48 hr
+1 μM PJ34
Aβ 48 hr
+10 μM 2-APB
RhodZin-3
RhodZin-3
MitoTracker
MitoTracker
b
RhodZin-3 (/Aβ)
1.0
0.8
0.6
0.4
0.2
0.0
*
***
Aβ
+PJ34
Aβ
+2-APB
MitoTracker (/Aβ)
2.0
1.6
1.2
0.8
0.4
0.0
***
***
Aβ
+PJ34
Aβ
+2-APB
c
+1 μM PJ34
Aspect ratio
4
3
2
1
Aβ 48 hr
1 2 3 4 5 6 7 8 9
Form factor
d
+10 μM 2-APB
Aspect ratio
4
3
2
1
Aβ 48 hr
1 2 3 4 5 6 7 8 9
Form factor
e
Form factor
6
4
2
0
***
***
Aβ
+PJ34
Aβ
+2-APB
Aspect ratio
3
2
1
0
**
**
Aβ
+PJ34
Aβ
+2-APB

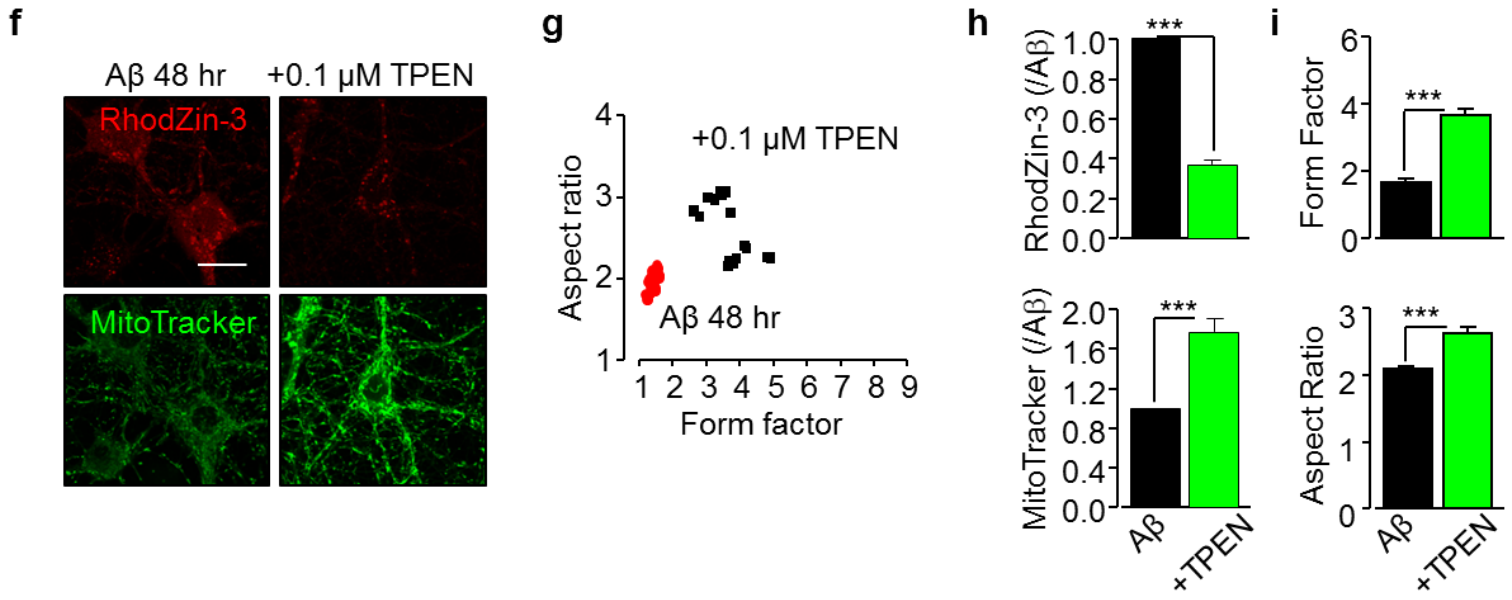

Figure 4.7 PARP/TRPM2 inhibitors and Zn^{2+} chelator attenuate $A\beta_{42}$-induced mitochondrial Zn^{2+} accumulation and fragmentation

(**a, f**) Representative confocal RhodZin-3 and MitoTracker Green staining images of WT hippocampal neurons exposed to 1 μM $A\beta_{42}$ for 48 hr with or without treatment with 1 μM PJ34, 10 μM 2-APB (**a**) or 0.1 μM TPEN (**f**). Scale bar is 10 μm. (**b, h**) Summary of the mean fluorescence intensity of RhodZin-3 (*left panel* in **b** and *top panel* in **h**) and MitoTracker Green (*right panel* in **b** and *bottom panel* in **h**) under indicated conditions, normalized to that in neurons treated with $A\beta_{42}$ alone. (**c, d, g**) Scatter plots of mitochondrial aspect ratio and form factor in WT hippocampal neurons treated with or without PJ34 (**c**), 2-APB (**d**) or TPEN (**g**). Black squares, red circles represent hippocampal neurons treated with or without inhibitors, respectively. (**e, i**) Summary of the mean aspect ratio and form factor of mitochondria derived from computer-assisted analysis in hippocampal neurons under indicated conditions. The data were from 3-4 independent experiments with each examining 15-20 neurons. *, $P < 0.05$, **, $P < 0.01$ and ***, $P < 0.001$ indicate significant difference from neurons treated with $A\beta_{42}$ alone.

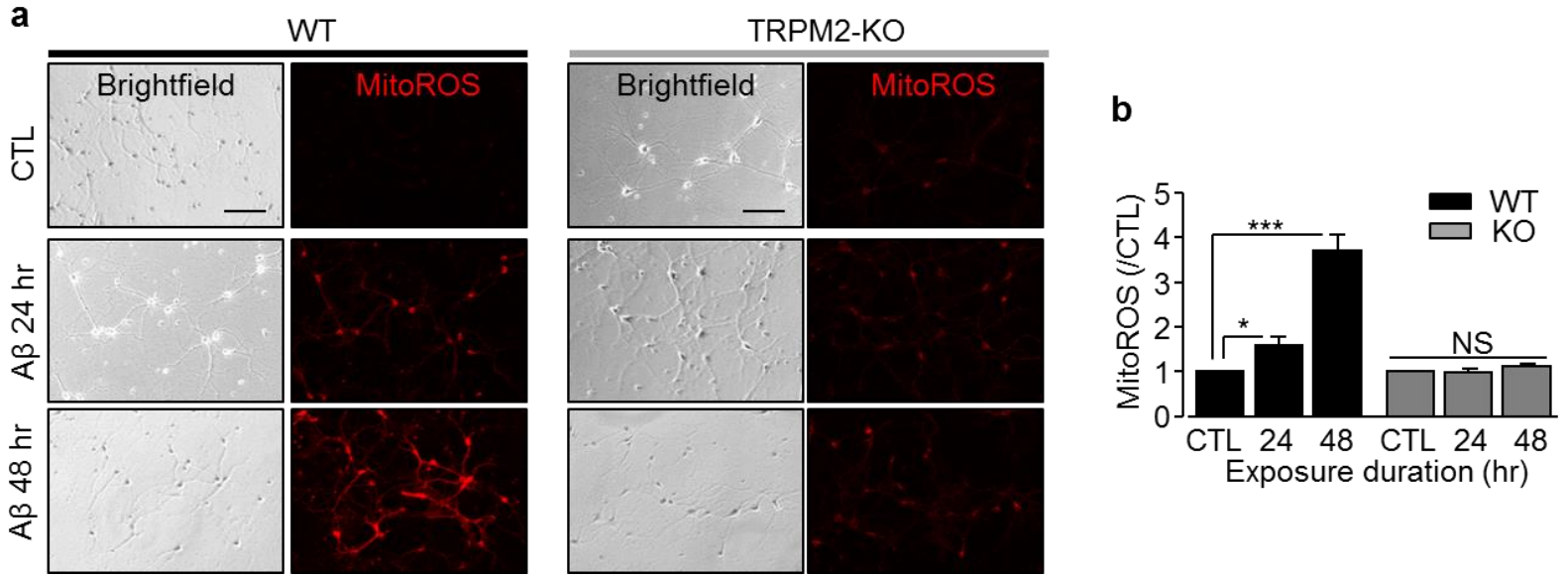
a
WT
TRPM2-KO
Brightfield
MitoROS
Brightfield
MitoROS
CTL
Aβ 24 hr
Aβ 48 hr
b
MitoROS (/CTL)
0
1
2
3
4
5
***
*
NS
WT
KO
CTL
24
48
CTL
24
48
Exposure duration (hr)

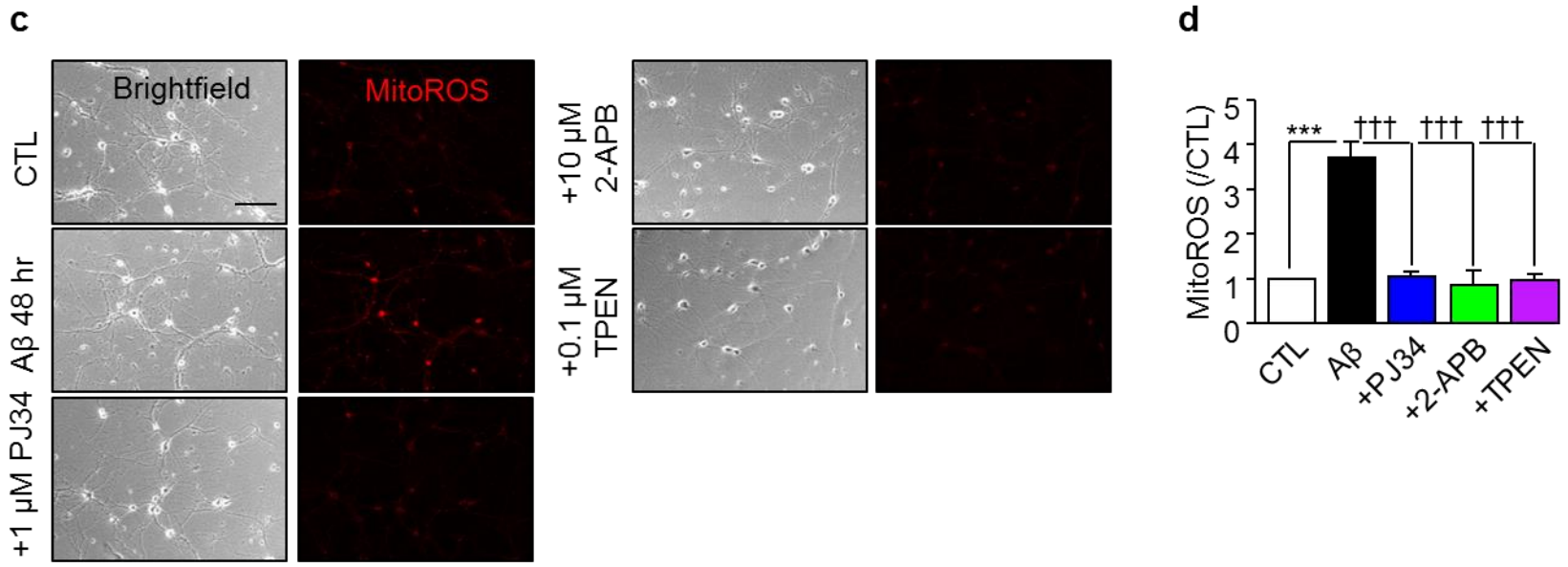

Figure 4.8 $A\beta_{42}$-induced TRPM2-dependent mitochondrial ROS production

(**a, c**) Representative images showing the MitoTracker Red CM-H_2Xros staining (MitoROS, red) in WT and TRPM2-KO hippocampal neurons under control (CTL) and treatment with 1 μM $A\beta_{42}$ for 24 or 48 hr (**a**), and WT hippocampal neurons untreated (CTL) or treated with 1 μM Aβ for 48 hr with or without pre-treatment with 1 μM PJ34, 10 μM 2-APB or 0.1 μM TPEN (**c**). Scale bar is 100 μm. (**b, d**) Summary of the mean MitoROS fluorescence intensity represent the mitochondrial ROS generation under indicated conditions, normalized to that in neurons under control conditions. The data were from 3 independent experiments with each experiment examining 350-500 neurons. *, $P < 0.05$; and ***, $P < 0.001$ indicate difference from neurons under the control conditions. †††, $P < 0.001$ indicates difference from neurons exposed with $A\beta_{42}$ alone. NS, stand for no significant difference.

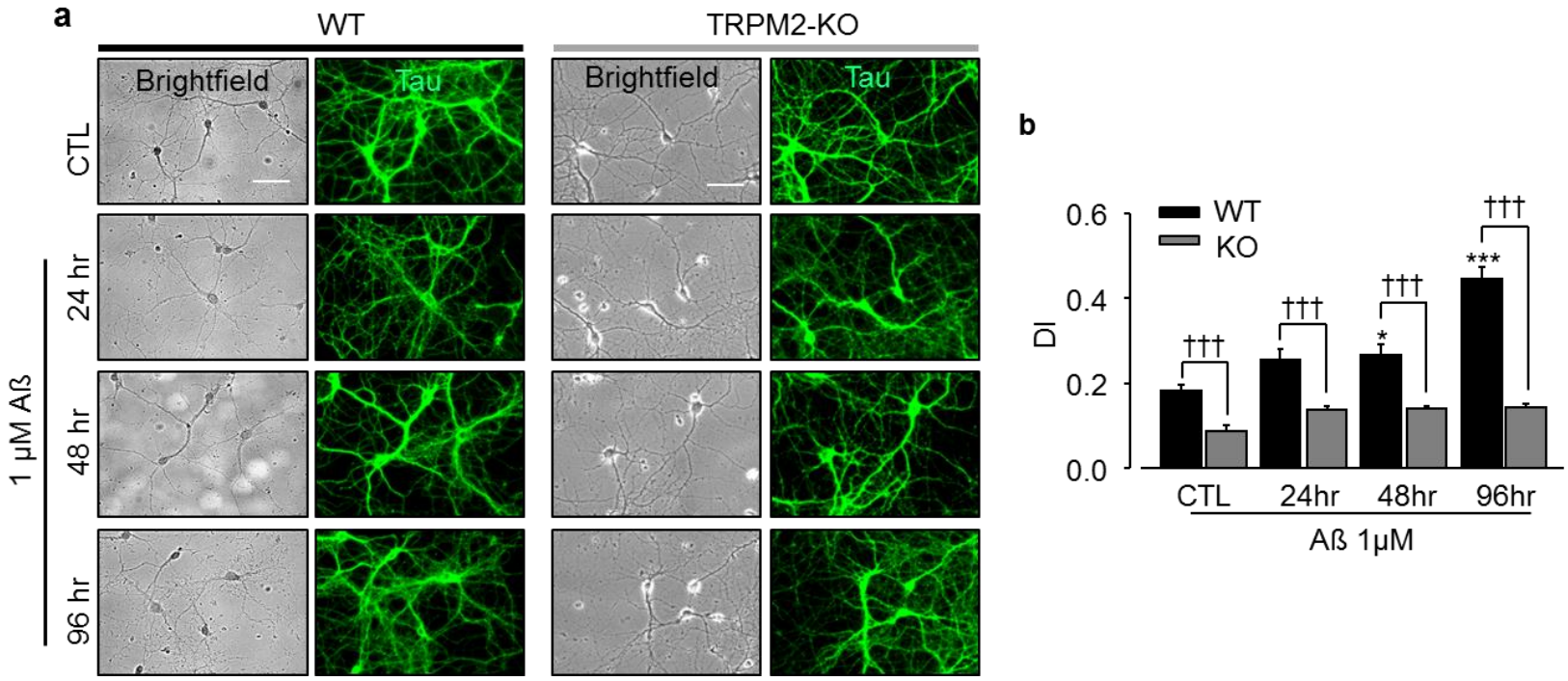

Figure 4.9 TRPM2 activation mediates axonal degeneration in hippocampal neurons induced by $A\beta_{42}$

(**a**) Representative immunofluorescent confocal images of hippocampal neurons labelled with an anti-Tau antibody (green) in hippocampal neurons from WT and TRPM2-KO neurons treated under indicated conditions. Scale bar is 100 µm. (**b**) Quantification of the axon degeneration index (DI) of WT and TRPM2-KO hippocampal neurons under indicated conditions. The results were from 3-5 (60-80 cells of each independent experiment), *, $P < 0.05$ and ***, $P < 0.001$ indicate significant difference relative to control; †, $P < 0.05$ and †††, $P < 0.001$ for comparison between WT and TRPM2-KO neurons.

4.2.5 The PKC/NOX signalling pathway is engaged in $A\beta_{42}$-induced hippocampal neurotoxicity

The results so far showed that $A\beta_{42}$ induces mitochondrial ROS generation. As introduced in previous chapters, ROS can activate PKC which in turn stimulates NOX, an important source of ROS inducing neuronal death implicated in ischemic stroke and neurodegenerative diseases. Experiments were performed to examine whether the PKC/NOX signalling pathway was engaged in $A\beta_{42}$-induced neurotoxicity by determining the effects of GÖ6976, apocynin, DPI and GKT137831 on $A\beta_{42}$-induced neurotoxicity and ROS generation. $A\beta_{42}$-induced neurotoxicity was significantly attenuated by treatment with 10-30 nM GÖ6976, prior to and during exposure to $A\beta_{42}$ (**Fig. 4.10**). Similarly, $A\beta_{42}$ induced neurotoxicity was virtually reversed by treatment with 10-30 µM apocynin (**Fig. 4.10**) or significantly inhibited by treatment with 1 nM DPI (**Fig. 4.10**) or 1-10 µM GKT137831 (**Fig. 4.10**). $A\beta_{42}$ also induced substantial increase in cellular oxidative stress or ROS generation, as shown using DCFH-DA (**Fig. 4.11**). Such $A\beta_{42}$-induced oxidative stress was prohibited by treatment with 10 nM GÖ6976, 30 µM apocynin, 1 nM DPI or 10 µM GKT137831 (**Fig. 4.11**). To further investigate the role of PKC/NOX-mediated ROS generation in $A\beta_{42}$-induced neurotoxicity, effects of the above-described PKC and NOX inhibitors were determined on $A\beta_{42}$-induced increase in the $[Zn^{2+}]_i$, lysosomal dysfunction, mitochondrial Zn^{2+} accumulation, and loss and dysfunction of mitochondria as well as mitochondrial ROS production (**Fig. 4.12-4.14**). Treatment with 10 nM GÖ6976, prior to and during exposure to $A\beta_{42}$, strongly or completely inhibited $A\beta_{42}$-induced increase in the $[Zn^{2+}]_i$ (**Fig. 4.12**), lysosomal dysfunction (**Fig. 4.12**), mitochondrial Zn^{2+} accumulation (**Fig. 4.12**), mitochondrial loss and fragmentation as well as mitochondrial ROS production (**Fig. 4.12** and **Fig. 4.14**). Similarly, treatment with 30 µM apocynin or 10 µM GKT137831 resulted in a strong inhibition of $A\beta_{42}$-induced increase in the $[Zn^{2+}]_i$ (**Fig. 4.13**), lysosomal dysfunction (**Fig. 4.13**), mitochondrial Zn^{2+} accumulation (**Fig. 4.13**), mitochondrial loss (**Fig.**

4.13) and fragmentation (**Fig. 4.13**) and mitochondrial ROS production (**Fig. 4.14**). These results clearly support the notion that the ROS-generating PKC/NOX signalling pathway is a critical component in the mechanisms mediating $A\beta_{42}$-induced neurotoxicity.

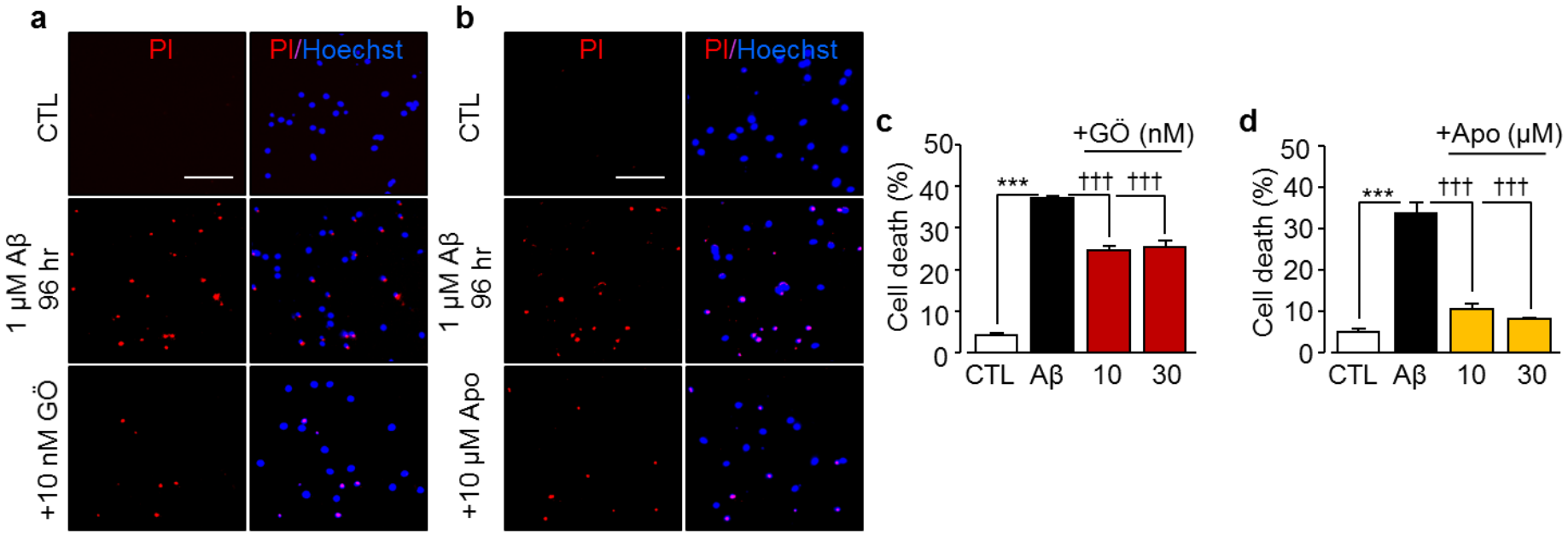
a
PI
PI/Hoechst
CTL
1 μM Aβ
96 hr
+10 nM GÖ
b
PI
PI/Hoechst
CTL
1 μM Aβ
96 hr
+10 μM Apo
c
+GÖ (nM)
Cell death (%)
50
40
30
20
10
0
***
†††
†††
CTL
Aβ
10
30
d
+Apo (μM)
Cell death (%)
50
40
30
20
10
0
***
†††
†††
CTL
Aβ
10
30

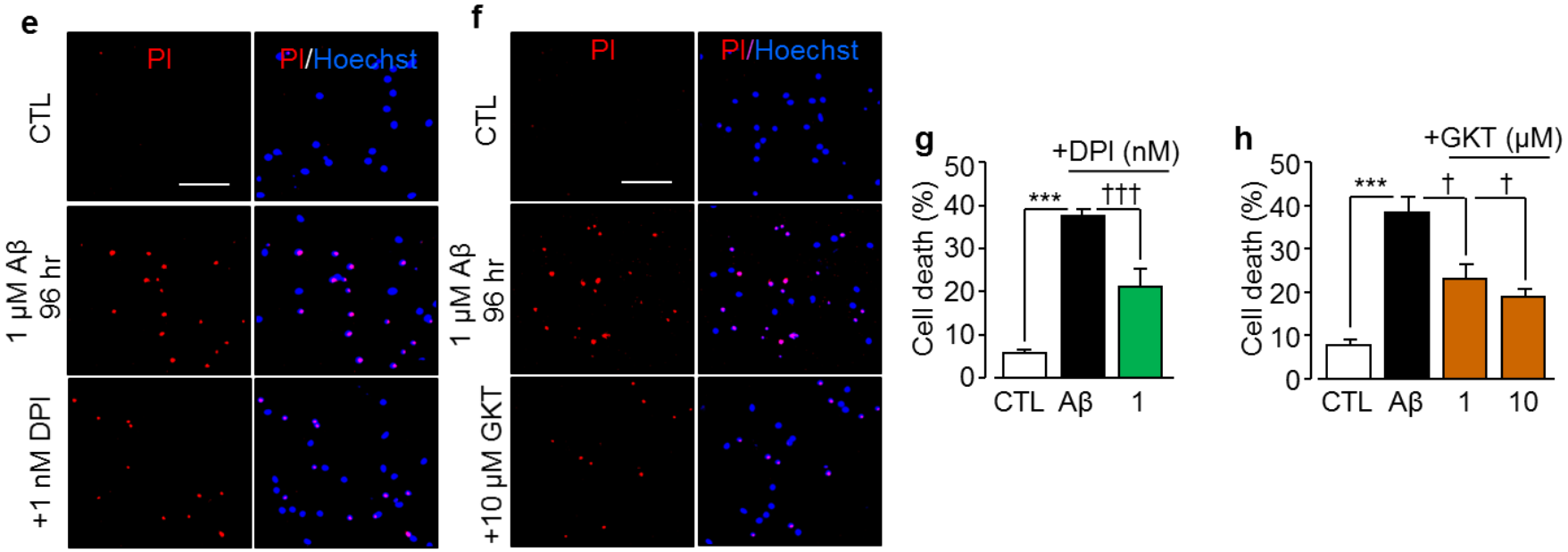

Figure 4.10 A critical role of the PKC/NOX signalling pathway in $A\beta_{42}$-induced hippocampal toxicity

(**a**, **b, e, f**). Representative images showing PI and PI/Hoechst staining images in hippocampal neurons under control (CTL) or exposure to 1 μM $A\beta_{42}$ for 96 hr treated with or without treatment with 10 nM GÖ6976 (GÖ) (**a**), 10 μM apocynin (Apo) (**b**), 1 nM DPI (**e**) or 10 μM GKT137831 (GKT) (**f**). Scale bar is 100 μm. (**c, d, g, h**) Summary of the mean percentage of PI positive neurons under indicated conditions, from 3-5 independent experiment with each examining 400-600 neurons. ***, $P < 0.001$ indicates difference from neurons under control conditions. †, $P < 0.05$ and †††, $P < 0.001$ indicate difference from neurons exposed to $A\beta_{42}$ alone.

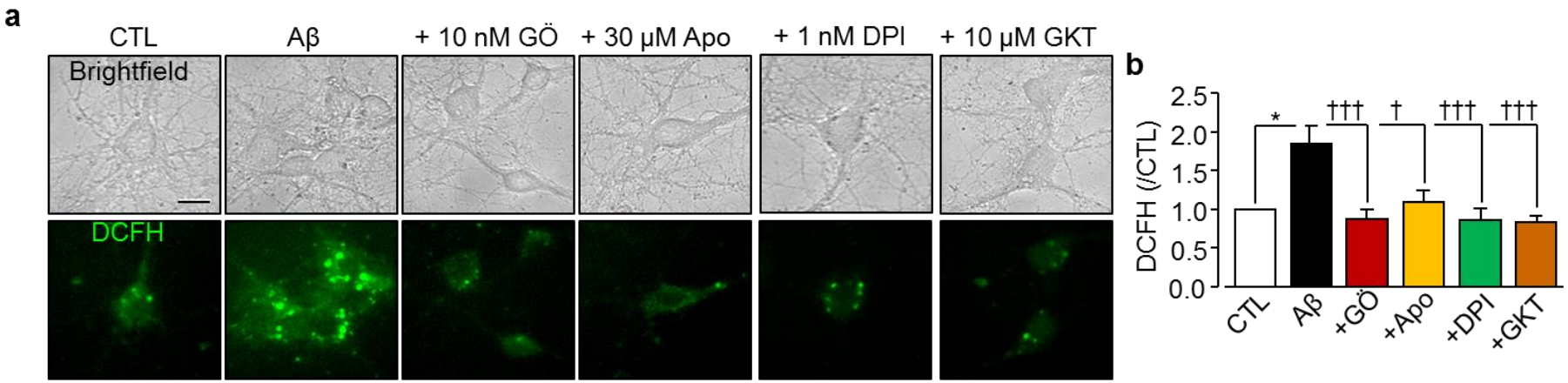

Figure 4.11 The PKC/NOX signalling pathway contributes in $A\beta_{42}$-induced oxidative stress

(**a**) Representative images showing the DCFH-DA fluorescence (oxidative stress or ROS generation) in hippocampal neurons under control (CTL) condition and exposure to 1 μM $A\beta_{42}$ for 48 hr with or without treatment with 10 nM GÖ6976 (GÖ), 30 μM apocynin (Apo), 1 nM DPI, or 10 μM GKT137831 (GKT). Scale bar is 10 μm. (**b**) Summary of the mean DCFH-DA fluorescence intensity in neurons under indicated conditions normalized to the basal level under control conditions, from 3-4 independent experiments with each examining 15-60 neurons. *, $P < 0.05$ indicates difference from the basal level. †, $P < 0.05$ and †††, $P < 0.001$ indicate difference from that in neurons exposed with $A\beta_{42}$ alone.

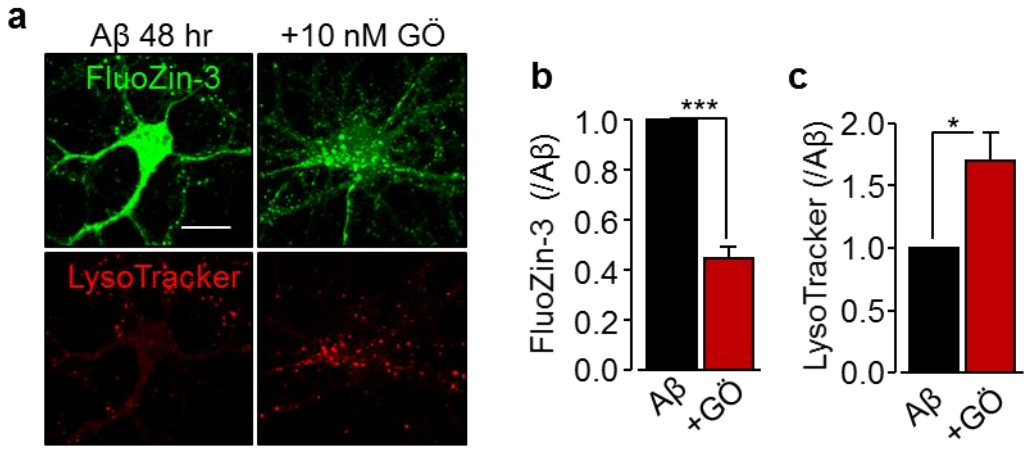
a
Aβ 48 hr
+10 nM GÖ
FluoZin-3
LysoTracker
b
***
FluoZin-3 (/Aβ)
1.0
0.8
0.6
0.4
0.2
0.0
Aβ
+GÖ
c
*
LysoTracker (/Aβ)
2.0
1.5
1.0
0.5
0.0
Aβ
+GÖ

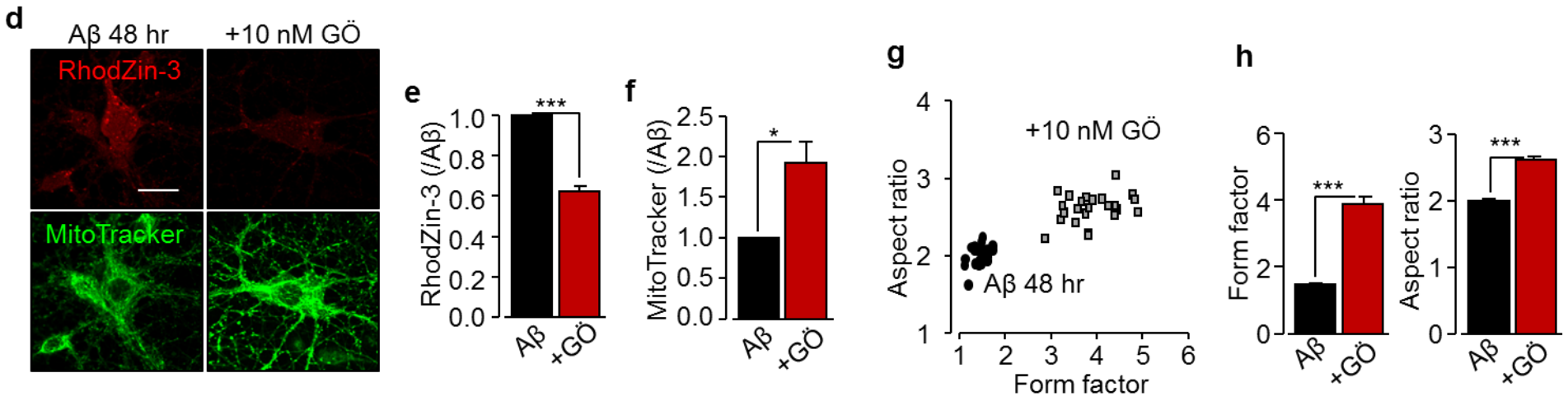

Figure 4.12 PKC activation mediates $A\beta_{42}$-induced increase in the $[Zn^{2+}]_i$, lysosomal dysfunction, mitochondrial Zn^{2+} accumulation, loss and fragmentation of mitochondria in hippocampal neurons

(**a**) Representative confocal images showing the FluoZin-3 and LysoTracker staining in hippocampal neurons treated with 1 μM $A\beta_{42}$ for 48 hr with or without the treatment with 10 nM GÖ6976 (GÖ). Scale bar is 10 μm. (**b, c**) Summary of the mean fluorescence intensity of FluoZin-3 (**b**) or LysoTracker (**c**) under indicated conditions normalized to that in neurons exposed to $A\beta_{42}$ alone, from 3-4 independent experiments with each examining 10-12 neurons. *, $P < 0.05$ and ***, $P < 0.001$ indicate the difference from neurons exposed with $A\beta_{42}$ alone. (**d**) Representative confocal images showing the RhodZin-3 and MitoTracker Green staining in hippocampal neurons exposed to 1 μM $A\beta_{42}$ for 48 hr with or without 10 nM GÖ6976. Scale bar is 10 μm. (**e, f**) Summary of the mean fluorescence intensity of RhodZin-3 (**e**) and MitoTracker (**f**) under indicated conditions normalized to that in neurons exposed with $A\beta_{42}$ alone. (**g**) Scatter plots of mitochondrial aspect ratio and form factor in cultured WT hippocampal neurons treated with or without GÖ6976. Black circles and grey squares represent hippocampal neurons treated with or without GÖ6976, respectively. (**h**) Summary of the mean form factor and aspect ratio value of mitochondria under indicated conditions. The data were from 4 independent experiments with each examining 15-20 neurons. *, $P < 0.05$, **, $P < 0.01$ and ***, $P < 0.001$ indicate the difference from neurons exposed with $A\beta_{42}$ alone.

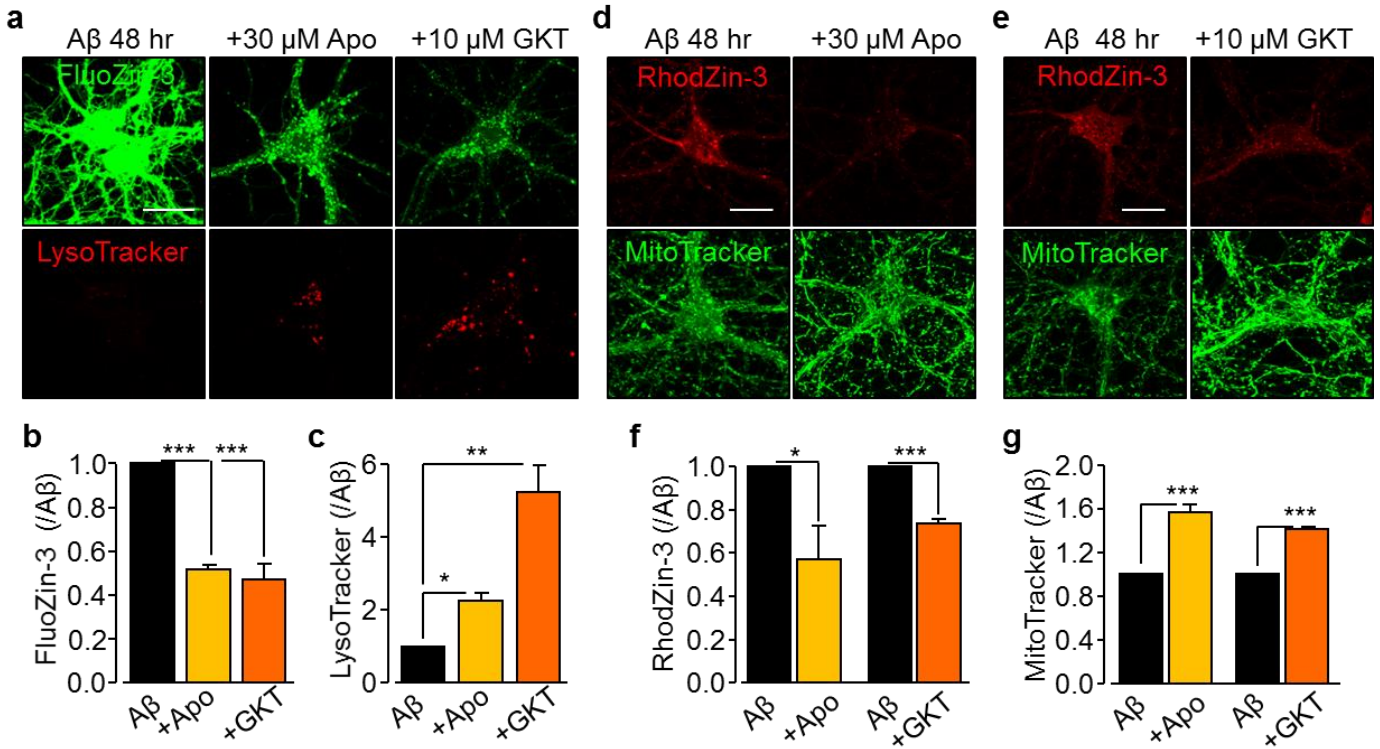
a
Aβ 48 hr
+30 μM Apo
+10 μM GKT
FluoZin-3
LysoTracker
d
Aβ 48 hr
+30 μM Apo
RhodZin-3
MitoTracker
e
Aβ 48 hr
+10 μM GKT
RhodZin-3
MitoTracker
b
FluoZin-3 (/Aβ)
c
LysoTracker (/Aβ)
f
RhodZin-3 (/Aβ)
g
MitoTracker (/Aβ)
Aβ
+Apo
+GKT

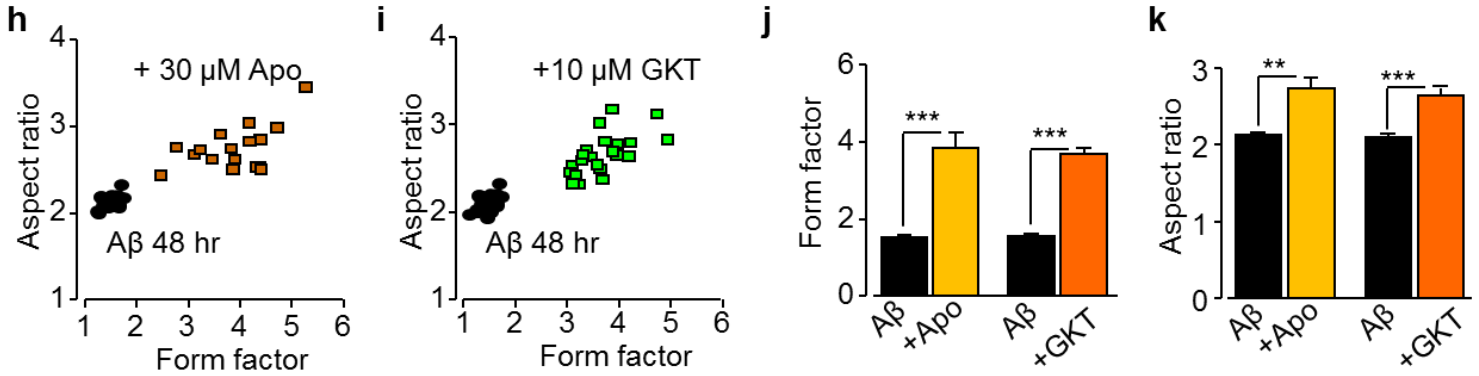

Figure 4.13 Critical dependence of $A\beta_{42}$-induced increase in the $[Zn^{2+}]_i$, lysosomal dysfunction, mitochondrial Zn^{2+} accumulation, the loss and fragmentation of mitochondria on PKC activation

(**a**) Representative confocal images showing the FluoZin-3 and LysoTracker staining in hippocampal neurons treated with 1 μM $A\beta_{42}$ for 48 hr with or without treatment with 30 μM apocynin (Apo) or 10 μM GKT137831 (GKT). Scale bar is 10 μm. (**b, c**) Summary of the mean fluorescence intensity of FluoZin-3 (**b**) or LysoTracker (**c**) under indicated conditions normalized to that in neurons exposed to $A\beta_{42}$ alone, from 3-4 independent experiments with each examining 10-12 neurons. *, $P < 0.05$, **, $P < 0.01$ and ***, $P < 0.001$ indicate the difference from neurons exposed with $A\beta_{42}$ alone. (**d, e**) Representative confocal images showing the RhodZin-3 and MitoTracker Green staining in hippocampal neurons exposed to 1 μM Aβ for 48 hr with or without 30 μM apocynin (**d**) or 10 μM GKT137831 (**e**). Scale bar is 10 μm. (**f, g**) Summary of the mean fluorescence intensity of RhodZin-3 (**f**) and MitoTracker (**g**) under indicated conditions normalized to that in neurons exposed with $A\beta_{42}$ alone. (**h, i**) Scatter plots of mitochondrial aspect ratio and form factor in cultured WT hippocampal neurons treated with or without apocynin (**h**) or GKT137831 (**i**). Red or green squares and black circles represent hippocampal neurons treated with or without inhibitors, respectively. (**j, k**) Summary of the mean form factor and aspect ratio values of mitochondria under indicated conditions. The data were from 3-4 independent experiments with each examining 15-20 neurons. *, $P < 0.05$, **, $P < 0.01$ and ***, $P < 0.001$ indicate difference from neurons exposed with $A\beta_{42}$ alone.

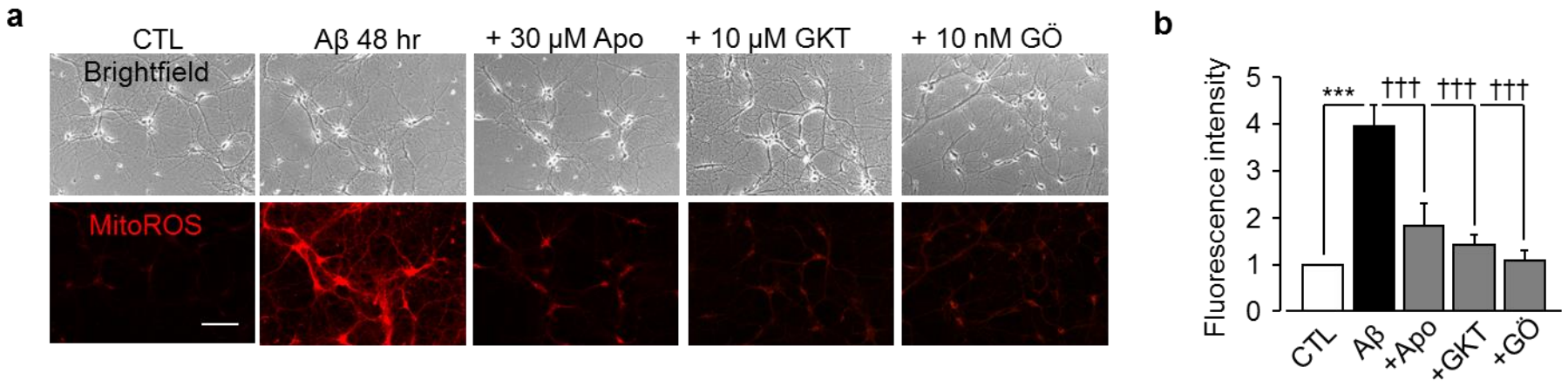

Figure 4.14 Inhibition of the PKC/NOX signalling pathway prevents $A\beta_{42}$-induced mitochondrial ROS generation

(**a**) Representative images showing the MitoROS fluorescence (mitochondrial ROS production) in hippocampal neurons under control (CTL) condition and exposure to 1 μM $A\beta_{42}$ for 48 hr with or without treatment with, 30 μM apocynin (Apo), 10 μM GKT137831 (GKT) or 10 nM GÖ6976 (GÖ). Scale bar is 100 μm. (**b**) Summary of the mean fluorescence intensity of MitoROS in neurons under indicated conditions normalized to the basal level under control conditions, from 3-4 independent experiments with each examining 15-60 neurons. ***, $P < 0.001$ indicates difference from the basal level. †††, $P < 0.001$ indicates difference from that in neurons exposed with $A\beta_{42}$ alone.

4.2.6 The MEK/ERK signalling pathway is vital in $A\beta_{42}$-induced hippocampal neurotoxicity

As discussed in the Introduction chapter (see section **1.3.4.3**), PARP-1 dependent production of ADPR represents a major mechanism in ROS-induced TRPM2 channel activation. ROS-induced PARP-1 activation is long known as an important neurotoxicity-inducing factor (Moroni, 2008). A recent study has reported that ROS stimulates PARP-1 via the activation of MAPK/ERK pathway (Domercq et al., 2013). In addition, Ras and Pyk2 are well-known to act as upstream signalling kinases that activate the MEK/ERK signalling pathway (Chang et al., 2003; Agell et al., 2002). Therefore, the role of MEK/ERK signalling pathways in $A\beta_{42}$-induced neurotoxicity was investigated. $A\beta_{42}$-induced neuronal death was significantly reduced by treatment with 10-100 nM PF431396, a Pyk2 inhibitor, but not with farnesylthiosalicylic acid (FTS) (**Fig. 4.15**), a Ras inhibitor. The viability of hippocampal neuronal cells in response to $A\beta_{42}$ was also substantially increased in the presence of 10-100 nM U0126, a MEK/ERK inhibitor (**Fig. 4.15**), indicating the importance of the MEK/ERK signalling pathway in $A\beta_{42}$-induced neurotoxicity.

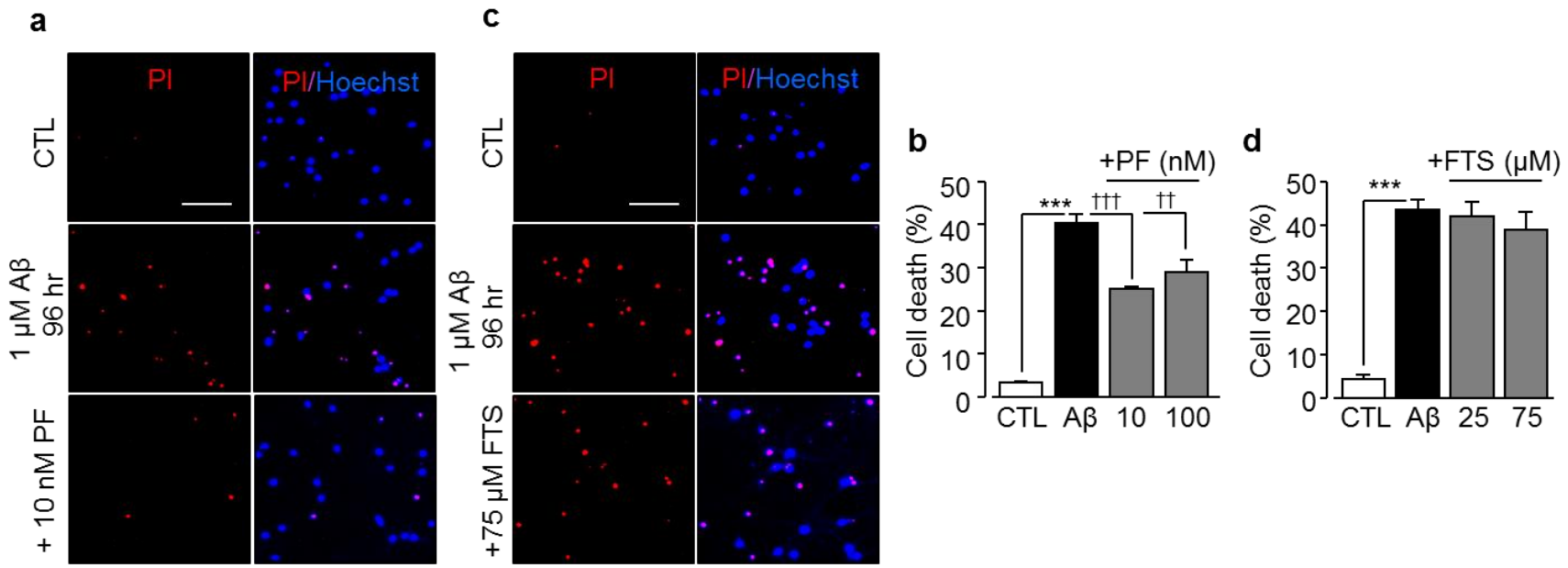
a
PI
PI/Hoechst
CTL
1 μM Aβ 96 hr
+ 10 nM PF
c
PI
PI/Hoechst
CTL
1 μM Aβ 96 hr
+75 μM FTS
b
+PF (nM)
Cell death (%)
50
40
30
20
10
0
***
†††
††
CTL
Aβ
10
100
d
+FTS (μM)
Cell death (%)
50
40
30
20
10
0
***
CTL
Aβ
25
75

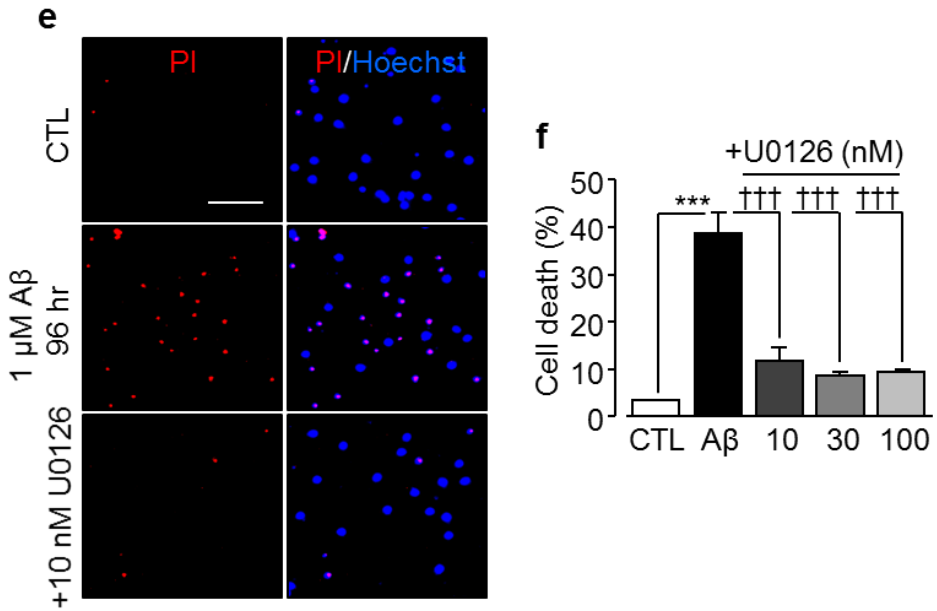

Figure 4.15 A critical role of the MEK/ERK signalling pathway in $A\beta_{42}$-induced hippocampal neurotoxicity

(**a, c, e**) Representative images showing PI and PI/Hoechst staining of hippocampal neurons under control (CTL) or exposure to 1 μM $A\beta_{42}$ for 96 hr with or without treatment with 10 nM PF431396 (PF) (**a**), 75 μM FTS (**c**) or 10 nM U0126 (**e**). Scale bar is 100 μm. (**b, d, f**) Summary of the mean percentage of PI positive neurons under indicated conditions, from 3 independent experiments with each examining 400-650 neurons. ***, $P < 0.001$ indicates the difference from neurons under control conditions. ††, $P < 0.01$ and †††, $P < 0.001$ indicate difference from neurons exposed with 1 μM $A\beta_{42}$ alone.

4.3 Discussion

The study described in this chapter presents experimental evidence using genetic and pharmacological approaches to show a host of intracellular events via coupling with the PKC/NOX and MEK/ERK signalling pathway form a positive feedback mechanism mediating $A\beta_{42}$-induced TRPM2 channel activation and neurotoxicity in hippocampal neurons (**Fig. 4.16**). These findings provide novel and mechanistic insights into AD pathogenesis.

It is well recognized that neurotoxicity resulting from the excessive Aβ generation is crucial in AD pathogenesis, for which multiple molecular and cellular mechanisms have been proposed. Consistently with Aβ-induced oxidative stress and TRPM2 channel as an oxidative stress-sensitive channel, recent studies have revealed an important role for TRPM2 channel in Aβ-induced vascular dysfunction, synaptic loss and age-related cognitive impairment (Ostapchenko et al., 2015; Park et al., 2014). The study described in this chapter showed that $A\beta_{42}$-induced neurotoxicity in hippocampal neurons was ablated by genetic depletion of the TRPM2 expression (**Fig. 4.1**) and attenuated by pharmacological inhibition of the PARP-1 dependent TRPM2 channel activation or activity (**Fig. 4.2**), providing strong evidence at the cell level to confirm a critical role for TRPM2 channel in $A\beta_{42}$-induced neurodegeneration.

Despite the recent revelation of the close causative relationship of the TRPM2 channel with AD, it remained elusive how the TRPM2 channel is activated and leads to neurodegeneration. Cytosolic Ca^{2+} is known as a ubiquitous signal in diverse cell functions, including cell death, contributing to NMDAR-dependent neuronal excitotoxicity in ischemia stroke (see section **1.4.2.1** in the Introduction chapter) and neurodegeneration in the pathogenesis of AD and PD. However, there is increasing evidence to show that TRPM2 channel is critical in the deregulation of intracellular Zn^{2+} homeostasis, evidenced by recent findings (Ye et al., 2014; Manna

et al., 2015) and the results shown in the previous chapter. An increase in the $[Ca^{2+}]_i$ resulting from TRPM2-mediated Ca^{2+} influx and intracellular Ca^{2+} release is not obligatory for cell death but is required mainly for facilitating the TRPM2 channel activation. As shown in this chapter, exposure to $A\beta_{42}$ failed to increase the $[Ca^{2+}]_i$ (**Fig. 4.4**) in hippocampal neurons. However, the $[Zn^{2+}]_i$ was considerably elevated by exposure to $A\beta_{42}$ (**Fig. 4.4**), and such $A\beta_{42}$-induced increase in the $[Zn^{2+}]_i$ as well as neurotoxicity was completely ablated by TPEN (**Fig. 4.4** and **Fig. 4.5**). There was no $A\beta_{42}$-induced increase in the $[Zn^{2+}]_i$ in TRPM2-KO neurons (**Fig. 4.5**) and $A\beta_{42}$ induced increase in the $[Zn^{2+}]_i$ was suppressed by PARP-1 and TRPM2 inhibitors (**Fig. 4.5**). Taken together, these results provide clear evidence to support TRPM2-dependent increase in $[Zn^{2+}]_i$ is critical in $A\beta_{42}$-induced hippocampal neurotoxicity.

$A\beta_{42}$ is a damage-associated molecular pattern molecule, which can be endocytosed into lysosome and as a result causes lysosomal dysfunction and cathepsin B release into cytosol (Halle et al., 2008). In this chapter, I found that exposure of hippocampal neurons to $A\beta_{42}$ led to massive increase in the $[Zn^{2+}]_i$, accompanied with the lysosomal dysfunction as indicated by significant decline in LysoTracker fluorescence intensity (**Fig. 4.5**). Additionally, $A\beta_{42}$-induced, as discussed below, the generation of excessive ROS (**Fig. 4.11**), which was known to induce damage of the lysosomal membrane integrity in hippocampal neurons as described by results presented in the previous chapter and previous studies (Boya and Kroemer, 2008).

The results shown in previous chapter support strong correlation of a rise in the $[Zn^{2+}]_i$ with the loss or dysfunction of mitochondria and the generation of excessive ROS. Indeed, $A\beta_{42}$ induced an increase in the $[Zn^{2+}]_i$ and also led to the mitochondrial Zn^{2+} accumulation (**Fig. 4.6**), alterations in mitochondrial morphologies (**Fig. 4.6**), and excessive ROS generation (**Fig. 4.8**). These events in mitochondria were completely prevented by TPEN as well as TRPM2-KO (**Figs.**

4.6-4.8). These results provide evidence to support that TRPM2-dependent mitochondrial dysfunction and excessive mitochondrial ROS generation. In addition, it is known that Zn^{2+} induces opening of the mPTP and the release of pro-apoptotic signalling pathway (Sensi et al., 2009). Consistently, $A\beta_{42}$-induced neurotoxicity was sensitive to the inhibition of caspase-dependent apoptosis (**Fig. 4.3**).

Neuronal cell death results from the damage to axons as well as cell bodies. Axonal degeneration can be induced by ROS and ROS-induced mitochondrial dysfunction (Barrientos et al., 2011; Court and Coleman, 2012). Recent studies show axonal degeneration is linked to Aβ accumulation and $A\beta_{42}$-induced neuronal cell death (Alobuia et al., 2013; Christensen et al., 2014). Exposure to $A\beta_{42}$ triggered significant axonal degeneration (**Fig. 4.9**), similar to H_2O_2-induced axonal degeneration described in the previous chapter. Such axonal destruction was attenuated by TRPM2-KO, suggesting the importance of the TRPM2 channel in $A\beta_{42}$-induced impairment of axons, which may result from ROS generation and mitochondrial dysfunction.

As already introduced in the previous chapters, Zn^{2+} can induce NOX activation to generate ROS in cultured neurons in addition to the mitochondrial ROS generation (Sensi et al., 2009). In fact, NOX-mediated ROS generation plays a crucial role in inducing neurotoxicity implicated in the pathogenesis of ischemic stroke and AD (Tang et al., 2012; Block, 2008). As shown in the present study, $A\beta_{42}$-induced neurotoxicity and cellular oxidative stress were strongly suppressed or prohibited by apocynin, DPI, and GKT137831 (**Figs. 4.10-4.11**), consistent with the role of NOX1 and NOX4 in hippocampal neurons (Kahles et al., 2010; Radermacher et al., 2013). Notably, $A\beta_{42}$-induced neurotoxicity was attenuated by GÖ6976 (**Fig. 4.10**), and so was $A\beta_{42}$-induced cellular oxidative stress (**Fig. 4.11**), supporting the notion that Zn^{2+} stimulates NOX through promoting PKC activation. Furthermore, $A\beta_{42}$-induced increase in the $[Zn^{2+}]_i$ as well as lysosomal dysfunction, mitochondrial Zn^{2+} accumulation and mitochondrial ROS generation were entirely or largely reversed

by PKC and NOX inhibitors (**Figs. 4.12-4.14**). These results indicate the PKC/NOX-mediated ROS-generation as a part of the mechanisms for $A\beta_{42}$-induced lysosomal dysfunction and increase in the $[Zn^{2+}]_i$ that leads to the mitochondrial Zn^{2+} accumulation, alterations in mitochondria, and mitochondrial ROS generation. As discussed in the Introduction chapter (see **Fig. 1.5** and section **1.3.4.3**), PARP-1 together with PARG in the nucleus is critically involved in ROS-induced DNA repair mechanism, in which ADPR is generated as a by-product (Ko and Ren, 2012). The ERK activation had been recently reported to result in PARP-1 activation, mediating oligodendrocyte death in OGD/R model (Domercq et al., 2013). Here, the results showed that $A\beta_{42}$-induced neurotoxicity in hippocampal neurons were completely prevented by U0126, a MEK/ERK inhibitor (**Fig. 4.15**). In addition to PKC, Ras and Pyk2 are two well-known kinases upstream of MEK/ERK. $A\beta_{42}$-induced neurotoxicity was modestly but significantly attenuated by PF431396, a Pyk2 inhibitor, but not FTS, a Ras inhibitor (**Fig. 4.15**). Taken together, the MEK/ERK signalling pathway acts as a critical signal in $A\beta_{42}$-induced PARP-1 activation, leading to the ADPR generation and TRPM2 channel activation.

In conclusion, the study presented in this chapter shows evidence to demonstrate that $A\beta_{42}$ induces multiple events from lysosomal dysfunction and Zn^{2+} release to mitochondrial Zn^{2+} accumulation, the loss and dysfunction of mitochondria, and mitochondrial ROS generation, which are coupled with the PKC/NOX pathway and the MEK/ERK signalling pathway to form a positive feedback mechanism underlying $A\beta_{42}$-induced TRPM2-dependent neurotoxicity in hippocampal neurons. These findings provide novel and mechanistic insights into the pathogenesis of AD.

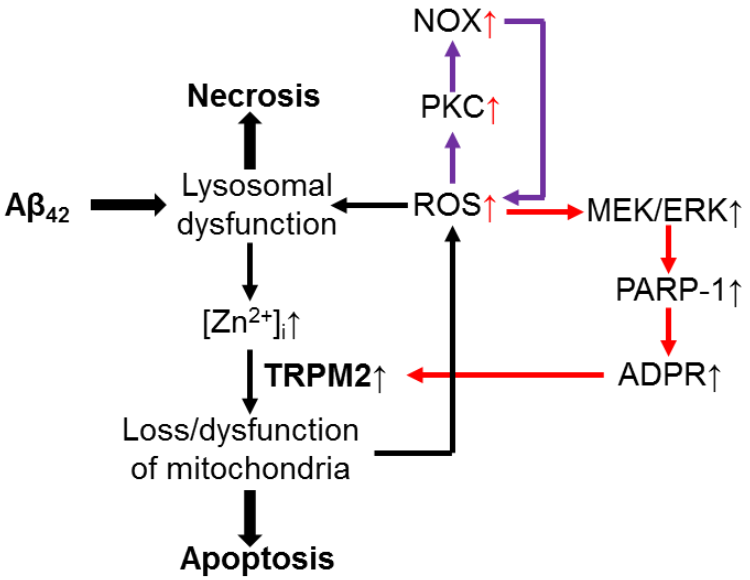

Figure 4.16 A schematic diagram summarizing the positive feedback mechanism underlying $A\beta_{42}$-induced TRPM2-dependent neurotoxicity

$A\beta_{42}$ can be internalized via endocytosis into lysosome, leading to the lysosomal dysfunction and Zn^{2+} release and subsequent increase in the $[Zn^{2+}]_i$. An increase in the $[Zn^{2+}]_i$ leads to TRPM2 channel-dependent mitochondrial Zn^{2+} accumulation that induces the loss and dysfunction of mitochondria and excessive mitochondrial ROS generation. ROS causes further lysosomal dysfunction and, in addition, activates the PKC/NOX signalling pathway to generate excessive ROS and the MEK/ERK signalling pathway to promote PARP-1 dependent ADPR generation and TRPM2 channel activation. (NOX: Nicotinamide adenine dinucleotide phosphate oxidase; PKC: Protein kinase C; ROS: Reactive oxygen species; ERK: Extracellular signal regulated kinase; MEK: MAPK/ERK kinase; ADPR: Adenosine diphosphate-ribose; PARP-1: Poly(ADP-ribose) polymerase-1; $[Zn^{2+}]_i$: Intracellular Zn^{2+} concentration.)

Chapter 5

General Discussion and Conclusions

5.1 Summary and general discussion

The results presented in this thesis define the molecular mechanisms and signalling pathways in TRPM2-mediated neuronal death in response to H_2O_2 or $A\beta_{42}$. These findings provide novel insights into the mechanisms of oxidative stress-induced neuronal death that is closely related to post-ischemic stroke and neurodegeneration diseases.

Most of previous studies have considered TRPM2 channel-dependent Ca^{2+} dysregulation as a pivotal factor in oxidative stress induced neuronal death. However, the study described in this thesis and recent studies (Ye et al., 2014; Manna et al., 2015) have revealed that TRPM2 channel activation-mediated rapid and dramatic increase in the $[Zn^{2+}]_i$ plays a predominant role in oxidative stress-induced neuronal death. Indeed, both H_2O_2 and $A\beta_{42}$ triggered considerable increase in the $[Zn^{2+}]_i$ and cell death in WT hippocampal neurons; pharmacological or genetic inhibition of the TRPM2 channel not only attenuated the increase in the $[Zn^{2+}]_i$ but also abolished neuronal death induced by H_2O_2 or $A\beta_{42}$.

Both H_2O_2 and $A\beta_{42}$ led to prominent lysosomal dysfunction, in accompany with a drastic increase in the $[Zn^{2+}]_i$, implicating that lysosomal dysfunction results in the release of lysosomal Zn^{2+} to cytosol (Hwang et al., 2008). H_2O_2- or $A\beta_{42}$-induced lysosomal dysfunction was ablated by pharmacological or genetic inhibition of the TRPM2 channel, suggesting a strong dependence of the TRPM2 channel. Given the co-localization of the TRPM2 immunoreactivity with LysoTracker, it is likely that the TRPM2 channel mediates the lysosomal Zn^{2+} release that is responsible for H_2O_2- or $A\beta_{42}$-induced increase in the $[Zn^{2+}]_i$ in hippocampal neurons. Moreover, lysosomal dysfunction results in the release of proteolytic enzymes, such as cathepsin B, which are responsible for the apoptotic/necrotic neuronal death. H_2O_2- or $A\beta_{42}$-induced hippocampal neuron death was sensitive to the inhibition by IM-54, Ac-DVED-CMK and necrostatin-1, further supporting that necrosis, apoptosis and

necroptosis are all involved in the complex mechanisms for H_2O_2- or $A\beta_{42}$-induced hippocampal neuron death.

Exposure to H_2O_2 or $A\beta_{42}$ induced considerable mitochondrial Zn^{2+} accumulation, mitochondrial loss, mitochondrial fragmentation, Cyt-c release and mitochondrial ROS generation. Similar mitochondrial effects were observed in hippocampal neurons exposed to bafilomycin A1 that induces lysosomal dysfunction. Those mitochondrial effects were prevented by treatment with TPEN, suggesting that lysosomal dysfunction and an increase in the $[Zn^{2+}]_i$ trigger the mitochondrial Zn^{2+} accumulation, which in turn causes mitochondrial loss and dysfunction, Cyt-c release and mitochondrial ROS generation. Cyt-c release from mitochondria is known to activate caspase-dependent apoptosis (Jiang and Wang, 2004). As discussed above, Ac-DVED-CMK acts as a potent inhibitor of caspase-3, significantly prevented H_2O_2- or $A\beta_{42}$-induced hippocampal neuron death. The immunofluorescent imaging supports strong mitochondrial localization of the TRPM2 protein. H_2O_2- or $A\beta_{42}$-induced mitochondrial effects were also abolished by pharmacological or genetic inhibition of the TRPM2 channel. Moreover, ADPR significantly enhanced mitochondrial Zn^{2+} uptake in mitochondria isolated from WT but not TRPM2-KO hippocampal neurons. These results provide further evidence to support the hypothesis that the mitochondrial TRPM2 channel mediates mitochondrial Zn^{2+} accumulation. Such TRPM2-dependent mitochondrial Zn^{2+} influx leads to the mitochondrial dysfunction and ROS generation, which may associate with the axonal degeneration of hippocampal neurons in response to H_2O_2 or $A\beta_{42}$. On the other hand, H_2O_2-induced mitochondrial ROS accumulation and cell death in WT hippocampal neurons were also attenuated by pharmacological inhibition of the mitochondrial NCX and MCU. However, such inhibition failed to reduce H_2O_2-induced cell death in TRPM2-KO neurons. The results suggest the functional interplay between TRPM2 channel and mitochondrial NCX and MCU plays a role in $A\beta_{42}$-induced mitochondrial Zn^{2+} accumulation.

H_2O_2- or $A\beta_{42}$-induced neurotoxicity was strongly suppressed by apocynin, DPI, and GKT137831, indicating the contribution of NOX-induced oxidative stress in hippocampal neuron death (Kahles et al., 2010; Radermacher et al., 2013). Notably, $A\beta_{42}$-induced neurotoxicity and oxidative stress were attenuated by GÖ6976, implicating that $A\beta_{42}$ initiates the NOX activation by promoting PKC activation. Furthermore, $A\beta_{42}$-induced increase in the $[Zn^{2+}]_i$, lysosomal dysfunction and mitochondrial effects were largely reversed by the PKC and NOX inhibitors. These results indicate the PKC/NOX-mediated generation of ROS contributes to $A\beta_{42}$-induced increase in the $[Zn^{2+}]_i$ that in turn leads to the mitochondrial ROS generation. It is shown in this thesis that $A\beta_{42}$-induced neurotoxicity in hippocampal neurons was significantly attenuated by U0126, a MEK/ERK inhibitor, and by PF431396, an inhibitor of Pyk2 which is a critical upstream kinase of the MEK/ERK signalling pathway. Given that the ERK activation stimulates the PARP-1 activation and cell death in OGD/R model (Domercq et al., 2013), $A\beta_{42}$-induced ERK activation may initiate the PARP-1 activation, leading to enhanced ADPR generation and TRPM2 channel activation.

5.2 Future works

5.2.1 Alternative methods for the measurement of neuronal death

The main method used in the present study to examine neuronal death is PI staining, a membrane impermeable indicator for cell death, particularly necrotic cell death that is accompanied with the loss of the membrane integrity. It was shown that not only necrosis, but also apoptosis and necroptosis are involved in H_2O_2 and $A\beta_{42}$-induced hippocampal neuron death. Therefore, alternative methods will be adopted in future study to investigate the hippocampal neuronal death.

5.2.2 The expression and function of TRPM2 channel in lysosomes and mitochondria

The results suggested that the TRPM2 channel contributes in mediating the lysosomal Zn^{2+} release, particularly mitochondria Zn^{2+} influx in hippocampal neurons in response to exposure to H_2O_2 and $A\beta_{42}$. Further investigations are required to show the lysosomal expression of TRPM2 channel and its role and mechanisms in lysosomal Zn^{2+} release. Further experiments are also required to determine the location of the mitochondria TRPM2 channel, and more importantly, the mechanisms underlying the TRPM2 channel activation. In addition, efforts are needed to establish the role of functional interplay between TRPM2 channel and mitochondrial NCX and MCU in mediating ROS-induced mitochondrial Zn^{2+} accumulation and ROS generation.

5.2.3 The contribution of MT proteins in H_2O_2- or $A\beta_{42}$-induced increase in the $[Zn^{2+}]_i$

Both H_2O_2- and $A\beta_{42}$-induced increase in the $[Zn^{2+}]_i$ were almost completely abolished in TRPM2-KO neurons, suggesting a predominat role of the TRPM2 channel in regulating the $[Zn^{2+}]_i$. However, the MT proteins are also known as an important Zn^{2+} store within cytosol. The mitochondrial ROS generation and also NOX-mediated ROS generation may induce Zn^{2+} release from the MT proteins. Clearly, further studies are required to provide a clear understanding of the possible role of this distinct mechanism in ROS- and $A\beta_{42}$-induced increase in the $[Zn^{2+}]_i$.

5.2.4 The mechanisms of TRPM2-dependent axonal degeneration

H_2O_2- or $A\beta_{42}$-induced considerable axonal degeneration in WT hippocampal neurons was largely abolished by TRPM2-KO, suggesuing an important role for the TRPM2 channel in mediating ROS-induced axonal degeneration. ROS-induced mitochondria dysfunction had been shown to be associated with axonal

degeneration, further studies are required to understand whether TRPM2 channel mediates ROS-induced axon impairment by initiating mitochondrial dysfunction.

5.2.5 The mechanisms for the activation of the MEK signalling pathway

The results presented in this thesis suggest the Pyk2-dependent activation of the MEK/ERK pathway contributes to H_2O_2- or $A\beta_{42}$-induced hippocampal neuron death. Further investigations are needed to disclose the mechanisms of how Pyk2 is activated in hippocampal neurons.

5.2.6 The role of TRPM2 channel in TNF-α, acidic pH or NMDA-induced neuronal death

The present study has observed a number of interesting observations. Firstly, TNF-α has been reported to facilitate the TRPM2 channel activation (Roberge et al., 2014). In this study, I examined TNF-α induced cell death in hippocampal neurons. The results showed that TNF-α triggered WT hippocampal neuron death in a time- and concentration-dependent manner (**Fig. 5.1**). TNF-α-induced neuronal death was substantially decreased in TRPM2-KO neurons (**Fig. 5.1**), strongly suggesting a substantial role for TRPM2 channel in mediating TNF-α induced hippocampal neuron death.

Secondly, in addition to ROS production, the acidification- and glutamate-induced neuronal death also occur during reperfusion. Activation of the acid sensing ion channels (ASICs), particularly ASIC1a, and the NMDA subtype of the ionotropic receptors for glutamate, have been reported to be critical for inducing post-ischemic neuronal death (Li et al., 2015). PI staining assay showed hippocampal neuron death was induced by the treatment with pH 6.0 for 2 hr followed by culturing in normal medium for further 24 hr (**Fig. 5.2**), or exposure to 100 μM NMDA for 30 min and culturing in NMDA-free medium for further 24 hr (**Fig. 5.2**). Such condition induced strong hippocampal neuron death, which was significantly reduced in

TRPM2-KO neurons (**Fig. 5.2**). Collectively, the results provide evidence to suggest a role for TRPM2 channel in mediating NMDA- and acid pH-induced neuronal death. Future experiments are required to provide mechanistic insights into these preliminary results.

5.3 Conclusions

The TRPM2 channel is potently activated by ROS and thus confers diverse cell types including hippocampal neurons with susceptibility to ROS-induced cell death. The study presented in this thesis investiagted the molecular mechanisms underlying TRPM2-mediated hippocampal neuronal death. The results support that the TRPM2 channel in mitochondria integrates multiple molecular mechanisms and signalling pathways that form a positive feedback loop that drives hippocampal neuronal death in response to ROS and $A\beta_{42}$. Such novel and mechanistic insights into the pathogenesis of post-ischemic stroke damage and AD should be beneficial to the development of novel therapeutics treating these ROS-related neurodegenerative conditions.

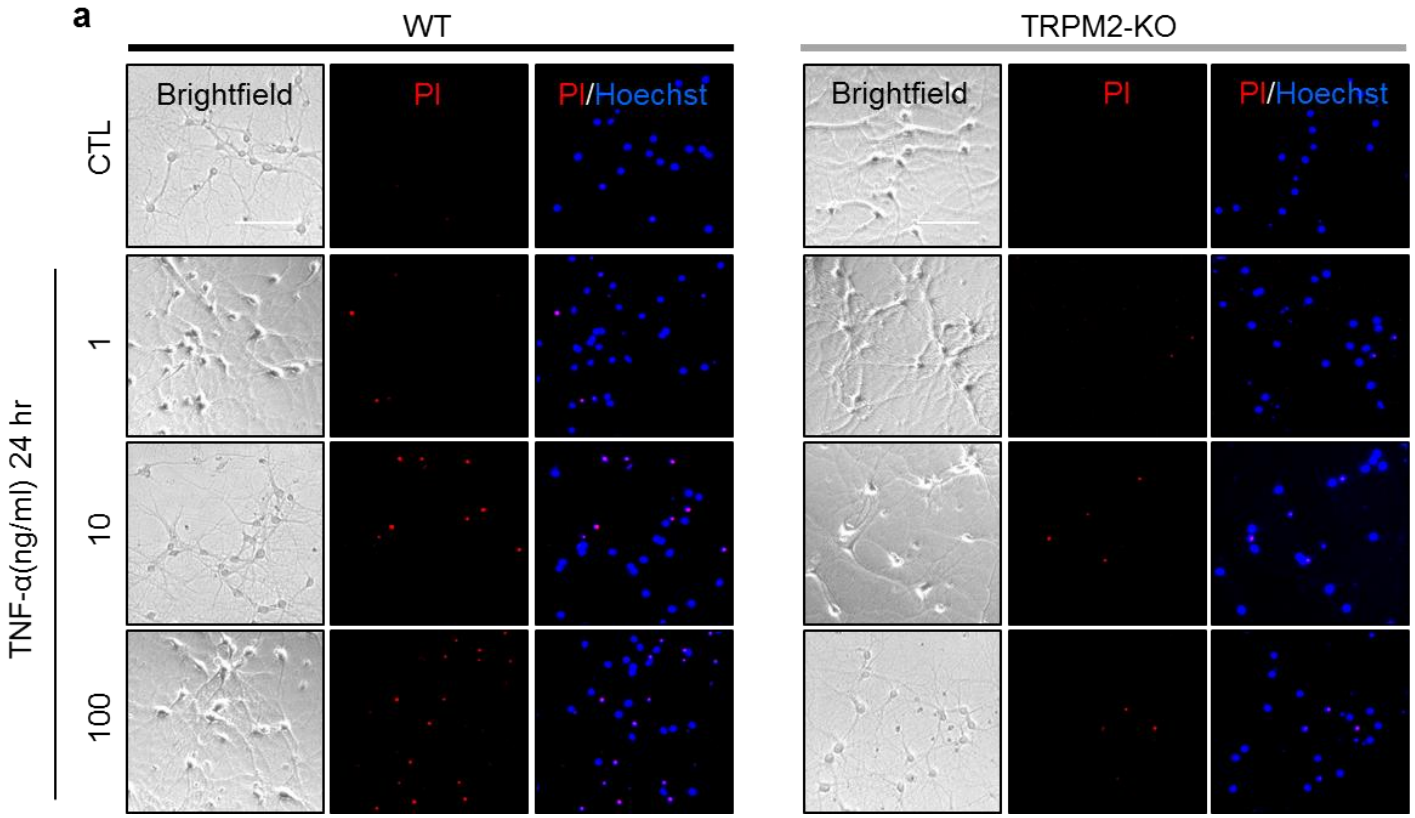
a
WT
TRPM2-KO
Brightfield
PI
PI/Hoechst
Brightfield
PI
PI/Hoechst
CTL
1
10
100
TNF-α(ng/ml) 24 hr

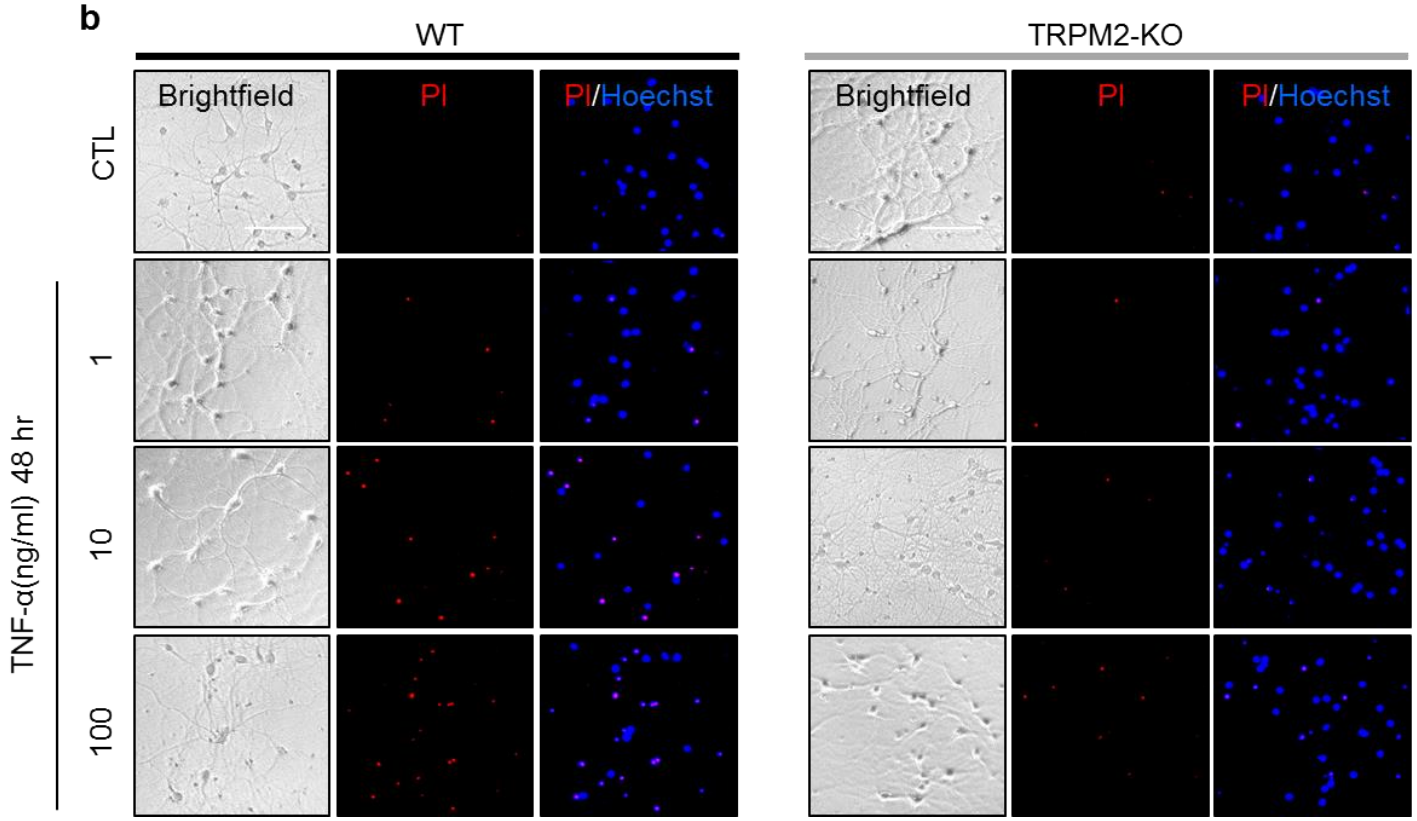
b
WT
TRPM2-KO
Brightfield
PI
PI/Hoechst
Brightfield
PI
PI/Hoechst
CTL
1
10
100
TNF-α(ng/ml) 48 hr

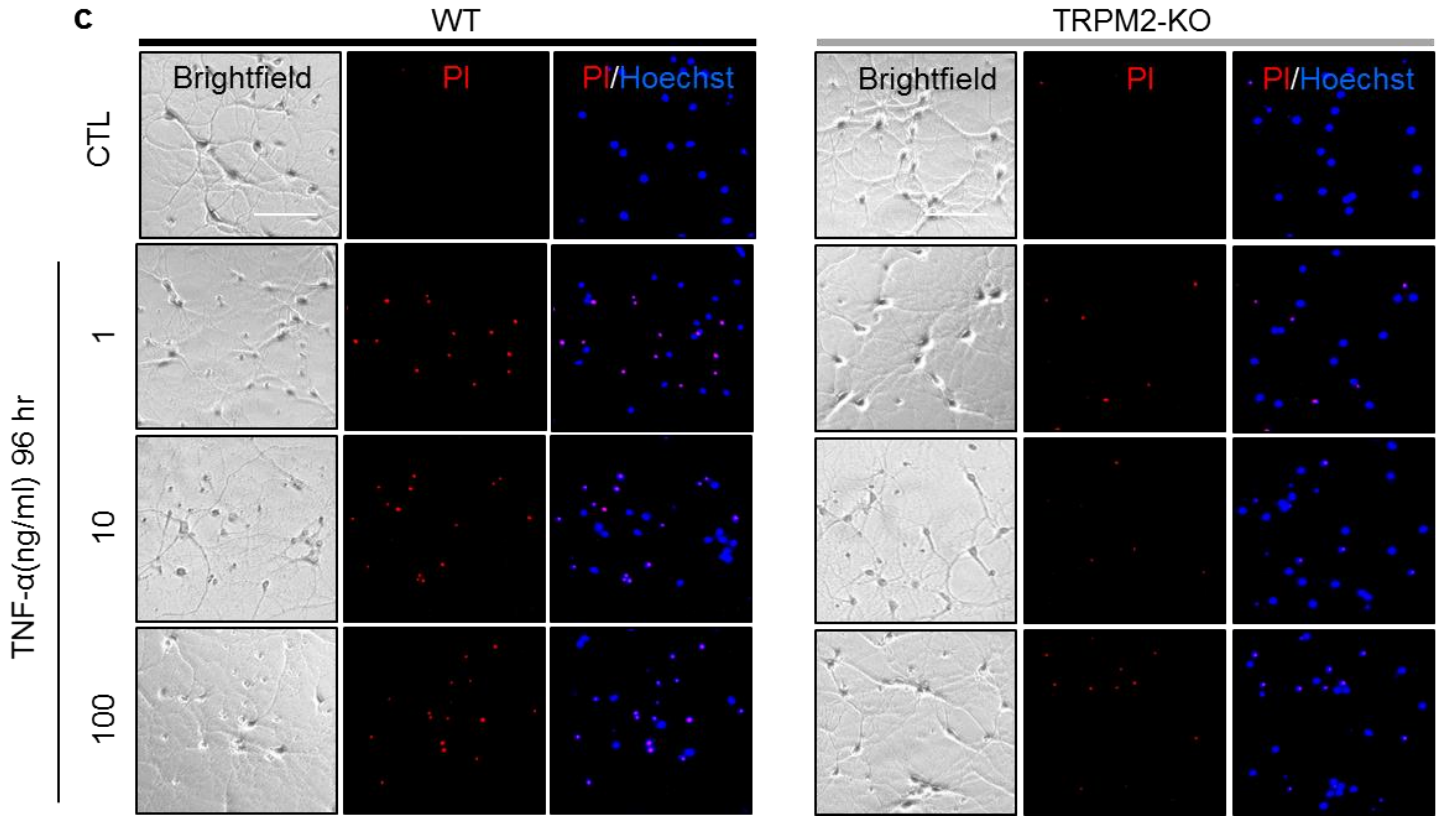
c
WT
TRPM2-KO
Brightfield
PI
PI/Hoechst
Brightfield
PI
PI/Hoechst
CTL
1
10
100
TNF-α(ng/ml) 96 hr

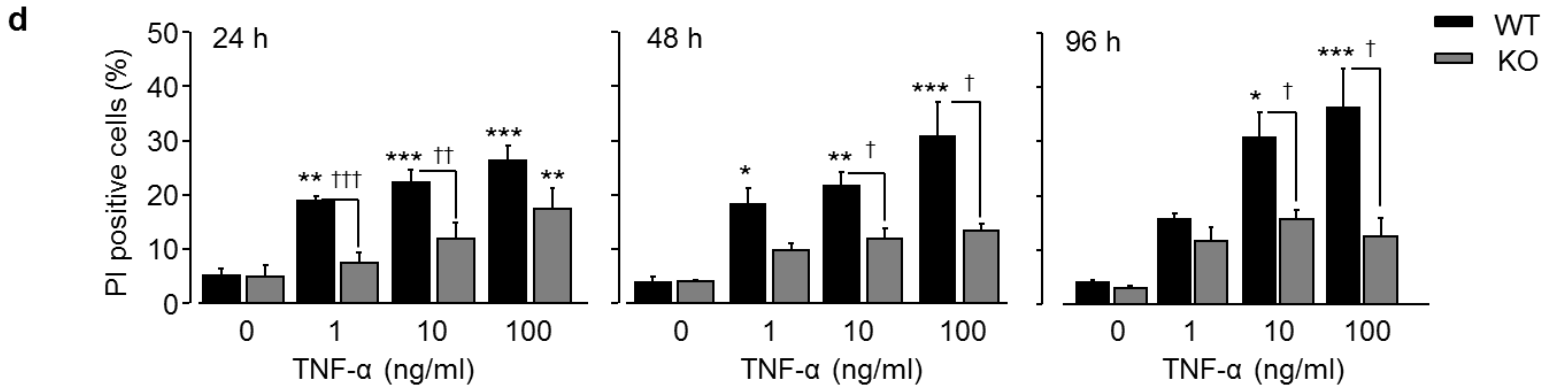

Figure 5.1 TNF-α induces TRPM2-dependent hippocampal neuron death

(**a**-**c**) Representative images showing PI staining of WT or TRPM2-KO hippocampal neurons after treatment with TNF-α at indicated concentrations and durations. Each panel consists of a brightfield image showing cells, PI staining image showing dead cells and a merged image of PI and Hoechst staining. Scale bar is 100 µm. (**d**) Summary of the mean percentage of PI positive cell at indicated conditions from 3-5 independent experiment (400-650 cell of each independent experiment). Black and grey bars showing WT neurons and TRPM2-KO neurons, respectively. *, P <0.05, **, P < 0.01 and ***, P < 0.001 indicate significant difference relative to untreated cells (CTL); †, P < 0.05, ††, P < 0.01 and †††, P < 0.001 for the comparison between WT neurons and TRPM2-KO neurons.

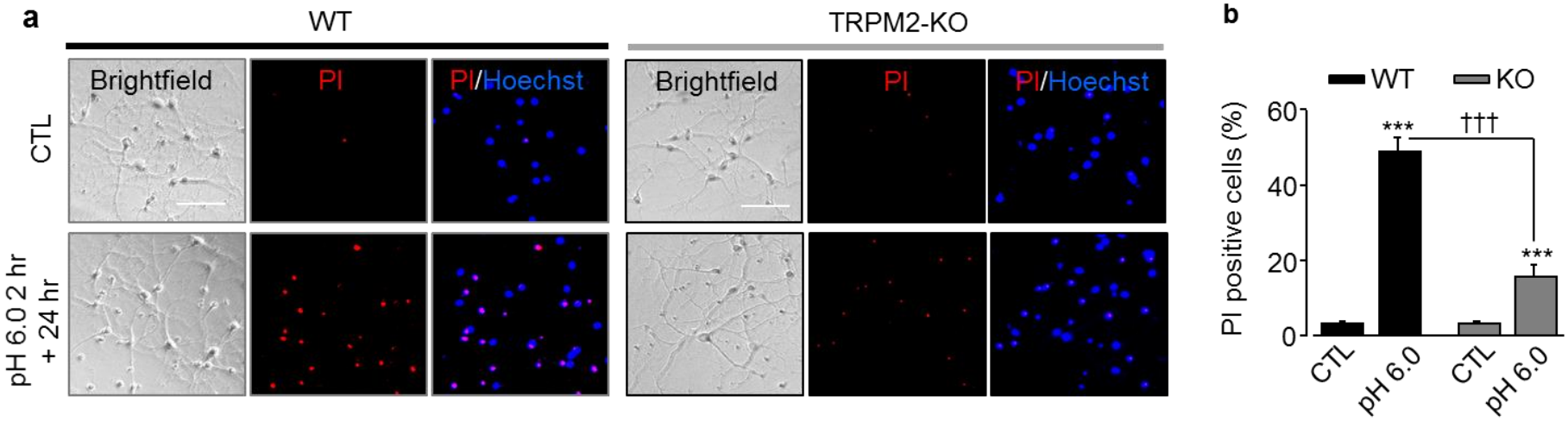
a
WT
TRPM2-KO
Brightfield
PI
PI/Hoechst
CTL
pH 6.0 2 hr
+ 24 hr
b
WT
KO
PI positive cells (%)
60
40
20
0
***
†††
CTL
pH 6.0

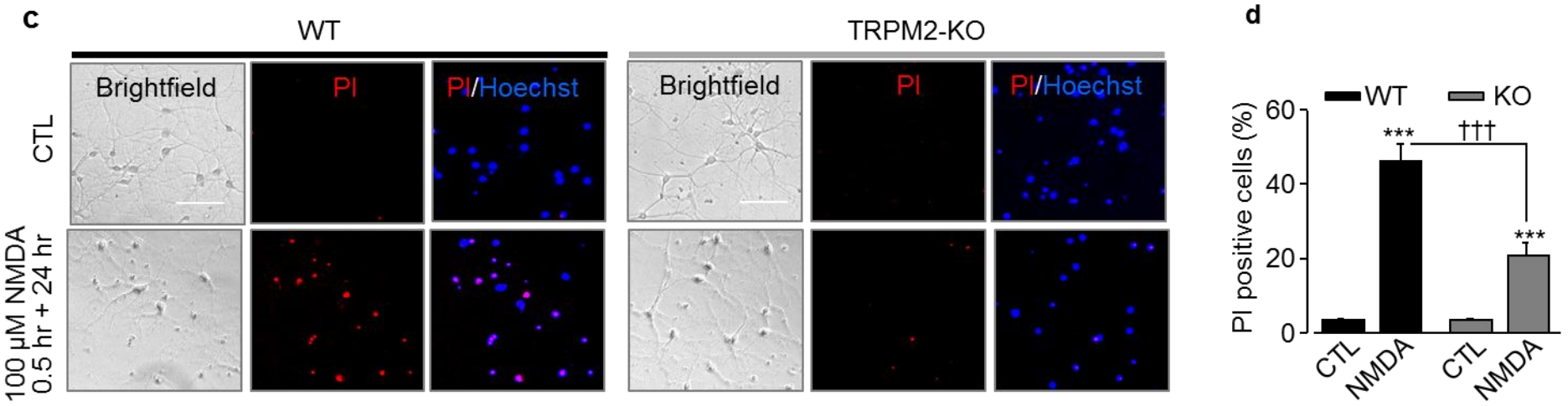

Figure 5.2 TRPM2 deficiency reduces acidic pH- and NMDA-induced hippocampal neuron death

(**a, c**) Representative PI and PI/Hoechst staining images showing acidic pH (pH 6.0) (**a**) or 100 µM NMDA (**c**) induced death in WT or TRPM2-KO hippocampal neurons. Scale bar is 100 µm. (**b, d**) The mean percentage of PI positive cells in hippocampal neurons treated with indicated conditions from 3 independent experiments (300-500 cells of each independent experiment), ***, $P < 0.001$ indicates significant difference relative to control (CTL), and †††, $P < 0.001$ for the comparison between WT neurons and TRPM2-KO neurons.

List of References

Aarts, M., Iihara, K., Wei, W.L., Xiong, Z.G., Arundine, M., Cerwinski, W., MacDonald, J.F. and Tymianski, M. 2003. A key role for TRPM7 channels in anoxic neuronal death. *Cell*. 115(7), pp.863-877.

Aarts, M., Liu, Y., Liu, L., Besshoh, S., Arundine, M., Gurd, J.W., Wang, Y.T., Salter, M.W. and Tymianski, M. 2002. Treatment of ischemic brain damage by perturbing NMDA receptor- PSD-95 protein interactions. *Science*. 298(5594), pp.846-850.

Abramov, A.Y., Jacobson, J., Wientjes, F., Hothersall, J., Canevari, L. and Duchen, M.R. 2005. Expression and modulation of an NADPH oxidase in mammalian astrocytes. *J Neurosci*. 25(40), pp.9176-9184.

Adlard, P.A., Parncutt, J.M., Finkelstein, D.I. and Bush, A.I. 2010. Cognitive loss in zinc transporter-3 knock-out mice: a phenocopy for the synaptic and memory deficits of Alzheimer's disease? *J Neurosci*. 30(5), pp.1631-1636.

Agell, N., Bachs, O., Rocamora, N. and Villalonga, P. 2002. Modulation of the Ras/Raf/MEK/ERK pathway by Ca^{2+}, and calmodulin. *Cell Signal*. 14(8), pp.649-654.

Alano, C.C., Garnier, P., Ying, W.H., Higashi, Y., Kauppinen, T.M. and Swanson, R.A. 2010. NAD^+ Depletion Is Necessary and Sufficient for Poly(ADP-Ribose) Polymerase-1-Mediated Neuronal Death. *J Neurosci*. 30(8), pp.2967-2978.

Alim, I., Teves, L., Li, R., Mori, Y. and Tymianski, M. 2013. Modulation of NMDAR subunit expression by TRPM2 channels regulates neuronal vulnerability to ischemic cell death. *J Neurosci*. 33(44), pp.17264-17277.

Alobuia, W.M., Xia, W. and Vohra, B.P.S. 2013. Axon degeneration is key component of neuronal death in amyloid-beta toxicity. *Neurochem Int*. 63(8), pp.782-789.

Amantea, D., Nappi, G., Bernardi, G., Bagetta, G. and Corasaniti, M.T. 2009. Post-ischemic brain damage: pathophysiology and role of inflammatory mediators. *FEBS J.* 276(1), pp.13-26.

Ameziane-El-Hassani, R., Morand, S., Boucher, J.L., Frapart, Y.M., Apostolou, D., Agnandji, D., Gnidehou, S., Ohayon, R., Noel-Hudson, M.S., Francon, J., Lalaoui,

K., Virion, A. and Dupuy, C. 2005. Dual oxidase-2 has an intrinsic Ca^{2+}-dependent H_2O_2-generating activity. *J Biol Chem*. 280(34), pp.30046-30054.

Amo, T., Saiki, S., Sawayama, T., Sato, S. and Hattori, N. 2014. Detailed analysis of mitochondrial respiratory chain defects caused by loss of PINK1. *Neurosci Lett*. 580, pp.37-40.

Aoyama, T., Paik, Y.H., Watanabe, S., Laleu, B., Gaggini, F., Fioraso-Cartier, L., Molango, S., Heitz, F., Merlot, C., Szyndralewiez, C., Page, P. and Brenner, D.A. 2012. Nicotinamide Adenine Dinucleotide Phosphate Oxidase in Experimental Liver Fibrosis: GKT137831 as a Novel Potential Therapeutic Agent. *Hepatology*. 56(6), pp.2316-2327.

Audo, I., Kohl, S., Leroy, B.P., Munier, F.L., Guillonneau, X., Mohand-Said, S., Bujakowska, K., Nandrot, E.F., Lorenz, B., Preising, M., Kellner, U., Renner, A.B., Bernd, A., Antonio, A., Moskova-Doumanova, V., Lancelot, M.E., Poloschek, C.M., Drumare, I., Defoort-Dhellemmes, S., Wissinger, B., Leveillard, T., Hamel, C.P., Schorderet, D.F., De Baere, E., Berger, W., Jacobson, S.G., Zrenner, E., Sahel, J.A., Bhattacharya, S.S. and Zeitz, C. 2009. TRPM1 Is Mutated in Patients with Autosomal-Recessive Complete Congenital Stationary Night Blindness. *Am J Hum Genet*. 85(5), pp.720-729.

Babior, B.M. 2004. NADPH oxidase. *Curr Opin Immunol*. 16(1), pp.42-47.

Banfi, B., Molnar, G., Maturana, A., Steger, K., Hegedus, B., Demaurex, N. and Krause, K.H. 2001. A Ca^{2+}-activated NADPH oxidase in testis, spleen, and lymph nodes. *J Biol Chem*. 276(40), pp.37594-37601.

Bano, D. and Nicotera, P. 2007. Ca^{2+} signals and neuronal death in brain ischemia. *Stroke*. 38(2 Suppl), pp.674-676.

Barrientos, S.A., Martinez, N.W., Yoo, S., Jara, J.S., Zamorano, S., Hetz, C., Twiss, J.L., Alvarez, J. and Court, F.A. 2011. Axonal Degeneration Is Mediated by the Mitochondrial Permeability Transition Pore. *J Neurosci*. 31(3), pp.966-978.

Bartels, A.L. and Leenders, K.L. 2009. Parkinson's disease: the syndrome, the pathogenesis and pathophysiology. *Cortex*. 45(8), pp.915-921.

Baud, O., Greene, A.E., Li, J.R., Wang, H., Volpe, J.J. and Rosenberg, P.A. 2004. Glutathione peroxidase-catalase cooperativity is required for resistance to hydrogen peroxide by mature rat oligodendrocytes. *J Neurosci*. 24(7), pp.1531-1540.

Bautista, D.M., Siemens, J., Glazer, J.M., Tsuruda, P.R., Basbaum, A.I., Stucky, C.L., Jordt, S.E. and Julius, D. 2007. The menthol receptor TRPM8 is the principal detector of environmental cold. *Nature*. 448(7150), pp.204-208.

Beaudoin, G.M., 3rd, Lee, S.H., Singh, D., Yuan, Y., Ng, Y.G., Reichardt, L.F. and Arikkath, J. 2012. Culturing pyramidal neurons from the early postnatal mouse hippocampus and cortex. *Nat Protoc*. 7(9), pp.1741-1754.

Bechtel, W. and Bauer, G. 2009. Catalase protects tumor cells from apoptosis induction by intercellular ROS signaling. *Anticancer Res*. 29(11), pp.4541-4557.

Beck, A., Kolisek, M., Bagley, L.A., Fleig, A. and Penner, R. 2006. Nicotinic acid adenine dinucleotide phosphate and cyclic ADP-ribose regulate TRPM2 channels in T lymphocytes. *FASEB J*. 20(7), pp.962-964.

Bedard, K. and Krause, K.H. 2007. The NOX family of ROS-generating NADPH oxidases: physiology and pathophysiology. *Physiol Rev*. 87(1), pp.245-313.

Belizario, J., Vieira-Cordeiro, L. and Enns, S. 2015. Necroptotic Cell Death Signaling and Execution Pathway: Lessons from Knockout Mice. *Mediators Inflamm*. 2015, p128076.

Benilova, I., Karran, E. and De Strooper, B. 2012. The toxic Abeta oligomer and Alzheimer's disease: an emperor in need of clothes. *Nat Neurosci*. 15(3), pp.349-357.

Bhattacharyya, A., Chattopadhyay, R., Mitra, S. and Crowe, S.E. 2014. Oxidative stress: an essential factor in the pathogenesis of gastrointestinal mucosal diseases. *Physiol Rev*. 94(2), pp.329-354.

Bian, M., Liu, J., Hong, X., Yu, M., Huang, Y., Sheng, Z., Fei, J. and Huang, F. 2012. Overexpression of parkin ameliorates dopaminergic neurodegeneration induced by 1- methyl-4-phenyl-1, 2, 3, 6-tetrahydropyridine in mice. *PLoS One*. 7(6), pe39953.

Bianca, V.D., Dusi, S., Bianchini, E., Dal Pra, I. and Rossi, F. 1999. Beta-amyloid activates the $O_2^{\cdot -}$ forming NADPH oxidase in microglia, monocytes, and neutrophils. A possible inflammatory mechanism of neuronal damage in Alzheimer's disease. *J Biol Chem*. 274(22), pp.15493-15499.

Block, M.L. 2008. NADPH oxidase as a therapeutic target in Alzheimer's disease. *BMC Neurosci*. 9.

Boothby, L.A. and Doering, P.L. 2005. Vitamin C and vitamin E for Alzheimer's disease. *Ann Pharmacother*. 39(12), pp.2073-2080.

Boya, P. and Kroemer, G. 2008. Lysosomal membrane permeabilization in cell death. *Oncogene*. 27(50), pp.6434-6451.

Brinkmann, V., Reichard, U., Goosmann, C., Fauler, B., Uhlemann, Y., Weiss, D.S., Weinrauch, Y. and Zychlinsky, A. 2004. Neutrophil extracellular traps kill bacteria. *Science*. 303(5663), pp.1532-1535.

Brown, A.M., Kristal, B.S., Effron, M.S., Shestopalov, A.I., Ullucci, P.A., Sheu, K.F., Blass, J.P. and Cooper, A.J. 2000. Zn^{2+} inhibits alpha-ketoglutarate-stimulated mitochondrial respiration and the isolated alpha-ketoglutarate dehydrogenase complex. *J Biol Chem*. 275(18), pp.13441-13447.

Butterfield, D.A. and Lauderback, C.M. 2002. Lipid peroxidation and protein oxidation in Alzheimer's disease brain: potential causes and consequences involving amyloid beta-peptide-associated free radical oxidative stress. *Free Radic Biol Med*. 32(11), pp.1050-1060.

Cali, T., Ottolini, D. and Brini, M. 2012. Mitochondrial Ca^{2+} and neurodegeneration. *Cell Calcium*. 52(1), pp.73-85.

Cande, C., Cohen, I., Daugas, E., Ravagnan, L., Larochette, N., Zamzami, N. and Kroemer, G. 2002. Apoptosis-inducing factor (AIF): a novel caspase-independent death effector released from mitochondria. *Biochimie*. 84(2-3), pp.215-222.

Cape, J.L., Bowman, M.K. and Kramer, D.M. 2007. A semiquinone intermediate generated at the Q_o site of the cytochrome bc1 complex: importance for the Q-cycle and superoxide production. *Proc Natl Acad Sci U S A*. 104(19), pp.7887-7892.

Casley, C.S., Canevari, L., Land, J.M., Clark, J.B. and Sharpe, M.A. 2002. Beta-amyloid inhibits integrated mitochondrial respiration and key enzyme activities. *J Neurochem*. 80(1), pp.91-100.

Chang, F., Steelman, L.S., Lee, J.T., Shelton, J.G., Navolanic, P.M., Blalock, W.L., Franklin, R.A. and McCubrey, J.A. 2003. Signal transduction mediated by the Ras/Raf/MEK/ERK pathway from cytokine receptors to transcription factors: potential targeting for therapeutic intervention. *Leukemia*. 17(7), pp.1263-1293.

Chaudhuri, D., Sancak, Y., Mootha, V.K. and Clapham, D.E. 2013. MCU encodes the pore conducting mitochondrial calcium currents. *Elife*. 2, pe00704.

Chen, D., Yu, J. and Zhang, L. 2016. Necroptosis: an alternative cell death program defending against cancer. *Biochim Biophys Acta*. 1865(2), pp.228-236.

Chen, G.L., Zeng, B., Eastmond, S., Elsenussi, S.E., Boa, A.N. and Xu, S.Z. 2012. Pharmacological comparison of novel synthetic fenamate analogues with econazole and 2-APB on the inhibition of TRPM2 channels. *Br J Pharmacol*. 167(6), pp.1232-1243.

Chen, H., Song, Y.S. and Chan, P.H. 2009. Inhibition of NADPH oxidase is neuroprotective after ischemia-reperfusion. *J Cereb Blood Flow Metab*. 29(7), pp.1262-1272.

Chen, H., Yoshioka, H., Kim, G.S., Jung, J.E., Okami, N., Sakata, H., Maier, C.M., Narasimhan, P., Goeders, C.E. and Chan, P.H. 2011. Oxidative stress in ischemic brain damage: mechanisms of cell death and potential molecular targets for neuroprotection. *Antioxid Redox Signal*. 14(8), pp.1505-1517.

Chen, Q., Vazquez, E.J., Moghaddas, S., Hoppel, C.L. and Lesnefsky, E.J. 2003. Production of reactive oxygen species by mitochondria: central role of complex III. *J Biol Chem*. 278(38), pp.36027-36031.

Chen, S.J., Hoffman, N.E., Shanmughapriya, S., Bao, L., Keefer, K., Conrad, K., Merali, S., Takahashi, Y., Abraham, T., Hirschler-Laszkiewicz, I., Wang, J., Zhang, X.Q., Song, J., Barrero, C., Shi, Y., Kawasawa, Y.I., Bayerl, M., Sun, T., Barbour, M., Wang, H.G., Madesh, M., Cheung, J.Y. and Miller, B.A. 2014. A splice variant of the human ion channel TRPM2 modulates neuroblastoma tumor growth through hypoxia-inducible factor (HIF)-1/2α. *J Biol Chem*. 289(52), pp.36284-36302.

Cheng, G., Cao, Z., Xu, X., van Meir, E.G. and Lambeth, J.D. 2001. Homologs of gp91^{phox}: cloning and tissue expression of Nox3, Nox4, and Nox5. *Gene*. 269(1-2), pp.131-140.

Cheng, H., Beck, A., Launay, P., Gross, S.A., Stokes, A.J., Kinet, J.P., Fleig, A. and Penner, R. 2007. TRPM4 controls insulin secretion in pancreatic β-cells. *Cell Calcium*. 41(1), pp.51-61.

Christensen, D.Z., Huettenrauch, M., Mitkovski, M., Pradier, L. and Wirths, O. 2014. Axonal degeneration in an Alzheimer mouse model is PS1 gene dose dependent and linked to intraneuronal Abeta accumulation. *Front Aging Neurosci.* 6, p139.

Chung, H.J., Huang, Y.H., Lau, L.F. and Huganir, R.L. 2004. Regulation of the NMDA receptor complex and trafficking by activity-dependent phosphorylation of the NR2B subunit PDZ ligand. *J Neurosci*. 24(45), pp.10248-10259.

Cipriani, A., Saunders, K., Attenburrow, M.J., Stefaniak, J., Panchal, P., Stockton, S., Lane, T.A., Tunbridge, E.M., Geddes, J.R. and Harrison, P.J. 2016. A systematic review of calcium channel antagonists in bipolar disorder and some considerations for their future development. *Mol Psychiatry*. 21(10), pp.1324-1332.

Clausen, A., McClanahan, T., Ji, S.G. and Weiss, J.H. 2013. Mechanisms of rapid reactive oxygen species generation in response to cytosolic Ca^{2+} or Zn^{2+} loads in cortical neurons. *PLoS One*. 8(12), pe83347.

Cole, T.B., Robbins, C.A., Wenzel, H.J., Schwartzkroin, P.A. and Palmiter, R.D. 2000. Seizures and neuronal damage in mice lacking vesicular zinc. *Epilepsy Res*. 39(2), pp.153-169.

Cole, T.B., Wenzel, H.J., Kafer, K.E., Schwartzkroin, P.A. and Palmiter, R.D. 1999. Elimination of zinc from synaptic vesicles in the intact mouse brain by disruption of the ZnT3 gene. *Proc Natl Acad Sci U S A*. 96(4), pp.1716-1721.

Collins, T.P., Bayliss, R., Churchill, G.C., Galione, A. and Terrar, D.A. 2011. NAADP influences excitation-contraction coupling by releasing calcium from lysosomes in atrial myocytes. *Cell Calcium*. 50(5), pp.449-458.

Cooke, M.S., Evans, M.D., Dizdaroglu, M. and Lunec, J. 2003. Oxidative DNA damage: mechanisms, mutation, and disease. *FASEB J*. 17(10), pp.1195-1214.

Court, F.A. and Coleman, M.P. 2012. Mitochondria as a central sensor for axonal degenerative stimuli. *Trends Neurosci*. 35(6), pp.364-372.

Coyle, C.H., Martinez, L.J., Coleman, M.C., Spitz, D.R., Weintraub, N.L. and Kader, K.N. 2006. Mechanisms of H_2O_2-induced oxidative stress in endothelial cells. *Free Radic Biol Med*. 40(12), pp.2206-2213.

Coyoy, A., Valencia, A., Guemez-Gamboa, A. and Moran, J. 2008. Role of NADPH oxidase in the apoptotic death of cultured cerebellar granule neurons. *Free Radic Biol Med*. 45(8), pp.1056-1064.

Crow, M.T., Mani, K., Nam, Y.J. and Kitsis, R.N. 2004. The mitochondrial death pathway and cardiac myocyte apoptosis. *Circ Res*. 95(10), pp.957-970.

Danscher, G., Jo, S.M., Varea, E., Wang, Z., Cole, T.B. and Schroder, H.D. 2001. Inhibitory zinc-enriched terminals in mouse spinal cord. *Neuroscience*. 105(4), pp.941-947.

Dantzer, F., Ame, J.C., Schreiber, V., Nakamura, J., Menissier-de Murcia, J. and de Murcia, G. 2006. Poly(ADP-ribose) polymerase-1 activation during DNA damage and repair. *Methods Enzymol*. 409, pp.493-510.

De Felice, F.G., Velasco, P.T., Lambert, M.P., Viola, K., Fernandez, S.J., Ferreira, S.T. and Klein, W.L. 2007. A beta oligomers induce neuronal oxidative stress through an N-methyl-D-aspartate receptor-dependent mechanism that is blocked by the Alzheimer drug memantine. *J Biol Chem*. 282(15), pp.11590-11601.

De Vos, K.J., Allan, V.J., Grierson, A.J. and Sheetz, M.P. 2005. Mitochondrial function and actin regulate dynamin-related protein 1-dependent mitochondrial fission. *Curr Biol*. 15(7), pp.678-683.

Deb, P., Sharma, S. and Hassan, K.M. 2010. Pathophysiologic mechanisms of acute ischemic stroke: An overview with emphasis on therapeutic significance beyond thrombolysis. *Pathophysiology*. 17(3), pp.197-218.

Deeds, J., Cronin, F. and Duncan, L.M. 2000. Patterns of melastatin mRNA expression in melanocytic tumors. *Hum Pathol*. 31(11), pp.1346-1356.

Dempsey, E.C., Newton, A.C., Mochly-Rosen, D., Fields, A.P., Reyland, M.E., Insel, P.A. and Messing, R.O. 2000. Protein kinase C isozymes and the regulation of diverse cell responses. *Am J Physiol Lung Cell Mol Physiol*. 279(3), pp.L429-438.

Deshpande, A., Mina, E., Glabe, C. and Busciglio, J. 2006. Different conformations of amyloid beta induce neurotoxicity by distinct mechanisms in human cortical neurons. *J Neurosci*. 26(22), pp.6011-6018.

Di, A., Gao, X.P., Qian, F., Kawamura, T., Han, J., Hecquet, C., Ye, R.D., Vogel, S.M. and Malik, A.B. 2011. The redox-sensitive cation channel TRPM2 modulates phagocyte ROS production and inflammation. *Nat Immunol*. 13(1), pp.29-34.

Dias, V., Junn, E. and Mouradian, M.M. 2013. The role of oxidative stress in Parkinson's disease. *J Parkinsons Dis*. 3(4), pp.461-491.

Dineley, K.E., Richards, L.L., Votyakova, T.V. and Reynolds, I.J. 2005. Zinc causes loss of membrane potential and elevates reactive oxygen species in rat brain mitochondria. *Mitochondrion*. 5(1), pp.55-65.

Doens, D. and Fernandez, P.L. 2014. Microglia receptors and their implications in the response to amyloid beta for Alzheimer's disease pathogenesis. *J Neuroinflammation*. 11.

Dolle, C., Rack, J.G. and Ziegler, M. 2013. NAD and ADP-ribose metabolism in mitochondria. *FEBS J*. 280(15), pp.3530-3541.

Domercq, M., Mato, S., Soria, F.N., Sanchez-gomez, M.V., Alberdi, E. and Matute, C. 2013. Zn^{2+}-induced ERK activation mediates PARP-1-dependent ischemic-reoxygenation damage to oligodendrocytes. *Glia*. 61(3), pp.383-393.

Doyle, K.P., Simon, R.P. and Stenzel-Poore, M.P. 2008. Mechanisms of ischemic brain damage. *Neuropharmacology*. 55(3), pp.310-318.

Drummond, G.R., Selemidis, S., Griendling, K.K. and Sobey, C.G. 2011. Combating oxidative stress in vascular disease: NADPH oxidases as therapeutic targets. *Nat Rev Drug Discov*. 10(6), pp.453-471.

Du, H. and Yan, S.S. 2010. Mitochondrial permeability transition pore in Alzheimer's disease: cyclophilin D and amyloid beta. *Biochim Biophys Acta*. 1802(1), pp.198-204.

Du, J., Xie, J. and Yue, L. 2009a. Intracellular calcium activates TRPM2 and its alternative spliced isoforms. *Proc Natl Acad Sci U S A*. 106(17), pp.7239-7244.

Du, J., Xie, J. and Yue, L. 2009b. Modulation of TRPM2 by acidic pH and the underlying mechanisms for pH sensitivity. *J Gen Physiol*. 134(6), pp.471-488.

Duncan, L.M., Deeds, J., Hunter, J., Shao, J., Holmgren, L.M., Woolf, E.A., Tepper, R.I. and Shyjan, A.W. 1998. Down-regulation of the novel gene melastatin

correlates with potential for melanoma metastasis. *Cancer Res*. 58(7), pp.1515-1520.

Earley, S., Waldron, B.J. and Brayden, J.E. 2004. Critical role for transient receptor potential channel TRPM4 in myogenic constriction of cerebral arteries. *Circ Res*. 95(9), pp.922-929.

Eigel, B.N., Gursahani, H. and Hadley, R.W. 2004. ROS are required for rapid reactivation of Na^+/Ca^{2+} exchanger in hypoxic reoxygenated guinea pig ventricular myocytes. *Am J Physiol Heart Circ Physiol*. 286(3), pp.H955-963.

El-Benna, J., Dang, P.M., Gougerot-Pocidalo, M.A., Marie, J.C. and Braut-Boucher, F. 2009. $p47^{phox}$, the phagocyte NADPH oxidase/NOX2 organizer: structure, phosphorylation and implication in diseases. *Exp Mol Med*. 41(4), pp.217-225.

Elmore, S. 2007. Apoptosis: a review of programmed cell death. *Toxicol Pathol*. 35(4), pp.495-516.

Falcon-Perez, J.M. and Dell'Angelica, E.C. 2007. Zinc transporter 2 (SLC30A2) can suppress the vesicular zinc defect of adaptor protein 3-depleted fibroblasts by promoting zinc accumulation in lysosomes. *Exp Cell Res*. 313(7), pp.1473-1483.

Fato, R., Bergamini, C., Bortolus, M., Maniero, A.L., Leoni, S., Ohnishi, T. and Lenaz, G. 2009. Differential effects of mitochondrial Complex I inhibitors on production of reactive oxygen species. *Biochim Biophys Acta*. 1787(5), pp.384-392.

Fauconnier, J., Meli, A.C., Thireau, J., Roberge, S., Shan, J., Sassi, Y., Reiken, S.R., Rauzier, J.M., Marchand, A., Chauvier, D., Cassan, C., Crozier, C., Bideaux, P., Lompre, A.M., Jacotot, E., Marks, A.R. and Lacampagne, A. 2011. Ryanodine receptor leak mediated by caspase-8 activation leads to left ventricular injury after myocardial ischemia-reperfusion. *Proc Natl Acad Sci U S A*. 108(32), pp.13258-13263.

Feng, S., Li, H., Tai, Y., Huang, J., Su, Y., Abramowitz, J., Zhu, M.X., Birnbaumer, L. and Wang, Y. 2013. Canonical transient receptor potential 3 channels regulate mitochondrial calcium uptake. *Proc Natl Acad Sci U S A*. 110(27), pp.11011-11016.

Festjens, N., Vanden Berghe, T. and Vandenabeele, P. 2006. Necrosis, a well-orchestrated form of cell demise: signalling cascades, important mediators and concomitant immune response. *Biochim Biophys Acta*. 1757(9-10), pp.1371-1387.

Fiers, W., Beyaert, R., Declercq, W. and Vandenabeele, P. 1999. More than one way to die: apoptosis, necrosis and reactive oxygen damage. *Oncogene*. 18(54), pp.7719-7730.

Fleig, A. and Penner, R. 2004. The TRPM ion channel subfamily: molecular, biophysical and functional features. *Trends Pharmacol Sci*. 25(12), pp.633-639.

Fonfria, E., Marshall, I.C., Boyfield, I., Skaper, S.D., Hughes, J.P., Owen, D.E., Zhang, W., Miller, B.A., Benham, C.D. and McNulty, S. 2005. Amyloid beta-peptide(1-42) and hydrogen peroxide-induced toxicity are mediated by TRPM2 in rat primary striatal cultures. *J Neurochem*. 95(3), pp.715-723.

Fonfria, E., Marshall, I.C.B., Benham, C.D., Boyfield, I., Brown, J.D., Hill, K., Hughes, J.P., Skaper, S.D. and McNulty, S. 2004. TRPM2 channel opening in response to oxidative stress is dependent on activation of poly(ADP-ribose) polymerase. *Br J Pharmacol*. 143(1), pp.186-192.

Fonfria, E., Mattei, C., Hill, K., Brown, J.T., Randall, A., Benham, C.D., Skaper, S.D., Campbell, C.A., Crook, B., Murdock, P.R., Wilson, J.M., Maurio, F.P., Owen, D.E., Tilling, P.L. and McNulty, S. 2006. TRPM2 is elevated in the tMCAO stroke model, transcriptionally regulated, and functionally expressed in C13 microglia. *J Recept Signal Transduct Res*. 26(3), pp.179-198.

Forman, H.J. and Torres, M. 2002. Reactive oxygen species and cell signaling: respiratory burst in macrophage signaling. *Am J Respir Crit Care Med*. 166(12 Pt 2), pp.S4-8.

Freland, L. and Beaulieu, J.M. 2012. Inhibition of GSK3 by lithium, from single molecules to signaling networks. *Front Mol Neurosci*. 5, p14.

Fukai, T. and Ushio-Fukai, M. 2011. Superoxide dismutases: role in redox signaling, vascular function, and diseases. *Antioxid Redox Signal*. 15(6), pp.1583-1606.

Galluzzi, L. and Kroemer, G. 2008. Necroptosis: a specialized pathway of programmed necrosis. *Cell*. 135(7), pp.1161-1163.

Garrido, C., Galluzzi, L., Brunet, M., Puig, P.E., Didelot, C. and Kroemer, G. 2006. Mechanisms of cytochrome c release from mitochondria. *Cell Death Differ*. 13(9), pp.1423-1433.

Gasser, A., Glassmeier, G., Fliegert, R., Langhorst, M.F., Meinke, S., Hein, D., Kruger, S., Weber, K., Heiner, I., Oppenheimer, N., Schwarz, J.R. and Guse, A.H. 2006. Activation of T cell calcium influx by the second messenger ADP-ribose. *J Biol Chem*. 281(5), pp.2489-2496.

Gees, M., Colsoul, B. and Nilius, B. 2010. The role of transient receptor potential cation channels in Ca^{2+} signaling. *Cold Spring Harb Perspect Biol*. 2(10), pa003962.

Gilon, P. and Henquin, J.C. 2001. Mechanisms and physiological significance of the cholinergic control of pancreatic beta-cell function. *Endocr Rev*. 22(5), pp.565-604.

Gorlach, A., Bertram, K., Hudecova, S. and Krizanova, O. 2015. Calcium and ROS: A mutual interplay. *Redox Biol*. 6, pp.260-271.

Granger, D.N. and Kvietys, P.R. 2015. Reperfusion injury and reactive oxygen species: The evolution of a concept. *Redox Biol*. 6, pp.524-551.

Griendling, K.K., Sorescu, D. and Ushio-Fukai, M. 2000. NADPH oxidase: role in cardiovascular biology and disease. *Circ Res*. 86(5), pp.494-501.

Grimm, C., Kraft, R., Sauerbruch, S., Schultz, G. and Harteneck, C. 2003. Molecular and functional characterization of the melastatin-related cation channel TRPM3. *J Biol Chem*. 278(24), pp.21493-21501.

Grubisha, O., Rafty, L.A., Takanishi, C.L., Xu, X., Tong, L., Perraud, A.L., Scharenberg, A.M. and Denu, J.M. 2006. Metabolite of SIR2 reaction modulates TRPM2 ion channel. *J Biol Chem*. 281(20), pp.14057-14065.

Grupe, M., Myers, G., Penner, R. and Fleig, A. 2010. Activation of store-operated I(CRAC) by hydrogen peroxide. *Cell Calcium*. 48(1), pp.1-9.

Guicciardi, M.E., Leist, M. and Gores, G.J. 2004. Lysosomes in cell death. *Oncogene*. 23(16), pp.2881-2890.

Haass, C. and Selkoe, D.J. 2007. Soluble protein oligomers in neurodegeneration: lessons from the Alzheimer's amyloid beta-peptide. *Nat Rev Mol Cell Biol*. 8(2), pp.101-112.

Hagmeyer, S., Haderspeck, J.C. and Grabrucker, A.M. 2014. Behavioral impairments in animal models for zinc deficiency. *Front Behav Neurosci*. 8, p443.

Halle, A., Hornung, V., Petzold, G.C., Stewart, C.R., Monks, B.G., Reinheckel, T., Fitzgerald, K.A., Latz, E., Moore, K.J. and Golenbock, D.T. 2008. The NALP3 inflammasome is involved in the innate immune response to amyloid-beta. *Nat Immunol*. 9(8), pp.857-865.

Han, B.H., Zhou, M.L., Johnson, A.W., Singh, I., Liao, F., Vellimana, A.K., Nelson, J.W., Milner, E., Cirrito, J.R., Basak, J., Yoo, M., Dietrich, H.H., Holtzman, D.M. and Zipfel, G.J. 2015. Contribution of reactive oxygen species to cerebral amyloid angiopathy, vasomotor dysfunction, and microhemorrhage in aged Tg2576 mice. *Proc Natl Acad Sci U S A*. 112(8), pp.E881-890.

Hara, Y., Wakamori, M., Ishii, M., Maeno, E., Nishida, M., Yoshida, T., Yamada, H., Shimizu, S., Mori, E., Kudoh, J., Shimizu, N., Kurose, H., Okada, Y., Imoto, K. and Mori, Y. 2002. LTRPC2 Ca^{2+}-permeable channel activated by changes in redox status confers susceptibility to cell death. *Mol Cell*. 9(1), pp.163-173.

Haraguchi, K., Kawamoto, A., Isami, K., Maeda, S., Kusano, A., Asakura, K., Shirakawa, H., Mori, Y., Nakagawa, T. and Kaneko, S. 2012. TRPM2 Contributes to Inflammatory and Neuropathic Pain through the Aggravation of Pronociceptive Inflammatory Responses in Mice. *J Neurosci*. 32(11), pp.3931-3941.

Hardingham, G.E. and Bading, H. 2010. Synaptic versus extrasynaptic NMDA receptor signalling: implications for neurodegenerative disorders. *Nat Rev Neurosci*. 11(10), pp.682-696.

Harrison, R. 2004. Physiological roles of xanthine oxidoreductase. *Drug Metab Rev*. 36(2), pp.363-375.

Hayashi, T., Ishimori, C., Takahashi-Niki, K., Taira, T., Kim, Y.C., Maita, H., Maita, C., Ariga, H. and Iguchi-Ariga, S.M. 2009. DJ-1 binds to mitochondrial complex I and maintains its activity. *Biochem Biophys Res Commun*. 390(3), pp.667-672.

He, S., Wang, L., Miao, L., Wang, T., Du, F., Zhao, L. and Wang, X. 2009. Receptor interacting protein kinase-3 determines cellular necrotic response to TNF-α. *Cell*. 137(6), pp.1100-1111.

Hecquet, C.M., Ahmmed, G.U., Vogel, S.M. and Malik, A.B. 2008. Role of TRPM2 channel in mediating H_2O_2-induced Ca^{2+} entry and endothelial hyperpermeability. *Circ Res*. 102(3), pp.347-355.

Hecquet, C.M., Zhang, M., Mittal, M., Vogel, S.M., Di, A., Gao, X.P., Bonini, M.G. and Malik, A.B. 2014. Cooperative Interaction of trp Melastatin Channel Transient Receptor Potential (TRPM2) With Its Splice Variant TRPM2 Short Variant Is Essential for Endothelial Cell Apoptosis. *Circ Res*. 114(3), pp.469-479.

Held, K., Kichko, T., De Clercq, K., Klaassen, H., Van Bree, R., Vanherck, J.C., Marchand, A., Reeh, P.W., Chaltin, P., Voets, T. and Vriens, J. 2015. Activation of TRPM3 by a potent synthetic ligand reveals a role in peptide release. *Proc Natl Acad Sci U S A*. 112(11), pp.E1363-E1372.

Hill, K., Benham, C.D., McNulty, S. and Randall, A.D. 2004a. Flufenamic acid is a pH-dependent antagonist of TRPM2 channels. *Neuropharmacology*. 47(3), pp.450-460.

Hill, K., McNulty, S. and Randall, A.D. 2004b. Inhibition of TRPM2 channels by the antifungal agents clotrimazole and econazole. *Naunyn Schmiedebergs Arch Pharmacol*. 370(4), pp.227-237.

Hiroi, T., Wajima, T., Negoro, T., Ishii, M., Nakano, Y., Kiuchi, Y., Mori, Y. and Shimizu, S. 2013. Neutrophil TRPM2 channels are implicated in the exacerbation of myocardial ischaemia/reperfusion injury. *Cardiovasc Res*. 97(2), pp.271-281.

Hirst, J., Carroll, J., Fearnley, I.M., Shannon, R.J. and Walker, J.E. 2003. The nuclear encoded subunits of complex I from bovine heart mitochondria. *Biochim Biophys Acta*. 1604(3), pp.135-150.

Hirst, J., King, M.S. and Pryde, K.R. 2008. The production of reactive oxygen species by complex I. *Biochem Soc Trans*. 36(Pt 5), pp.976-980.

Hossmann, K.A. 2006. Pathophysiology and therapy of experimental stroke. *Cell Mol Neurobiol*. 26(7-8), pp.1057-1083.

Huang, K., Zhang, J., O'Neill, K.L., Gurumurthy, C.B., Quadros, R.M., Tu, Y. and Luo, X. 2016. Cleavage by Caspase-8 and Mitochondrial Membrane Association Activate the BH3-only Protein Bid during TRAIL-induced Apoptosis. *J Biol Chem*. 291(22), pp.11843-11851.

Huang, L.P. and Tepaamorndech, S. 2013. The SLC30 family of zinc transporters-A review of current understanding of their biological and pathophysiological roles. *Mol Aspects Med*. 34(2-3), pp.548-560.

Hwang, J.J., Lee, S.J., Kim, T.Y., Cho, J.H. and Koh, J.Y. 2008. Zinc and 4-hydroxy-2-nonenal mediate lysosomal membrane permeabilization induced by H_2O_2 in cultured hippocampal neurons. *J Neurosci*. 28(12), pp.3114-3122.

Hwang, O. 2013. Role of oxidative stress in Parkinson's disease. *Exp Neurobiol*. 22(1), pp.11-17.

Inamura, K., Sano, Y., Mochizuki, S., Yokoi, H., Miyake, A., Nozawa, K., Kitada, C., Matsushime, H. and Furuichi, K. 2003. Response to ADP-ribose by activation of TRPM2 in the CRI-G1 insulinoma cell line. *J Membr Biol*. 191(3), pp.201-207.

Iordanov, I., Mihalyi, C., Toth, B. and Csanady, L. 2016. The proposed channel-enzyme transient receptor potential melastatin 2 does not possess ADP ribose hydrolase activity. *Elife*. 5.

Irrcher, I., Aleyasin, H., Seifert, E.L., Hewitt, S.J., Chhabra, S., Phillips, M., Lutz, A.K., Rousseaux, M.W., Bevilacqua, L., Jahani-Asl, A., Callaghan, S., MacLaurin, J.G., Winklhofer, K.F., Rizzu, P., Rippstein, P., Kim, R.H., Chen, C.X., Fon, E.A., Slack, R.S., Harper, M.E., McBride, H.M., Mak, T.W. and Park, D.S. 2010. Loss of the Parkinson's disease-linked gene DJ-1 perturbs mitochondrial dynamics. *Hum Mol Genet*. 19(19), pp.3734-3746.

Ishii, M., Hagiwara, T., Mori, Y. and Shimizu, S. 2014. Involvement of TRPM2 and L-type Ca^{2+} channels in Ca^{2+} entry and cell death induced by hydrogen peroxide in rat beta-cell line RIN-5F. *J Toxicol Sci*. 39(2), pp.199-209.

Ishii, M., Shimizu, S., Hara, Y., Hagiwara, T., Miyazaki, A., Mori, Y. and Kiuchi, Y. 2006. Intracellular-produced hydroxyl radical mediates H_2O_2-induced Ca^{2+} influx and cell death in rat beta-cell line RIN-5F. *Cell Calcium*. 39(6), pp.487-494.

Jang, Y., Lee, S.H., Lee, B., Jung, S., Khalid, A., Uchida, K., Tominaga, M., Jeon, D. and Oh, U. 2015. TRPM2, a Susceptibility Gene for Bipolar Disorder, Regulates Glycogen Synthase Kinase-3 Activity in the Brain. *J Neurosci*. 35(34), pp.11811-11823.

Jaquet, V., Marcoux, J., Forest, E., Leidal, K.G., McCormick, S., Westermaier, Y., Perozzo, R., Plastre, O., Fioraso-Cartier, L., Diebold, B., Scapozza, L., Nauseef, W.M., Fieschi, F., Krause, K.H. and Bedard, K. 2011. NADPH oxidase (NOX) isoforms are inhibited by celastrol with a dual mode of action. *Br J Pharmacol*. 164(2b), pp.507-520.

Jia, J., Verma, S., Nakayama, S., Quillinan, N., Grafe, M.R., Hurn, P.D. and Herson, P.S. 2011. Sex differences in neuroprotection provided by inhibition of TRPM2 channels following experimental stroke. *J Cereb Blood Flow Metab*. 31(11), pp.2160-2168.

Jiang, D., Sullivan, P.G., Sensi, S.L., Steward, O. and Weiss, J.H. 2001. Zn^{2+} induces permeability transition pore opening and release of pro-apoptotic peptides from neuronal mitochondria. *J Biol Chem*. 276(50), pp.47524-47529.

Jiang, L.H., Yang, W., Zou, J. and Beech, D.J. 2010. TRPM2 channel properties, functions and therapeutic potentials. *Expert Opin Ther Targets*. 14(9), pp.973-988.

Jiang, X. and Wang, X. 2004. Cytochrome C-mediated apoptosis. *Annu Rev Biochem*. 73, pp.87-106.

Jin, R., Yang, G.J. and Li, G.H. 2010. Inflammatory mechanisms in ischemic stroke: role of inflammatory cells. *J Leukoc Biol*. 87(5), pp.779-789.

Johnson, D.K., Schillinger, K.J., Kwait, D.M., Hughes, C.V., McNamara, E.J., Ishmael, F., O'Donnell, R.W., Chang, M.M., Hogg, M.G., Dordick, J.S., Santhanam, L., Ziegler, L.M. and Holland, J.A. 2002. Inhibition of NADPH oxidase activation in endothelial cells by ortho-methoxy-substituted catechols. *Endothelium*. 9(3), pp.191-203.

Joza, N., Susin, S.A., Daugas, E., Stanford, W.L., Cho, S.K., Li, C.Y., Sasaki, T., Elia, A.J., Cheng, H.Y., Ravagnan, L., Ferri, K.F., Zamzami, N., Wakeham, A., Hakem, R., Yoshida, H., Kong, Y.Y., Mak, T.W., Zuniga-Pflucker, J.C., Kroemer, G. and Penninger, J.M. 2001. Essential role of the mitochondrial apoptosis-inducing factor in programmed cell death. *Nature*. 410(6828), pp.549-554.

Kahles, T., Kohnen, A., Heumueller, S., Rappert, A., Bechmann, I., Liebner, S., Wittko, I.M., Neumann-Haefelin, T., Steinmetz, H., Schroeder, K. and Brandes, R.P. 2010. NADPH oxidase NOX1 contributes to ischemic injury in experimental stroke in mice. *Neurobiol Dis*. 40(1), pp.185-192.

Kalogeris, T., Baines, C.P., Krenz, M. and Korthuis, R.J. 2012. Cell biology of ischemia/reperfusion injury. *Int Rev Cell Mol Biol*. 298, pp.229-317.

Kambe, T., Tsuji, T., Hashimoto, A. and Itsumura, N. 2015. The Physiological, Biochemical, and Molecular Roles of Zinc Transporters in Zinc Homeostasis and Metabolism. *Physiol Rev*. 95(3), pp.749-784.

Kaneko, S., Kawakami, S., Hara, Y., Wakamori, M., Itoh, E., Minami, T., Takada, Y., Kume, T., Katsuki, H., Mori, Y. and Akaike, A. 2006. A critical role of TRPM2 in neuronal cell death by hydrogen peroxide. *J Pharmacol Sci*. 101(1), pp.66-76.

Kang, Y.J. 2006. Metallothionein redox cycle and function. *Exp Biol Med (Maywood)*. 231(9), pp.1459-1467.

Kashio, M., Sokabe, T., Shintaku, K., Uematsu, T., Fukuta, N., Kobayashi, N., Mori, Y. and Tominaga, M. 2012. Redox signal-mediated sensitization of transient receptor potential melastatin 2 (TRPM2) to temperature affects macrophage functions. *Proc Natl Acad Sci U S A*. 109(17), pp.6745-6750.

Kashio, M. and Tominaga, M. 2015. Redox Signal-mediated Enhancement of the Temperature Sensitivity of Transient Receptor Potential Melastatin 2 (TRPM2) Elevates Glucose-induced Insulin Secretion from Pancreatic Islets. *J Biol Chem*. 290(19), pp.12435-12442.

Kawase, M., Murakami, K., Fujimura, M., Morita-Fujimura, Y., Gasche, Y., Kondo, T., Scott, R.W. and Chan, P.H. 1999. Exacerbation of delayed cell injury after transient global ischemia in mutant mice with Cu/Zn superoxide dismutase deficiency. *Stroke*. 30(9), pp.1962-1968.

Kerchner, G.A., Canzoniero, L.M.T., Yu, S.P., Ling, C. and Choi, D.W. 2000. Zn^{2+} current is mediated by voltage-gated Ca^{2+} channels and enhanced by extracellular acidity in mouse cortical neurones. *J Physiol*. 528(1), pp.39-52.

Kim, E.K. and Choi, E.J. 2010. Pathological roles of MAPK signaling pathways in human diseases. *Biochim Biophys Acta*. 1802(4), pp.396-405.

Kim, Y.H. and Koh, J.Y. 2002. The role of NADPH oxidase and neuronal nitric oxide synthase in zinc-induced poly(ADP-ribose) polymerase activation and cell death in cortical culture. *Exp Neurol*. 177(2), pp.407-418.

Kim, Y.S., Kim, S.S., Cho, J.J., Choi, D.H., Hwang, O., Shin, D.H., Chun, H.S., Beal, M.F. and Joh, T.H. 2005. Matrix metalloproteinase-3: A novel signaling proteinase from apoptotic neuronal cells that activates microglia. *J Neurosci*. 25(14), pp.3701-3711.

Kirino, T. 2000. Delayed neuronal death. *Neuropathology*. 20 Suppl, pp.S95-97.

Ko, H.L. and Ren, E.C. 2012. Functional Aspects of PARP1 in DNA Repair and Transcription. *Biomolecules*. 2(4), pp.524-548.

Koh, J.Y., Suh, S.W., Gwag, B.J., He, Y.Y., Hsu, C.Y. and Choi, D.W. 1996. The role of zinc in selective neuronal death after transient global cerebral ischemia. *Science*. 272(5264), pp.1013-1016.

Koike, C., Obara, T., Uriu, Y., Numata, T., Sanuki, R., Miyata, K., Koyasu, T., Ueno, S., Funabiki, K., Tani, A., Ueda, H., Kondo, M., Mori, Y., Tachibana, M. and Furukawa, T. 2010. TRPM1 is a component of the retinal ON bipolar cell transduction channel in the mGluR6 cascade. *Proc Natl Acad Sci U S A*. 107(1), pp.332-337.

Kokjohn, T.A. and Roher, A.E. 2009. Amyloid precursor protein transgenic mouse models and Alzheimer's disease: understanding the paradigms, limitations, and contributions. *Alzheimers Dement*. 5(4), pp.340-347.

Kolisek, M., Beck, A., Fleig, A. and Penner, R. 2005. Cyclic ADP-ribose and hydrogen peroxide synergize with ADP-ribose in the activation of TRPM2 channels. *Mol Cell*. 18(1), pp.61-69.

Koopman, W.J., Visch, H.J., Verkaart, S., van den Heuvel, L.W., Smeitink, J.A. and Willems, P.H. 2005. Mitochondrial network complexity and pathological decrease in complex I activity are tightly correlated in isolated human complex I deficiency. *Am J Physiol Cell Physiol*. 289(4), pp.C881-890.

Kraemer, B.R., Snow, J.P., Vollbrecht, P., Pathak, A., Valentine, W.M., Deutch, A.Y. and Carter, B.D. 2014. A role for the p75 neurotrophin receptor in axonal degeneration and apoptosis induced by oxidative stress. *J Biol Chem*. 289(31), pp.21205-21216.

Kraft, R., Grimm, C., Frenzel, H. and Harteneck, C. 2006. Inhibition of TRPM2 cation channels by N-(p-amylcinnamoyl)anthranilic acid. *Br J Pharmacol*. 148(3), pp.264-273.

Kraft, R., Grimm, C., Grosse, K., Hoffmann, A., Sauerbruch, S., Kettenmann, H., Schultz, G. and Harteneck, C. 2004. Hydrogen peroxide and ADP-ribose induce TRPM2-mediated calcium influx and cation currents in microglia. *Am J Physiol Cell Physiol*. 286(1), pp.C129-137.

Kuhn, F.J. and Luckhoff, A. 2004. Sites of the NUDT9-H domain critical for ADP-ribose activation of the cation channel TRPM2. *J Biol Chem*. 279(45), pp.46431-46437.

Kukic, I., Kelleher, S.L. and Kiselyov, K. 2014. Zn^{2+} efflux through lysosomal exocytosis prevents Zn^{2+}-induced toxicity. *J Cell Sci*. 127(14), pp.3094-3103.

Kushnareva, Y., Murphy, A.N. and Andreyev, A. 2002. Complex I-mediated reactive oxygen species generation: modulation by cytochrome-c and NADP oxidation-reduction state. *Biochem J*. 368(Pt 2), pp.545-553.

Kussmaul, L. and Hirst, J. 2006. The mechanism of superoxide production by NADH:ubiquinone oxidoreductase (complex I) from bovine heart mitochondria. *Proc Natl Acad Sci U S A*. 103(20), pp.7607-7612.

LaFerla, F.M., Green, K.N. and Oddo, S. 2007. Intracellular amyloid-beta in Alzheimer's disease. *Nat Rev Neurosci*. 8(7), pp.499-509.

Lai, T.W., Zhang, S. and Wang, Y.T. 2014. Excitotoxicity and stroke: identifying novel targets for neuroprotection. *Prog Neurobiol*. 115, pp.157-188.

Lambeth, J.D. 2004. NOX enzymes and the biology of reactive oxygen. *Nat Rev Immunol*. 4(3), pp.181-189.

Lambeth, J.D., Cheng, G., Arnold, R.S. and Edens, W.A. 2000. Novel homologs of $gp91^{phox}$. *Trends Biochem Sci*. 25(10), pp.459-461.

Lange, I., Yamamoto, S., Partida-Sanchez, S., Mori, Y., Fleig, A. and Penner, R. 2009. TRPM2 Functions as a Lysosomal Ca^{2+}-Release Channel in beta Cells. *Sci Signal*. 2(71).

Launay, P., Fleig, A., Perraud, A.L., Scharenberg, A.M., Penner, R. and Kinet, J.P. 2002. TRPM4 is a Ca^{2+}-activated nonselective cation channel mediating cell membrane depolarization. *Cell*. 109(3), pp.397-407.

Lee, C.R., Machold, R.P., Witkovsky, P. and Rice, M.E. 2013. TRPM2 channels are required for NMDA-induced burst firing and contribute to H_2O_2-dependent modulation in substantia nigra pars reticulata GABAergic neurons. *J Neurosci*. 33(3), pp.1157-1168.

Lee, S.J., Cho, K.S. and Koh, J.Y. 2009. Oxidative injury triggers autophagy in astrocytes: the role of endogenous zinc. *Glia*. 57(12), pp.1351-1361.

Lee, S.J. and Koh, J.Y. 2010. Roles of zinc and metallothionein-3 in oxidative stress-induced lysosomal dysfunction, cell death, and autophagy in neurons and astrocytes. *Mol Brain*. 3(1), p30.

Lewis, E.M., Sergeant, S., Ledford, B., Stull, N., Dinauer, M.C. and McPhail, L.C. 2010. Phosphorylation of $p22^{phox}$ on threonine 147 enhances NADPH oxidase activity by promoting $p47^{phox}$ binding. *J Biol Chem*. 285(5), pp.2959-2967.

Li, C.K., Meng, L., Li, X., Li, D.L. and Jiang, L.H. 2015. Non-NMDAR neuronal Ca^{2+}-permeable channels in delayed neuronal death and as potential therapeutic targets for ischemic brain damage. *Expert Opin Ther Targets*. 19(7), pp.879-892.

Li, M., Liu, Z., Zhuan, L., Wang, T., Guo, S., Wang, S., Liu, J. and Ye, Z. 2013. Effects of apocynin on oxidative stress and expression of apoptosis-related genes in testes of diabetic rats. *Mol Med Rep*. 7(1), pp.47-52.

Li, W.G., Miller, F.J., Jr., Zhang, H.J., Spitz, D.R., Oberley, L.W. and Weintraub, N.L. 2001. H_2O_2-induced O_2 production by a non-phagocytic NADPH oxidase causes oxidant injury. *J Biol Chem*. 276(31), pp.29251-29256.

Link, T.A. and von Jagow, G. 1995. Zinc ions inhibit the Q_P center of bovine heart mitochondrial bc_1 complex by blocking a protonatable group. *J Biol Chem*. 270(42), pp.25001-25006.

Linkermann, A. and Green, D.R. 2014. Necroptosis. *N Engl J Med*. 370(5), pp.455-465.

Lo, E.H., Dalkara, T. and Moskowitz, M.A. 2003. Mechanisms, challenges and opportunities in stroke. *Nat Rev Neurosci*. 4(5), pp.399-415.

Locksley, R.M., Killeen, N. and Lenardo, M.J. 2001. The TNF and TNF receptor superfamilies: integrating mammalian biology. *Cell*. 104(4), pp.487-501.

Lovell, M.A. 2009. A potential role for alterations of zinc and zinc transport proteins in the progression of Alzheimer's disease. *J Alzheimers Dis*. 16(3), pp.471-483.

Manna, P.T., Munsey, T.S., Abuarab, N., Li, F., Asipu, A., Howell, G., Sedo, A., Yang, W., Naylor, J., Beech, D.J., Jiang, L.H. and Sivaprasadarao, A. 2015.

TRPM2-mediated intracellular Zn^{2+} release triggers pancreatic beta-cell death. *Biochem J*. 466(3), pp.537-546.

Maret, W. and Vallee, B.L. 1998. Thiolate ligands in metallothionein confer redox activity on zinc clusters. *Proc Natl Acad Sci U S A*. 95(7), pp.3478-3482.

Marin, P., Israel, M., Glowinski, J. and Premont, J. 2000. Routes of zinc entry in mouse cortical neurons: role in zinc-induced neurotoxicity. *Eur J Neurosci*. 12(1), pp.8-18.

Martel, M.A., Soriano, F.X., Baxter, P., Rickman, C., Duncan, R., Wyllie, D.J.A. and Hardingham, G.E. 2009. Inhibiting pro-death NMDA receptor signaling dependent on the NR2 PDZ ligand may not affect synaptic function or synaptic NMDA receptor signaling to gene expression. *Channels*. 3(1), pp.12-15.

Masella, R., Di Benedetto, R., Vari, R., Filesi, C. and Giovannini, C. 2005. Novel mechanisms of natural antioxidant compounds in biological systems: involvement of glutathione and glutathione-related enzymes. *J Nutr Biochem*. 16(10), pp.577-586.

Massullo, P., Sumoza-Toledo, A., Bhagat, H. and Partida-Sanchez, S. 2006. TRPM channels, calcium and redox sensors during innate immune responses. *Semin Cell Dev Biol*. 17(6), pp.654-666.

Mattson, M.P., Duan, W., Pedersen, W.A. and Culmsee, C. 2001. Neurodegenerative disorders and ischemic brain diseases. *Apoptosis*. 6(1-2), pp.69-81.

McCord, M.C. and Aizenman, E. 2014. The role of intracellular zinc release in aging, oxidative stress, and Alzheimer's disease. *Front Aging Neurosci*. 6, p77.

McCubrey, J.A., Steelman, L.S., Chappell, W.H., Abrams, S.L., Wong, E.W., Chang, F., Lehmann, B., Terrian, D.M., Milella, M., Tafuri, A., Stivala, F., Libra, M., Basecke, J., Evangelisti, C., Martelli, A.M. and Franklin, R.A. 2007. Roles of the Raf/MEK/ERK pathway in cell growth, malignant transformation and drug resistance. *Biochim Biophys Acta*. 1773(8), pp.1263-1284.

McHugh, D., Flemming, R., Xu, S.Z., Perraud, A.L. and Beech, D.J. 2003. Critical intracellular Ca^{2+} dependence of transient receptor potential melastatin 2 (TRPM2) cation channel activation. *J Biol Chem*. 278(13), pp.11002-11006.

McQuillin, A., Bass, N.J., Kalsi, G., Lawrence, J., Puri, V., Choudhury, K., Detera-Wadleigh, S.D., Curtis, D. and Gurling, H.M. 2006. Fine mapping of a susceptibility locus for bipolar and genetically related unipolar affective disorders, to a region containing the C21ORF29 and TRPM2 genes on chromosome 21q22.3. *Mol Psychiatry*. 11(2), pp.134-142.

Medvedeva, Y.V., Lin, B., Shuttleworth, C.W. and Weiss, J.H. 2009. Intracellular Zn^{2+} accumulation contributes to synaptic failure, mitochondrial depolarization, and cell death in an acute slice oxygen-glucose deprivation model of ischemia. *J Neurosci*. 29(4), pp.1105-1114.

Medvedeva, Y.V. and Weiss, J.H. 2014. Intramitochondrial Zn^{2+} accumulation via the Ca^{2+} uniporter contributes to acute ischemic neurodegeneration. *Neurobiol Dis*. 68, pp.137-144.

Melzer, N., Hicking, G., Gobel, K. and Wiendl, H. 2012. TRPM2 cation channels modulate T cell effector functions and contribute to autoimmune CNS inflammation. *PLoS One*. 7(10), pe47617.

Micheau, O. and Tschopp, J. 2003. Induction of TNF receptor I-mediated apoptosis via two sequential signaling complexes. *Cell*. 114(2), pp.181-190.

Miller, B.A. 2006. The role of TRP channels in oxidative stress-induced cell death. *J Membr Biol*. 209(1), pp.31-41.

Miller, B.A. and Zhang, W.Y. 2011. TRP Channels as Mediators of Oxidative Stress. *Adv Exp Med Biol*. 704, pp.531-544.

Mittal, M., Siddiqui, M.R., Tran, K., Reddy, S.P. and Malik, A.B. 2014. Reactive oxygen species in inflammation and tissue injury. *Antioxid Redox Signal*. 20(7), pp.1126-1167.

Miyake, T., Shirakawa, H., Kusano, A., Sakimoto, S., Konno, M., Nakagawa, T., Mori, Y. and Kaneko, S. 2014. TRPM2 contributes to LPS/IFNγ-induced production of nitric oxide via the p38/JNK pathway in microglia. *Biochem Biophys Res Commun*. 444(2), pp.212-217.

Monteilh-Zoller, M.K., Hermosura, M.C., Nadler, M.J., Scharenberg, A.M., Penner, R. and Fleig, A. 2003. TRPM7 provides an ion channel mechanism for cellular entry of trace metal ions. *J Gen Physiol*. 121(1), pp.49-60.

Montell, C. 2001. Physiology, phylogeny, and functions of the TRP superfamily of cation channels. *Sci STKE*. 2001(90), pre1.

Montell, C. 2005. The TRP superfamily of cation channels. *Sci STKE*. 2005(272), pre3.

Moore, D.J., West, A.B., Dawson, V.L. and Dawson, T.M. 2005. Molecular pathophysiology of Parkinson's disease. *Annu Rev Neurosci*. 28, pp.57-87.

Moreira, P.I., Santos, M.S., Moreno, A. and Oliveira, C. 2001. Amyloid beta-peptide promotes permeability transition pore in brain mitochondria. *Biosci Rep*. 21(6), pp.789-800.

Moroni, F. 2008. Poly(ADP-ribose)polymerase 1 (PARP-1) and postischemic brain damage. *Curr Opin Pharmacol*. 8(1), pp.96-103.

Morris, D.R. and Levenson, C.W. 2012. Ion channels and zinc: mechanisms of neurotoxicity and neurodegeneration. *J Toxicol*. 2012, p785647.

Mucke, L. and Selkoe, D.J. 2012. Neurotoxicity of amyloid beta-protein: synaptic and network dysfunction. *Cold Spring Harb Perspect Med*. 2(7), pa006338.

Muftuoglu, M., Elibol, B., Dalmizrak, O., Ercan, A., Kulaksiz, G., Ogus, H., Dalkara, T. and Ozer, N. 2004. Mitochondrial complex I and IV activities in leukocytes from patients with parkin mutations. *Mov Disord*. 19(5), pp.544-548.

Munoz, P., Huenchuguala, S., Paris, I. and Segura-Aguilar, J. 2012. Dopamine oxidation and autophagy. *Parkinsons Dis*. 2012, p920953.

Muoio, D.M. and Newgard, C.B. 2008. Mechanisms of disease: Molecular and metabolic mechanisms of insulin resistance and beta-cell failure in type 2 diabetes. *Nat Rev Mol Cell Biol*. 9(3), pp.193-205.

Murakami, K., Kondo, T., Kawase, M., Li, Y.B., Sato, S., Chen, S.F. and Chan, P.H. 1998. Mitochondrial susceptibility to oxidative stress exacerbates cerebral infarction that follows permanent focal cerebral ischemia in mutant mice with manganese superoxide dismutase deficiency. *J Neurosci*. 18(1), pp.205-213.

Murphy, M.P. 2009. How mitochondria produce reactive oxygen species. *Biochem J*. 417, pp.1-13.

Murphy, M.P. and LeVine, H., 3rd. 2010. Alzheimer's disease and the amyloid-beta peptide. *J Alzheimers Dis*. 19(1), pp.311-323.

Nadler, M.J., Hermosura, M.C., Inabe, K., Perraud, A.L., Zhu, Q., Stokes, A.J., Kurosaki, T., Kinet, J.P., Penner, R., Scharenberg, A.M. and Fleig, A. 2001. LTRPC7 is a Mg.ATP-regulated divalent cation channel required for cell viability. *Nature*. 411(6837), pp.590-595.

Nicolle, M.M., Gonzalez, J., Sugaya, K., Baskerville, K.A., Bryan, D., Lund, K., Gallagher, M. and McKinney, M. 2001. Signatures of hippocampal oxidative stress in aged spatial learning-impaired rodents. *Neuroscience*. 107(3), pp.415-431.

Nilius, B., Prenen, J., Droogmans, G., Voets, T., Vennekens, R., Freichel, M., Wissenbach, U. and Flockerzi, V. 2003. Voltage dependence of the Ca^{2+}-activated cation channel TRPM4. *J Biol Chem*. 278(33), pp.30813-30820.

Nimse, S.B. and Pal, D. 2015. Free radicals, natural antioxidants, and their reaction mechanisms. *Rsc Advances*. 5(35), pp.27986-28006.

Noh, K.M., Kim, Y.H. and Koh, J.Y. 1999. Mediation by membrane protein kinase C of zinc-induced oxidative neuronal injury in mouse cortical cultures. *J Neurochem*. 72(4), pp.1609-1616.

Noh, K.M. and Koh, J.Y. 2000. Induction and activation by zinc of NADPH oxidase in cultured cortical neurons and astrocytes. *J Neurosci*. 20(23), pRC111.

O'Brien, R.J. and Wong, P.C. 2011. Amyloid precursor protein processing and Alzheimer's disease. *Annu Rev Neurosci*. 34, pp.185-204.

O'Donnell, B.V., Tew, D.G., Jones, O.T. and England, P.J. 1993. Studies on the inhibitory mechanism of iodonium compounds with special reference to neutrophil NADPH oxidase. *Biochem J*. 290 (Pt 1), pp.41-49.

O'Donnell, V.B., Smith, G.C. and Jones, O.T. 1994. Involvement of phenyl radicals in iodonium inhibition of flavoenzymes. *Mol Pharmacol*. 46(4), pp.778-785.

Ohana, E., Segal, D., Palty, R., Dien, T.T., Moran, A., Sensi, S.L., Weiss, J.H., Hershfinkel, M. and Sekler, I. 2004. A sodium zinc exchange mechanism is mediating extrusion of zinc in mammalian cells. *J Biol Chem*. 279(6), pp.4278-4284.

Olagnier, D., Peri, S., Steel, C., van Montfoort, N., Chiang, C., Beljanski, V., Slifker, M., He, Z., Nichols, C.N., Lin, R., Balachandran, S. and Hiscott, J. 2014. Cellular oxidative stress response controls the antiviral and apoptotic programs in dengue virus-infected dendritic cells. *PLoS Pathog*. 10(12), pe1004566.

Olah, M.E., Jackson, M.F., Li, H., Perez, Y., Sun, H.S., Kiyonaka, S., Mori, Y., Tymianski, M. and MacDonald, J.F. 2009. Ca^{2+}-dependent induction of TRPM2 currents in hippocampal neurons. *J Physiol*. 587(Pt 5), pp.965-979.

Orfanelli, U., Wenke, A.K., Doglioni, C., Russo, V., Bosserhoff, A.K. and Lavorgna, G. 2008. Identification of novel sense and antisense transcription at the TRPM2 locus in cancer. *Cell Res*. 18(11), pp.1128-1140.

Orrenius, S., Gogvadze, V. and Zhivotovsky, B. 2007. Mitochondrial oxidative stress: implications for cell death. *Annu Rev Pharmacol Toxicol*. 47, pp.143-183.

Ostapchenko, V.G., Chen, M., Guzman, M.S., Xie, Y.F., Lavine, N., Fan, J., Beraldo, F.H., Martyn, A.C., Belrose, J.C., Mori, Y., MacDonald, J.F., Prado, V.F., Prado, M.A. and Jackson, M.F. 2015. The Transient Receptor Potential Melastatin 2 (TRPM2) Channel Contributes to beta-Amyloid Oligomer-Related Neurotoxicity and Memory Impairment. *J Neurosci*. 35(45), pp.15157-15169.

Osyczka, A., Moser, C.C. and Dutton, P.L. 2005. Fixing the Q cycle. *Trends Biochem Sci*. 30(4), pp.176-182.

Oz, A. and Celik, O. 2017. Curcumin inhibits oxidative stress-induced TRPM2 channel activation, calcium ion entry and apoptosis values in SH-SY5Y neuroblastoma cells: Involvement of transfection procedure. *Mol Membr Biol*. pp.1-13.

Paiva, C.N. and Bozza, M.T. 2014. Are Reactive Oxygen Species Always Detrimental to Pathogens? *Antioxid Redox Signal*. 20(6), pp.1000-1037.

Palacino, J.J., Sagi, D., Goldberg, M.S., Krauss, S., Motz, C., Wacker, M., Klose, J. and Shen, J. 2004. Mitochondrial dysfunction and oxidative damage in parkin-deficient mice. *J Biol Chem*. 279(18), pp.18614-18622.

Palmiter, R.D., Cole, T.B., Quaife, C.J. and Findley, S.D. 1996. ZnT-3, a putative transporter of zinc into synaptic vesicles. *Proc Natl Acad Sci U S A*. 93(25), pp.14934-14939.

Panday, A., Sahoo, M.K., Osorio, D. and Batra, S. 2015. NADPH oxidases: an overview from structure to innate immunity-associated pathologies. *Cell Mol Immunol*. 12(1), pp.5-23.

Park, H.S., Jung, H.Y., Park, E.Y., Kim, J., Lee, W.J. and Bae, Y.S. 2004. Cutting edge: Direct interaction of TLR4 with NADPH oxidase 4 isozyme is essential for lipopolysaccharide-induced production of reactive oxygen species and activation of NF-κB. *J Immunol*. 173(6), pp.3589-3593.

Park, L., Anrather, J., Zhou, P., Frys, K., Pitstick, R., Younkin, S., Carlson, G.A. and Iadecola, C. 2005. NADPH-oxidase-derived reactive oxygen species mediate the cerebrovascular dysfunction induced by the amyloid beta peptide. *J Neurosci*. 25(7), pp.1769-1777.

Park, L., Wang, G., Moore, J., Girouard, H., Zhou, P., Anrather, J. and Iadecola, C. 2014. The key role of transient receptor potential melastatin-2 channels in amyloid-beta-induced neurovascular dysfunction. *Nat Commun*. 5.

Park, L., Zhou, P., Pitstick, R., Capone, C., Anrather, J., Norris, E.H., Younkin, L., Younkin, S., Carlson, G., McEwen, B.S. and Iadecola, C. 2008. Nox2-derived radicals contribute to neurovascular and behavioral dysfunction in mice overexpressing the amyloid precursor protein. *Proc Natl Acad Sci U S A*. 105(4), pp.1347-1352.

Parker, W.D., Jr., Parks, J.K. and Swerdlow, R.H. 2008. Complex I deficiency in Parkinson's disease frontal cortex. *Brain Res*. 1189, pp.215-218.

Peier, A.M., Moqrich, A., Hergarden, A.C., Reeve, A.J., Andersson, D.A., Story, G.M., Earley, T.J., Dragoni, I., McIntyre, P., Bevan, S. and Patapoutian, A. 2002. A TRP channel that senses cold stimuli and menthol. *Cell*. 108(5), pp.705-715.

Perez, C.A., Huang, L., Rong, M., Kozak, J.A., Preuss, A.K., Zhang, H., Max, M. and Margolskee, R.F. 2002. A transient receptor potential channel expressed in taste receptor cells. *Nat Neurosci*. 5(11), pp.1169-1176.

Perraud, A.L., Fleig, A., Dunn, C.A., Bagley, L.A., Launay, P., Schmitz, C., Stokes, A.J., Zhu, Q., Bessman, M.J., Penner, R., Kinet, J.P. and Scharenberg, A.M. 2001. ADP-ribose gating of the calcium-permeable LTRPC2 channel revealed by Nudix motif homology. *Nature*. 411(6837), pp.595-599.

Perraud, A.L., Takanishi, C.L., Shen, B., Kang, S., Smith, M.K., Schmitz, C., Knowles, H.M., Ferraris, D., Li, W., Zhang, J., Stoddard, B.L. and Scharenberg, A.M. 2005. Accumulation of free ADP-ribose from mitochondria mediates oxidative stress-induced gating of TRPM2 cation channels. *J Biol Chem*. 280(7), pp.6138-6148.

Petronio, M.S., Zeraik, M.L., Fonseca, L.M. and Ximenes, V.F. 2013. Apocynin: chemical and biophysical properties of a NADPH oxidase inhibitor. *Molecules*. 18(3), pp.2821-2839.

Pisoschi, A.M. and Pop, A. 2015. The role of antioxidants in the chemistry of oxidative stress: A review. *Eur J Med Chem*. 97, pp.55-74.

Pochwat, B., Nowak, G. and Szewczyk, B. 2015. Relationship between Zinc (Zn^{2+}) and Glutamate Receptors in the Processes Underlying Neurodegeneration. *Neural Plast*.

Poewe, W., Seppi, K., Tanner, C.M., Halliday, G.M., Brundin, P., Volkmann, J., Schrag, A.E. and Lang, A.E. 2017. Parkinson disease. *Nat Rev Dis Primers*. 3.

Pozueta, J., Lefort, R. and Shelanski, M.L. 2013. Synaptic changes in Alzheimer's disease and its models. *Neuroscience*. 251, pp.51-65.

Pratico, D. and Sung, S. 2004. Lipid peroxidation and oxidative imbalance: Early functional events in Alzheimer's disease. *J Alzheimers Dis*. 6(2), pp.171-175.

Qian, L., Flood, P.M. and Hong, J.S. 2010. Neuroinflammation is a key player in Parkinson's disease and a prime target for therapy. *J Neural Transm (Vienna)*. 117(8), pp.971-979.

Qin, Y., Thomas, D., Fontaine, C.P. and Colvin, R.A. 2008. Mechanisms of Zn^{2+} efflux in cultured cortical neurons. *J Neurochem*. 107(5), pp.1304-1313.

Qin, Y., Thomas, D., Fontaine, C.P. and Colvin, R.A. 2009. Silencing of ZnT1 reduces Zn^{2+} efflux in cultured cortical neurons. *Neurosci Lett*. 450(2), pp.206-210.

Querfurth, H.W. and LaFerla, F.M. 2010. Alzheimer's disease. *N Engl J Med*. 362(4), pp.329-344.

Quillinan, N., Grewal, H., Klawitter, J. and Herson, P.S. 2014. Sex Steroids Do Not Modulate TRPM2-Mediated Injury in Females following Middle Cerebral Artery Occlusion(1,2,3). *eNeuro*. 1(1).

Raad, H., Paclet, M.H., Boussetta, T., Kroviarski, Y., Morel, F., Quinn, M.T., Gougerot-Pocidalo, M.A., Dang, P.M. and El-Benna, J. 2009. Regulation of the phagocyte NADPH oxidase activity: phosphorylation of gp91^{phox}/NOX2 by protein kinase C enhances its diaphorase activity and binding to Rac2, p67^{phox}, and p47^{phox}. *FASEB J*. 23(4), pp.1011-1022.

Radermacher, K.A., Wingler, K., Langhauser, F., Altenhofer, S., Kleikers, P., Hermans, J.J.R., de Angelis, M.H., Kleinschnitz, C. and Schmidt, H.H.H.W. 2013. Neuroprotection After Stroke by Targeting NOX4 As a Source of Oxidative Stress. *Antioxid Redox Signal*. 18(12), pp.1418-1427.

Ray, P.D., Huang, B.W. and Tsuji, Y. 2012. Reactive oxygen species (ROS) homeostasis and redox regulation in cellular signaling. *Cell Signal*. 24(5), pp.981-990.

Reddy, P.H., Manczak, M., Mao, P., Calkins, M.J., Reddy, A.P. and Shirendeb, U. 2010. Amyloid-beta and mitochondria in aging and Alzheimer's disease: implications for synaptic damage and cognitive decline. *J Alzheimers Dis*. 20 Suppl 2, pp.S499-512.

Reinehr, R., Gorg, B., Becker, S., Qvartskhava, N., Bidmon, H.J., Selbach, O., Haas, H.L., Schliess, F. and Haussinger, D. 2007. Hypoosmotic swelling and ammonia increase oxidative stress by NADPH oxidase in cultured astrocytes and vital brain slices. *Glia*. 55(7), pp.758-771.

Rissman, R.A., Poon, W.W., Blurton-Jones, M., Oddo, S., Torp, R., Vitek, M.P., LaFerla, F.M., Rohn, T.T. and Cotman, C.W. 2004. Caspase-cleavage of tau is an early event in Alzheimer disease tangle pathology. *J Clin Invest*. 114(1), pp.121-130.

Rivlin-Etzion, M., Marmor, O., Saban, G., Rosin, B., Haber, S.N., Vaadia, E., Prut, Y. and Bergman, H. 2008. Low-pass filter properties of basal ganglia cortical muscle loops in the normal and MPTP primate model of parkinsonism. *J Neurosci*. 28(3), pp.633-649.

Rizzuto, R., De Stefani, D., Raffaello, A. and Mammucari, C. 2012. Mitochondria as sensors and regulators of calcium signalling. *Nat Rev Mol Cell Biol*. 13(9), pp.566-578.

Roberge, S., Roussel, J., Andersson, D.C., Meli, A.C., Vidal, B., Blandel, F., Lanner, J.T., Le Guennec, J.Y., Katz, A., Westerblad, H., Lacampagne, A. and Fauconnier, J. 2014. TNF-α-mediated caspase-8 activation induces ROS production and TRPM2 activation in adult ventricular myocytes. *Cardiovasc Res*. 103(1), pp.90-99.

Rock, K.L. and Kono, H. 2008. The inflammatory response to cell death. *Annu Rev Pathol*. 3, pp.99-126.

Roedding, A.S., Gao, A.F., Au-Yeung, W., Scarcelli, T., Li, P.P. and Warsh, J.J. 2012. Effect of oxidative stress on TRPM2 and TRPC3 channels in B lymphoblast cells in bipolar disorder. *Bipolar Disord*. 14(2), pp.151-161.

Roedding, A.S., Tong, S.Y., Au-Yeung, W., Li, P.P. and Warsh, J.J. 2013. Chronic oxidative stress modulates TRPC3 and TRPM2 channel expression and function in rat primary cortical neurons: relevance to the pathophysiology of bipolar disorder. *Brain Res*. 1517, pp.16-27.

Rohn, T.T. and Head, E. 2009. Caspases as therapeutic targets in Alzheimer's disease: Is it time to "cut" to the chase? *Int J Clin Exp Pathol*. 2(2), pp.108-118.

Ruiz, C., Casarejos, M.J., Gomez, A., Solano, R., de Yebenes, J.G. and Mena, M.A. 2012. Protection by glia-conditioned medium in a cell model of Huntington disease. *PLoS Curr*. 4, pe4fbca54a2028b.

Ruttkay-Nedecky, B., Nejdl, L., Gumulec, J., Zitka, O., Masarik, M., Eckschlager, T., Stiborova, M., Adam, V. and Kizek, R. 2013. The role of metallothionein in oxidative stress. *Int J Mol Sci*. 14(3), pp.6044-6066.

Saelens, X., Festjens, N., Vande Walle, L., van Gurp, M., van Loo, G. and Vandenabeele, P. 2004. Toxic proteins released from mitochondria in cell death. *Oncogene*. 23(16), pp.2861-2874.

Salminen, A., Kauppinen, A., Suuronen, T., Kaarniranta, K. and Ojala, J. 2009. ER stress in Alzheimer's disease: a novel neuronal trigger for inflammation and Alzheimer's pathology. *J Neuroinflammation*. 6, p41.

Sanderson, T.H., Reynolds, C.A., Kumar, R., Przyklenk, K. and Huttemann, M. 2013. Molecular mechanisms of ischemia-reperfusion injury in brain: pivotal role of the mitochondrial membrane potential in reactive oxygen species generation. *Mol Neurobiol*. 47(1), pp.9-23.

Sano, Y., Inamura, K., Miyake, A., Mochizuki, S., Yokoi, H., Matsushime, H. and Furuichi, K. 2001. Immunocyte Ca^{2+} influx system mediated by LTRPC2. *Science*. 293(5533), pp.1327-1330.

Santo-Domingo, J. and Demaurex, N. 2010. Calcium uptake mechanisms of mitochondria. *Biochim Biophys Acta*. 1797(6-7), pp.907-912.

Sasaki, Y., Vohra, B.P.S., Lund, F.E. and Milbrandt, J. 2009. Nicotinamide Mononucleotide Adenylyl Transferase-Mediated Axonal Protection Requires Enzymatic Activity But Not Increased Levels of Neuronal Nicotinamide Adenine Dinucleotide. *J Neurosci*. 29(17), pp.5525-5535.

Scheltens, P., Blennow, K., Breteler, M.M., de Strooper, B., Frisoni, G.B., Salloway, S. and Van der Flier, W.M. 2016. Alzheimer's disease. *Lancet*. 388(10043), pp.505-517.

Schrader, M. and Fahimi, H.D. 2006. Peroxisomes and oxidative stress. *Biochim Biophys Acta*. 1763(12), pp.1755-1766.

Schreiber, V., Dantzer, F., Ame, J.C. and de Murcia, G. 2006. Poly(ADP-ribose): novel functions for an old molecule. *Nat Rev Mol Cell Biol*. 7(7), pp.517-528.

Sensi, S.L., Paoletti, P., Bush, A.I. and Sekler, I. 2009. Zinc in the physiology and pathology of the CNS. *Nat Rev Neurosci*. 10(11), pp.780-791.

Sensi, S.L., Paoletti, P., Koh, J.Y., Aizenman, E., Bush, A.I. and Hershfinkel, M. 2011. The neurophysiology and pathology of brain zinc. *J Neurosci*. 31(45), pp.16076-16085.

Sensi, S.L., Ton-That, D., Sullivan, P.G., Jonas, E.A., Gee, K.R., Kaczmarek, L.K. and Weiss, J.H. 2003. Modulation of mitochondrial function by endogenous Zn^{2+} pools. *Proc Natl Acad Sci U S A*. 100(10), pp.6157-6162.

Shamas-Din, A., Kale, J., Leber, B. and Andrews, D.W. 2013. Mechanisms of action of Bcl-2 family proteins. *Cold Spring Harb Perspect Biol*. 5(4), pa008714.

Sharov, V.S., Dremina, E.S., Galeva, N.A., Williams, T.D. and Schoneich, C. 2006. Quantitative mapping of oxidation-sensitive cysteine residues in SERCA in vivo and in vitro by HPLC-electrospray-tandem MS: selective protein oxidation during biological aging. *Biochem J*. 394(Pt 3), pp.605-615.

Sharpley, M.S. and Hirst, J. 2006. The inhibition of mitochondrial complex I (NADH: ubiquinone oxidoreductase) by Zn^{2+}. *J Biol Chem*. 281(46), pp.34803-34809.

Sheline, C.T., Behrens, M.M. and Choi, D.W. 2000. Zinc-induced cortical neuronal death: contribution of energy failure attributable to loss of NAD^+ and inhibition of glycolysis. *J Neurosci*. 20(9), pp.3139-3146.

Shimizu, S., Yonezawa, R., Hagiwara, T., Yoshida, T., Takahashi, N., Hamano, S., Negoro, T., Toda, T., Wakamori, M., Mori, Y. and Ishii, M. 2014. Inhibitory effects of AG490 on H_2O_2-induced TRPM2-mediated Ca^{2+} entry. *Eur J Pharmacol*. 742, pp.22-30.

Shimizu, T., Macey, T.A., Quillinan, N., Klawitter, J., Perraud, A.L., Traystman, R.J. and Herson, P.S. 2013. Androgen and PARP-1 regulation of TRPM2 channels after ischemic injury. *J Cereb Blood Flow Metab*. 33(10), pp.1549-1555.

Shuttleworth, C.W. and Weiss, J.H. 2011. Zinc: new clues to diverse roles in brain ischemia. *Trends Pharmacol Sci*. 32(8), pp.480-486.

Sindreu, C., Palmiter, R.D. and Storm, D.R. 2011. Zinc transporter ZnT-3 regulates presynaptic Erk1/2 signaling and hippocampus-dependent memory. *Proc Natl Acad Sci U S A*. 108(8), pp.3366-3370.

Sirk, D., Zhu, Z., Wadia, J.S., Shulyakova, N., Phan, N., Fong, J. and Mills, L.R. 2007. Chronic exposure to sub-lethal beta-amyloid (Aβ) inhibits the import of nuclear-encoded proteins to mitochondria in differentiated PC12 cells. *J Neurochem*. 103(5), pp.1989-2003.

Slee, E.A., Adrain, C. and Martin, S.J. 2001. Executioner caspase-3, -6, and -7 perform distinct, non-redundant roles during the demolition phase of apoptosis. *J Biol Chem*. 276(10), pp.7320-7326.

Smart, T.G., Hosie, A.M. and Miller, P.S. 2004. Zn^{2+} ions: modulators of excitatory and inhibitory synaptic activity. *Neuroscientist*. 10(5), pp.432-442.

So, K., Haraguchi, K., Asakura, K., Isami, K., Sakimoto, S., Shirakawa, H., Mori, Y., Nakagawa, T. and Kaneko, S. 2015. Involvement of TRPM2 in a wide range of inflammatory and neuropathic pain mouse models. *J Pharmacol Sci*. 127(3), pp.237-243.

Son, Y., Kim, S., Chung, H.T. and Pae, H.O. 2013. Reactive oxygen species in the activation of MAP kinases. *Methods Enzymol*. 528, pp.27-48.

Song, K., Wang, H., Kamm, G.B., Pohle, J., Reis, F.D., Heppenstall, P., Wende, H. and Siemens, J. 2016. The TRPM2 channel is a hypothalamic heat sensor that limits fever and can drive hypothermia. *Science*. 353(6306), pp.1393-1398.

Sousa, S.C., Maciel, E.N., Vercesi, A.E. and Castilho, R.F. 2003. Ca^{2+}-induced oxidative stress in brain mitochondria treated with the respiratory chain inhibitor rotenone. *FEBS Lett*. 543(1-3), pp.179-183.

Spahl, D.U., Berendji-Grun, D., Suschek, C.V., Kolb-Bachofen, V. and Kroncke, K.D. 2003. Regulation of zinc homeostasis by inducible NO synthase-derived NO: Nuclear translocation and intranuclear metallothionein Zn^{2+} release. *Proc Natl Acad Sci U S A*. 100(24), pp.13952-13957.

Stadtman, E.R. and Levine, R.L. 2000. Protein oxidation. *Ann N Y Acad Sci*. 899, pp.191-208.

Starkov, A.A., Fiskum, G., Chinopoulos, C., Lorenzo, B.J., Browne, S.E., Patel, M.S. and Beal, M.F. 2004. Mitochondrial alpha-ketoglutarate dehydrogenase complex generates reactive oxygen species. *J Neurosci*. 24(36), pp.7779-7788.

Starkus, J., Beck, A., Fleig, A. and Penner, R. 2007. Regulation of TRPM2 by extra- and intracellular calcium. *J Gen Physiol*. 130(4), pp.427-440.

Starkus, J.G., Fleig, A. and Penner, R. 2010. The calcium-permeable non-selective cation channel TRPM2 is modulated by cellular acidification. *J Physiol*. 588(8), pp.1227-1240.

Stork, C.J. and Li, Y.V. 2009. Rising zinc: a significant cause of ischemic neuronal death in the CA1 region of rat hippocampus. *J Cereb Blood Flow Metab*. 29(8), pp.1399-1408.

Straub, R.E., Lehner, T., Luo, Y., Loth, J.E., Shao, W., Sharpe, L., Alexander, J.R., Das, K., Simon, R., Fieve, R.R. and et al. 1994. A possible vulnerability locus for bipolar affective disorder on chromosome 21q22.3. *Nat Genet*. 8(3), pp.291-296.

Sumoza-Toledo, A., Lange, I., Cortado, H., Bhagat, H., Mori, Y., Fleig, A., Penner, R. and Partida-Sanchez, S. 2011. Dendritic cell maturation and chemotaxis is regulated by TRPM2-mediated lysosomal Ca^{2+} release. *FASEB J*. 25(10), pp.3529-3542.

Sun, H.S., Jackson, M.F., Martin, L.J., Jansen, K., Teves, L., Cui, H., Kiyonaka, S., Mori, Y., Jones, M., Forder, J.P., Golde, T.E., Orser, B.A., Macdonald, J.F. and Tymianski, M. 2009. Suppression of hippocampal TRPM7 protein prevents delayed neuronal death in brain ischemia. *Nat Neurosci*. 12(10), pp.1300-1307.

Sun, L., Wang, H., Wang, Z., He, S., Chen, S., Liao, D., Wang, L., Yan, J., Liu, W., Lei, X. and Wang, X. 2012. Mixed lineage kinase domain-like protein mediates necrosis signaling downstream of RIP3 kinase. *Cell*. 148(1-2), pp.213-227.

Sun, Y., Sukumaran, P., Selvaraj, S., Cilz, N.I., Schaar, A., Lei, S. and Singh, B.B. 2016. TRPM2 Promotes Neurotoxin MPP^+/MPTP-Induced Cell Death. *Mol Neurobiol*.

Swomley, A.M., Forster, S., Keeney, J.T., Triplett, J., Zhang, Z., Sultana, R. and Butterfield, D.A. 2014. Abeta, oxidative stress in Alzheimer disease: evidence based on proteomics studies. *Biochim Biophys Acta*. 1842(8), pp.1248-1257.

Takahashi, N. and Mori, Y. 2011. TRP channels as sensors and signal integrators of redox status changes. *Front Pharmacol*. 2.

Takuma, H., Tomiyama, T., Kuida, K. and Mori, H. 2004. Amyloid beta peptide-induced cerebral neuronal loss is mediated by caspase-3 in vivo. *J Neuropathol Exp Neurol*. 63(3), pp.255-261.

Tammariello, S.P., Quinn, M.T. and Estus, S. 2000. NADPH oxidase contributes directly to oxidative stress and apoptosis in nerve growth factor-deprived sympathetic neurons. *J Neurosci*. 20(1), pRC53.

Tan, C.H. and McNaughton, P.A. 2016. The TRPM2 ion channel is required for sensitivity to warmth. *Nature*. 536(7617), pp.460-3.

Tanaka, Y., Tran, P.O., Harmon, J. and Robertson, R.P. 2002. A role for glutathione peroxidase in protecting pancreatic beta cells against oxidative stress in a model of glucose toxicity. *Proc Natl Acad Sci U S A*. 99(19), pp.12363-12368.

Tang, X.N., Cairns, B., Kim, J.Y. and Yenari, M.A. 2012. NADPH oxidase in stroke and cerebrovascular disease. *Neurol Res*. 34(4), pp.338-345.

Toda, T., Yamamoto, S., Yonezawa, R., Mori, Y. and Shimizu, S. 2016. Inhibitory effects of Tyrphostin AG-related compounds on oxidative stress-sensitive transient receptor potential channel activation. *Eur J Pharmacol*. 786, pp.19-28.

Togashi, K., Hara, Y., Tominaga, T., Higashi, T., Konishi, Y., Mori, Y. and Tominaga, M. 2006. TRPM2 activation by cyclic ADP-ribose at body temperature is involved in insulin secretion. *EMBO J*. 25(9), pp.1804-1815.

Togashi, K., Inada, H. and Tominaga, M. 2008. Inhibition of the transient receptor potential cation channel TRPM2 by 2-aminoethoxydiphenyl borate (2-APB). *Br J Pharmacol*. 153(6), pp.1324-1330.

Tong, Q., Zhang, W., Conrad, K., Mostoller, K., Cheung, J.Y., Peterson, B.Z. and Miller, B.A. 2006. Regulation of the transient receptor potential channel TRPM2 by the Ca^{2+} sensor calmodulin. *J Biol Chem*. 281(14), pp.9076-9085.

Tong, X.K., Nicolakakis, N., Kocharyan, A. and Hamel, E. 2005. Vascular remodeling versus amyloid beta-induced oxidative stress in the cerebrovascular dysfunctions associated with Alzheimer's disease. *J Neurosci*. 25(48), pp.11165-11174.

Toth, B. and Csanady, L. 2010. Identification of direct and indirect effectors of the transient receptor potential melastatin 2 (TRPM2) cation channel. *J Biol Chem*. 285(39), pp.30091-30102.

Toth, B., Iordanov, I. and Csanady, L. 2015. Ruling out pyridine dinucleotides as true TRPM2 channel activators reveals novel direct agonist ADP-ribose-2 '-phosphate. *J Gen Physiol*. 145(5), pp.419-430.

Traber, M.G. and Stevens, J.F. 2011. Vitamins C and E: beneficial effects from a mechanistic perspective. *Free Radic Biol Med*. 51(5), pp.1000-1013.

Troy, C.M., Rabacchi, S.A., Friedman, W.J., Frappier, T.F., Brown, K. and Shelanski, M.L. 2000. Caspase-2 mediates neuronal cell death induced by beta-amyloid. *J Neurosci*. 20(4), pp.1386-1392.

Turrens, J.F. 2003. Mitochondrial formation of reactive oxygen species. *J Physiol*. 552(Pt 2), pp.335-344.

Uchida, K., Dezaki, K., Damdindorj, B., Inada, H., Shiuchi, T., Mori, Y., Yada, T., Minokoshi, Y. and Tominaga, M. 2011. Lack of TRPM2 Impaired Insulin Secretion and Glucose Metabolisms in Mice. *Diabetes*. 60(1), pp.119-126.

Uemura, T., Kudoh, J., Noda, S., Kanba, S. and Shimizu, N. 2005. Characterization of human and mouse TRPM2 genes: identification of a novel N-terminal truncated protein specifically expressed in human striatum. *Biochem Biophys Res Commun*. 328(4), pp.1232-1243.

Uttara, B., Singh, A.V., Zamboni, P. and Mahajan, R.T. 2009. Oxidative stress and neurodegenerative diseases: a review of upstream and downstream antioxidant therapeutic options. *Curr Neuropharmacol*. 7(1), pp.65-74.

Valko, M., Leibfritz, D., Moncol, J., Cronin, M.T., Mazur, M. and Telser, J. 2007. Free radicals and antioxidants in normal physiological functions and human disease. *Int J Biochem Cell Biol*. 39(1), pp.44-84.

Vallet, P., Charnay, Y., Steger, K., Ogier-Denis, E., Kovari, E., Herrmann, F., Michel, J.P. and Szanto, I. 2005. Neuronal expression of the NADPH oxidase NOX4, and its regulation in mouse experimental brain ischemia. *Neuroscience*. 132(2), pp.233-238.

Vandenabeele, P., Galluzzi, L., Vanden Berghe, T. and Kroemer, G. 2010. Molecular mechanisms of necroptosis: an ordered cellular explosion. *Nat Rev Mol Cell Biol*. 11(10), pp.700-714.

Vandenbroucke, E., Mehta, D., Minshall, R. and Malik, A.B. 2008. Regulation of endothelial junctional permeability. *Ann N Y Acad Sci*. 1123, pp.134-145.

Vercammen, D., Beyaert, R., Denecker, G., Goossens, V., Van Loo, G., Declercq, W., Grooten, J., Fiers, W. and Vandenabeele, P. 1998. Inhibition of caspases increases the sensitivity of L929 cells to necrosis mediated by tumor necrosis factor. *J Exp Med*. 187(9), pp.1477-1485.

Verma, S., Quillinan, N., Yang, Y.F., Nakayama, S., Cheng, J., Kelley, M.H. and Herson, P.S. 2012. TRPM2 channel activation following in vitro ischemia contributes to male hippocampal cell death. *Neurosci Lett*. 530(1), pp.41-46.

Vila, M. and Przedborski, S. 2003. Targeting programmed cell death in neurodegenerative diseases. *Nat Rev Neurosci*. 4(5), pp.365-375.

Voets, T., Nilius, B., Hoefs, S., van der Kemp, A.W., Droogmans, G., Bindels, R.J. and Hoenderop, J.G. 2004. TRPM6 forms the Mg^{2+} influx channel involved in intestinal and renal Mg^{2+} absorption. *J Biol Chem*. 279(1), pp.19-25.

Walder, R.Y., Landau, D., Meyer, P., Shalev, H., Tsolia, M., Borochowitz, Z., Boettger, M.B., Beck, G.E., Englehardt, R.K., Carmi, R. and Sheffield, V.C. 2002. Mutation of TRPM6 causes familial hypomagnesemia with secondary hypocalcemia. *Nat Genet*. 31(2), pp.171-174.

Walseth, T.F. and Lee, H.C. 1993. Synthesis and characterization of antagonists of cyclic-ADP-ribose-induced Ca^{2+} release. *Biochim Biophys Acta*. 1178(3), pp.235-242.

Wang, F., Dufner-Beattie, J., Kim, B.E., Petris, M.J., Andrews, G. and Eide, D.J. 2004. Zinc-stimulated endocytosis controls activity of the mouse ZIP1 and ZIP3 zinc uptake transporters. *J Biol Chem*. 279(23), pp.24631-24639.

Wang, H., Ma, J., Tan, Y., Wang, Z., Sheng, C., Chen, S. and Ding, J. 2010. Amyloid-beta1-42 induces reactive oxygen species-mediated autophagic cell death in U87 and SH-SY5Y cells. *J Alzheimers Dis*. 21(2), pp.597-610.

Wang, L., Du, F. and Wang, X. 2008. TNF-α induces two distinct caspase-8 activation pathways. *Cell*. 133(4), pp.693-703.

Wang, Q.Q., Liu, Y.J. and Zhou, J.W. 2015. Neuroinflammation in Parkinson's disease and its potential as therapeutic target. *Transl Neurodegener*. 4.

Wang, X. and Michaelis, E.K. 2010. Selective neuronal vulnerability to oxidative stress in the brain. *Front Aging Neurosci*. 2, p12.

Wang, X., Wang, W., Li, L., Perry, G., Lee, H.G. and Zhu, X. 2014. Oxidative stress and mitochondrial dysfunction in Alzheimer's disease. *Biochim Biophys Acta*. 1842(8), pp.1240-1247.

Wehage, E., Eisfeld, J., Heiner, I., Jungling, E., Zitt, C. and Luckhoff, A. 2002. Activation of the cation channel long transient receptor potential channel 2 (LTRPC2) by hydrogen peroxide. A splice variant reveals a mode of activation independent of ADP-ribose. *J Biol Chem*. 277(26), pp.23150-23156.

Wehrhahn, J., Kraft, R., Harteneck, C. and Hauschildt, S. 2010. Transient Receptor Potential Melastatin 2 Is Required for Lipopolysaccharide-Induced Cytokine Production in Human Monocytes. *J Immunol*. 184(5), pp.2386-2393.

Wei, H. and Yu, X. 2016. Functions of PARylation in DNA Damage Repair Pathways. *Genomics Proteomics Bioinformatics*. 14(3), pp.131-139.

Williams, G.S., Boyman, L., Chikando, A.C., Khairallah, R.J. and Lederer, W.J. 2013. Mitochondrial calcium uptake. *Proc Natl Acad Sci U S A*. 110(26), pp.10479-10486.

Williams, T.I., Lynn, B.C., Markesbery, W.R. and Lovell, M.A. 2006. Increased levels of 4-hydroxynonenal and acrolein, neurotoxic markers of lipid peroxidation, in the brain in Mild Cognitive Impairment and early Alzheimer's disease. *Neurobiol Aging*. 27(8), pp.1094-1099.

Wilms, H., Rosenstiel, P., Sievers, J., Deuschl, G., Zecca, L. and Lucius, R. 2003. Activation of microglia by human neuromelanin is NF-κB dependent and involves p38 mitogen-activated protein kinase: implications for Parkinson's disease. *FASEB J*. 17(3), pp.500-502.

Wong, J.L., Creton, R. and Wessel, G.M. 2004. The oxidative burst at fertilization is dependent upon activation of the dual oxidase Udx1. *Dev Cell*. 7(6), pp.801-814.

Wood-Kaczmar, A., Gandhi, S., Yao, Z., Abramov, A.S.Y., Miljan, E.A., Keen, G., Stanyer, L., Hargreaves, I., Klupsch, K., Deas, E., Downward, J., Mansfield, L., Jat, P., Taylor, J., Heales, S., Duchen, M.R., Latchman, D., Tabrizi, S.J. and Wood, N.W. 2008. PINK1 Is Necessary for Long Term Survival and Mitochondrial Function in Human Dopaminergic Neurons. *PloS One*. 3(6).

Xie, Z., Chang, C. and Zhou, Z. 2014. Molecular mechanisms in autoimmune type 1 diabetes: a critical review. *Clin Rev Allergy Immunol*. 47(2), pp.174-192.

Xu, C., Li, P.P., Cooke, R.G., Parikh, S.V., Wang, K., Kennedy, J.L. and Warsh, J.J. 2009. TRPM2 variants and bipolar disorder risk: confirmation in a family-based association study. *Bipolar Disord*. 11(1), pp.1-10.

Xu, C., Macciardi, F., Li, P.P., Yoon, I.S., Cooke, R.G., Hughes, B., Parikh, S.V., McIntyre, R.S., Kennedy, J.L. and Warsh, J.J. 2006. Association of the putative susceptibility gene, transient receptor potential protein melastatin type 2, with bipolar disorder. *Am J Med Genet B Neuropsychiatr Genet*. 141B(1), pp.36-43.

Xu, S., Zhang, R., Niu, J., Cui, D., Xie, B., Zhang, B., Lu, K., Yu, W., Wang, X. and Zhang, Q. 2012. Oxidative stress mediated-alterations of the microRNA expression profile in mouse hippocampal neurons. *Int J Mol Sci*. 13(12), pp.16945-16960.

Yamamoto, S., Shimizu, S., Kiyonaka, S., Takahashi, N., Wajima, T., Hara, Y., Negoro, T., Hiroi, T., Kiuchi, Y., Okada, T., Kaneko, S., Lange, I., Fleig, A., Penner, R., Nishi, M., Takeshima, H. and Mori, Y. 2008. TRPM2-mediated Ca^{2+} influx induces chemokine production in monocytes that aggravates inflammatory neutrophil infiltration. *Nat Med*. 14(7), pp.738-747.

Yamamoto, S., Toda, T., Yonezawa, R., Negoro, T. and Shimizu, S. 2017. Tyrphostin AG-related compounds attenuate H_2O_2-induced TRPM2-dependent and -independent cellular responses. *J Pharmacol Sci*. 134(1), pp.68-74.

Yan, Y., Wei, C.L., Zhang, W.R., Cheng, H.P. and Liu, J. 2006. Cross-talk between calcium and reactive oxygen species signaling. *Acta Pharmacol Sin*. 27(7), pp.821-826.

Yang, K.T., Chang, W.L., Yang, P.C., Chien, C.L., Lai, M.S., Su, M.J. and Wu, M.L. 2006. Activation of the transient receptor potential M2 channel and poly(ADP-ribose) polymerase is involved in oxidative stress-induced cardiomyocyte death. *Cell Death Differ*. 13(10), pp.1815-1826.

Yang, W., Zou, J., Xia, R., Vaal, M.L., Seymour, V.A., Luo, J., Beech, D.J. and Jiang, L.H. 2010. State-dependent inhibition of TRPM2 channel by acidic pH. *J Biol Chem*. 285(40), pp.30411-30418.

Ye, B., Maret, W. and Vallee, B.L. 2001. Zinc metallothionein imported into liver mitochondria modulates respiration. *Proc Natl Acad Sci U S A*. 98(5), pp.2317-2322.

Ye, M., Yang, W., Ainscough, J.F., Hu, X.P., Li, X., Sedo, A., Zhang, X.H., Zhang, X., Chen, Z., Li, X.M., Beech, D.J., Sivaprasadarao, A., Luo, J.H. and Jiang, L.H. 2014. TRPM2 channel deficiency prevents delayed cytosolic Zn^{2+} accumulation and CA1 pyramidal neuronal death after transient global ischemia. *Cell Death Dis*. 5, pe1541.

Yilmaz, G. and Granger, D.N. 2008. Cell adhesion molecules and ischemic stroke. *Neurol Res*. 30(8), pp.783-793.

Yin, H.Z., Sensi, S.L., Ogoshi, F. and Weiss, J.H. 2002. Blockade of Ca^{2+}-permeable AMPA/kainate channels decreases oxygen-glucose deprivation-induced Zn^{2+} accumulation and neuronal loss in hippocampal pyramidal neurons. *J Neurosci*. 22(4), pp.1273-1279.

Yoon, I.S., Li, P.P., Siu, K.P., Kennedy, J.L., Macciardi, F., Cooke, R.G., Parikh, S.V. and Warsh, J.J. 2001. Altered TRPC7 gene expression in bipolar-I disorder. *Biol Psychiatry*. 50(8), pp.620-626.

Yosida, M., Dezaki, K., Uchida, K., Kodera, S., Lam, N.V., Ito, K., Rita, R.S., Yamada, H., Shimomura, K., Ishikawa, S., Sugawara, H., Kawakami, M., Tominaga, M., Yada, T. and Kakei, M. 2014. Involvement of cAMP/EPAC/TRPM2 Activation in Glucose- and Incretin-Induced Insulin Secretion. *Diabetes*. 63(10), pp.3394-3403.

Youdim, M.B., Edmondson, D. and Tipton, K.F. 2006. The therapeutic potential of monoamine oxidase inhibitors. *Nat Rev Neurosci*. 7(4), pp.295-309.

Yu, P., Xue, X., Zhang, J., Hu, X., Wu, Y., Jiang, L.H., Jin, H., Luo, J., Zhang, L., Liu, Z. and Yang, W. 2017. Identification of the ADPR binding pocket in the NUDT9 homology domain of TRPM2. *J Gen Physiol*. 149(2), pp.219-235.

Zaidi, A. 2010. Plasma membrane Ca-ATPases: Targets of oxidative stress in brain aging and neurodegeneration. *World J Biol Chem*. 1(9), pp.271-280.

Zangar, R.C., Davydov, D.R. and Verma, S. 2004. Mechanisms that regulate production of reactive oxygen species by cytochrome P450. *Toxicol Appl Pharmacol*. 199(3), pp.316-331.

Zecca, L., Wilms, H., Geick, S., Claasen, J.H., Brandenburg, L.O., Holzknecht, C., Panizza, M.L., Zucca, F.A., Deuschl, G., Sievers, J. and Lucius, R. 2008. Human neuromelanin induces neuroinflammation and neurodegeneration in the rat substantia nigra: implications for Parkinson's disease. *Acta Neuropathol*. 116(1), pp.47-55.

Zhang, L., Shimoji, M., Thomas, B., Moore, D.J., Yu, S.W., Marupudi, N.I., Torp, R., Torgner, I.A., Ottersen, O.P., Dawson, T.M. and Dawson, V.L. 2005. Mitochondrial localization of the Parkinson's disease related protein DJ-1: implications for pathogenesis. *Hum Mol Genet*. 14(14), pp.2063-2073.

Zhang, Q.G., Laird, M.D., Han, D., Nguyen, K., Scott, E., Dong, Y., Dhandapani, K.M. and Brann, D.W. 2012. Critical Role of NADPH Oxidase in Neuronal Oxidative Damage and Microglia Activation following Traumatic Brain Injury. *PloS One*. 7(4).

Zhang, W., Chu, X., Tong, Q., Cheung, J.Y., Conrad, K., Masker, K. and Miller, B.A. 2003. A novel TRPM2 isoform inhibits calcium influx and susceptibility to cell death. *J Biol Chem*. 278(18), pp.16222-16229.

Zhang, W. and Liu, H.T. 2002. MAPK signal pathways in the regulation of cell proliferation in mammalian cells. *Cell Res*. 12(1), pp.9-18.

Zhang, W., Wang, T.G., Pei, Z., Miller, D.S., Wu, X.F., Block, M.L., Wilson, B., Zhang, W.Q., Zhou, Y., Hong, J.S. and Zhang, J. 2005. Aggregated alpha-synuclein activates microglia: a process leading to disease progression in Parkinson's disease. *FASEB J*. 19(6), pp.533-542.

Zhang, W.Y., Hirschler-Laszkiewicz, I., Tong, Q., Conrad, K., Sun, S.C., Penn, L., Barber, D.L., Stahl, R., Carey, D.J., Cheung, J.Y. and Miller, B.A. 2006. TRPM2 is an ion channel that modulates hematopoietic cell death through activation of caspases and PARP cleavage. *Am J Physiol Cell Physiol*. 290(4), pp.C1146-C1159.

Zhao, J., Jitkaew, S., Cai, Z.Y., Choksi, S., Li, Q.N., Luo, J. and Liu, Z.G. 2012. Mixed lineage kinase domain-like is a key receptor interacting protein 3 downstream component of TNF-induced necrosis. *Proc Natl Acad Sci U S A*. 109(14), pp.5322-5327.

Zhivotovsky, B. and Orrenius, S. 2011. Calcium and cell death mechanisms: a perspective from the cell death community. *Cell Calcium*. 50(3), pp.211-221.

Zhou, W. and Yuan, J. 2014. Necroptosis in health and diseases. *Semin Cell Dev Biol*. 35, pp.14-23.

Zhu, X., Su, B., Wang, X., Smith, M.A. and Perry, G. 2007. Causes of oxidative stress in Alzheimer disease. *Cell Mol Life Sci*. 64(17), pp.2202-2210.

Zlokovic, B.V. 2011. Neurovascular pathways to neurodegeneration in Alzheimer's disease and other disorders. *Nat Rev Neurosci*. 12(12), pp.723-738.

Zorov, D.B., Juhaszova, M. and Sollott, S.J. 2014. Mitochondrial reactive oxygen species (ROS) and ROS-induced ROS release. *Physiol Rev*. 94(3), pp.909-950.

Zou, J., Ainscough, J.F., Yang, W., Sedo, A., Yu, S.P., Mei, Z.Z., Sivaprasadarao, A., Beech, D.J. and Jiang, L.H. 2013. A differential role of macrophage TRPM2 channels in Ca^{2+} signaling and cell death in early responses to H_2O_2. *Am J Physiol Cell Physiol*. 305(1), pp.C61-C69.